Unveiling Cellular Dynamics: Exploring Human Disease Progression and Therapeutic Potential through Organoid Models and Single-Cell Technologies

Inauguraldissertation

zur

Erlangung der Würde eines Doktors der Philosophie

vorgelegt der

Philosophisch-Naturwissenschaftlichen Fakultät

der Universität Basel

von

Bruno Gjeta

Basel, 2024

Genehmigt von der Philosophisch-Naturwissenschaftlichen Fakultät

auf Antrag von

Erstbetreuer: Dr. Jarrett Grayson Camp

Zusätzlicher Erstbetreuer: Prof. Dr. Verdon Taylor

Zweitbetreuer: Prof. Dr. Primo Leo Schär

Externe Expertin: Prof. Dr. Sarah Amalia Teichmann

Prof. Dr. Marcel Mayor

Dekan

Basel, den 14.11.2023

ACKNOWLEDGEMENTS

I am profoundly grateful to the multitude of individuals within the IHB community who have provided unwavering trust, steadfast support, invaluable encouragement, and expert guidance throughout my journey. These remarkable individuals have not only been colleagues but have evolved into cherished friends, forming an integral part of my IHB experience.

Foremost among these luminaries is my esteemed supervisor and mentor, Dr. Gray Camp. His unyielding dedication to scientific excellence, boundless optimism, and masterful craftsmanship in research have consistently inspired me. Gray, you have been a beacon of encouragement, propelling me to explore new horizons, master novel skills, and ascend to greater heights. Your belief in my potential has been the driving force behind my progress, and for that, I extend my deepest gratitude. The impact of this thesis would be incomplete without the invaluable feedback and insights of Prof. Dr. Barbara Treutlein and the extended Camp and Treutlein groups. Your contributions have shaped my work and amplified its significance.

The joint Treutlein and Camp Labs have transcended the status of a workspace, becoming a second home that encapsulates both joyous triumphs and challenging setbacks. To all my fellow lab members, I extend my heartfelt appreciation for sharing in both the jubilant moments and the arduous struggles. Participating in this lab has been an extraordinary privilege, and I would unhesitatingly embark on this journey again under your guidance. A special mention goes to Ryo Okuda with whom I've woven strong bonds and collaborated closely on our collective journey. Your camaraderie and dedication have made our collaboration a source of learning and growth that I genuinely treasure. I cannot overlook the contributions of Umut Kilik and Christoph Harmel, whose comedy bits and music presence in the lab have been invaluable.

I must also acknowledge the sage wisdom and scholarly guidance bestowed upon me by my thesis committee members, Prof. Dr. Verdon Taylor and Prof. Dr. Primo Leo Schaer. Their perceptive insights and intellectual mentorship have significantly enriched my work.

I express my heartfelt gratitude to my family. Your unwavering support, shared uncertainties, perpetual cheerfulness, and boundless encouragement have been my bedrock. In my closing words, my heartfelt appreciation extends to my friends and every individual who played a role, no matter how large or small, in shaping this journey and making this thesis a reality.

TABLE OF CONTENTS

ACKNOWLEDGEMENTS 3

TABLE OF CONTENTS 4

1. SUMMARY 5
2. INTRODUCTION 7
   1- HUMAN DEVELOPMENT AND DISEASE 7
   2- ADVENT OF A NEW TECHNOLOGY 7
   3- SELF ORGANIZATION AND CELLULAR CROSSTALK 8
3. ADVANCEMENTS IN ORGANOID TECHNOLOGY 10
   1- UNLEASHING THE POTENTIAL OF 3D MULTICELLULAR STRUCTURES ... 10
   2- STEM CELL DERIVED ORGANOIDS 11
   3- CANCER ORGANOIDS 13
   4- HUMAN ORGANOIDS AND THEIR ROLE IN ADVANCING BIOMEDICAL RESEARCH 15
   5- LIMITATIONS OF ORGANOID MODELS 18
4. PROBING NEW HORIZONS WITH SINGLE CELL TRANSCRIPTOMICS 20
   1- EMERGING TECHNOLOGIES 20
   2- BASICS OF DATA ANALYTICS 21
   3- INTERCELLULAR COMMUNICATION ANALYSIS 23
   4- GENE REGULATORY NETWORK INFERENCE 24
   5- DIFFERENTIATION TRAJECTORY INFERENCE 27
5. SCOPE OF THE DISSERTATION 30
6. RECONSTRUCTING CELL INTERACTIONS AND STATE TRAJECTORIES IN PANCREATIC CANCER STROMAL TUMOROIDS 31
   1- BACKGROUND 31
   2- OBJECTIVES 32
   3- RESULTS 33
   4- CHALLENGES AND FUTURE PERSPECTIVES 51
7. HUMAN INTESTINAL ORGANOIDS WITH AN AUTOLOGOUS TISSUE-RESIDENT IMMUNE COMPARTMENT 56
   1- BACKGROUND 56
   2- OBJECTIVES 57
   3- RESULTS 57
   4- CHALLENGES AND FUTURE PERSPECTIVES 70
8. CONCLUSIVE REMARKS 72
9. APPENDIX 73
10. REFERENCES 88
11. RESUME 129

SUMMARY

Human disease progression is a highly dynamic process characterized by cellular-level decision-making. It is crucial to employ appropriate technologies, with spatial and temporal resolution, as well as reliable model systems, to study and understand disease progression dynamics. Over the past decade, the emergence of single-cell technologies has facilitated such studies, enabling high-resolution molecular phenotyping of multicellular systems. Moreover, while much of our current knowledge of disease phenotypes has been derived from research on model organisms, organoid cultures have emerged as a viable alternative to bridge the gap to human systems. By recapitulating the cytoarchitecture and cellular complexity of human tissues, organoids offer an opportunity to investigate human-specific traits and obtain more representative outcomes for therapeutics. In this thesis, we leverage state-of-the-art human organoid models and single-cell transcriptome technologies to characterize the morphological and molecular changes associated with pancreatic cancer progression and acute intestinal inflammation. These two areas represent clinically relevant concerns with unmet therapeutic needs, and patient-specific models might bring new inroads into therapy development. We establish novel multi-lineage organoid models for both disease areas and investigate the onset and progression of abnormal cell states over time. Our focus lies particularly on intercellular communication, and we describe dynamic gene regulatory networks that underlie the observed transitions in cell states.

In the first project, we developed a modular stroma-rich tumoroid culture system that models pancreatic ductal adenocarcinoma (PDAC). This system successfully recreates the interactions between cancer, endothelial, and fibroblast cells, mimicking various aspects of primary tumors. Communication between different cell lineages within the cancer microenvironment can enhance cancer cell behavior and influence therapeutic responses. However, generating a complex cancer microenvironment *in vitro* has been a significant challenge. Our tumoroids consist of interconnected vessels, desmoplastic fibroblasts, and glandular cancer cell phenotypes that develop over time. By employing time-course single-cell transcriptome measurements, we demonstrate that tumoroid formation activates fibroblasts, leading to alterations in the extracellular matrix composition and the induction of specific signal-response signatures and metabolic changes in cancer cells. We identify Syndecan 1 (SDC1) and Peroxisome proliferator-activated receptor gamma (PPARG) as crucial receptor and metabolic nodes involved in cancer cell response to signals from cancer-associated fibroblasts (CAFs), and we show that blocking SDC1 disrupts cancer cell growth within the tumoroid. Analysis of tumoroids from multiple PDAC patients reveals the coexistence of subpopulations associated with classical and basal phenotypes, as well as the presence of migratory cancer cells characterized by a distinct transcriptional signature related to metastasis. This migration signature develops over time, reflecting a stress response mechanism that correlates with a worse clinical outcome.

In the second project, we turn our attention to the intricate relationship between the immune system and the intestinal epithelium. The intestine, a complex mucosal epithelial tissue responsible for food digestion and nutrient absorption, is a highly regenerating yet vulnerable tissue exposed to microbic flora. Perturbations in the delicate balance between epithelial and tissue-resident immune cells can contribute to autoimmune diseases and cancer. However, the dynamics of this relationship have remained elusive due to the lack of suitable experimental protocols for harvesting and cultivating fragile gut-resident immune

cells. In this study, we developed a 3D organoid model that combines human intestinal epithelium with autologous intraepithelial lymphocytes (IELs). This model enables us to characterize IEL populations under homeostatic and activated conditions and uncover the underlying processes and interactions involved in inflammatory responses. Our results demonstrate that IELs naturally integrate into the epithelium and dynamically survey both the organoids and the surrounding extracellular matrix. By performing single-cell transcriptome profiling (scRNA-seq), we identify a differential enrichment of cytoskeletal genes in IELs compared to matched peripheral blood mononuclear cells (PBMCs) and provide an explanation for their increased motility and intrinsic ability to inspect the epithelium. Unlike PBMCs, *in vitro* IELs exhibit rapid responses to cancer-targeting biologics, which are known to raise safety concerns in the intestine. This led to unwanted inflammation against healthy epithelium, a consistent adverse outcome observed clinically. Through time-course experiments and scRNA-seq profiling, we characterize critical IEL populations, uncovering key state trajectories and interactions that drive activation dynamics and result in adverse effects. We propose the antagonization of rho-associated kinases 1 & 2, key cytoskeletal modulators, as well as tumor necrosis factor alpha (TNFa), as a potential strategy to mitigate drug-induced inflammation.

Taken together, our comprehensive analyses and modular developmental systems serve as powerful tools to explore dynamic cell states and interactions, as well as to pave the way for the discovery of personalized therapies. We illustrate how our innovative models, particularly the immune-competent intestinal organoids, serve as better predictors of immunomodulatory drug responses.

INTRODUCTION

HUMAN DEVELOPMENT AND DISEASE

Human development is a truly extraordinary process that demands a high-magnification lens to comprehend fully. It all begins with a single cell, the zygote, which eventually gives rise to the entire human body. During this fascinating journey, cells undergo a series of remarkable changes: they grow, multiply, change shape, and differentiate into specialized cell types, each with its own unique function. What is truly astonishing is how this cellular diversification, or symmetry breaking, occurs from initially uniform conditions. These diversifications result from a complex interplay of stochastic fluctuations and cell interactions, which are further sustained and amplified through intricate feedback loops. A symphony of microenvironmental signals directed by evolved gene regulatory networks (GRNs) orchestrate a self-organizing sequence of events that controls the precise positioning of cells and fine-tunes cell function. As organized structures emerge, they mature and intricately interconnect, culminating in the formation of the various tissues, organs, and complex systems that constitute a fully developed multicellular organism. Despite the complexity and puzzling nature of these developmental processes, they exhibit an astonishing resilience to perturbations and remain highly reproducible across different individuals.

However, the human body's robustness is not infallible. At times, failures occur, triggered by mutations, whether somatic or germline, or environmental pressures, causing disruptions in the harmonious system. This can lead to the emergence of aberrant states, representing harmful deviations from the normal structural integrity of tissues or an individual's physiological condition. These aberrant states manifest in a multitude of diseases, each with unique characteristics classified according to their origin, affected organs, and prognosis. Regardless of their specific manifestations, they all share a common trait: the potential to significantly impact an individual's quality of life and life expectancy. In the face of these challenges, fundamental research becomes an invaluable tool. It delves deep into the mechanisms underlying the onset and progression of disease phenotypes, providing crucial insights that serve as the foundation for developing therapies. These treatments aim to either mitigate the detrimental effects of aberrant states or restore essential homeostasis, ultimately striving to enhance both the length and quality of human life.

ADVENT OF A NEW TECHNOLOGY

Since the beginning of the last century, biological research has dedicated substantial attention to investigating the function and morphology of *in vitro* cultured tissues. Early groundbreaking reports demonstrated the use of *ex vivo* cultured neurites, providing a platform for microscopic observations (Harrison *et al.,* 1907). Over the years, cell culture techniques have become increasingly sophisticated, allowing for the study of more complex systems. In the mid-1970s, cultures of squamous epithelial colonies, resembling human epidermis with keratinization in the upper layers and cell proliferation in the bottom layers, were developed from single cells (Rheinwald and Green, 1975).

To create more physiologically relevant models that overcome the limitations of two-dimensional (2D) cultures, researchers introduced artificial extracellular matrix (ECM) (Orkin *et al.,* 1977). This groundbreaking advancement enabled the development of the first three-dimensional (3D) *in vitro* cultures derived from mammary glands (Barcellos-Hoff *et al.,* 1989). In the last decade, the emergence of 3D organotypic culture systems, commonly known as organoids, has revolutionized the study of various multicellular complex tissues. Organoids offer researchers an accessible and tractable method to study tissues, circumventing the lack of primary human tissue and providing excellent potential for mechanistic and manipulative studies. Notably, organoids are especially suitable for genetic and morphogenetic manipulation, single-cell studies, and drug screenings.

SELF ORGANIZATION AND CELLULAR CROSSTALK

Organoids are 3D *in vitro* models capable of recapitulating key aspects of spatio-temporal patterning observed during organ development, while mimicking their physiology and cytoarchitecture (Clevers, 2016; Zhao *et al.,* 2022). These versatile structures can be derived from pluripotent, embryonic, adult stem cells, or cancer cells and undergo spontaneous self-organization in the presence of specific niche and growth factors (Clevers, 2016; Fatehullah *et al.,* 2016; Lancaster and Knoblich, 2014; Rossi *et al.,* 2018). A debate ensues regarding whether organoids truly exhibit self-organization, as some systems necessitate exogenous growth factors to trigger the process. The emergence of localized signaling sources which, when stabilized, can act as references for patterning, in a genetically encoded self-assembly model may also explain organoid formation (Turner *et al.,* 2016). However, it has been observed that intestinal organoids undergo symmetry breaking even without external differentiation cues and subsequently initiate self-patterning and self-sorting to achieve equilibrium at homeostatic conditions (Serra *et al.,* 2019). In the context of organoids, self-organization refers to the emergence of a system-autonomous, asymmetric higher-order structure from an initially homogeneous state under a uniform signaling environment.

Central to the remarkable transformations during self-organization is the ability of a cell to exchange signals within the local neighborhood. Intricate signaling networks enable cell interactions, coordination of activities, fate decisions, tissue patterning, and migration. For example, during early human brain development, a cascade of morphogenetic events is triggered. The forebrain develops from the anterior-most section of the neural tube in response to a WNT morphogenetic gradient, while a spreading SHH signaling gradient from the neural tube floorplate instructs ventral fates and counters WNT and BMP signals from the cortical hem and neural tube roofplate responsible for dorsal forebrain specification. Additionally, the Pallial-Subpallial Boundary (PSB) secretes soluble Frizzle-like Receptor Proteins (sFRPs) that restrict WNT signaling to cortical structures, further refining the spatial context-dependent crosstalk of different cell types (Martinez *et al.,* 2012; Martinez-Ferre & Martinez, 2012; Puelles & Martinez, 2013). Mediating these crucial physiological processes are ligand-receptor complexes. Binding of ligands to their cognate receptors activates cell-specific signaling pathways that can induce profound changes in metabolism and transcriptional profiles. Consequently, mapping these ligand-receptor interactions becomes fundamental to understanding cellular behavior and decoding responses to microenvironmental cues. Organoid systems offer a fascinating tool that enables

observation of localized interactions and manipulation of morphogens and other signaling molecules under controlled conditions.

ADVANCEMENTS IN ORGANOID TECHNOLOGY

UNLEASHING THE POTENTIAL OF 3D MULTICELLULAR STRUCTURES

Organoids have emerged as valuable 3D *in vitro* models, capable of mimicking the physiology and cytoarchitecture of various organs, such as the pancreas, intestine, stomach, brain, and liver (Barker *et al.,* 2010; Dahl-Jensen and Grapin-Botton, 2017; Eiraku *et al.,* 2011; Greggio *et al.,* 2013; Huch *et al.,* 2013; Huch *et al.,* 2013; Lancaster and Knoblich, 2014; Lancaster *et al.,* 2013; Rookmaaker *et al.,* 2015; Rossi *et al.,* 2018; Sasai, 2013; Sato and Clevers, 2013; Sato *et al.,* 2011; Sato *et al.,* 2009; Simunovic and Brivanlou, 2017; Werner *et al.,* 2017). Depending on the biological materials used, organoids can be categorized into three main types: pluripotent stem cell (PSC)-derived, adult stem cell (ASC)-derived, and cancer organoids. The PSC-derived organoids encompass diverse tissue types, such as thyroid, kidney, optic cup, retinal, and cerebral organoids (Kurmann *et al.,* 2015; Takasato *et al.,* 2014; Eiraku *et al.,* 2011; Shirai *et al.,* 2016; Lancaster *et al.,* 2013). Furthermore, embryoids and gastruloids, which originate from clusters of differentiating embryonic stem cells (ESC), have been created to mimic the initial developmental stages of embryos, the determination of cell type identities, and the establishment of body axes (Beccari *et al.,* 2018; Harrison *et al.,* 2017; Rossi *et al.,* 2018; Simunovic & Brivanlou, 2017; van den Brink *et al.,* 2014). ASC-derived organoids comprise various tissue models, including mammary gland, salivary gland, lung, pancreatic, colon, and small intestinal organoids (Olabi *et al.,* 2018; Butler *et al.,* 2016; Loomans *et al.,* 2018; Yui *et al.,* 2012; Sato *et al.,* 2009). Moreover, patient-derived cancer specimens embedded in a 3D matrix can also grow into organoids known as tumor organoids (tumoroids). Several tumoroids have been established (Boj *et al.,* 2015; Broutier *et al.,* 2017; Gao *et al.,* 2014; Hubert *et al.,* 2016; Lee *et al.,* 2018; Sachs *et al.,* 2018; Sato *et al.,* 2011; Van de Wetering *et al.,* 2015; Vlachogiannis *et al.,* 2018), providing a more accurate and robust predictive model for the efficacy of anticancer drugs and the identification of new compounds (Vlachogiannis *et al.,* 2018).

Despite their diversity, all organoid systems share a common defining feature: they originate from progenitor cells with intrinsic self-organizing capacity, driving the formation of complex multicellular 3D structures with emergent properties surpassing those of individual components. This spatial organization establishes a stem cell niche, facilitates the expansion of progenitor cells, and supports the development and maintenance of differentiated cells. However, variations exist in cell-type composition between individual organoids, batches, and stem cell lines. Researchers are trying to addressorganoid heterogeneity by developing highly reproducible organoid protocols across different lines (Velasco *et al.,* 2019; Yoon *et al.,* 2019). Additionally, organoid morphogenesis is influenced by the composition and physical properties of the extracellular matrix (ECM). Current methods for organoid generation involve the use of exogenous ECM components, like Matrigel (SelectScience https://www.selectscience.net/application-articles/tuning-the-elastic-moduli-of-corning-matrigel-and-collagen-i-3d-matrices-by-varying-the-protein-concentration/?artid=46305), or endogenous ECM progressively deposited by the organoid

itself. Moreover, the need for exogenous ECM may vary based on tissue model and developmental stage. Whereas exogenous ECM inclusion promotes the initial establishment of tissue polarity, it may become dispensable following fate specification (Martins-Costa *et al.,* 2022). Efforts are currently underway to develop substitute techniques for ECM support that can overcome the ill-defined and variable Matrigel composition (Kozlowski *et al.,* 2021; Ranga *et al.,* 2016). Developing new materials with optimum stiffness for specific tissues is critical for symmetry-breaking events in organoids (Ranga *et al.,* 2016; Y. Zheng *et al.,* 2019).

STEM CELL DERIVED ORGANOIDS

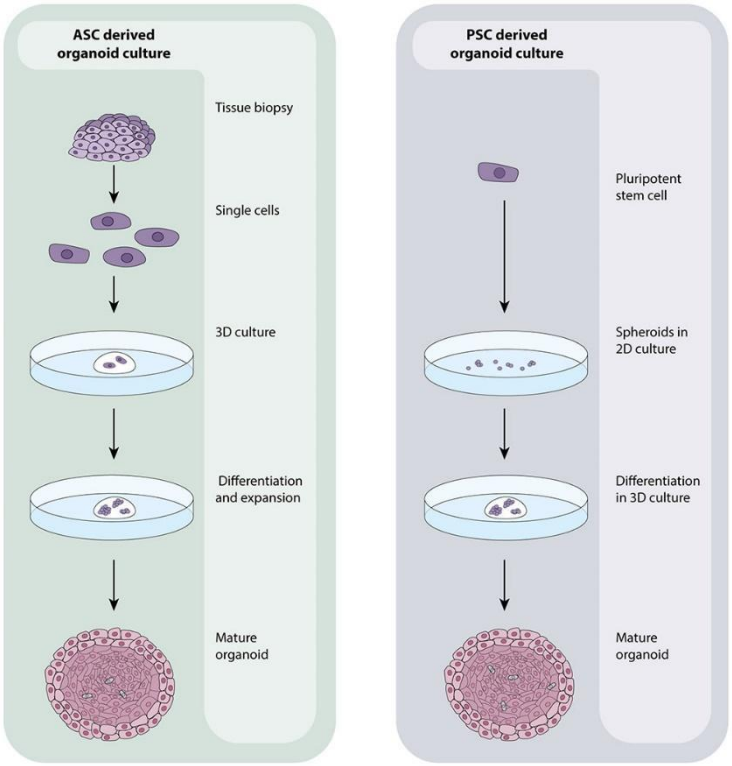

Figure 1: Stem cell-derived organoids formation. *Organoids derived from ASCs are generated by breaking down patient-derived tissues followed by cultivating them in a synthetic extracellular matrix. On the other hand, organoids derived from PSCs originate from individual stem cells, initially forming spheroids in a suspension culture, and subsequently being transferred to a three-dimensional environment where they are exposed to morphogens. Adapted from Iakobachvili and Peters (2017).*

Stem cell-derived organoids encompass (induced)-pluripotent stem cells (iPSCs) and tissue-resident fetal and adult stem cells (FSCs, ASCs), and they have been generated by mimicking the biochemical and physical cues of tissue development and homeostasis (Fig. 1) (Iakobachvili & Peters, 2017; Lancaster & Knoblich, 2014).

General strategies for the development of iPSC-derived organoids involve a stereotypical sequence of specific morphogen regiments, designed to follow the step-wise developmental stages and allow the correct patterning of a desired tissue type *in vitro* (Fig. 2) (McCauley & Wells, 2017). Nodal and Wnt signals, depending on the time point of delivery, promote endoderm and mesoderm fates (Gadue *et al.,* 2006). These inputs are the major determinants of PSC germ layer identity which is established *in vivo* during gastrulation through the migration of epiblast cells across the primitive streak (Ciruna & Rossant, 2001). In the absence of other triggering cues during this stage, neural determination is induced in the tissue. Therefore, if induced iPSCs are grown without the presence of the instructive signals, they will naturally develop into neuroepithelial cells (Eiraku *et al.,* 2008). To date, two approaches prevail in the production of 3D human brain tissue cultures. The first is based on culturing the neuroepithelium in permissive media, resulting in the generation of multiple brain structures within the same organoid (Kadoshima *et al.,* 2013; Lancaster *et al.,* 2013). Alternatively, signaling molecules or other directive cues can be used to control patterning of the neuroepithelium towards defined structures, such as cortex, ventral telencephalon, hypothalamus, or thalamus (Eiraku *et al.,* 2008; Kadoshima *et al.,* 2013; Pajca *et al.,* 2015; Bagley *et al.,* 2017; Birey *et al.,* 2017; Xiang *et al.,* 2017;

Qian *et al.,* 2016; Xiang *et al.,* 2019). Fusion of two or more brain structures has been explored to study neuronal migration or enable the formation of inter-region neuronal connections (Bagley *et al.,* 2017; Birey *et al.,* 2017; Duan *et al.,* 2019; Pasca, 2018).

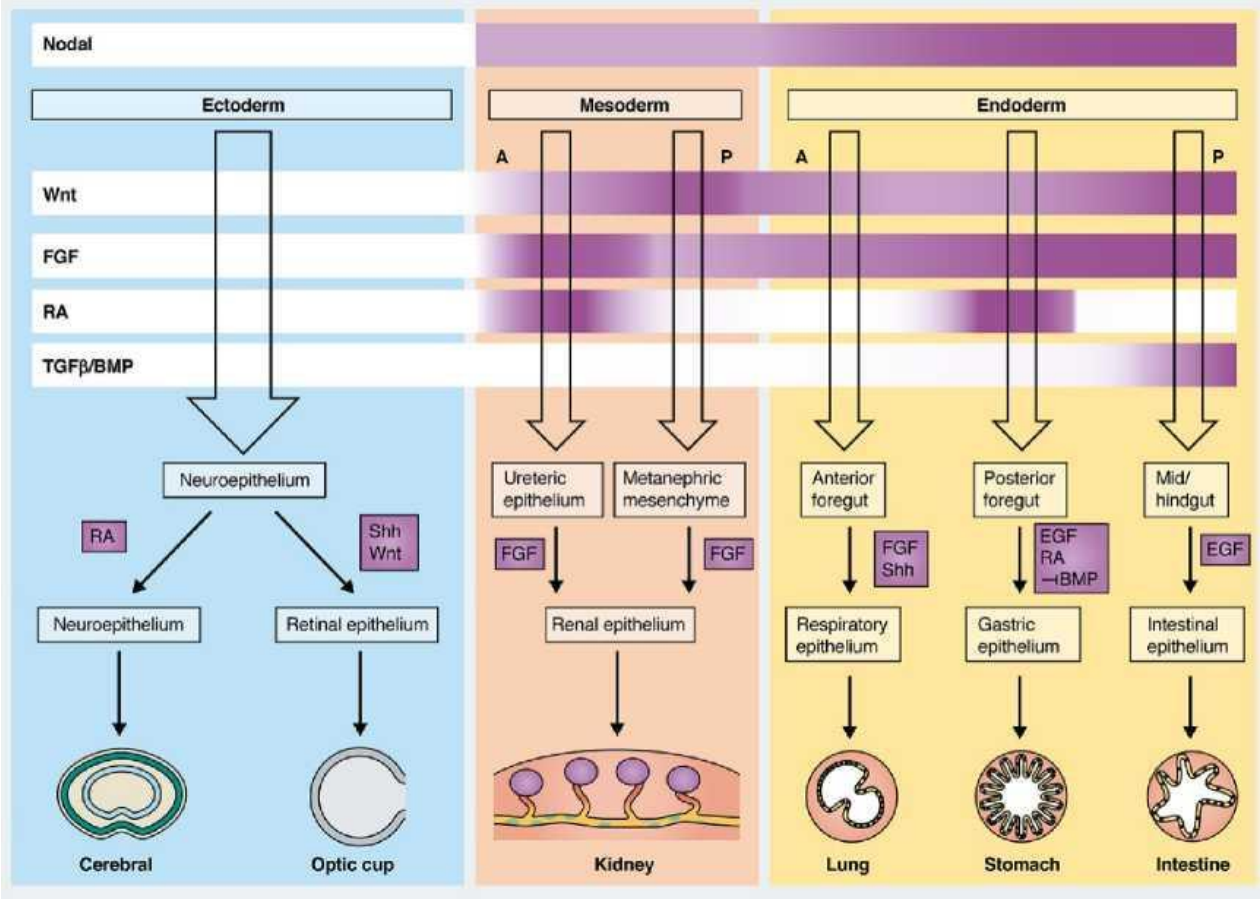

Figure 2: PSC-derived organoid generation mimics developmental stages. *Cultivating pluripotent stem cells (PSCs) with precise mixtures and concentrations of morphogens, which replicate the sequence of events in embryonic development, enables the patterning of germ layer identity and subsequent generation of organoids that closely resemble a diverse range of tissues. Adapted from McCauley and Wells (2017).*

Likewise, tissue-specific cues can also be employed to create organoids originating from mesoderm and endoderm. The patterning of endoderm and mesoderm along the anterior-posterior axis is guided by spatio-temporal signaling gradients of Wnt, fibroblast growth factor (FGF), retinoic acid (RA), and transforming growth factor (TGF) / bone morphogenetic protein (BMP) (Kubo *et al.,* 2004). Accurate activation of Wnt signaling, followed by the FGF, leads to the formation of anterior-posterior mesoderm. Thereafter, modulation of RA cues allows for the patterning of ureteric epithelium and metanephric mesenchyme (Taguchi *et al.,* 2014; Takasato *et al.,* 2014). Notably, extended exposure of mesodermal lineages to Wnt and FGF signals has the potential to produce kidney organoids (Taguchi *et al.,* 2014). Expression of the transcription factor Cdx2, following Wnt and FGF activation, promotes posterior endoderm and commitment to mid/hindgut fate (Spence *et al.,* 2011). In contrast, BMP signaling inhibition leading to Cdx2 repression results in the formation of foregut endoderm (Fausett *et al.,* 2014; McCracken *et al.,* 2014). At this stage, additional inhibition of RA signaling promotes anterior endoderm fate that leads towards lung organoid formation (Dye *et al.,* 2015). Conversely, stimulation with RA factors guide the acquisition of posterior foregut identity enabling the generation of gastric organoids

(McCracken *et al.,* 2014). BMP stimulation drives the acquisition of the most posterior endodermal fates giving rise to intestinal organoids (Spence *et al.,* 2011).

Fate restriction of iPSCs to a specific germ layer during culture may impact the functionality of an organoid system when the desired tissue is a complex mixture of cells with diverse developmental origins. Neural organoid protocols, as described above, initially restrict their potential to neuroectoderm-derived fates, precluding the presence of microglia and endothelial cells within the organoid. To address this limitation, several protocols have been developed leading to the successful incorporation of microglia-like cells in retinal organoids (Chichagova *et al.,* 2023) along with structures resembling blood vessels and microglia within cortical organoids (Sun *et al.,* 2022). Furthermore, the ectopic expression of transcription factors specific to myeloid and endothelial cells has been outlined as a potential strategy for the inherent generation of endothelial cells and microglia within cortical organoids (Cakir *et al.,* 2019; Cakir *et al.,* 2022). Altogether, this shows how key steps driving embryo development can be engineered to direct differentiation of iPSCs and allows the generation of diverse organoid systems. Despite holding great potential and enabling the generation of a wide array of tissues in a patient-specific context, iPSC-derived organoids result in models that more closely resemble embryonic rather than adult tissues (Eiraku *et al.,* 2011; McCracken *et al.,* 2014; Rossi *et al.,* 2018). Additionally, since PSC-derived organoids usually require culture for extended periods of time, they tend to suffer from the lack of perfusing oxygen, which impacts the survival of the inner-most regions and overall maturation of the different cell types. Good results in mitigating these caveats have been observed by the transplantation of the organoids into living animal models. Indeed, neural organoid transplantation into the brain of living rodents (Daviaud *et al.,* 2018; Dong *et al.,* 2021; Jgamadze *et al.,* 2023; Mansour *et al.,* 2018; Revah *et al.,* 2022) results in the vascularization of organoid tissue (Daviaud *et al.,* 2018; Mansour *et al.,* 2018) and functional integration of circuits, which serve as a hybrid model with behavioral output (Revah *et al.,* 2022).

In contrast to PSC-derived models, ASC-derived organoids do not recapitulate developmental steps. Rather, this system takes advantage of the regenerative capacity of parent tissues, resulting in structures that are more reminiscent of adult physiology (Clevers, 2016). Consistently, growth conditions for ASC-derived organoids typically include factors controlling tissue repair or homeostasis. While the idea that organoids developed from ASCs essentially replicate tissue regeneration is not yet widely accepted, numerous discoveries support this theory. Several ASC-derived organoid models replicate the properties of tissues with either rapid cell replenishment or the ability to regenerate, like the small intestine, stomach, and lung. Furthermore, recent studies have shown that in liver, regenerative responses following acute damage involve induction of stem cells expressing Lgr5 (Huch *et al.,* 2013b). These cells have the potential to regenerate liver tissues as well as generate hepatic organoids. Likewise, in the lung, an organ characterized by low rate of cell division, instances of sudden damage result in an elevated count of actively dividing cells (Pardo-Saganta *et al.,* 2015), which can be used for the formation of cultured organoids (Tadokoro *et al.,* 2014).

CANCER ORGANOIDS

Cancer organotypic cultures, defined as 3D self-organizing aggregates of patient-derived tumor cells that are capable of mimicking critical phenotypic, genetic, and

histopathological hallmarks of the parent neoplastic tissue, have recently been established as a comparatively cost-efficient and archetypal platform to investigate human cancer heterogeneity and tumor microenvironment (TME) interactions *in vitro* (Fig. 3) (LeSavage *et al.,* 2022; Drost & Clevers, 2018).

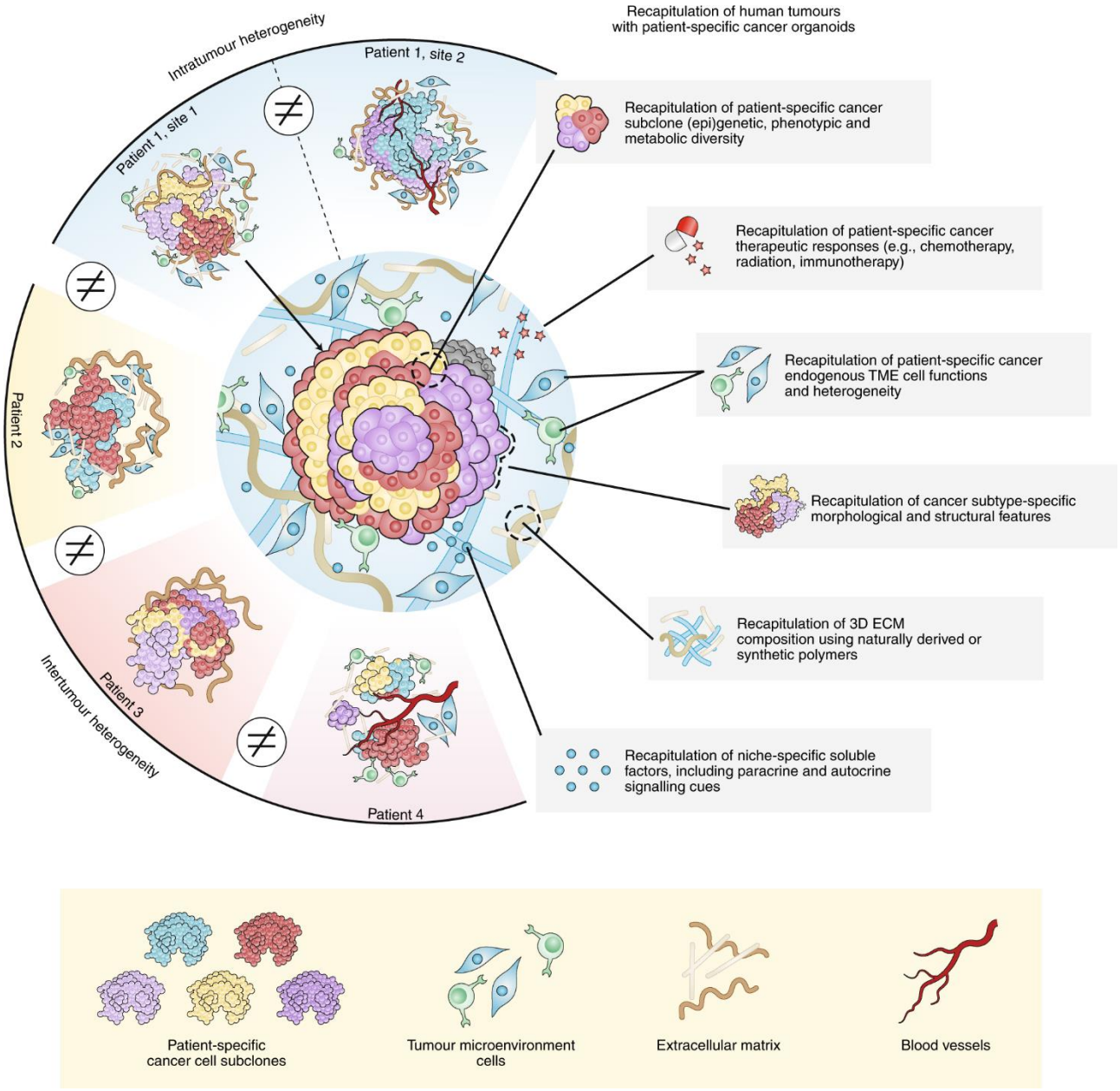

Figure 3: Cancer organoids mirror the distinctive traits of inter- and intratumoral heterogeneity. *Every patient's cancer has a range of unique cellular and environmental traits that contribute to the considerable biological variability observed within and between tumors. Patient-derived cancer organoid models have demonstrated the ability to faithfully reproduce this inherent diversity within and between tumors. Specifically, patient-derived cancer organoids can mimic the extensive (epi)genetic and phenotypic heterogeneity among different subclones of cancerous cells, together with the collective morphological features unique to each tumor. Additionally, cancer organoids provide a way to simulate the diversity of the tumor microenvironment (TME), including the presence and functions of non-cancerous cells, the signaling through specific soluble molecules, and changes in the composition of the extracellular matrix (ECM). Consequently, cancer organoids stand as poweful predictive tools for anti-cancer treatment responses in clinical personalized medicine. Adapted from LeSavage et al. (2022).*

Building upon established protocols for healthy gastrointestinal organoid generation, colorectal cancer (CRC) was among the first successfully developed patient-derived organoid tumor models (Sato *et al.,* 2009; Sato *et al.,* 2011). This seminal work paved the

way for the development of cancer organoids from several tumor types, which have provided a high-throughput platform for testing clinical as well as emerging cancer targeting treatments such as chemotherapy (Kopper *et al.,* 2019; Sachs *et al.,* 2018; Tiriac *et al.,* 2018; Vlachogiannis *et al.,* 2018), immunotherapy (Neal *et al.,* 2018), as well as radiation therapy (Ganesh *et al.,* 2019) in a patient-specific context. Moreover, numerous studies have taken advantage of cancer organoids for investigating disease progression and tumor niche factor requirements (Fujii *et al.,* 2016; Nanki *et al.,* 2018; Seino *et al.,* 2018). The capacity to cultivate, passage, and cryopreserve neoplastic cells while maintaining the parent's tumor genetic and histological traits, defines the attainment rate of organoid establishment from specific tumor subtypes. This has been described to be higher than 70% (Boj *et al.,* 2015; Neal *et al.,* 2018; Sachs *et al.,* 2018; Tiriac *et al.,* 2018), significantly better compared to the success rate of cancer cell lines establishbment which ranges between 20-30% (Kodack *et al.,* 2017). Additionally, through the co-culture of non-neoplastic cellular populations, such as cancer-associated fibroblasts (CAFs) (Ohlund *et al.,* 2017; Seino *et al.,* 2018) and immune cells (Neal *et al.,* 2018), *in vitro* cancer organoids offer unique advantages in modeling cell type diversity as well as heterotypic cell interactions within the tumor microenvironment.

To date, several 'living biobanks' of patient-derived cancer organoids, including colorectal (Fujii *et al.,* 2016; Sato *et al.,* 2011; van de Wetering *et al.,* 2015), pancreatic (Boj *et al.,* 2015; Seino *et al.,* 2018; Tiriac *et al.,* 2018), prostate (Gao *et al.,* 2014), ovarian (Hill *et al.,* 2018; Kopper *et al.,* 2019), bladder (Lee *et al.,* 2018), liver (Brouttier *et al.,* 2017), breast (Sachs *et al.,* 2018), lung (Kim *et al.,* 2019; Sachs *et al.,* 2019), esophagus (Li *et al.,* 2018), gastric (Nanki *et al.,* 2019), endometrium (Boretto *et al.,* 2019), and brain (Jacob *et al.,* 2020), have modeled interpatient heterogeneity. These studies highlight the maintenance of parent tumor (epi)genetic, proteomic, morphological, and pharmacotypic features in cancer organoids. Specifically, an all-encompassing cohort of 138 tumor samples from pancreatic cancer patients, covering both genetic and phenotypic variability, unveiled shared genetic and transcriptomic patterns linked to the effectiveness of cancer-fighting drugs (Tiriac *et al.,* 2018). Remarkably, studied organoids revealed pharmacological signatures that were, a posteriori, predictive of clinical outcomes for multiple patients after treatment (Tiriac *et al.,* 2018). Similarly, a living biobank of colo-rectal cancer (CRC) encompassing 55 patient-specific organoid lines, established from both primary and metastatic lesions, demonstrated the conservation of distinct histopathological features and genetic signatures of their *in vivo* counterparts (Fujii *et al.,* 2016). By meticulously examining the genetic traits and adjusting culture condition, cancer organoids are shown to effectively replicate heterogeneity in the genetic makeup among patients which impacts the needs of specific environmental factors within the organoids and the process of metastasis (Fujii *et al.,* 2016).

HUMAN ORGANOIDS AND THEIR ROLE IN ADVANCING BIOMEDICAL RESEARCH

Despite the undeniable successes that animal models have historically achieved, there is a critical bottleneck hindering biological research from addressing human-specific questions in understanding human biology and disease. Extrapolating results from animal models to humans has proven challenging and requires pre-existing insights into causative conditions or genes involved. To study a particular phenotype, animal models are commonly

established through precisely manipulating the genes responsible for inducing the specific disorder or by subjecting animals to detrimental environmental conditions. The mouse is one of the most frequently used animal models due to its mammalian similarity to humans and the possibility to establish genetically engineered strains. However, even with recent precision genome editing advancements mediated by CRISPR-Cas9, creating conventional transgenic mouse models still takes over a year (Wang *et al.*, 2013; Yang *et al.*, 2013; Yang *et al.*, 2014). Furthermore, certain human biological traits are not suitable to being recapitulated in animal model systems. Brain function, resulting from human-specific developmental events and mechanisms (Kanton *et al.,* 2019; Lui *et al.,* 2011), is significantly more complex in humans compared to murine counterparts. Given that human development unfolds over a much longer period of time than the models (Kuzawa *et al.,* 2014), human physiology diverges significantly from that of the laboratory mouse, and it is not surprising that substantial metabolic disparities exist between these two species. Besides, the genetic diversity inherent to humans, which is absent in inbred animal models, exerts a pivotal influence on the initiation, advancement, and drug reactions in various diseases. This underscores the imperative need to create model systems that are uniquely tailored to human biology for the advancement of personalized medical interventions.

To bridge the gap between animal models and humans, human stem cell-derived organoid culture has emerged as a promising solution (Fowler *et al.,* 2019; Lancaster & Huch, 2019, Schweiger & Jensen, 2016). Organoids offer a powerful platform to recreate human organ architecture and physiology with remarkable detail, surpassing the limitations of animal models. They maintain cellular heterogeneity and structure of parent tissues while preserving most advantages of *in vitro* systems, facilitating the study of processes that are challenging to address *in vivo*. Indeed, complex diseases involving multiple genes, including inflammatory bowel disease (IBD) and cancer, greatly benefit from organoid systems that can be established directly from patient biopsies, without the necessity of prior knowledge about the precise genes accountable for the observed phenotype (Drost & Clevers, 2018; Nanki *et al.,* 2020). Additionally, organotypic cultures enable quicker and more reliable results, are more easily attainable and can be readily expanded to reach an optimal sample size making large-scale studies of chemical and genetic perturbations feasible in conditions where physiological cell types and interactions are preserved (Rookmaaker *et al.,* 2015; Rossi *et al.,* 2018; Xavier da Silveira Dos Santos & Liberali, 2018).

Human organoids derived from biopsy samples or genetic manipulations have proven instrumental in studying the molecular pathogenesis of various illnesses and conducting drug screenings for personalized medicine (Lancaster & Huch, 2019; Michels *et al.,* 2020). Additionally, combining organoids with CRISPR-Cas9 genome editing has allowed researchers to model monogenic disorders like cystic fibrosis and test potential therapeutic strategies (Schwank *et al.,* 2013). This showcased the potential of adopting a comparable approach to produce autologous organoids for transplantation. Indeed, integration into mouse models aimed at restoring damaged tissues and cell therapy efficacy have been assessed using organoids (Rookmaaker *et al.,* 2015; Rossi *et al.,* 2018; Schweiger & Jensen, 2016). Furthermore, genetic manipulation of organoids has led to the identification of oncogenic driver mutations and their subsequent introduction into normal epithelial organoids has provided invaluable descriptions of the minimum set of mutations that can closely model a metastatic human colon cancer (Drost *et al.,* 2015; Matano *et al.,* 2015). Besides, conducting analysis of pooled CRISPR gRNA library screenings has enabled the

optimization of the effectiveness of organoid models in human genetic research (Michels *et al.,* 2020; Ringel *et al.,* 2020).

Beyond disease modeling, organoids are shedding light on human-specific traits (Fig. 4) (Pollen *et al.,* 2023). By directly comparing human and non-human primate brain organoids, researchers have unveiled features linked to enhanced cognition (Kanton *et al.,* 2019; Mora-Bermudez *et al.,* 2016; Pollen *et al.,* 2019). Specifically, comparing human, chimpanzee and macaque cerebral organoid development revealed human-selective gene regulatory features that persist into adulthood (Kanton *et al.,* 2019) and increased mTOR signaling in human outer radial glia (Pollen *et al.,* 2019). Furthermore, muscle and bone differentiation techniques using organoids provide insights into musculoskeletal changes, while intestine and colon organoids have been employed to study metabolic effects of diet and cooking innovations (Chal & Pourquié, 2017; Singh *et al.,* 2020). Acquisition of metabolic, morphological, and cognitive modifications that enabled humans to colonize diverse habitats and develop extraordinary technologies to explore the depths of outer space has been possible on the basis of genetic, molecular and developmental changes that often involve complex intercellular interactions.

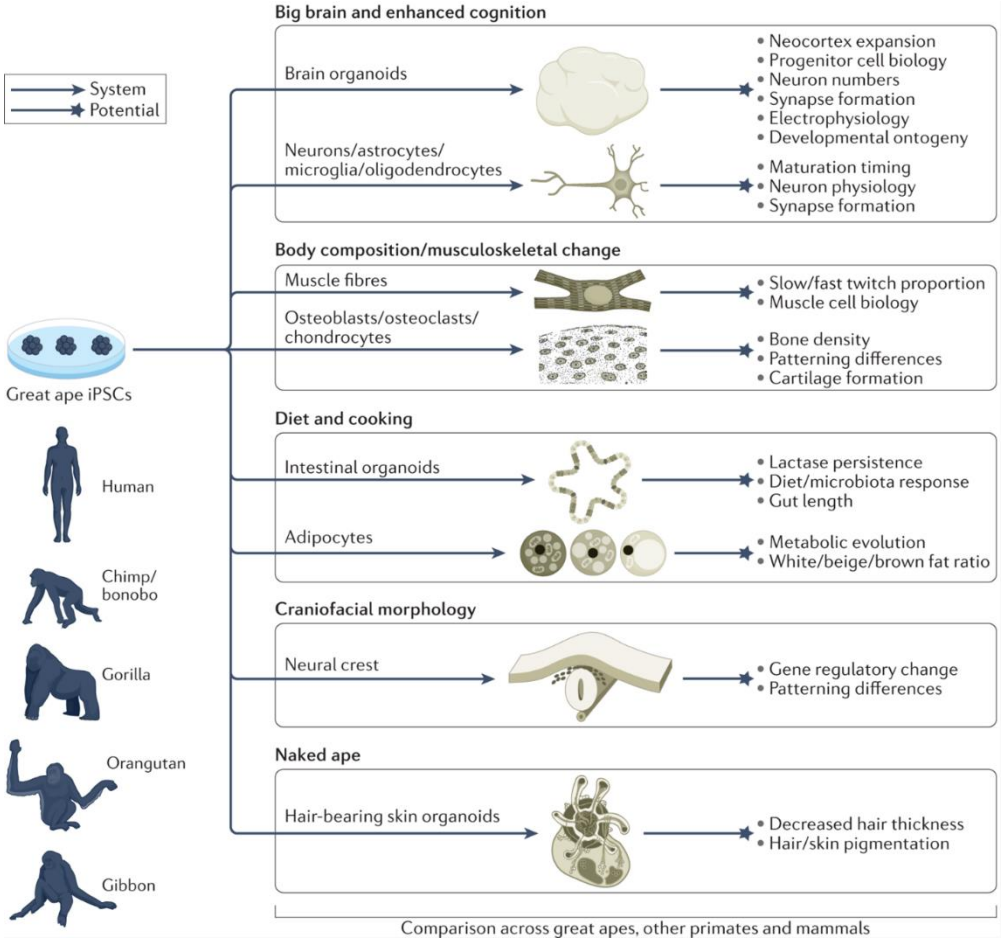

Figure 4: Primate-derived organoids to explore human-specific characteristics *Induced pluripotent stem cells (iPSCs) from large primates have the potential to delve into contemporary human features. Illustrated are instances of existing human in vitro model systems (arrows) and the possibility of investigating and comprehending traits unique to humans (stars). These stem cell and organoid models have the capacity to be extended to encompass great apes, along with other primates and mammals, facilitating the study of human molecular, cellular, and tissue functions under controlled conditions. Adapted from Pollen et al. (2023).*

When organoids patterned to selected germ layers or regions were insufficient, more complex assemblies of organoids have also been developed that could model human-specific biology (Sousa *et al.,* 2017; Aiello & Wheeler, 1995; Babbitt *et al.,* 2011). Remarkably, intestinal organoids are capable of replicating the contractions observed in the gut when paired with co-cultures of neural crest cells (Workman *et al.,* 2017), while the introduction of microglia and vascular cells could play a crucial role in emulating interactions

between the nervous and immune systems, as well as supporting the development of neurons (Cakir *et al.,* 2019; Popova *et al.,* 2021). Finally, organoids provide valuable insights from an evolutionary perspective, offering information about human health, disease susceptibility, and recent genetic changes (Fan *et al.,* 2016; Benton *et al.,* 2021). Understanding how our bodies are organized and how recent genetic changes affect disease risk can aid in personalized medical treatments.

Advancements in single-cell RNA sequencing (scRNA-seq) and high-content imaging technologies enable researchers to quantitatively investigate organoids at the single-cell level, providing unprecedented morphological and molecular insights of developmental and evolutionary processes and allowing the reconstruction of differentiation trajectories (Camp *et al.,* 2015; Kanton *et al.,* 2019; Mayr *et al.,* 2019; Quadrato *et al.,* 2017; Velasco *et al.,* 2019). In conclusion, human stem cell-derived organoids offer a transformative approach in biological research, providing an essential bridge between animal models and human biology. Their use in disease modeling, studying human-specific traits, and exploring evolutionary insights is accelerating progress in understanding human biology and advancing personalized medicine.

LIMITATIONS OF ORGANOID MODELS

Despite the numerous advantages outlined earlier, organotypic cultivation of human tissue remains a work in progress, with ongoing efforts to advance and standardize the technology. One pressing challenge in organoid research is the variability of the system, as different studies employ contrasting procedures to establish stem-cell derived organoids, lacking a broadly accepted standardized protocol. This inconsistency is evident in gut organoids that can be derived from human ASCs or PSCs (Sato *et al.,* 2009, Sato *et al.,* 2011, Spence *et al.,* 2011) as well as cerebral organoids derived from different cell lines (Kanton *et al.,* 2019). A recent breakthrough showcased the potential for further improvement by refining culture conditions, leading to better cellular diversity and culture efficiency (Velasco *et al.,* 2019, Yoon *et al.,* 2019). A collective effort is needed to establish clear guidelines and quality assessment methods which are of paramount importance in reducing variability among research groups. Leveraging single-cell transcriptomic and (epi)-genomic profiling, along with advanced analysis technologies, could prove crucial in achieving precise assays for benchmarking different organoid systems against their *in vivo* counterparts. Furthermore, human organoid models may encounter added variability due to individual distinctions including age and genetic makeup. While challenging, this variation provides the chance to explore the impact of population heterogeneity in human biology.

A clear drawback of organoid systems is their inability to simulate interorgan communication comprehensively. Human organoids can only mimic organ or tissue-specific microphysiology, a limitation that must be acknowledged when delving into this exciting research field. However, progress is underway to overcome this limitation by connecting multiple organoids to study communication between different organs (Bagley *et al.,* 2017, Birey *et al.,* 2017, Xiang *et al.,* 2017). Exciting prospects arise from the convergence of organoid research and organ-on-a-chip technology, potentially leading to an 'organoid-on-a-chip' technology (Zhang *et al.,* 2017). This could facilitate inter-organoid communication while the distinct organoid types are segregated in spatially isolated cultures.

Another challenge lies in defining the effect of extracellular matrix composition on organoid culture. The uncertainty surrounding matrix composition can significantly impact the results of chemical and genetic perturbation screening of human organoid models. Despite ongoing efforts (Kozlowski *et al.,* 2021, Ranga *et al.,* 2016), more work is needed to surmount this challenge, establish more faithful human model systems, and facilitate the application of human organotypic cultures to regenerative medicine, where compliance with "good manufacturing practice" necessitates the use of precisely defined raw materials. Moreover, ongoing efforts are being directed towards generating human organoid culture platforms tailored for large-scale production (Cowan *et al.*, 2020), advancing organoid-based high-content screening, and developing micro-organoids-on-a-chip as finely tuned miniature systems. In all these endeavors, acquiring the knowledge of crafting a synthetic and adaptable extracellular matrix will prove of paramount significance.

PROBING NEW HORIZONS WITH SINGLE CELL TRANSCRIPTOMICS

EMERGING TECHNOLOGIES

Single-cell messenger RNA sequencing (scRNA-seq) has undergone a revolutionary transformation, becoming one of the fastest-evolving techniques in the last decade. This powerful method enables the measurement of all messenger RNA molecules in individual cells, providing insights into the future expressed proteins and functional identity of each cell. Unlike bulk RNA sequencing approaches, scRNA-seq has illuminated an astonishing degree of cell type diversity, shedding new light on the complexity of physiological and developmental processes in human biology. Additionally, scRNA-seq is particularly well-suited for reconstructing comprehensive developmental differentiation trajectories due to its ability to capture a variety of differentiation states simultaneously (Nayak & Hasija, 2021). The fundamental strategy behind scRNA-seq methods involves "tagging" each cell's transcriptome with unique oligomeric barcodes. Following enzymatic tissue dissociation and permeabilization of cytoplasmic or nuclear membranes, messenger RNA (mRNA) molecules, together with barcodes uniquely identifying individual cells, undergo reverse transcription to cDNA. Since the number of collected transcripts for single-cell sequencing is scarce compared to bulk sequencing, an extensive amplification procedure is necessary. This procedure includes the introduction of a unique molecular identifier (UMI) to correctly assign all generated amplicons to their original transcripts. Moreover, in techniques such as massively parallel sequencing, the generation of cDNA libraries for individual cells involves the incorporation of additional adaptor and barcoding sequences to facilitate subsequent multiplexing of transcription reads.

Key distinctions among scRNA-seq techniques lie in the single-cell isolation procedure as well as in the particular chemistry used during the experiment. Plate-based assays, for instance, involve distribution of cells into multiwell plates or microfuge tubes before applying barcodes and initiating library construction (Hashimshony *et al.,* 2016; Islam *et al.,* 2011; Picelli *et al.,* 2013; Sasagawa *et al.,* 2013). Among these, SMART-seq2 is renowned chemistry used in plate-based methods for its exceptional sensitivity and the capacity to produce complete cDNA molecules (Picelli *et al.,* 2014). In contrast, droplet microfluidic-based assays rely on the encapsulation of single cells in microfluidic droplets, enabling the profiling of tens of thousands of cells per experiment (Jaitin *et al.,* 2014; Klein *et al.,* 2015; Macosko *et al.,* 2015; Treutlein *et al.,* 2014; Zheng *et al.,* 2017). Droplet microfluidic-based methods have gained popularity due to their accessibility, commercialization, and ability to characterize sample heterogeneity at single-cell resolution with high cell numbers. Both microfluidic- and plate-based techniques, however, require complete dissociation of the tissue sample, leading to over sequencing more abundant cell types and rare or other specific cell populations. To overcome this limitation, researchers have employed various strategies. For example, Fluorescence-Activated Cell Sorting (FACS) and Laser Capture Microdissection (LCM) have been used to enrich cells expressing specific markers or select specific sections of the tissue (Nichterwitz *et al.,* 2016).

Recent advances in the field have led to the development of techniques that address the single-cell isolation needs. SPLiT-seq (Split-Pool Ligation-based Transcriptome

sequencing) sequentially links barcodes to divided cell groups creating distinct sequence combinations for each pool (Rosenberg *et al.,* 2018). Similarly, Sci-RNA-seq utilizes combinatorial barcoding for increased efficiency (Cao *et al.,* 2017). Most recently, PIP-seq has simplified the single-cell droplet encapsulation process through a vortex-aided emulsification process (Clark *et al.,* 2023). These techniques have enabled a significant increase in the number of profiled cells, potentially reaching up to a million cells per experiment. In addition to increased cell profiling, recent developments have also allowed for the preservation of structural information in tissue samples while still capturing single-cell transcriptomes. Spatially resolved methods are distinguished based on the required resolution at the cellular or gene level. Some methods offer single-cell resolution with high gene coverage, such as MERFISH (Chen *et al.,* 2015). Others have lower spatial resolution (1-10 cells) but provide whole transcriptome coverage, such as Visium (Stahl *et al.,* 2016).

BASICS OF DATA ANALYTICS

Over the past few years, swift advancements and enhanced capacity for processing single-cell transcriptomics have resulted in the production of extensive volumes of data. To effectively process this data and extract useful biological information, specialized analysis pipelines have been developed. Two widely used and comprehensive sets of tools for analyzing scRNA-seq data are Seurat (R) (Stuart *et al.,* 2019) and Scanpy (Python) (Wolf *et al.,* 2018). To ensure the accurate processing of scRNA-seq data and eliminate spurious technical effects, following commonly accepted guidelines is crucial (Luecken & Theis, 2019; Nayak & Hasija, 2021):

1. Alignment and Counting:

   FASTQ files containing sequencing information need to be aligned to a reference genome and subsequently counted to generate a numeric matrix of transcript counts per detected cell barcode. However, gene dropout, caused by variable transcript capture efficiency rates and insufficient sequencing depth, results in a sparse matrix with many cells having a transcript count of zero.

2. Normalization and Stabilization:

   The transcriptomic landscape of individual cells is highly variable and needs to be adjusted through normalization procedures to enable reliable comparison of gene expression across different cells. Commonly, library size factor normalization and logarithmic transformation of the raw transcript count matrix, with pseudocount addition to all genes to avoid the zero-count problem, are applied. SCTransform (Hafemeister & Satija, 2019), integrated into recent versions of the Seurat analysis pipeline, introduces modeling approaches to stabilize transcript count variance and enhance the recovery of biological variation.

3. Quality Control (QC):

   Quality control checkpoints are necessary to discard dead or damaged cells, multiplets, or empty droplets that can occur during sample preparation. Strategies involve filtering cells based on their proportion of mitochondrial gene counts and total UMI or gene counts. Quantification and regression of ambient RNA can also be beneficial.

4. Scaling and Variation Regression:

Scaling normalized transcript counts across the dataset guarantees that genes with high expression do not dominate downstream analysis. Scaling is typically performed only on the highly variable genes to reduce computation time and memory resources. Additionally, regression of undesired sources of variation, such as mitochondrial or cell cycle gene expression, can significantly improve data quality and the recovery of interesting biological insights.

5. Data Integration:

When comparing cells from multiple experiments, data integration is required. Unlike batch-effect correction used for repetitions of the same experiment through linear algorithms, data integration employs non-linear algorithms to ensure similar cell states are grouped together, even when they belong to different samples. Several methods for data integration have been deployed, each optimized for specific settings and presenting different stringencies. When performing data integration, it is recommended to test multiple methods and monitor their performance to avoid overcorrection and the creation of technical artifacts. Notable integration algorithms include Harmony (Korsunsky, Millard, *et al.,* 2019), CCA/RPCA (Butler *et al.,* 2018), CSS/RSS (He *et al.,* 2020), MNN (Haghverdi *et al.,* 2018), and LIGER (Welch *et al.,* 2019).

6. Dimensionality Reduction:

Principal Component Analysis (PCA) is a key step in facilitating the analysis of high-dimensional single-cell transcriptomic data. It summarizes gene expression variation in Principal Components (PCs) ordered according to their information content. PCA is typically followed by non-linear dimensionality reduction methods, such as t-distributed Stochastic Neighbor Embedding projections (t-SNE) (Maaten & Hinton, 2008) and Uniform Approximation and Projection embedding (UMAP) (McInnes *et al.,* 2018). These methods highlight differences between cell populations and preserve the global structure of the data, making them efficient for large datasets. Other options include force-directed layouts like ForceAtlas2 (Jacomy *et al.,* 2014) and cluster-based visualizations like Partition-Based Graph Abstraction (PAGA) (Wolf *et al.,* 2019).

7. Clustering:

Grouping cells according to their transcriptional landscapes is a common practice achieved through clustering algorithms. Supervised methods rely on prior knowledge about the data, such as the number of expected clusters or specific marker genes. On the other hand, unsupervised methods do not make any a priori assumptions and are especially useful for exploratory analyses. These algorithms act on network representations of the data, such as the shared nearest neighbor (SNN)-based graph from Seurat, and identify communities in the dataset through an optimization process. The resulting clusters are linked to biologically meaningful information and may represent different cell types or states. Identification of biologically meaningful clusters may require several iterations and parameter tweaking, such as clustering resolution (Yu *et al.,* 2022).

After completing this pipeline, a plethora of downstream analyses can be performed for deeper insights. Common subsequent steps include differential expression (DE) analysis, cell type heterogeneity analysis, gene set enrichment analysis (GSEA), gene regulatory

network (GRN) inference, differentiation trajectory inference, and intercellular signaling analysis.

INTERCELLULAR COMMUNICATION ANALYSIS

The exponential growth of scRNA-seq has enabled the measurement of ligands and receptors' expression in multiple cell types, providing valuable insights into intercellular communication networks that are fundamental to tissue function in homeostasis and disease. To identify ligand-receptor interactions from scRNA-seq data, researchers need to annotate complex relationships and use statistical methods to integrate resources and select relevant interactions. Several methods have been published to investigate context-dependent crosstalk of different cell types and their role in physiological processes. Most of these methods rely on lists of binary ligand-receptor pairs and filter interactions based on expression levels or the number of cells expressing specific interactors in cell populations (Camp *et al.,* 2017; Pavličev *et al.,* 2017; Puram *et al.,* 2017; Skelly *et al.,* 2018). Other approaches include hierarchical clustering to construct interaction graphs of ligand-receptor modules (Cohen *et al.,* 2018), one-sided Wilcoxon rank-sum test on ligand-receptor pairs' mean expression product (Kumar *et al.,* 2018), and enrichment of shared interactions between two cell populations against a background model (Boisset *et al.,* 2018; Joost *et al.,* 2018).

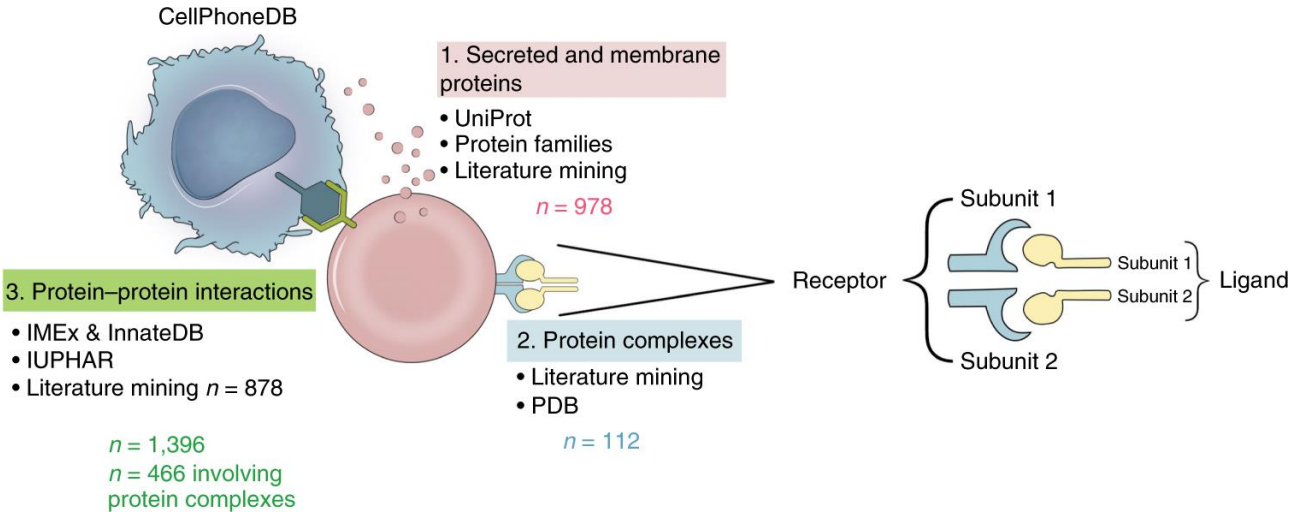

Figure 5: Overview of CellPhoneDB database. *(1) Proteins that are secreted and those located in the cell membrane are held within the protein_input category; (2) complexes of proteins are kept in the complex_input category; and (3) interactions between different proteins are recorded in the interaction_input category. This data has been compiled from www.CellPhoneDB.org. The CellPhoneDB database contains a cumulative count of 978 proteins: 501 belong to the secreted category, while 585 are membrane-bound proteins. These proteins partake in 1,396 interactions; among all the proteins housed in CellPhoneDB, 466 form heteromers. Within this dataset, there are 474 interactions involving secreted proteins and 490 interactions involving solely membrane proteins. Notably, there are a combined total of 250 interactions that encompass integrins. Adapted from Efremova et al. (2020).*

CellPhoneDB v2.0 stands out from other methods by accurately representing ligand-receptor complexes and considering their multi-subunit architecture, which can influence binding affinity and downstream signal transduction (Fig. 5) (Efremova *et al.,* 2020). It relies on public resources and manual curation to annotate proteins involved in cell-cell communication and employs a statistical framework to predict enriched cellular interactions from single-cell transcriptomics data. The CellPhoneDB pipeline involves subsampling of input data through geometric sketching and pooling of cells based on cluster annotations. Enriched ligand-receptor interactions between cell populations are identified based on

expression and detection rates of queried genes and cell-population specificity calculated through empirical shuffling. Specificity is crucial to highlight informative communication between selected cell populations and filter out ubiquitously expressed genes. Finally, predicted molecular interactions can be used to generate potential cell-cell communication networks.

In contrast, NicheNet focuses on the functional understanding of cell-cell communication by considering the influence of sender-cell ligands on receiver-cell gene expression (Browaeys *et al.,* 2020). NicheNet combines gene expression data of interacting cells with a prior model representing ligand-to-target signaling paths. NicheNet's prior model aims at overcoming simple ligand-receptor interactions to predict ligands' influence on the expression profiles in another cell while tracking which signaling mediators may be involved. This is the result of a model-based parameter optimization to integrate multiple complementary data sources covering ligand-receptor, signal transduction, and gene regulatory interactions. Network propagation is then employed to compute a ligand-target regulatory potential score, indicating the regulators' downstream location in the signaling network of the ligand. NicheNet's analysis pipeline provides a ranking of ligands that most likely affect gene expression in receiver cells, along with potential signaling paths, offering a comprehensive assessment of the signaling transduction cascade.

Recently, CellChat (Jin *et al.,* 2021) has been developed to infer, visualize, and analyze intercellular communications from scRNA-seq data. Similar to CellPhoneDB v2.0, CellChat provides a comprehensive and manually curated signaling molecule interaction database, accounting for known structural composition of ligand-receptor complexes. Additionally, it considers soluble agonists and antagonists, stimulatory and inhibitory membrane-bound co-receptors, as key components of the signaling process. CellChat employs mass action models, along with differential expression analysis and statistical tests on cell groups or continuous state trajectories, for inferring cell-state specific signaling communications. To characterize and compare the inferred intercellular communications within complex tissues, CellChat offers social network analysis, pattern recognition, and manifold learning approaches.

Despite the potential benefits, intercellular communication analysis has some limitations to consider. Ligand-receptor interaction databases are not complete but continuously updated and refined. Additionally, while statistical methods may prioritize cell-type-enriched interactions, non-significant p-values do not imply absence of interactions. Moreover, current methods predict cell-cell communication without considering spatial proximity or phosphorylation status of receptor complexes. Multimodal approaches integrating spatial information, phosphorylation dynamics, and ligand diffusion rates can significantly enhance the accuracy of intercellular signaling predictions.

GENE REGULATORY NETWORK INFERENCE

Cells coordinate their activities through complex gene regulatory networks (GRNs), where the interplay between chromatin states and transcription factors (TFs) modulates transcription rates of target genes. Understanding these regulatory dynamics is crucial for unraveling cellular identity and its disruptions in disease. GRNs, represented as graphs, can incorporate multiple components of gene regulation, including TFs, splicing factors, non-coding RNAs, microRNAs, and metabolites. Historically, GRNs were inferred from bulk -

omics data or literature. However, the advent of single-cell technologies, particularly multimodal profiling, has sparked an explosion of novel GRN inference methods (Klein *et al.,* 2015; Macosko *et al.,* 2015; Treutlein *et al.,* 2014; Zheng *et al.,* 2017; Chen *et al.,* 2019; Liu *et al.,* 2019).

GRN inference involves summarizing complex gene regulation events into interpretable network structures using computational methods and observational data. Inferred interactions in GRNs can be directed or undirected, signed or weighted. Weighted gene co-expression network analysis (WGCNA) (Langfelder *et al.,* 2008) is a simple unsupervised method that identifies modules of co-expressed genes. However, it lacks causal regulatory links and has a high number of false positive associations. To address these limitations, methods like GENIE3 distinguish TFs from target genes based on prior knowledge (Huynh-Thu *et al.,* 2010). SCENIC, tailored to scRNA-seq data, is an extension of GENIE3 and generates cell type-specific GRNs by leveraging TF-gene co-expression patterns and TF binding motif enrichment on gene promoter regions and cis-regulatory elements (CREs) (Aibar *et al.,* 2017). GRNBoost2, incorporated into SCENIC, provides a faster implementation of GRN reconstruction (Moerman *et al.,* 2019). However, inference from transcriptomics data alone may still produce false positives since chromatin accessibility is ignored. Nevertheless, inference from transcriptomics data alone is still prone to false positives given that processes such as chromatin accessibility are ignored.

The progress in profiling chromatin states using single-cell assay for transpose-accessible chromatin sequencing (scATAC-seq) (Buenrostro *et al.,* 2015) has enabled a significant refinement of GRN reconstruction. Multimodal data can be paired or unpaired, depending on whether different profiling modalities have been performed on the same cell or not, and GRN inference methods differ in their input requirements. Some methods summarize read-outs across cell groups or build GRNs independently for each modality and then merge the results which overcomes the need for paired data. Others model both modalities simultaneously requiring prior integration approaches (Argelaguet *et al.,* 2021) or paired samples as input. To facilitate user experience, methods such as FigR, GLUE, and SOMatic implement and incorporate integration approaches into their analysis pipeline (Kartha *et al.,* 2022; Cao & Gao, 2022; Jansen *et al.,* 2019).

GRN inference from multimodal data is a stepwise process. Generally, CREs are associated with target genes according to genomic distance constraints. Subsequently, TFs are assigned to accessible CREs using binding motif annotations. Finally, a prediction of gene expression is modelled based on TF expression (Fig. 6). Distinct GRNs can be reconstructed for the same data inputs, even when inference methods implement similar modelling strategies, due to the numerous and highly heterogeneous TF biding motif databases and algorithms for predicting TF-CRE associations. To ensure reproducibility within the analysis pipeline, most methods fix the motif matcher algorithm used. A notable exception is SCENIC+ which introduces a comprehensive curated collection of TF binding motifs and allows analysis with multiple motif matcher algorithms such as cisTarget, DEM as well as HOMER (González-Blas *et al.,* 2022; Heinz *et al.,* 2010). Variability in GRN prediction methods is expanded by employing diverse genomic distance thresholds for linking open chromatin regions to their respective target genes. Functionally validated interactions are significantly enriched at short distances, closer than 10kb which represent the most common choice, while substantially decreasing past 100 kb (Kim & Wysocka, 2023). Nevertheless, medium range distances covering up to 100 kb or large distal sites up

to 1 Mb are known to be relevant to transcriptional regulation (Kim & Wysocka, 2023) and their effects should not be ignored. However, it is important to consider that different cutoffs will likely impact the GRN inference results.

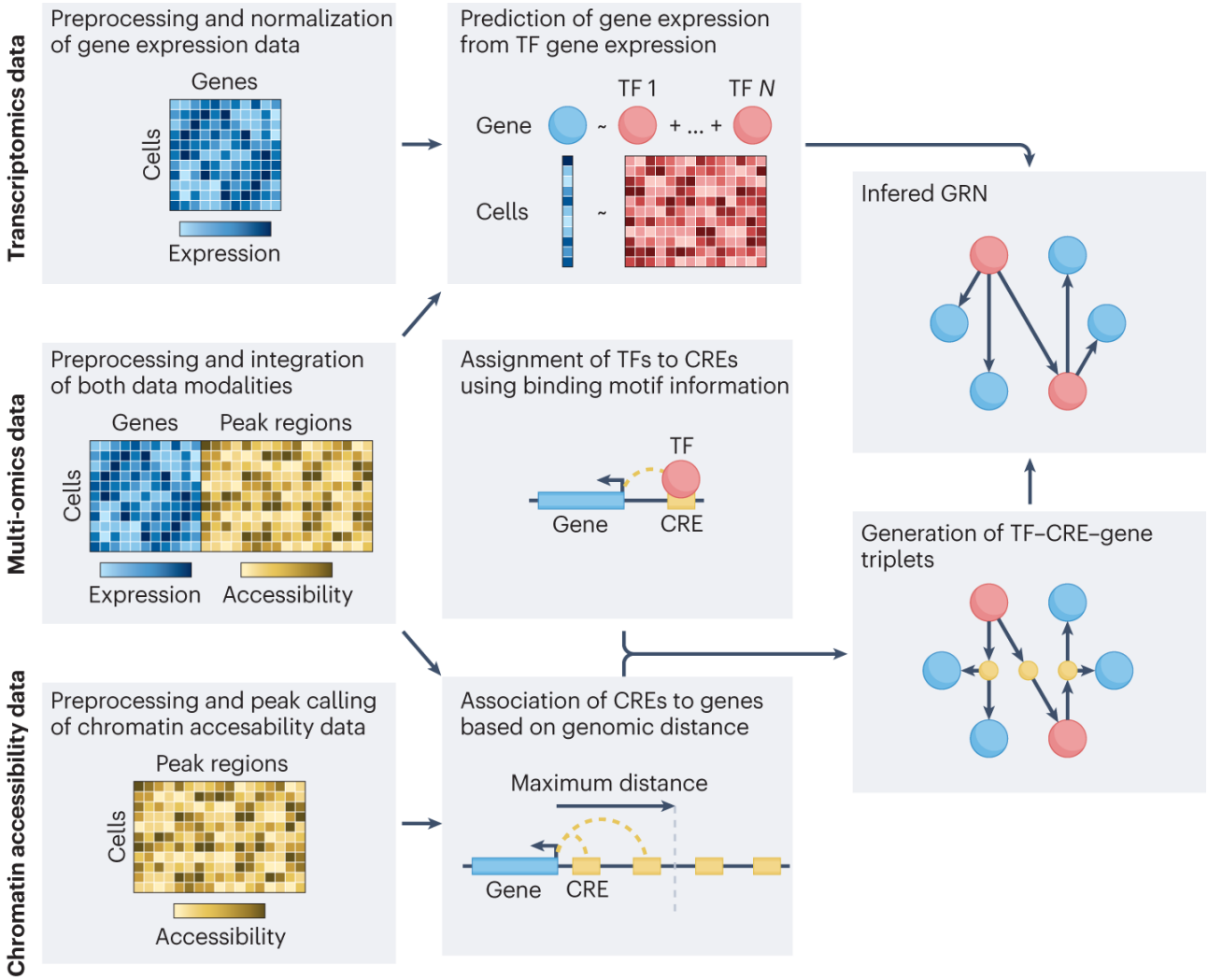

Figure 6: Overview of gene regulatory network (GRN) inference methods. *The process of inferring gene regulatory networks (GRNs) involves various stages that depend on the type of data collected from the studied samples. In the case of transcriptomics data, the initial steps encompass preprocessing and normalization to create a matrix reflecting gene expression levels across different samples or cells. To identify genes capable of regulating others, a list of established transcription factor (TF) genes is sourced from external references. Predicting interactions between TFs and target genes comes next; this involves constructing models that aim to anticipate observed gene expression by considering TF transcript abundance, ultimately resulting in associations between TFs and genes that are then consolidated to depict a comprehensive GRN. For chromatin accessibility data, the first actions entail preprocessing and identifying peaks to generate a matrix indicating the accessibility status of cis-regulatory elements (CREs) across samples or cells. Associating CREs with genes is achieved based on specific genomic distance thresholds. To predict TF binding to CREs, databases containing TF binding motifs and algorithms that match these motifs are employed. The outcome is the prediction of TF-CRE-gene complex interactions which are simplified to TF-gene pairs and aggregated into a cohesive GRN. In cases where samples are profiled using both transcriptomics and chromatin accessibility modalities (multi-omics data), the preprocessing steps are applied to each independently. If required, integration is performed on data from unmatched modalities. With both sets of data available, the methodology can simultaneously utilize the three aforementioned modeling stages to establish TF-CRE-gene triplets, which are then simplified and merged into a unified GRN.* *Adapted from Badia-i-Mompel et al. (2023).*

Following the above-described steps, GRN inference methods create a candidate scaffold network of TF-CRE-target triplets. To reconstruct the final GRN structure, TF-CRE-target dependencies are then modelled either linearly, for example in FigR, or non-linearly, for example in SCENIC+ which builds random forests to describe relationships between variables. The latter modelling strategy can accommodate complex interactions such as synergistic effects which are widely acknowledged to underline transcriptional processes

(Zuin *et al.,* 2022). Meanwhile, linear modelling benefits from its simplicity in formulation and increased interpretability. The significance of the inferred regulatory interactions can be assessed using frequentist or Bayesian statistical frameworks. Even though Bayesian methods excel in integrating pre-existing domain knowledge into the newly inferred GRN structure, frequentist methods tend to be faster, more scalable, and more accurate in the absence of high-quality prior knowledge. Some methods, including FigR and SCENIC+, implement frequentist statistical frameworks, while others like CellOracle and Pando offer multiple modeling strategies to the user (Kamimoto *et al.,* 2023; Fleck *et al.,* 2022). Additionally, scMEGA and IReNA leverage trajectories to infer linear and non-linear GRNs, respectively, when no distinct cell groups are defined (Li *et al.,* 2023; Jiang *et al.,* 2022).

Despite the valuable biological insights provided by GRN inference methods, the input data may not directly capture various regulatory mechanisms, such as TF protein abundance, TF cooperation with cofactors, alternative transcript splicing, post-translational protein modifications, and genome structure. Indeed, just the expression of a TF or the presence of accessible promoter regions may not be informative enough and poorly correlate with active gene transcription (Kim & Wysocka, 2023). Including and measuring these aspects can lead to more representative GRNs that better capture gene regulation *in vivo*.

DIFFERENTIATION TRAJECTORY INFERENCE

The dynamic interplay between intercellular signaling exchanges and gene regulatory network fluctuations drives a continuous spectrum of cell state transitions. Single-cell RNA sequencing has the remarkable capability to capture multiple cell states in a single snapshot, enabling computational modeling of differentiation trajectories. Trajectory Inference (TI) methods aim to order individual cells along a pseudo-temporal axis, representing the continuity of their gene expression profiles' transition. For simple processes like differentiation from one cell type to another or spatial distribution of related cells in a tissue, a single monotonic continuum can be adequately described. Such trajectories can be modeled with a trajectory structure consisting of a single lineage, and cell loadings along the first principal component, which explains most of the variation of the dataset, can be interpreted as pseudo-times. However, when the topology of the phenomenon to be modeled is more complex, such as bifurcating, tree-like, or cycling trajectories, more appropriate methods are required.

Monocle was among the first TI methods applied to scRNA-seq data. Derived as an extension of a previous algorithm, Monocle accommodates single-cell variation and allows for ordering multiple cell fates from a common progenitor cell type in pseudotime (Trapnell *et al.,* 2014; Magwene *et al.,* 2003). Monocle's pseudotemporal order maximizes the transcriptional similarity between successive pairs of cells. Thus, it reflects progress through differentiation rather than sample profiling time. This algorithm reduces high-dimensional expression profiles using independent component analysis (ICA), computes a minimum spanning tree (MST) on cells, and finds the longest path through the tree, representing the longest sequence of transcriptionally similar cells. Finally, it uses this sequence to produce a trajectory of an individual cell's progress through differentiation. By examining cells away from the main path, Monocle identifies alternative trajectories through the MST, it ordered and connects them to the main structure while annotating each cell with trajectory and

pseudotime values. With this approach Monocle aims at reconstructing branched biological processes without prior knowledge of specific genes distinguishing cell fates.

Another method, diffusion pseudotime (DPT), uses random-walk-based distance to order scRNA-seq data (Haghverdi *et al.,* 2016). Diffusion maps, a non-linear dimensionality reduction method, organize data by defining coordinates based on dominant eigenvectors of a transition matrix which describes random walks between cells at distinct stages of differentiation. This approach to dimensionality reduction strongly reduces noise and allows to represent branching trajectories. DPT computes a transition matrix by convolving Gaussians centered at nearby cells, effectively constructing a weighted nearest-neighbor graph. Random walks, of any length, through the graph determine the probability of each cell transitioning to any other cell, essentially a proxy for cell fate commitment. Finally, the DPT between pairs of cells is calculated as the Euclidean distance between their respective transition probability vectors and the pseudotemporal ordering can be reconstructed by computing DPT between the selected root and all other cells. Branching points in DPT are identified by measuring the correlation of pseudotime sequences along trajectories that start from the root and from a cell x with maximal DPT with respect to the root. While these sequences are anticorrelated on their connecting trajectory, they become correlated in a separate branch leading to a cell y. Branching points are thus identified by cells for which the two sequences switch from anticorrelated to correlated behavior. Postulating that differentiation speed is inversely proportional to cell density in the trajectory allows for metastable states to be recognized by pseudotimes with high densities. DPT's computational efficiency and applicability to large-scale single-cell data make it greatly advantageous.

RNA velocity, first implemented in Velocyto, describes the rate of gene expression change for an individual gene based on the proportion of its processed and nascent transcript mRNA molecules (La Manno *et al.,* 2018). Following the inference of nascent versus processed mRNA abundance proportion, which is stable in a transcriptional equilibrium, deviation between observations and steady-state identify velocities. This concept allows the reconstruction of directed temporal dynamics, with positive velocity indicating upregulation, when unspliced mRNA abundance exceeds steady-state expectations, and negative velocity indicating downregulation. Integration of velocities over several genes can subsequently be leveraged for the prediction of each cell's forthcoming state identity. Deriving the steady-state equilibrium proportion involves two key underlying concepts which are often violated, particularly when analyzing heterogeneous populations characterized by subunits with different kinetics. First, on the gene level, the complete splicing dynamics encompassing transcriptional activation, inhibition and equilibrium mRNA proportions are observed. Second, at the cell level, every gene exhibits identical splicing kinetics. scVelo was subsequently developed to address these limitations and refine RNA velocity analysis through a dynamical model based on likelihood maximization which allows for the complete solution of transcriptional activity of splicing processes (Bergen *et al.,* 2020). scVelo infers transcription, processing and catabolism kinetics of individual genes, as well as an inherently shared latent time with an effective expectation-maximization (EM) approach. The cell's internal clock, represented by the latent time and grounded only on transcriptional dynamics, precisely describes a cell's position within the biological process under examination and accommodates both the magnitude and direction of temporal

progression. This enabled generalization of RNA velocity to systems with transient cell states, commonly observed during development and response to perturbations.

In summary, organoids and single-cell technologies provide exciting new opportunities to model and understand human-specific and patient-specific biology, providing new inroads for therapy development.

SCOPE OF THE DISSERTATION

The aim of this doctoral thesis is to investigate human disease progression using organoid models, focusing on the highly dynamic processes characterized by cellular-level decision-making. The study primarily centers on two clinically relevant disease areas with unmet therapeutic needs: pancreatic cancer progression and acute intestinal inflammation. The findings from this research are expected to contribute valuable insights to the fields of cell biology, disease pathology, and personalized medicine.

To explore these conditions comprehensively, the research leverages cutting-edge technologies with spatial and temporal resolution, including single-cell transcriptomics and multiplexed imaging, and utilizes complex human organoid models. Over the past decade, single-cell technologies have emerged as a powerful tool, enabling high-resolution molecular phenotyping of multicellular systems. Moreover, organoids have proven to be a promising alternative to traditional model organisms, as they recapitulate the aspects of cytoarchitecture and cellular complexity of human tissues, offering opportunities to investigate human-specific traits and obtain more representative outcomes for therapeutic interventions. Specifically, this work involves the establishment and characterization of novel multi-lineage organoid models for each disease area.

For pancreatic cancer, a modular stroma-rich tumoroid culture system is developed to model pancreatic ductal adenocarcinoma (PDAC). This system enables the recreation of interactions between cancer, endothelial, and fibroblast cells, mimicking various aspects of primary tumors. The focus here is on studying the intercellular communication and dynamic gene regulatory networks that underlie the observed transitions in cell states during tumoroid formation and cancer progression.

The thesis also delves into the intricate relationship between the immune system and the intestinal epithelium. To address this, a 3D organoid model is developed, combining human intestinal epithelium with autologous intraepithelial lymphocytes (IELs). This model allows for the characterization of IEL populations and their interactions under homeostatic and activated conditions, particularly in the context of inflammatory responses. The research investigates the differential gene expression and state trajectories of IELs, as well as the impact of immunomodulatory drug responses on the intestinal epithelium.

My personal contribution to this body of work was to drive the analysis of the genomics data generated for each of the projects, providing deep characterization of our organoid models and uncovering biological insights into mechanisms amenable for therapeutic interventions.

RECONSTRUCTING CELL INTERACTIONS AND STATE TRAJECTORIES IN PANCREATIC CANCER STROMAL TUMOROIDS

Ryo Okuda[1,3,10*], Bruno Gjeta[3,4,10*], Ashley Maynard[6], Doris Popovic[5], Marina Signer[5], Qianhui Yu[3,10], Zhisong He[6], Malgorzata Santel[6], Makiko Seimiya[6], Soichiro Morinaga[7], Yohei Miyagi[8], Tomoyuki Yamaguchi[9], Yasuharu Ueno[2], Hideki Taniguichi[1,2,#], Barbara Treutlein[6,#], J. Gray Camp[3,4,10,#]

[1] Department of Regenerative Medicine, Yokohama City University Graduate School of Medicine, Kanagawa, Japan.

[2] Division of Regenerative Medicine, Center for Stem Cell Biology and Regenerative Medicine, the Institute of Medical Science, the University of Tokyo, Tokyo, Japan

[3] Institute of Molecular and Clinical Ophthalmology Basel, Switzerland

[4] University of Basel, Basel, Switzerland

[5] Roche Institute for Translational Bioengineering (ITB), Roche Pharma Research and Early Development, Roche Innovation Center Basel, Switzerland

[6] Department of Biosystems Science and Engineering, ETH Zürich, Basel, Switzerland

[7] Department of Hepato-Biliary and Pancreatic Surgery, Kanagawa Cancer Center, Kanagawa, Japan

[8] Molecular Pathology and Genetics Division, Kanagawa Cancer Center Research Institute, Kanagawa, Japan

[9] Laboratory of Regenerative Medicine, School of Life Sciences, Tokyo University of Pharmacy and Life Sciences, Tokyo, Japan

[10] Current affiliation: Roche Institute for Translational Bioengineering (ITB), Roche Pharma Research and Early Development, Roche Innovation Center Basel, Switzerland

[*] These authors contributed equally

[#] Corresponding authors

Contribution

This chapter represents work that has been published as a pre-print (https://www.biorxiv.org/content/10.1101/2022.02.14.480334v1) and is in revision at a journal after peer-review. I performed all single-cell genomic data analysis presented in this manuscript.

BACKGROUND

Pancreatic ductal adenocarcinoma (PDAC) stands as one of the most aggressive and challenging forms of cancer (Rahib *et al.,* 2014; Rawla *et al.,* 2019; Siegel *et al.,* 2018). It ranks as the 7th leading cause of cancer-related mortality worldwide, with a meager 8% five-year survival rate. The primary reason for the high mortality rate is the prevalence of

systemic metastasis upon clinical diagnosis (Makohon-Moore & Iacobuzio-Donahue, 2016; Ryan *et al.,* 2014), which is further exacerbated by the lack of early detection and effective treatment options (Castellanos *et al.,* 2011). The pathogenic progression of PDAC is governed by critical genetic factors, such as KRAS hyperactivating mutations observed in over 90% of clinical cases, and the frequent loss of function in tumor suppressor genes TP53, SMAD4, CDKN2A (Dunne & Hezel, 2015). These mutations converge on specific signaling pathways, including KRAS, TGF-β, WNT, Notch signaling, as well as DNA repair and chromatin dynamics (Bailey *et al.,* 2016; Waddell *et al.,* 2015), which are indispensable to the dysregulated cellular processes in primary tumor cells driving tumor progression (Neureiter *et al.,* 2014). PDAC wounds exhibit striking intra-tumoral heterogeneity (ITH), with a dense stroma component that can comprise over 70% of the tumor mass, often intertwined with normal pancreatic tissue (Biankin & Maitra, 2015). This ITH within the tumor microenvironment (TME) originates from distinct regional tissue states, influencing cancer phenotypes and impacting key clinical metrics of disease progression (Grunwald *et al.,* 2021; Kong *et al.,* 2011; Krebs *et al.,* 2017; Moncada *et al.,* 2020; Ohlund *et al.,* 2014). However, the complexity of ITH spatio-temporal dynamics cannot be solely explained by DNA somatic mutations (Jamal-Hanjani *et al.,* 2017), and few studies have explored the contribution of the tumor microenvironment to ITH. Among the central components of PDAC stroma are cancer-associated fibroblasts (CAFs), which play a pivotal role in orchestrating various features of the TME, including the secretion of cytokines regulating cancer growth and shaping evolutionary pressures that support malignancy (Sahai *et al.,* 2020). The microenvironmental pressures within the primary tumor induce cancer cells to acquire specific metabolic and cell state signatures, facilitating their adaptation to current conditions and paving the way for future colonization into other organ niches (Bertero *et al.,* 2019; Lehuede *et al.,* 2016; Li *et al.,* 2019; Morris *et al.,* 2016; Schild *et al.,* 2018). Understanding the diverse and dynamic pressures within the tumor has been challenging, especially when attempting to comprehend how CAF-cancer cell interactions generate a multitude of cell states. Despite the confirmation of metastasis-specific mutations (Campbell *et al.,* 2010; Makohon-Moore *et al.,* 2017), the mechanisms underlying metastasis in PDAC remain poorly understood, impeding their translation into clinical practice. Fortunately, advancements in cancer research offer promising avenues for progress. Cancer cystic organoids (CCOs) derived from patients provide exceptional opportunities to study cancer cell biology (Sato *et al.,* 2011; Tuveson & Clevers, 2019). *In vitro* co-culturing of cancer cells and CAFs has already started yielding valuable insights into their interactions (Ohlund *et al.,* 2017; Seino *et al.,* 2018). Additionally, single-cell sequencing has enabled the reconstruction of cell state continuums within complex developing tissues, offering predictions of cell interactions based on receptor and ligand expression patterns between cell types (Treutlein *et al.,* 2014; Camp *et al.,* 2017). These technological advancements hold promise for identifying novel diagnostic markers and therapeutic targets, thereby bringing us closer to better approaches in combating PDAC.

OBJECTIVES

In this project, we set out to establish a stroma-rich tumoroid co-culture system to understand PDAC cancer-CAF interactions in controlled environments, and to explore developmental processes within tumoroids using single-cell transcriptome sequencing, with spatial and temporal resolution, as well as image-based phenotyping. By doing so, we learn

about principles associated with intratumoral heterogeneity that might be leveraged for therapy development in PDAC and other cancers.

RESULTS

Cancer research has traditionally relied on 2D cancer cell lines or cancer cyst organoids derived from biopsies to study diseases. We generated cancer cyst organoids (CCOs) from PDAC patient primary biopsies, which we stably cultured according to previously published protocols (Boj *et al.,* 2015). However, scRNA-seq revealed limited heterogeneity in CCO cultures (Fig. 7A-H), despite them maintaining a tumor-like character compared to healthy pancreatic tissue (Fig. 7I-L). In an effort to overcome this limitation, we devised a groundbreaking *in vitro* model that incorporates patient-derived cancer and cancer-associated fibroblast (CAF) cells, along with endothelial cells (ECs), in a 3D tumoroid culture system (Fig. 8A). This novel, complex, and modular model offers improved control and reliability, enabling a deeper investigation of tumor processes. However, we note that the CAFs and ECs were not derived from the same patient, and the same CAF and EC lines were used throughout our study. Over 24 hours, the cells form a spherical culture (Fig. 8B) and, through extended cultivation of stroma-rich tumoroids, we observed the emergence of CAF produced ECM, EC organization into vessel networks and glandular cancer cell structures (Fig. 8C-E). To comprehensively understand the differences from previous approaches, we performed single-cell transcriptomics analysis and compared the new model to its individual components cultured separately (Fig. 8F).

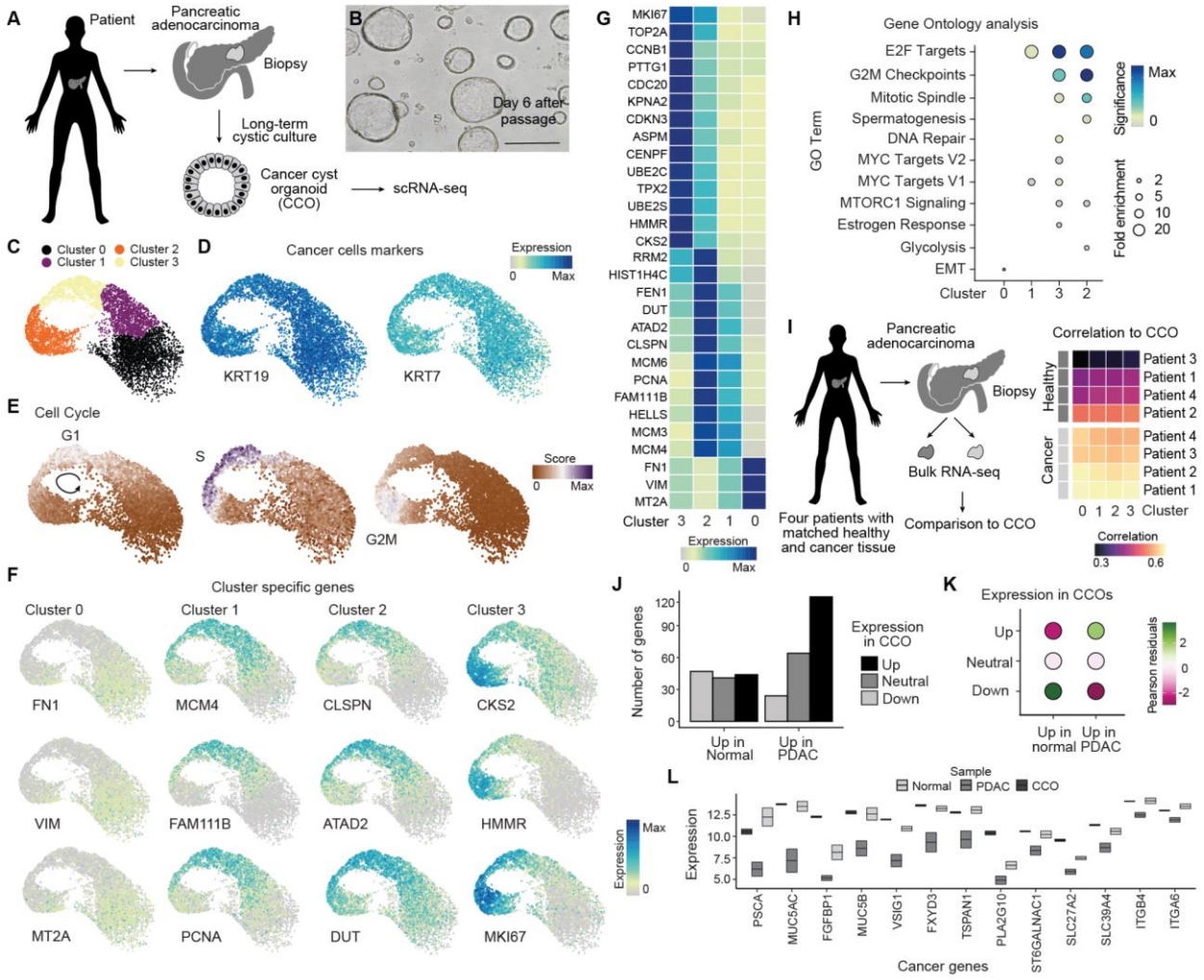

Figure 7: Single-cell transcriptome analysis of pancreatic cancer cyst organoid cultures and comparison to primary cancer tissue. *A) Cancer cyst organoid (CCO) lines were established from PDAC patient biopsies. CCOs were propagated over multiple passages, and after day 7 of culture post-passage, CCOs were subjected to scRNA-seq. Scale bar:400um. B) Brightfield image of CCOs in a 3D Matrigel culture 6 days after passage. C) UMAP cell embedding of CCO scRNA-seq data colored by cluster. D-F) Feature plots of PDAC cancer cell markers Keratin (KRT19 and KRT17), correlation to cell cycle states (e) and cluster markers (f). G) Heatmap showing normalized cluster marker expression. H) Gene ontology analysis of genes enriched in each CCO cluster. Circles are colored based on significance (High p-value in blue, low in yellow/gray) and sized by fold enrichment. I) CCO pseudo-bulk samples, obtained through aggregation of single cells according to their respective cluster memberships, were compared to bulk transcriptome data from healthy and cancer tissue from TCGA cohort. Heatmap shows correlation (high, bright yellow; low, dark colors) of each cluster to the different patient specimens. J) Barplots show the number of genes that are differentially expressed between normal and PDAC tissue and are up-regulated (up), down-regulated (down), or not differentially expressed (neutral) in CCOs compared to primary pancreas cells. K) Dotplot shows similarity between CCO and pancreatic cancer signatures when compared to healthy pancreatic tissue (χ^2 test p-value = 1.6e-07). L) Boxplots show the expression distribution of pancreatic cancer markers as comparison between TCGA healthy and cancer samples and our CCO culture.*

This analysis revealed 12 cell populations and interestingly, distinct clustering of tumoroid-derived cell types compared to their single-culture counterparts, indicating significant transcriptional differences between the two modalities (Fig. 8G). Differential expression analysis between the 2D monoculture and 3D tumoroid counterparts at day 7 and day 14 revealed diverse changes that emerged in the tumoroid over time (Fig. 8H, 9A-B). Within tumoroids, a general hypoxia response characterized all cell types at day 7 and it was followed by angiogenic induction, extracellular component modulation, and metabolic adaptation signatures for the different cell types by day 14 (Fig. 9C-D). Strikingly, we found that tumoroid CAFs induced a consortium of extracellular matrix proteins (Collagens COL3A1, COL6A2, COL1A2, COL1A1; Fibronectin 1, FN1; Decorin, DCN) compared to the

2D CAFs, and tumoroid CAF-specific genes enriched in cancer hallmark processes for transforming growth factor beta (TGF-β) signaling, inflammatory response, and hypoxia. These data show that the multilineage tumoroid microenvironment induces strong morphological and molecular cell state changes across different cell types.

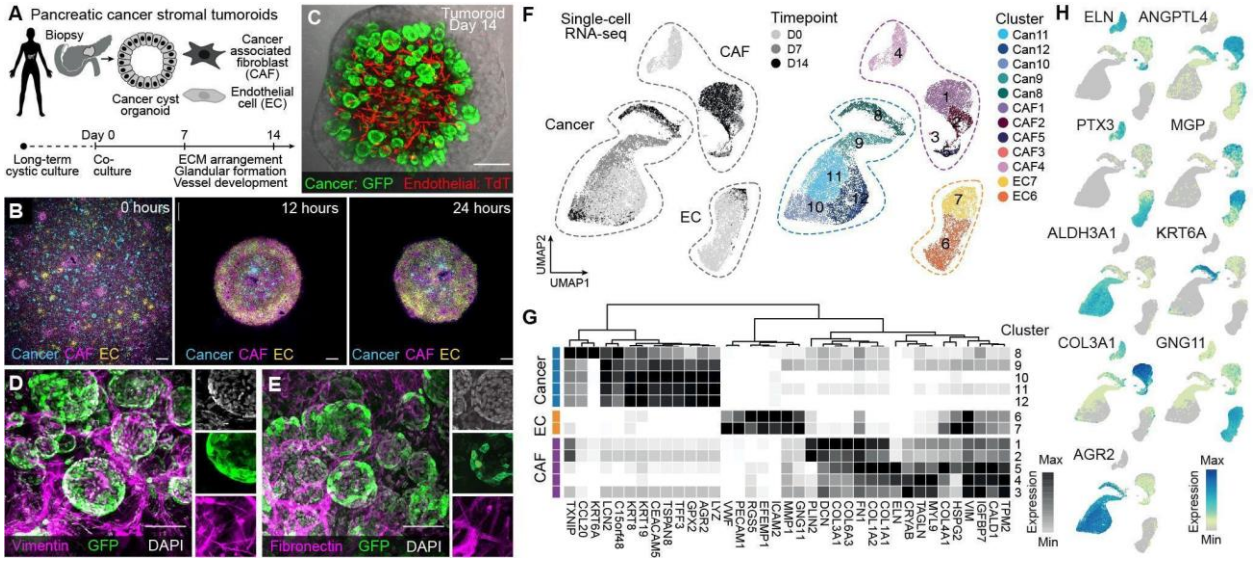

Figure 8: Generation and single-cell transcriptome characterization of pancreatic cancer stromal tumoroids. *A) Long-term cancer cyst organoid (CCO) cultures established from patients with pancreatic adenocarcinoma (PDAC) can be co-cultured in a 3D matrix with endothelial cells (EC) and cancer associated fibroblasts (CAF), which self-organized a complex tumoroid microenvironment. Over 14 days, fibrous connective tissue forms, vessels sprout and organize, and cancer cells form 3D glandular structures within multilineage tumoroids. B) Cancer cells (teal blue), cancer associated fibroblasts (CAFs, pink), and endothelial cells (ECs, yellow) expressing a reporter 0, 12, and 24 hours after co-culture. Scale bar: 10um. C) Day 14 tumoroid with cancer cells and ECs stably transformed with EGFP and TdT expression cassettes, respectively. Scale bar: 250um. D,E) Whole-mount immunohistochemistry on cleared tumoroids probing Vimentin (pink, D) and Fibronectin (pink, E). Cancer cells expressing EGFP; nuclei are marked with DAPI (white). Scale bar: 100ul. F) scRNA-seq was performed on the input cells in monoculture (Day 0) and on tumoroids after 7 and 14 days in co-culture. UMAP cell embedding of scRNA-seq data is colored by time point (left) and by cluster (right). G) Heatmap showing normalized expression of cluster marker genes. H) Feature plots showing expression of representative cell type marker genes from single-cell transcriptome data generated from tumoroids and input cells.*

To explore the cell state dynamics within the tumoroid, we first established a pseudotemporal trajectory for each cell type and identified genes that vary over the trajectory (Fig. 10, 9E-F). We observed that there were cells from both time points that covered the entire range of the trajectory, and for CAF we observed similar proportions of day 7 and day 14 CAFs along the CAF trajectory. We observed that the CAF pseudotemporal ordering reflected activation status, such that induction of collagens and cytokines could be observed along pseudotime (Fig. 10B). CAF temporal trajectory strongly resembles a transition from "normal" to "activated" stroma signatures in response to tumorigenic cells' presence in their proximity (Moffitt *et al.,* 2015) (Fig. 10C-D). This activated stroma signature has previously been shown to be prognostic, associated with worse clinical outcomes, and is characterized by the expression of genes that point to the role of CAF activation in tumor promotion (Moffitt *et al.,* 2015). The CAF activation signature includes Secreted protein acidic and cysteine rich (SPARC), Wnt pathway family members (WNT5A and WNT5B), Matrix metalloproteinases (*MMP2, MMP11 and MMP14*), and Fibroblast Activation Protein (FAP) (Moffitt *et al.,* 2015) (Fig. 10E).

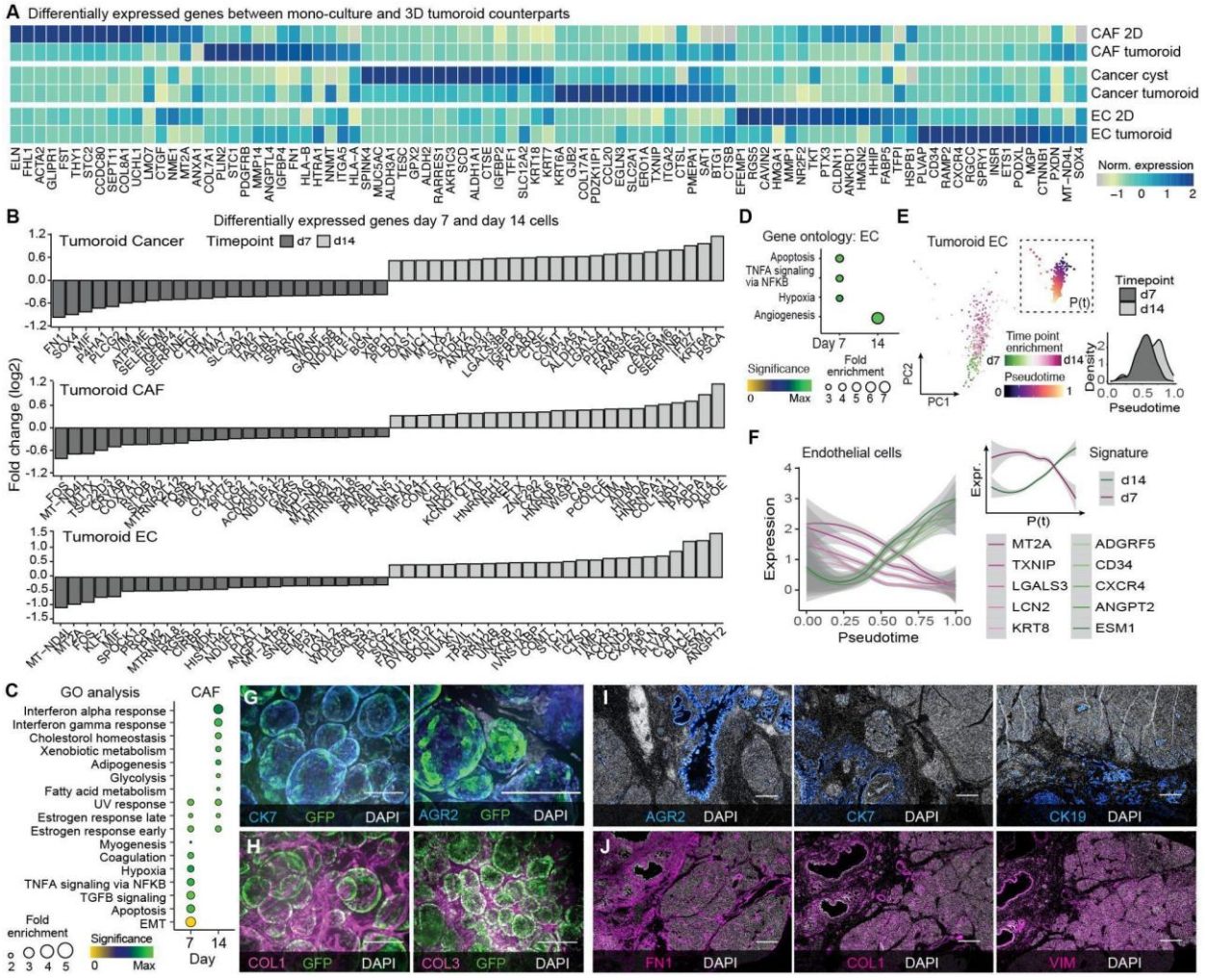

Figure 9: Comparison between 2D monoculture and 3D tumoroid cells and tumoroid time points. *A) Heatmap showing genes that are differentially expressed between tumoroid cell types and their input counterparts. B) Barplots show log-transformed fold change (log 2) for top DEGs between day 7 (dark grey) and day 14 (light grey) tumoroid cancer (top), CAF (middle), and EC (bottom) cells. C-D) Hallmark analysis of genes enriched in day 7 and day 14 tumoroid CAF (C) and endothelial cells (D). E) PCA embedding colored by expression of time specific signatures in tumoroid endothelial cells and insert colored by pseudotime. The right insert represents the density plot of tumoroid endothelial cells along the inferred pseudotime. F) Pseudotemporal expression profile of top DEGs between tumoroid endothelial cells at day 7 and day 14. Inset shows cumulative expression profiles of the DEGs. G) Immunofluorescence staining of cancer cell markers Cytokeratin 7 (CK7, blue, left) and Anterior Gradient 2 (AGR2, blue, right) in day 14 tumoroids. Cancer cells express GFP (green), Nuclei marked with DAPI (white). H) Immunofluorescence staining of extracellular matrix proteins Type I collagen (COL1, pink, left) and Collagen 3 (COL3, blue, right) in day 14 tumoroids. Cancer cells express GFP (green), Nuclei marked with DAPI (white). Scale bar:100um. I-J) Immunofluorescence staining of cancer markers AGR2, CK7, CK19 (blue, I), and extracellular matrix proteins Fibronectin (FN1), COL1, Vimentin (VIM) (pink, J) in the primary pancreatic cancer tissue. Scale bar:200um.*

Aligning tumoroid CAF cells along an activation trajectory allowed us to describe the process through dynamic gene regulatory interactions. Regulome analysis using SCENIC (Aibar *et al.*, 2017) suggested Early Growth Response 1 (EGR1) as a central transcriptional regulator that likely coordinates CAF activation (Fig. 11A-D), that is upstream of several growth factor signaling pathways (BMP2, NOTCH3, LIF, VEGFC) and ECM regulators (COL5A3, COL12A1, LAMA4, HAS2) (Fig. 10E). Whole-mount immunohistochemistry on cleared tumoroids stained for Collagen and Fibronectin revealed substantial ECM deposition surrounding cancer cells (Fig. 8D, 9G-H), and we validated these protein expression profiles in primary PDAC tissue from diagnostic biopsies (Fig. 9I-J). Along the EC trajectory, increased expression of Matrix Gla Protein (MGP), Angiopoietin-2 (ANGPT2), Endothelial cell-specific molecule 1 (ESM1) correlated with angiogenesis and TNF-α signaling that

increase over pseudotime and have highest expression in day 14 tumoroids (Fig. 9D-F). In contrast to CAF, for cancer cells there was a strong relationship between time point and position on the trajectory (Fig. 10F-G).

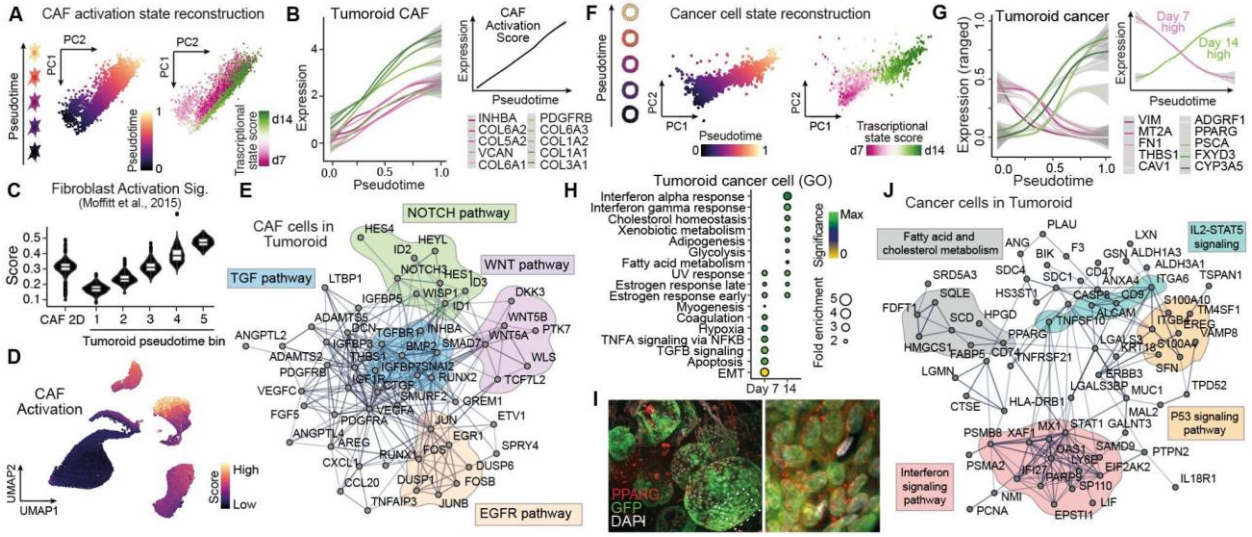

Figure 10: Cell state trajectory reconstruction reveals CAF activation and cancer cell persistence pathways induced during tumoroid development. *A) Principal component analysis (PCA) embedding representing tumoroid cancer-associated fibroblast (CAF) cells colored by pseudotime (left) and time point-specific signature (right). B) Expression of extracellular matrix protein encoding and other genes in CAFs ordered based on pseudotime reconstruction. Inset shows a CAF activation score previously established from primary PDAC cancer RNA-seq data (Moffitt et al., 2015). C) Distributions of CAF activation score in monoculture CAFs and tumoroid CAFs in 5 pseudotemporal bins. D) Tumoroid UMAP colored by CAF activation score. E) Protein-protein interactome from the STRING database with pathway annotation for CAF pseudotemporally up-regulated genes. F) PCA embedding representing tumoroid cancer cells colored by pseudotime (left) and time point-specific signature (right). G) Pseudotemporal expression profile of DEGs between tumoroid cancer cells at day 7 and 14. Inset shows cumulative expression profiles of the DEGs. H) Hallmark pathway enrichment on genes upregulated in day 7 or 14 cancer cells. I) Whole-mount immunohistochemistry on cleared tumoroids probing Peroxisome Proliferator Activated Receptor Gamma (PPARG). Cancer cells stably expressing EGFP (green); nuclei are marked with DAPI (white). Scale bar: 100ul. J) Protein-protein interactome from STRING database with pathway annotation for cancer cell pseudotemporally up-regulated genes.*

The cancer cell trajectory revealed initial induction of hypoxia-, apoptosis-, and epithelial-to-mesenchymal transition-related genes followed by adaption expression signatures associated with xenobiotic metabolism, cholesterol homeostasis, and interferon responses (Fig. 10G-H). Many of the genes that increase over pseudotime and peak at day 14 in tumoroid cancer cells, such as Peroxisome proliferator-activated receptor gamma (PPARG), Syndecan 1 (SDC1), Mucin 1 (MUC1), Kruppel-like factor 3 (KFL3), have been previously associated with poor disease outcome (Hinoda *et al.,* 2003; Yao *et al.,* 2019; Zhang *et al.,* 2015). We explored gene regulatory interactions to understand the underlying cell state progression in tumoroid cancer cells. Regulome analysis revealed transcription factors and their predicted targets that are differential along the cancer pseudotime and highlighted a predominant role of PPARG and KLF2/3 in coordinating the cancer cell responses within the tumoroid (Fig. 11E-G). Interestingly, the PPARG regulome linked fatty acid and cholesterol metabolism with the IL2-STAT5, P53, and the Interferon signaling pathways (Fig. 10I-J). Additionally, PPARG and its predicted target genes strongly associated with an immune cell devoid tumor tissue, as well as lower survival in the PDAC tumor cohort from the cancer genome atlas (TCGA) (Fig. 11H-K) (The Cancer Genome Atlas Research Network. Electronic address: andrew_aguirre@dfci.harvard.edu and Cancer The Genome Atlas Research Network, 2017). This potentially implicates PPARG not only in important metabolic pathways that regulate nutrient and energy resource management, but

also in limiting immune cell infiltration into the tumor tissue which maybe be beneficial to cancer cell survival yet very detrimental to patients' health conditions.

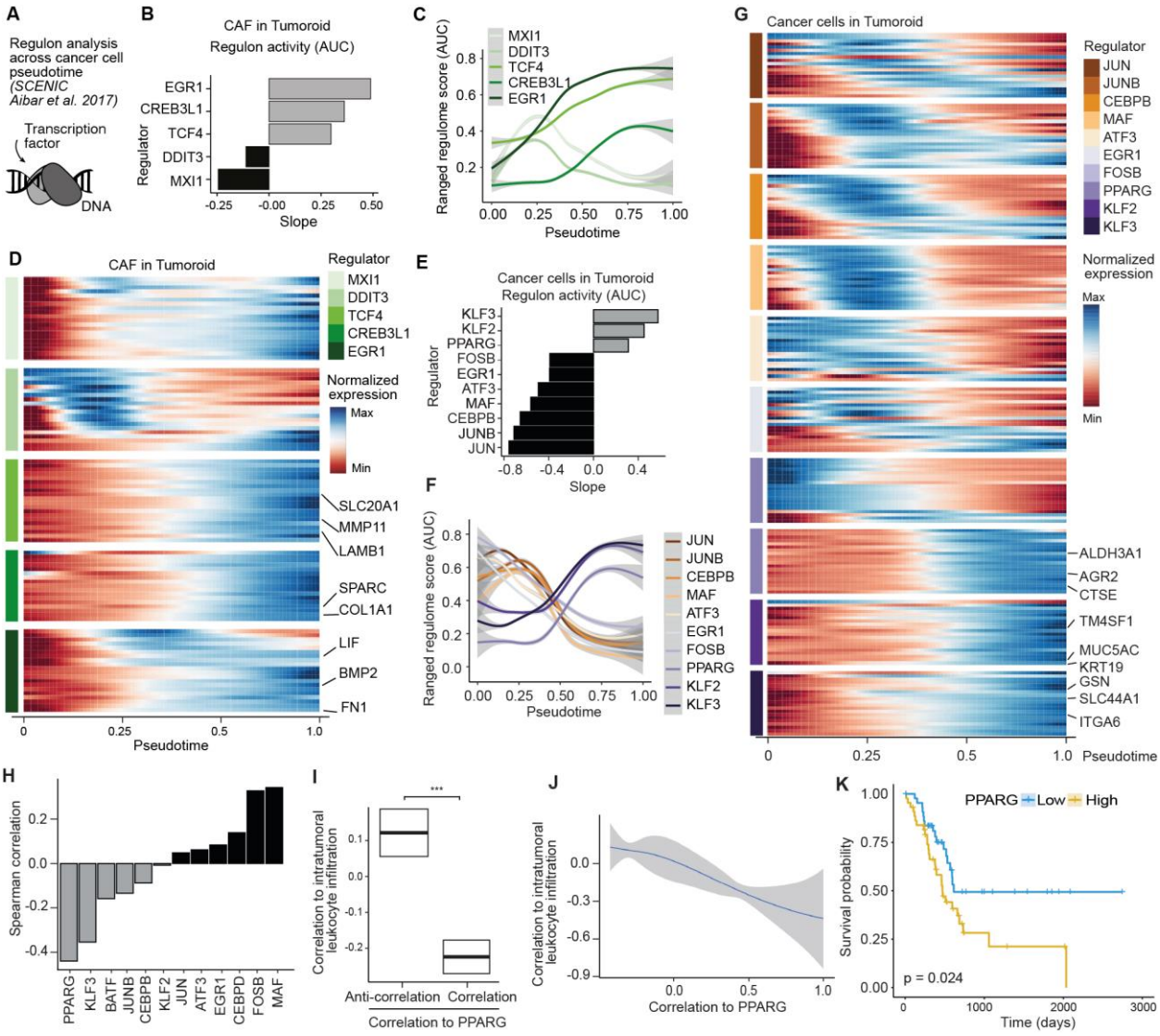

Figure 11: Regulon analysis of Tumoroid CAF and cancer cells. *A) SCENIC was used to infer regulatory network scores for tumoroid CAF and cancer cells. B) The expression slope over tumoroid CAF pseudotime is plotted for the top regulons based on area under the curve (AUC) metrics from SCENIC. C) Line plots show the ranged regulon score for each of the top regulators over tumoroid CAF pseudotime. D) Heatmap shows expression of predicted targets of each major regulator over tumoroid CAF pseudotime. E) The expression slope over tumoroid cancer pseudotime is plotted for the top regulons based on area under the curve (AUC) metrics from SCENIC. F) Line plots show normalized pseudotemporal expression of central cancer regulators. G) Heatmap shows expression of predicted targets of each major regulator over tumoroid cancer cell pseudotime. H) Spearman correlation score between expression of dynamic tumoroid cancer cell transcription factors (TFs) and percentage of tumor infiltrating immune cells in TCGA pancreatic cancer sample cohort. TFs show a wide range of values and note that PPARG registers the highest negative correlation score. I) Differential association of positively versus negatively PPARG correlated genes with percentage of intratumoral immune cell infiltration is statistically significant. One-sided t-test, *** indicates a p-value = 0.3e-12. J) Line plot showing gene correlation to PPARG expression versus percentage of infiltrating intratumoral immune cells. K) Kaplan-Meier curve showing significant association of high PPARG expression with poor prognosis in TCGA PDAC cohort.*

Altogether, these data showed that CAFs activated by day 7 within the tumoroid and suggested that CAF activation may induce endothelial and cancer cell hypoxic as well as metabolic transition responses which are relevant for primary pancreatic cancer progression. Our innovative CAF-tumoroid model shows great capacity to mimic *in vivo* PDAC features, facilitating a more nuanced understanding of tumor processes. The integration of patient-derived cancer and CAF cells, along with endothelial cells, in this

modular system offers a sophisticated platform for future cancer research, paving the way for improved therapeutic strategies and precision medicine approaches in the fight against pancreatic cancer.

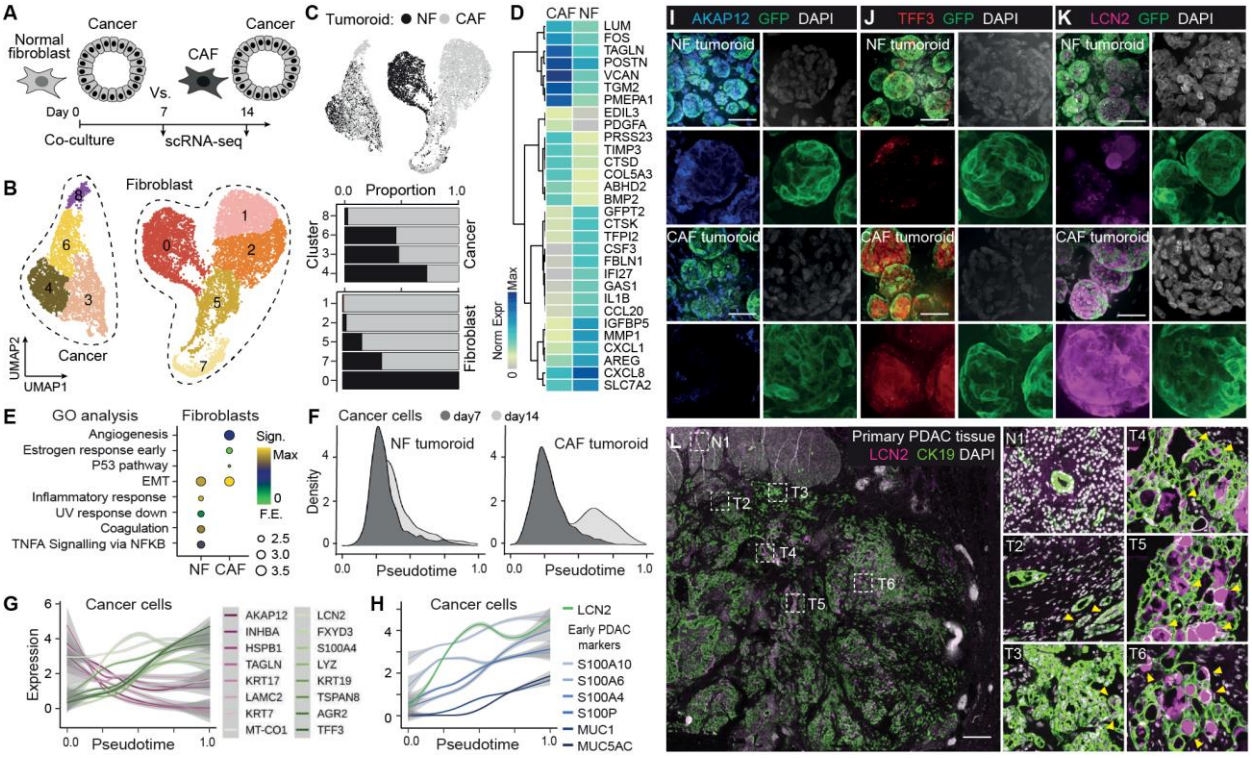

Figure 12: CAFs provide distinct signals from normal fibroblasts that associate with cancer cell state change in tumoroids. *A) Tumoroids containing normal, or cancer associated fibroblasts were generated and analyzed by scRNA-seq. B) UMAP embedding is colored and numbered by cluster, with cancer and fibroblast cells encircled and noted. C) UMAP with cells colored by tumoroid type (top). Stacked barplot shows proportion of cancer or fibroblast cells per cluster and colored by tumoroid type. Clusters are significantly enriched for tumoroid type (χ^2 p-value < 2.2e-16). D) Heatmap shows expression of DE genes by NF and CAF in the tumoroids. E) Hallmark enrichment for NF and CAF DE genes. F) Density plots showing proportion of cancer cells along an inferred pseudotime in the NF and CAF tumoroids. Day 14 cancer cells have altered profiles only in CAF tumoroids. G,H) Expression profiles of genes over cancer cell pseudotime that are DE between day 7 and day 14. Day 14 DE genes are also DE between cancer cells in NF and CAF tumoroids. I-K) Immunofluorescence of AKAP12 (I), TFF3 (J), and LCN2 (K) protein expression in NF and CAF tumoroids. Cancer cells stably express GFP, DAPI marks nuclei (white). Scale bar: 100um. L) Immunofluorescence of LCN2 and CK19 in Primary PDAC tissue. Insets show 1 location within non-cancerous pancreas tissue (N1) as well as 5 locations within the tumor (T2-6). Nuclei stained with DAPI (white). Scale bar: 1mm.*

To understand the specificity and impact of CAFs in shaping cancer cell state transitions, we developed a model in which cancer-associated fibroblasts were replaced by naïve fibroblasts (NFs derived from healthy pancreas tissue) in the tumoroid system (Fig. 12A). We analyzed and compared CAF- and NF-integrated tumoroid models using imaging and single-cell transcriptomics at day 7 and day 14. Our data showed significant clustering differences (Fig. 12B), with distinct transcriptional profiles translating into substantial structural disparities under the microscope (Fig. 13A-B). Specifically, we observed CAF tumoroids had larger glandular structures and more developed endothelial networks compared to NF tumoroids suggesting a difference in signaling cues between the two microenvironments (Fig. 13A-B). Single-cell transcriptome analysis enabled the identification of 9 distinct cell states, highlighted how NF (c0) and CAF (c1, c2) cells largely cluster apart and evidenced a cancer cell population (c8) which uniquely emerged within the CAF-integrated tumoroid model (χ^2 test p-value < 2.2e-16) (Fig. 12B-C).

Differentially expressed genes between NFs and CAFs show enrichments in both cases for epithelial-to-mesenchymal transition however, CAF-specific genes showed increased engagement in processes associated with angiogenesis, estrogen response, and the TP53 pathway (Fig. 12D-E, 13C-E). Inference of differentiation trajectories for cancer cells exposed to the two fibroblast types revealed a time-dependent segregation of cells along the pseudotemporal axis, such that day 14 cancer cells grown with CAFs were predominantly enriched at later stages of the trajectory compared to tumor cells grown with NFs (Fig. 12F). This result indicated the pivotal role of CAFs in supporting fast cancer cell state progression. We observed that genes specific to day 14 cancer cells co-cultured with CAF were involved in metabolic homeostasis and included many classical PDAC-associated genes such as TFF3, TSPAN8, AGR2, and S100 (Fig. 12G, 13F-H). Interestingly, we identify Lipocalin 2 (LCN2) as an early induced gene which could potentially serve as an early prognostic biomarker of subsequent cancer metabolic state response to activated CAF signaling (Fig. 12H). We validated low expression of AKAP12 and CAF-specific induction of PDAC signature genes TFF3 and LCN2 using immunohistochemistry in tumoroids (Fig. 12I-K). Additionally, we show that LCN2 exhibits heterogeneous expression within primary PDAC tissue (Fig. 12L).

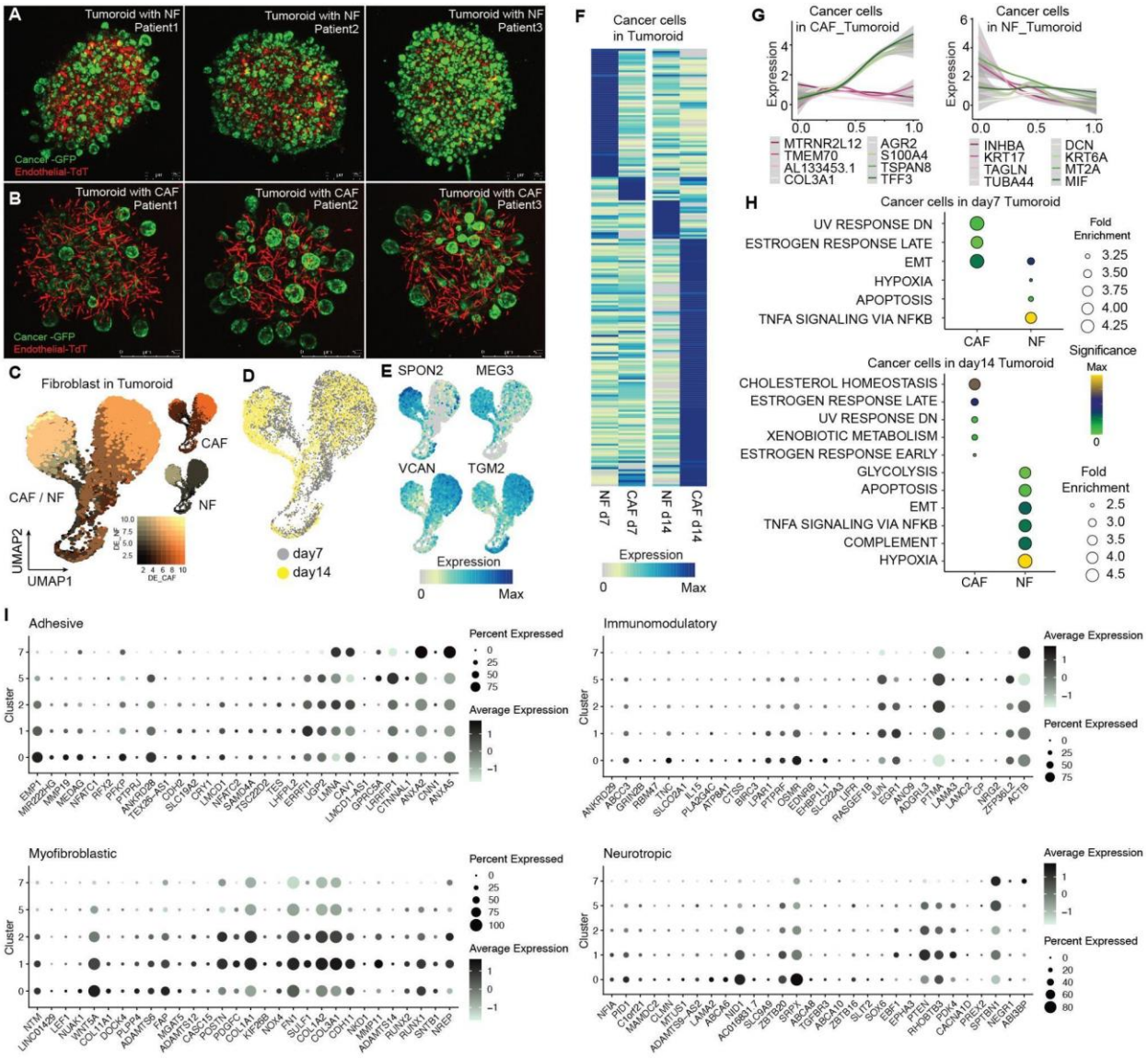

Figure 13: Comparison of NF and CAF tumoroids. *A,B) Images show tumoroids generated with normal fibroblasts (NFs, A - upper row) or cancer associated fibroblasts (CAFs, B - lower row) with endothelial cells labeled with TdTomato and cancer cells labeled with EGFP. Scale bar:250um. C-E) UMAP cell embedding from Fig. 2 showing normal and cancer associated fibroblasts colored by respective transcriptional signatures (C), tumoroid culture timepoint (D), or expression feature (E). F) Heatmap shows expression profiles of DEGs, at each timepoint, between cancer cells in tumoroids with NFs or CAFs. G) Pseudotemporal expression pattern of representative genes in cancer cells from NF and CAF tumoroids. H) Hallmark enrichment analysis in cancer cells within the different tumoroid types at 7 (top) and 14 (bottom) days of co-culture. Data shows how cancer cells within the CAF tumoroid change state and acquire new metabolic footprints, while cancer cells in contact with normal fibroblasts remain largely stable over the entire co-culture period. I) Dotplot showing the average expression (grey color scale) and percent of cells expressing (size of dot) of marker genes of previously described fibroblast states (Hwang et al. 2022) across the different tumoroid fibroblast clusters.*

To validate the tumoroid model's accuracy, we analyzed a cohort of 24 recently published primary PDAC scRNA-seq samples (Peng *et al.,* 2019). In our re-analysis of this dataset, we observed that the diverse cell types contributing to the tumor microenvironment could be grouped into at least 20 molecularly distinct populations at a coarse resolution (Fig. 14A, 15A-B). Tumoroid cancer and CAF cell populations showed strong relative similarity to the counterparts in the primary biopsies (Fig. 15C). Sub-clustering of the primary cancer cell populations revealed 8 distinct cancer cell clusters (Fig. 14B-C, 15D-E) that were ubiquitously yet heterogeneously represented in each patient sample (Fig. 15F). Interestingly, we found that tumoroid cancer cell states had strong transcriptional similarity

with multiple distinct cancer populations observed in the primary tissue demonstrating that our model can capture substantial intra-tumoral heterogeneity (Fig. 14D).

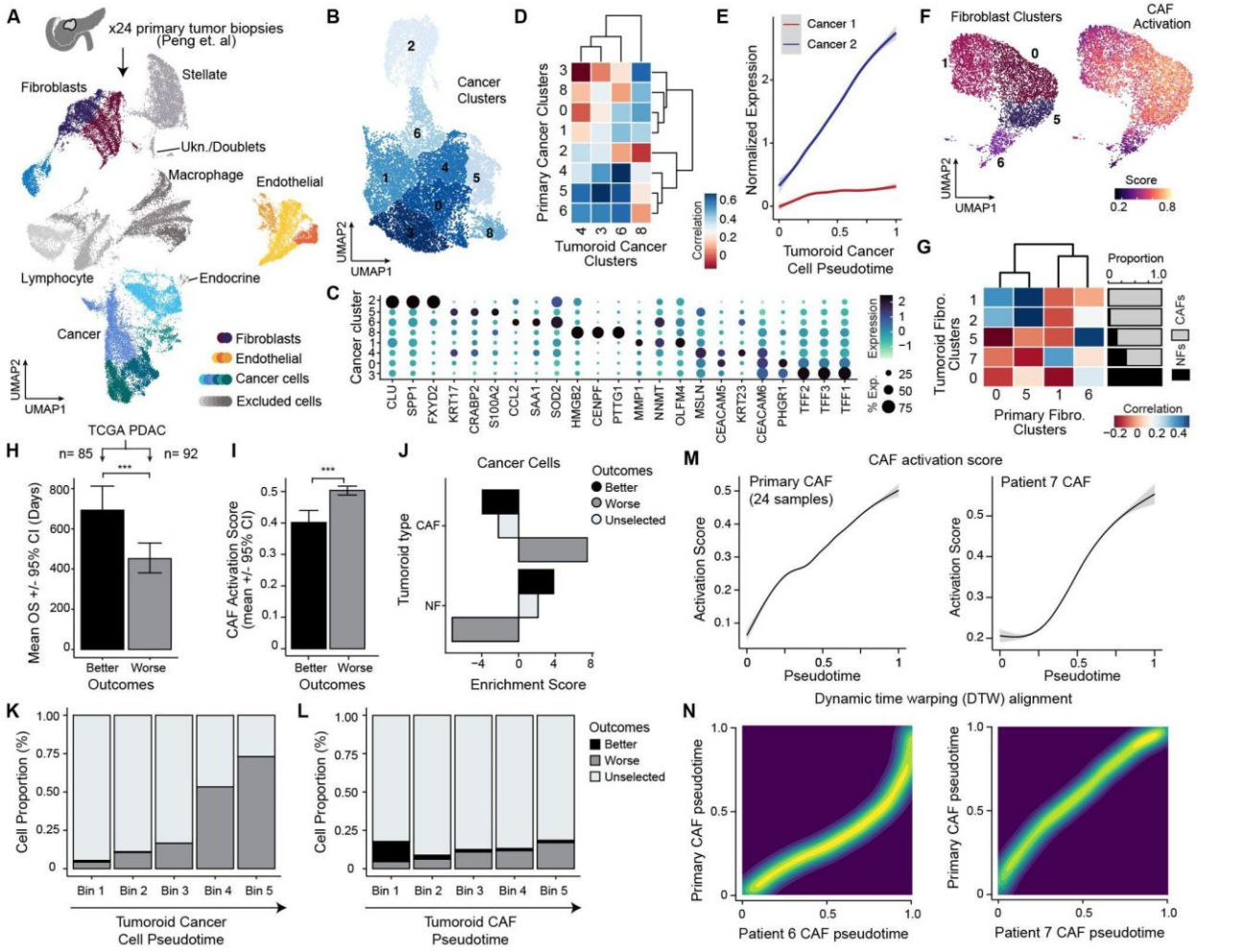

Figure 14: Tumoroids recapitulate cancer cell and CAF states observed in primary PDAC tissues. *A) Integrated UMAP embedding of a published single cell RNA-seq dataset from 24 primary PDAC resected samples (Peng et al., 2019), colored by cluster. B) UMAP embedding showing reclustering of cancer cells from primary resections colored by cluster. C) Dotplot shows expression profiles of top markers for identified cancer cell clusters. D) Spearman correlation scores between tumoroid cancer clusters and primary cancer clusters. Similar cancer states can be observed between tumoroids and primary tissues. E) Expression score of signatures for cancer cell states identified by Peng et al. on CAF co-cultured tumoroid cancer cells ordered by pseudotime. Note that, while the abnormal Cancer 1 phenotype seems to be undetectable in tumoroids, the alignment points towards an ever-increasing expression of the malignant Cancer 2 phenotypic profile. F) UMAP embedding of primary fibroblasts colored by cluster (left) and by expression of CAF activation score (right). G) Spearman correlation between tumoroid fibroblast clusters and primary PDAC fibroblast clusters; stacked barplot annotates tumoroid fibroblast clusters by proportion of normal fibroblasts (NF) and cancer-associated fibroblasts (CAF). CAF dominated tumoroid clusters achieve the highest similarity to the primary counterpart. H) Barplot showing the average overall survival time (OS) by vital status in TCGA PDAC cohort (one-sided t-test, *** indicates a p-value = 4.54e-04). I) Scissor selected tumoroid fibroblast cells significantly differ in their expression of activation signature; "Worse", denotes strong positive association to poor prognosis. "Better", denotes stronger association to a more favorable outcome (longer overall survival). One-sided t-test, *** indicates a p-value = 8.9e-07. J) Distribution of Scissor selected tumoroid cancer cells. CAF co-cultured cancer cells highly enriched for worse outcome association while NF co-cultured cancer cells enriched for better outcome association.* $\mathcal{X}^2$ *test, p-value < 2.2e-16. K-L) Stacked barplot showing proportions of Scissor classification in 5 pseudotime bins of CAF-tumoroid cancer (K) and CAF (L) cells. M) CAF activation score in primary CAFs (left) and an independent CAF line (right, patient 7, see supplemental figures) ordered by pseudotime. N) Density plot of pseudotime alignment comparison between primary CAFs (y-axis) and tumoroid CAFs (x-axis) from two patients (patient 6, left; patient 7, right) demonstrates independently computed tumoroid CAF trajectories can be aligned to a reconstructed primary CAF trajectory.*

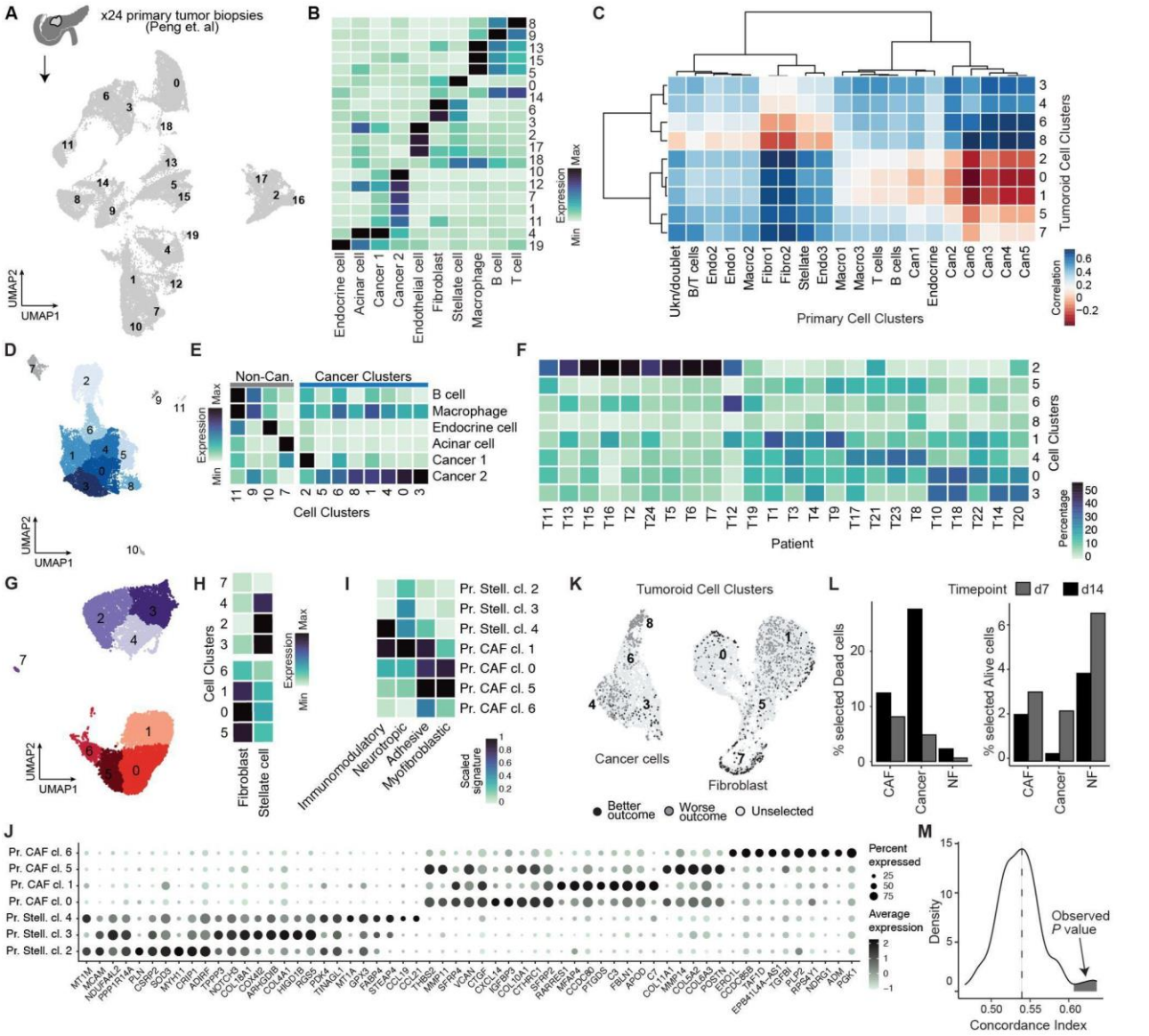

Figure 15: Comparison to primary PDAC and scissor analysis. *A,B) UMAP embedding of primary PDAC samples (A) and expression of specific cell type signatures (B) used for cluster annotation. C) Spearman correlation scores between primary PDAC clusters and tumoroid clusters. D,E) UMAP embedding of subsetted primary cancer cells (D) identifies impurities and refines cancer cell heterogeneity as shown by expression scores for cell type specific signatures (E). Note that true cancer cell clusters can be aligned on a Cancer 1 to Cancer 2 progression axis as reported by Peng et al. F) Heatmap representing proportions of cancer cell states in each primary sample: multiple states can coexist within the same patient. G,H) UMAP embedding of subsetted primary fibroblast and stellate cells (G) identifies impurities and refines fibroblast cell heterogeneity as shown by expression scores for cell type specific signatures (H). I,J) Average expression of fibroblast signatures .(Hwang et al. 2022) (I) and expression profiles of top markers for primary CAF and stellate cells. K) UMAP embedding of tumoroid cells colored by scissor selection group: "worse", denotes cells associated with worse outcome; "better", marks cells associated with protective phenotype. L) Barplot showing proportions of scissor selected tumoroid cells by cell type and timepoint. Right, day 14 system correlates with worse outcome with a significant enrichment in cancer cells; left, protective phenotype correlates with day 7 system with NF cells being the most representative. M) Scissor reliability significance test: analysis was performed 100 times on randomly permuted bulk labels with 3-fold CV. P-value is computed by the fraction of scores exceeding the score obtained with original labels, p-value = 0.04.*

Moreover, our comparative analysis revealed a close alignment of cancer cell states between tumoroid and primary tissues, strikingly recapitulating the progressive cancer 1 to cancer 2 transcriptional transition described *in vivo* by the original analysis (Peng *et al.*, 2019) (Fig. 14E). This result reinforces the relevance of our tumoroid model as an invaluable tool in PDAC research. Similarly, we observed that fibroblast cells from the primary samples showed an activation pattern that reflects the one emergent in our tumoroid model and,

tumoroid CAF states correlated with primary CAF states while NF states do not (Fig. 14F-G, 15G-J). Notably, activation status proved to be the major source of variability in primary CAF cells and aligning these along increasing activation score showed strong similarity to CAF state transitions observed in tumoroid samples from multiple fibroblast lines (Fig. 14M-N). Altogether, these data confirm that interactions between cancer and CAF in the tumoroid induce cancer cell phenotypes that are observed in primary tissues.

To assess the relevance of states observed in the tumoroid tissue to PDAC outcomes, we utilized the annotated data from TCGA. The TCGA PDAC cohort contains 177 bulk transcriptomes that could be stratified by outcome, revealing a significant difference in post-diagnosis survival time (Fig. 14H). Comparison of tumoroid cells to the bulk dataset using Cox hazard regression and the SCISSOR algorithm (Sun *et al.,* 2022) enabled critical observations regarding fibroblast activation scores and cancer cell state correlation to survival time. Notably, tumoroid fibroblasts negatively correlating with survival exhibited higher activation scores compared to those correlating with more favorable outcomes (Fig. 14I, 15K-L). Additionally, the CAF-tumoroid model showed significant enrichment in cancer cells negatively correlating with survival, surpassing the NF-tumoroid model (Fig. 14J). Remarkably, both cancer cell and fibroblast trajectories aligned with an increase in cells predictive of poor outcomes (Fig. 14K-L). These findings emphasize the reliability of the CAF-tumoroid model for PDAC research and suggest that the inferred trajectories faithfully recapitulate disease progression dynamics (Fig. 15M).

Acknowledging that our study primarily utilized a single CAF cell line, a notable concern could raise criticism on the reproducibility of results, we procured additional fresh samples and showcased tumoroid cultures in one such instance. We generated CAF and cancer cell lines from the same patient and grew them as 3D organoids either separately or as an autologous CAF/cancer stromal tumoroid (Fig. 16A). We collected transcriptional profiles from each modality at different timepoints and were able to identify 10 major populations representing mono-cultured CAF (c5, c6), tumoroid CAF (c1, c4), CCO condition (c3, c8, c9), tumoroid cancer (c2, c7) and growth factor supplemented cancer cell (c0) states (Fig. 16B-E). Evidently, these tumoroid cultures display marked differences when compared to the culture models of individual components (Fig. 16F), effectively recapitulating the same cell states delineated in our study for both cancer and CAF cells (Fig. 8G-H).

Particularly with regards to CAF cells, our tumoroid culture system demonstrates a significant enhancement in matching primary CAF states when compared to mono-culture models (Fig. 16G). Reference-based annotation analysis showed that tumoroid CAF states converge, independently of the patient line, to the same primary CAF states and revealed the absence of some primary CAF state signatures in our tumoroid models (Fig. 16H). Focusing on the activation signature genes, we observed some minor discrepancies in the set of genes expressed by our tumoroid models and the primary CAF cells (Fig. 16I). However overall, we could observe a striking overlap in the expression patterns of CAF activation (Fig. 16I-J).

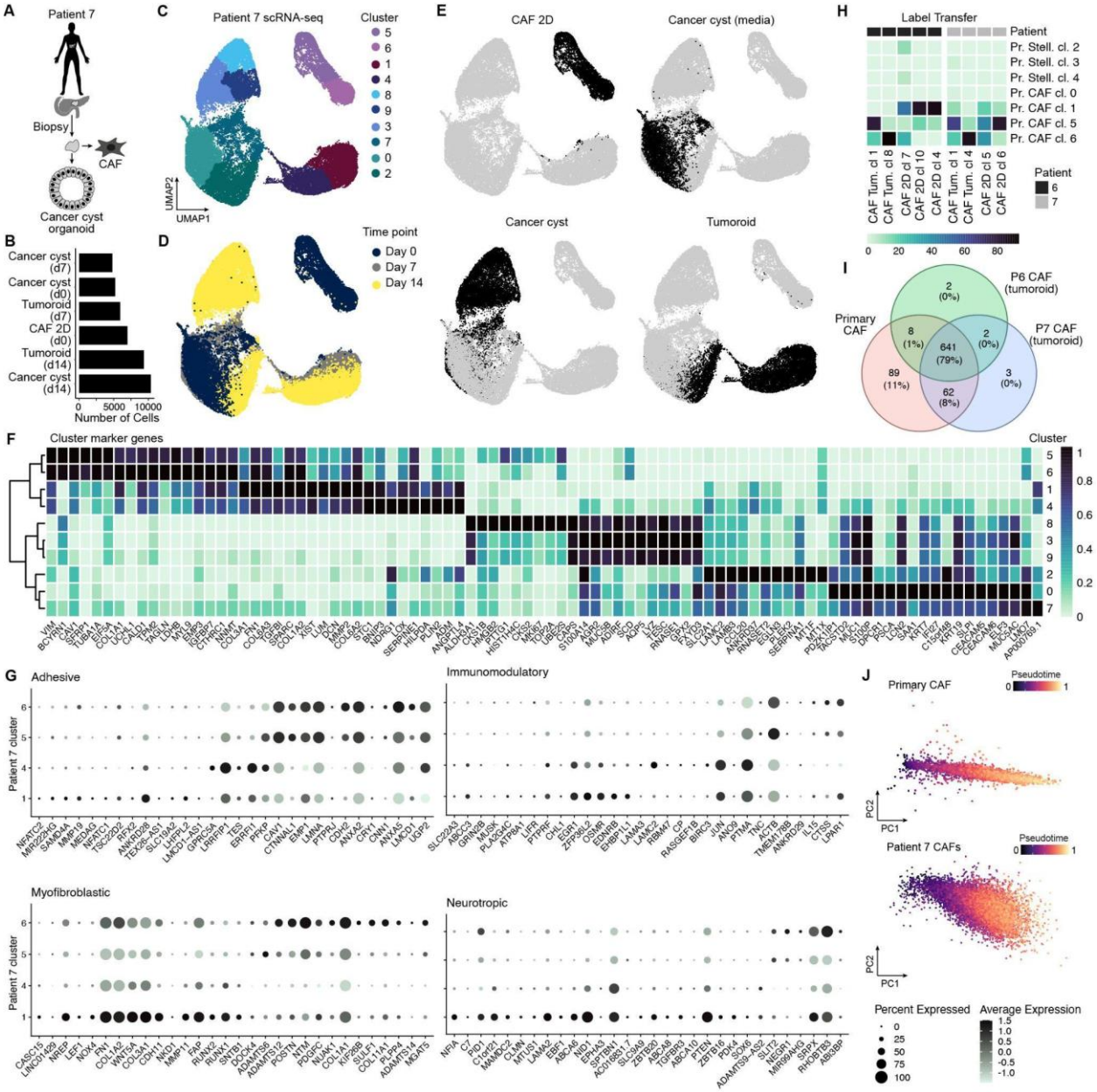

Figure 16: Single-cell transcriptome analysis of CAF state reproducibility. *A) Schematic representation of sample collection for autologous PDAC in-vitro models. B-E) Number of sequenced single-cells (B) and integrated UMAP embedding with emphasis on identified cell states (C), timepoint (D) or tested culture condition (E). Note that, in contrast to other conditions where cells rely on internal interactions to sustain the system, day 0 cancer cyst cells were cultured in growth factor supplemented media. F) Panel top cluster markers expression profiles. G) Dotplot showing the average expression (grey color scale) and percent of cells expressing (size of dot) of marker genes of previously described fibroblast states {REF} across the different clusters of CAFs. H) Heatmap highlighting results from label-transfer analysis from primary CAF states on tumoroid and 2D CAF states independently for each patient line. Tumoroid CAF states converge on the same set of primary CAF states. I) Venn diagram showing the overlap of expressed genes from the activation signature in CAFs from primary tissue (red), patient 6 tumoroid (green), and patient 7 tumoroid (blue). The number and percentage of overlapping genes are indicated. J) PCA analysis of primary biopsies as well as tumoroid cultures consistently shows how the major axis of variation for CAF cells correlates with the activation signature.*

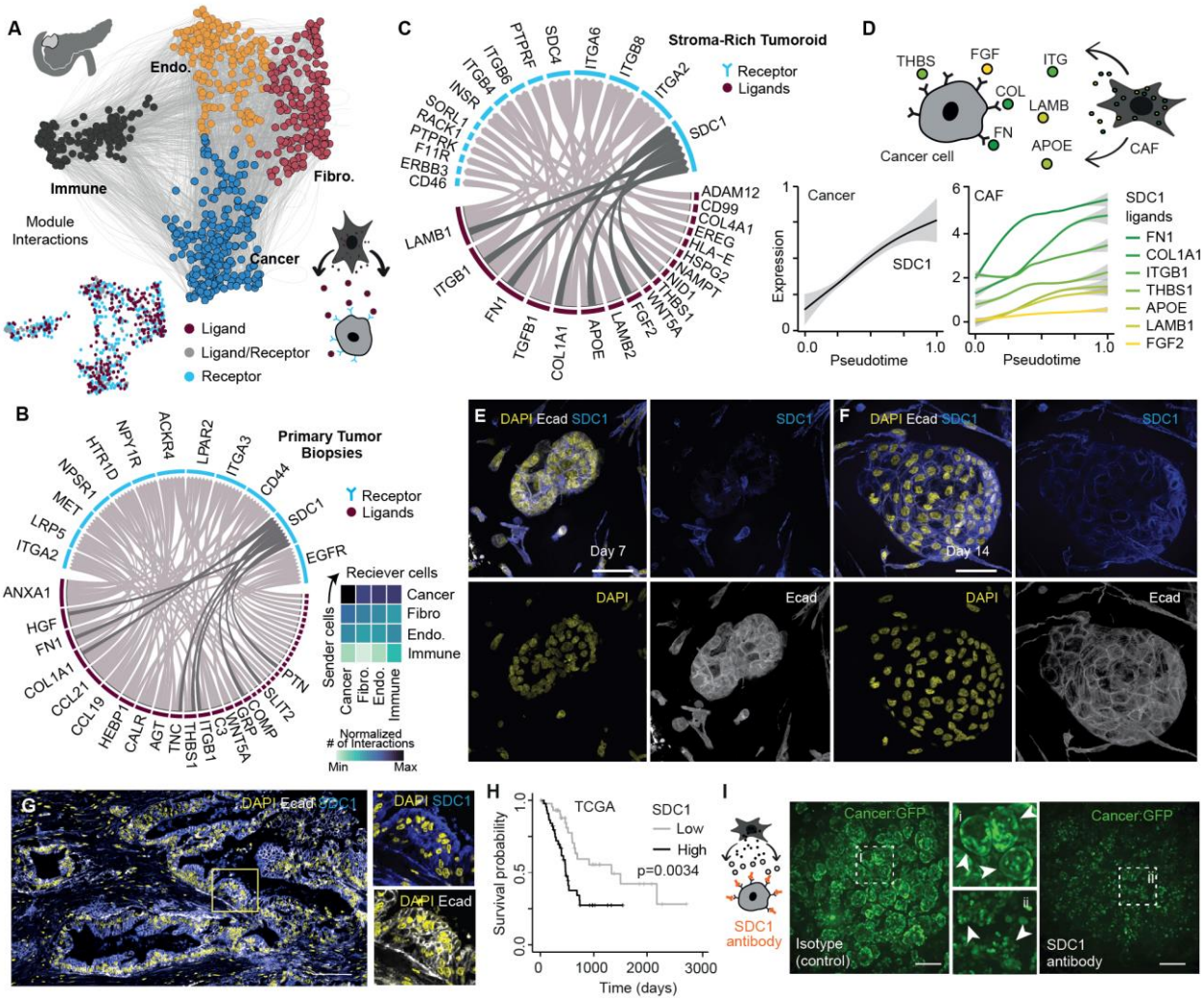

Figure 17: Interaction analysis identifies SDC1 as a dynamically expressed receptor in tumoroid cancer cells and SDC1-antibody block disrupts cancer cell glandular structure. *A) Network showing ligand-receptor (LR) pairing between major cell types in primary tissues, colored by cell type (top) and molecular function (bottom). B,C) Ribbon plots (Gu et al., 2014) showing CAF to cancer LR pairing in primary PDAC (B) and CAF-tumoroids (C). Inset heatmap in (B) shows magnitude of pairwise directed interactions between cell types. Syndecan 1 (SDC1)-ligand pairings are highlighted in dark gray. D) SDC1 (left) and predicted ligand (right) expression in cancer and CAF cells over pseudotime, respectively. E,F) Immunofluorescence showing SDC1 induction from day 7 (E) to day 14 (F) tumoroids. Scale bar:50um. G) Immunofluorescence staining of SDC1 in the primary pancreatic cancer tissue. Scale bar:100um. H) Kaplan–Meier plot showing that high expression of SDC1 in PDAC cancers from TCGA cohort is associated with poor prognosis. I) Schematic shows SDC1 antibody blocking experiment. GFP reporter expression in cancer cells on day 14 tumoroids incubated with isotype control (left, inset i) or SDC1 (right, inset ii) antibodies. Scale bar: 100um.*

To uncover the mechanisms driving cell state transitions, we explored microenvironmental interactions within the primary PDAC samples (Fig. 17A). Remarkably, we observed that cancer cells and CAFs exchanged the most signals, emphasizing the intimate relationship of these cell types within the tumor tissue (Fig. 17B). We identified Syndecan 1 (SDC1) and Epidermal Growth Factor Receptor (EGFR) as major cancer cell surface receptors predicted to interact with several CAF-secreted signals related to disease progression (Fig. 17B). Analyzing CAF-cancer interactions within tumoroid models, we observed that a significant proportion of directed interactions identified in primary samples could be observed in tumoroids (Fig. 18A-B).

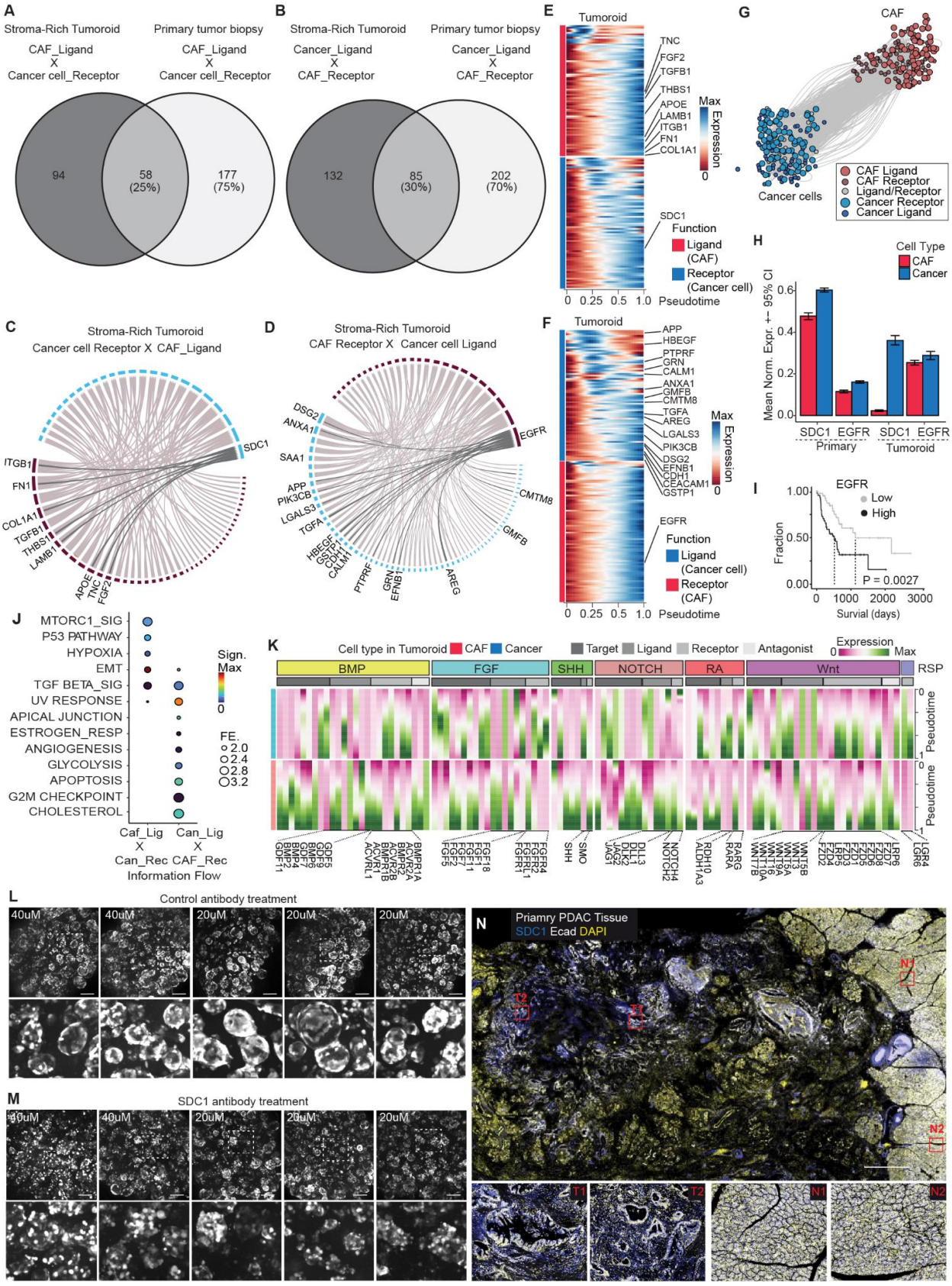

Figure 18: Expression of receptors and ligands in tumoroid CAF and cancer cells. *A,B) Venn diagram representing number of LR interactions between CAF and cancer cells: tumoroid model is able to recover over 25% of CAF to cancer interactions (A) and 30% of cancer to CAF interactions as compared to ground truth identified in independent primary PDAC sample cohort. C,D) Ribbon plot representing communication between tumoroid CAF (source) and cancer cells (target) highlighting SDC1 interactions (C) as well as tumoroid cancer cells (source) and CAF (target) highlighting EGFR interactions (D). E,F) Expression of CAF-specific ligands and cancer-specific receptors along respective pseudotemporal trajectories (E) as well as specular signaling dynamic (F). G) Network*

depicting all identified tumoroid CAF and cancer cell interactions. H) Expression of SDC1 and EGFR in CAF and cancer cells in tumoroids and primary PDAC biopsies. I) Survival analysis on TCGA pancreatic cancer cohort links EGFR overexpression to worse outcome. J) Hallmark enrichment of directed signaling through LR pairs between CAF and cancer cells in tumoroid model. K) Signaling molecules from curated annotations (Han et al., 2020) of major developmental pathways are dynamically expressed along CAF and cancer trajectories within tumoroids. L,M) GFP reporter expression in cancer cells on day 14 tumoroids treated with isotype control (L) or SDC1 (M) antibodies. Scale bar:100um. N) Immunofluorescence of SDC1 and E-Cadherin in primary PDAC tissue. Insets show 2 locations within non-cancerous pancreas tissue (N1-2) as well as 2 locations within the tumor (T1-2). Nuclei stained with DAPI (white). Scale bar: 2mm.

Consistent with the primary PDAC samples, we identified SDC1 acting as a cancer cell hub for the collection of CAF secreted ligands (Fig. 17C, 18C-G). Interestingly, we observed SDC1 and its predicted CAF-secreted ligands increasing in expression along the respective cell type trajectories in tumoroids (Fig. 17D). Previous studies have revealed that SDC1 is recycled to the cell membrane by Kirsten Rat Sarcoma Virus Oncogene Homolog (KRAS) activity and is a critical mediator of macropinocytosis in pancreatic cancer (Yao *et al.,* 2019). SDC1 is known to be a key cell surface adhesion molecule engaged in interactions with numerous ligands (e.g. THBS1, FGF2, TNC, FN1) (Bray *et al.,* 2019; Chen *et al.,* 2020; Jacquemin *et al.,* 2020; Ni *et al.,* 2017; Topalovski and Brekken, 2016), thereby regulating major pathways responsible for cell interactions within the microenvironment, and contributing to cancer progression, proliferation, metastasis and overall poor prognosis (Akl *et al.,* 2015). We also observed that EGFR expression is associated with CAF activation in the tumoroid (Fig. 18F), and primary PDAC tumors with high EGFR expression are associated with poor survival (Fig. 18I). EGFR inhibition shows promise as a co-target in mouse models and is FDA approved for PDAC treatment in humans (Blasco *et al.,* 2019; Garvey *et al.,* 2020). In contrast to EGFR, SDC1 showed higher expression and specificity in cancer cells of tumoroid and primary resections (Fig. 18H). More broadly, we observed that regulators of diverse signaling pathways are dynamically modulated in the tumoroid (Fig. 18K), providing a rich resource for future *in vitro* perturbation experiments to understand these complex interactions.

SDC1 specificity revealed by our analysis prompted us to investigate how the blockage of this receptor impacts cancer growth within the tumoroid. Through imaging of the tumoroid cultures, we confirmed a time-dependent increase in SDC1 expression, predominantly localized to the cell membrane of cancer cells (Fig. 17E-F). Expression of SDC1 protein in cancer cells was also validated on primary PDAC resections (Figure 17G, 18N). Furthermore, SDC1 overexpression significantly decreased survival in the TCGA PDAC cohort (Fig. 17H), and preliminary data indicate that blocking this receptor is detrimental to the tumoroid system (Fig. 17I, 18L-N). These findings suggest a crucial role for signaling through SDC1 in the development and dynamics of our model system, offering promising avenues for further research and therapeutic intervention. Overall, by accurately recapitulating PDAC cancer states and validating clinically relevant features, such as survival correlations, our multilineage tumoroid model emphasizes the significance of CAF-cancer interactions in PDAC disease progression and provides a powerful platform for manipulating and understanding CAF-cancer interactions with therapeutic relevance.

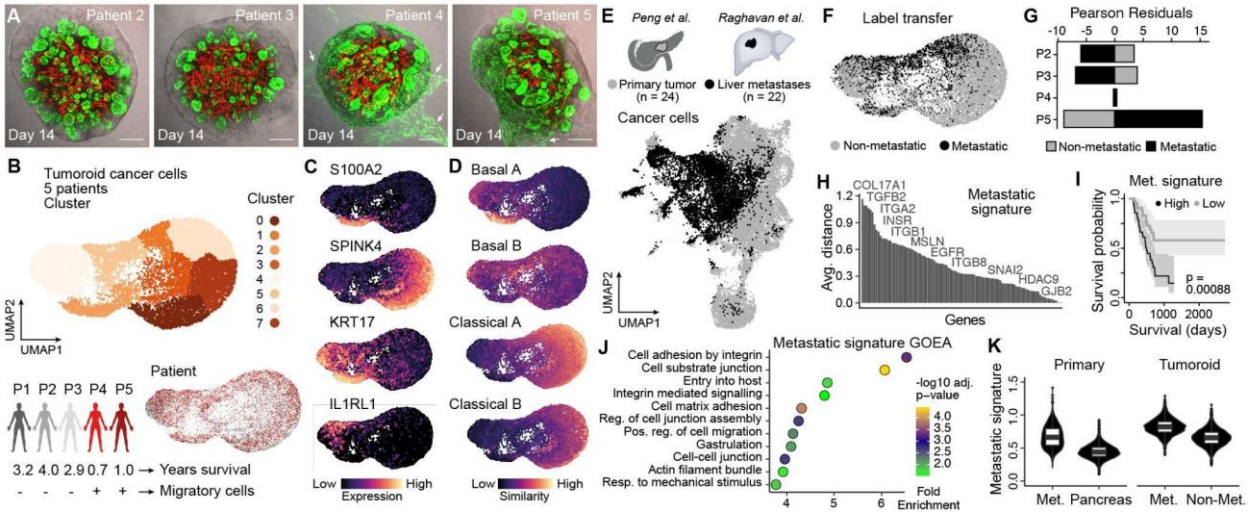

Figure 19: Patient-variable tumoroid migratory state signatures correlate with cancer prognosis. *A) CCO were established from 4 additional PDAC patients and co-cultured with CAFs and ECs to generate tumoroids. Images show cancer cells and ECs stably transformed with EGFP and TdT expression cassettes, respectively. Arrows highlight the presence of migratory-like cells in certain patient tumoroids. Scale bar: 250um. B) Cancer cell heterogeneity analysis of scRNA-seq data from tumoroids from 5 patients. UMAP embedding is colored by cluster (top). Approximate overall survival time (in years) and recurrence status are noted for each patient (bottom). C) Feature plot showing expression of selected marker genes. D) Feature plots showing expression scores of PDAC subtype signatures. Data suggests co-existence of cancer sub-populations within the same tumoroid. E) Integrated UMAP embedding of cancer cell transcriptome states from previously published scRNA-seq primary PDAC tissue (grey) and PDAC liver metastases (black). These data were used to identify a metastatic signature that differed between the two sets of samples and classify tumoroid cancer cells. F) Tumoroid UMAP colored by label transfer from primary PDAC (non-metastatic) or liver metastatic cancer cells. G) Barplot of Pearson residuals (Chi-square test) showing depletion and enrichment of non-metastatic (grey) and metastatic (black) label-transferred cells in tumoroids of each patient shown in panel A. H) Barplot showing the average expression difference between tumoroid cancer metastatic and non-metastatic DEGs. I) Kaplan–Meier (KM) plot showing that high expression of metastatic signature genes in PDAC cancers from TCGA dataset is associated with lower survival. J) Gene ontology enrichment of the metastatic signature genes. K) Distribution of metastatic signature gene expression in primary cancer tissue (PDAC, liver metastasis) and organoids from tumoroids with metastatic (patient 4, 5) and non-metastatic (patient 2,3) phenotypes.*

Moving forward, it is noteworthy that on day 14, our tumoroids exhibited intriguing characteristics. Upon microscopic examination, we observed the presence of detached cancer cells exhibiting a migratory phenotype in select cultures (Fig. 19A). This phenomenon appeared to be more pronounced in tumoroid cultures derived from patients with heightened susceptibility to metastasis and shorter overall survival rates. To understand the potential diversity of molecular profiles and cell behaviors between different patients, we generated single-cell transcriptome data from tumoroids from each patient, analyzed cancer heterogeneity separately, integrated cancer cell data from each individual, visualized cells in a UMAP embedding, and identified markers for each cluster (Fig. 19B-C, 20A-D). In the integrated analysis, we observed a diversity of cancer cell states and each individual contributed cells to all identified populations (Fig. 20E). Moreover, we report how each tumoroid cancer cluster could be classified based on signatures derived from different primary PDAC types (Classical A, B; Basal-like A, B) (Chan-Seng-Yue *et al.,* 2020) (Fig. 19D). Strikingly, we found that each tumoroid consisted of a heterogeneous mix of all the different PDAC cancer subtypes, and the proportions of these populations differed among patient tumoroids (Fig. 20F). These data suggest that PDAC types represent proportion differences among cancers, that the underlying cell states develop dynamically over time, and that tumoroids might be used to recapitulate PDAC type proportions. This facet, while not within the scope of this study, opens up future possibilities for assessing the emergence of diverse subtypes and characterizing the extent of plasticity and interplay among them *in vitro*.

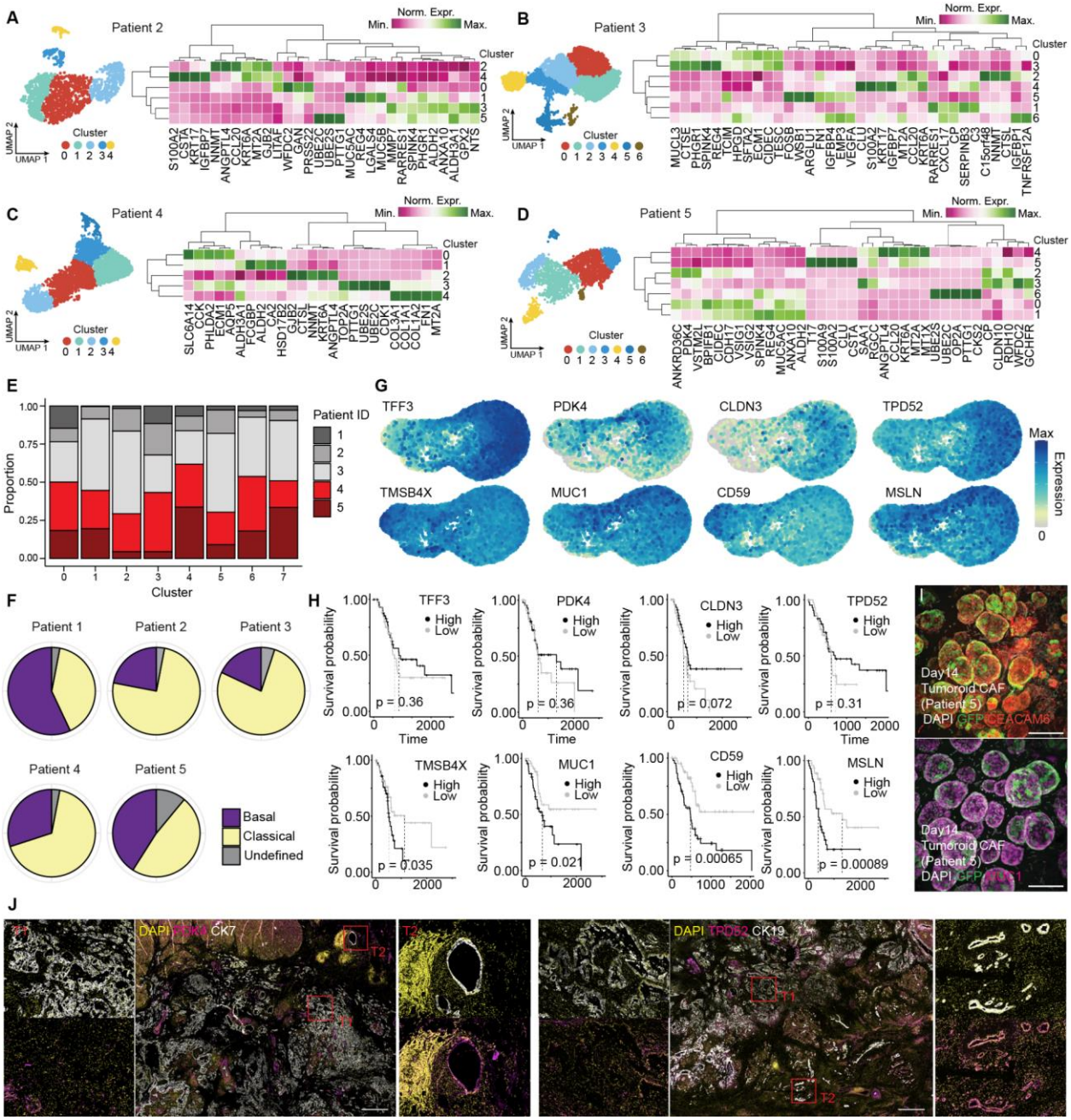

Figure 20: Heterogeneity analysis of tumoroid cancer cells from 5 patients. *A-D) Heterogeneity analysis in tumoroid cancer cells for each patient derived line showing selection of marker genes for cultures with no migratory cells (A,B) and cultures with migratory cells (C,D). Insets display individual UMAP embeddings color-coded by cluster. Note that the cluster colors are not comparable across samples. E) Proportion of cells in each cluster that are derived from each patient from the integrated heterogeneity analysis presented in Fig. 19. F) Pie chart shows the proportion of cells from each patient tumoroid classified into PDAC subtypes. The data shows how different subtypes co-exist within each patient-derived tumoroid. G) Feature plots on the integrated UMAP from Fig. 19 showing expression of genes enriched in tumoroids without (top row) and with (bottom row) migratory cells. H) Kaplan–Meier (KM) plot showing the relationship of gene expression in the Tumor Migration Signature (TMS, bottom) or in the non-TMS (top) and the survival times. Data is from the cancer genome atlas (TGCA). I) Immunofluorescence staining for CEACAM6 (red, top) and MUC1 (pink, bottom) on day 14 tumoroids from Patient 5. Cancer cells stably express GFP, DAPI marks nuclei (white). Scale bar:100um. J) Immunofluorescence of Pyruvate Dehydrogenase Kinase 4 (PDK4, pink, left) and Tumor Protein D52 (TPD52, pink, right) in primary aggressive PDAC tissue. Insets show 2 locations within 1 location within the well differentiated character (T1) as well as 1 location within the undifferentiated character (T2). Cancer cells stained with Cytokeratin 7 (CK7, white, left) and Cytokeratin 19 (CK19, white, right). Nuclei stained with DAPI (yellow). Scale bar: 2mm.*

Intrigued by the tumoroid cancer migratory phenotype, we endeavored to pinpoint a gene signature that could define this state. We integrated the primary PDAC cancer cells (Peng *et al.*, 2019) with an independent cohort of 19 PDAC-derived liver metastatic

resections (Raghavan *et al.,* 2021) (Fig. 19E) and used these data as basis for a reference-based annotation of our integrated tumoroid cancer cells (Fig. 19F). Remarkably, we observed that the 'metastatic' annotation was depleted in cancer cells from tumoroid cultures of patients with longer overall survival while being strongly enriched in the cancer cells derived from the patient with shortest post-diagnosis survival time and with proven history of recurrence (Fig. 19G). Differential expression analysis between 'metastatic' and 'non-metastatic' classes of tumoroid cancer cells revealed a Tumoroid Metastatic Signature (TMS) (Fig. 19H). Overexpression of the TMS showed a significant negative impact on patient survival from the TCGA cohort (Fig. 19I, 20G-J) and genes in this signature were over-represented in cellular processes involved with cytoskeleton dynamics, substrate interaction and cell migration (Fig. 19J). Finally, we validated that PDAC-derived liver metastasis biopsies show a significantly higher expression of TMS compared to the primary PDAC cells (Fig. 19K).

To summarize, our CAF-tumoroid model adeptly reproduces the trajectories of cancer and stromal cell states. We reveal that CAFs, in contrast to NFs, transmit distinct signals that sustain cancer cell states associated with unfavorable prognoses. Moreover, we uncover pivotal ligand-receptor interactions that can influence cancer cell organization and viability. Lastly, we present a discernible signature associated with tumoroid migratory behavior, which correlates with unfavorable clinical outcomes. Future work is needed to explore the link between the larger patient cohorts and their corresponding tumoroid avatars. In addition, similarly thorough analysis on more developed models that incorporate macrophages, monocytes and other immune cell types will be required to fully recapitulate the dynamic interlineage signaling axes prevalent in PDAC tumor microenvironments. Overall, our findings significantly advance our understanding of PDAC and underscore the utility of our innovative tumoroid model in advancing cancer research and precision medicine strategies.

CHALLENGES AND FUTURE PERSPECTIVES

As the utilization of patient-specific tumor organoid models becomes increasingly widespread, the establishment of standardized protocols for organoid generation that accommodate the intrinsic heterogeneity within tumors is crucial for their clinical success. Several challenges arise from the sourcing of tumor tissue for organoid generation, which contribute to variability resulting from clinical necessity and is outside the experimentalists' sphere of influence. The current models, primarily established from individual biopsy specimens or minute tissue fragments, do not adequately capture the profound patient-specific biological diversity and spatiotemporal evolution (Roerink *et al.,* 2018). This limitation in capturing the diversity of populations in organoid biobanks can result in flawed efforst in drug exploration and biomarker advancement, especially when there are differential responses to anticancer treatments in populations missing from the model (Boj *et al.,* 2015; Broutier *et al.,* 2017; Fujii *et al.,* 2016; Kopper *et al.,* 2019). Additionally, the presence of fast-growing cells in the samples can contaminate the tumor tissue thus limiting research aimed at describing neoplastic cell biology (Dijkstra *et al.,* 2020).

Efforts to standardize tumor tissue processing are essential to achieve more uniform cancer organoid cultures. Traditional methods involve completely dissociating patient-derived biopsies into cellular components using enzymatic and/or mechanical treatments, subsequently encased in a complex 3D matrix submerged in a nutrient-rich medium

(Driehuis *et al.,* 2020). However, these techniques often lead to limited reproducibility in sizes of cell clusters, inconsistently ranging from individual cells to aggregates of approximately 100 µm in diameter. Enzymatic treatment can lead to unintended cleaving of proteins located on the surface of the calls, requiring tissue-specific dissociation protocols (Driehuis *et al.,* 2020). Full tissue dissociation, while useful, disrupts complex cell-extracellular matrix (ECM) interactions and may negatively impact non-cancerous and non-epithelial cell populations. An alternative approach involving patient tissue mincing and encapsulation of millimeter-scale tumor fragments retains parent tissue structure and tumor microenvironment (TME) cell composition, but this method also results in limited reproducibility of fragment sizes, leading to uneven environments for encapsulated cells. Damage resulting directly from the mincing procedure or indirectly through gradients of oxygen and nutrients further reduces cell viability for organoid generation. Moreover, encapsulation of selected cell populations conserving reproducible interactions with the surrounding environment is extremely difficult under this processing procedure.

Despite challenges in standardizing clinical tissue collection, there are promising avenues for advancing cancer organoid culture protocols. Samples of flash-frozen tissue, thawed after months of cryopreservation, have been shown to maintain similar pharmacotropic profiles compared to tissue-matched fresh organotypic cultures established at the time of biopsy, offering a potential solution (Walsh *et al.,* 2016). Defining intra- and inter-tumoral heterogeneity is essential for standardization (Roerink *et al.,* 2018). Multiregion tissue sampling, utilizing primary and metastatic tumor lesion biopsies from individual patients, can help model the inherent complexity of intratumor heterogeneity and pharmacotropic responses (Kopper *et al.,* 2019; Vlachogiannis *et al.,* 2018). Although living biobanks of tumor organoids derived from various neoplastic tissue types provide valuable insights, the temporal evolution of patient-derived cancer organoids has not been extensively investigated, primarily due to the scarcity of available samples. Innovative approaches, such as genetically engineered organoids derived from healthy tissue and liquid biopsies, could offer more accessible alternatives for modeling and investigating cancer progression.

In tandem with endeavors to standardize neoplastic tissue collection, there has been a concurrent integration of technological innovations in microfabrication, microdissection, and microfluidic techniques aimed at streamlining the subsequent steps in tissue processing, organoid establishment, and pharmacotropic response assessments (Brandenberg *et al.,* 2020; Horowitz *et al.,* 2021; Li *et al.,* 2014). These innovative methodologies serve to streamline the identification of distinct cancer subpopulations and enable precise investigations into the impact of the starting number of cells on organoid derivation efficiency. Moreover, the realm of microphysiological systems now encompasses organoid/tumor-on-a-chip systems featuring heightened tissue complexity, offering the prospect of incorporating fully developed vasculature. This integration provides a distinctive vantage point for evaluating cancer extravasation and drug delivery processes (Chen *et al.,* 2017; Haase *et al.,* 2020). The ongoing enhancements of microfluidic devices are poised to play a pivotal role in faithfully replicating the unique cellular and anatomical variabilities found in patient-derived tumors. Enhanced techniques for quantitatively tracking organoid progression at the cellular level, including cellular barcoding (Umkehrer *et al.,* 2021) and machine learning-based image analysis (Kassis *et al.,* 2019), will complement these advancements in cancer modeling.

Constructing systems that mimic the natural structure and intricacy, encompassing the integration of pertinent cells from the tumor microenvironment, stands as another significant objective in cancer simulation. Recent efforts have been directed towards creating cultivation systems that faithfully replicate the diverse composition of TME cells and the interactions between different cell types, all aimed at assessing individualized immunotherapies (Neal *et al.,* 2018; Schnalzger *et al.,* 2019). The specific effects of cancer-associated fibroblasts (CAFs) on cancer organoid populations have revealed unique interactions and stroma-derived factors influencing epithelial-to-mesenchymal transition (EMT) and therapeutic responses (Ebbing *et al.,* 2019; Öhlund *et al.,* 2017). Meanwhile, distinct phenotypes observed in murine CAFs from patient-derived xenografts highlight the limitations of murine models in reconstructing the human TME (Ebbing *et al.,* 2019). These studies have resulted in the introduction of new biomarkers and therapeutic approaches for categorizing patients and tailoring treatments to their individual needs. Nevertheless, comprehensively examining the diverse functions TME cells fulfill in the advancement and maintenance of cancer organoids remains an unexplored area, mainly because reliable protocols enabling the simultaneous and extended culture of multiple cell types have not been established.

Cancer heterogeneity, driven by complex and reciprocal soluble factor signaling within the tumor microenvironment (TME), poses a critical challenge in developing effective cancer organoid models. In models comprising pure populations of neoplastic cells, external supplementation of signaling factors promoting cancer cell growth is necessary. To achieve the reproducibility required for clinical translation, standardized procedures for recombinant protein expression and isolation are essential. Advancements in liposomes based on phospholipids or cholesterol, coupled with the identification of the stabilizing role of afamin (Mihara *et al.,* 2016), a glycoprotein found in bovine serum, have led to enhanced stability and biological activity of *in vitro* protein expressed Wnt3a complexes (Tüysüz *et al.,* 2017; Willert *et al.,* 2003). Nevertheless, the use of some purified recombinant proteins may be limited by poor solubility and stability, resulting in diminished protein activity (Tüysüz *et al.,* 2017; Willert *et al.,* 2003). Additionally, the cost and scalability of medium cocktails containing multiple growth factors and nutrients can become prohibitive for high-throughput applications.

Conditioned medium from engineered mammalian cells producing R-spondin, Wnt3a, and/or Noggin soluble molecules, has significantly reduced costs and increased the access to cancer organotypic culture systems (Willert *et al.,* 2003). However, diluting the conditioned medium directly into complete formulations of organoid medium for preparation faces concerns in achieving standardized and consistent culture protocols. Batch-to-batch variability in conditioned medium, along with the presence of diverse molecules besides the protein(s) of interest, affects encapsulated cancer organoid phenotype and reaction to pharmaceutical treatment. Furthermore, the use, in conditioned medium, of residual animal-derived serum, such as fetal bovine serum (FBS), raises concerns about ill-defined components and the potential for undesired effects and infections (van der Valk *et al.,* 2010). Altogether, the dependence on conditioned medium and serum derived from animals during the cultivation of cancer organoids obstructs endeavors to create uniform models and restricts the ability to compare data consistently across various experiments and studies.

Alternative DNA-based protein synthesis methods, including insect or bacterial cell-based systems, could offer more scalable and cost-efficient avenues for producing medium

components with more permissive purification needs. Yet, bacterial systems could be vulnerable to the presence of endotoxins, and they frequently lack sufficient mechanisms to guide protein folding and perform necessary post-translational modifications that are essential for preserving the correct biological functionality of the target proteins. Overcoming these challenges, a unique expression and purification workflow for Gremlin 1 (GREM1) and R-spondin 1 (RSPO1) in Escherichia coli has demonstrated activity similar to proteins sourced from commercial vendors, with reduced endotoxin contamination and cost (Urbischek *et al.,* 2019). Moreover, tumor-associated signaling circuits can be modulated by custom-engineered agonists, offering an additional cost-efficient avenue with comparable biological functions (Janda *et al.,* 2017; Luca *et al.,* 2020; Miao *et al.,* 2020). The inclusion of these tailored agonists within cancer organoid cultures has the potential to yield fresh insights into the responses of distinct clonal subpopulations of cancer cells when subjected to the activation of precise signaling pathways.

The advancement of next-gen tumor organoid culture medium requires a patient-tailored comprehension of the tumor microenvironment *in vivo* and the establishment of standardized *in vitro* modeling. Although recent studies have discerned essential or nonessential components within the culture medium, they often focus on a limited number of interlinked biochemical networks such as WNT/R-spondin, EGF, TGF-beta and BMP. Furthermore, even though research indicates that altered expression of certain signaling molecules can initiate tumor formation without genetic changes (Tsukamoto *et al.,* 1988), the current categorization of patient-derived organoids into subgroups with distinct medium needs is frequently based solely on mutation status. Analysis through scRNA-seq along with multiplexed proteomic profiling of patient-specific TME soluble signaling molecules *in vivo* will offer crucial insights into medium formulation requirements (Kumar *et al.,* 2018). Coupled with advancements in characterization of collected human serum from matched patients to explore soluble factors that influence cancer phenotypes (Broutier *et al.,* 2017; Ebbing *et al.,* 2019), these analyses will provide an alternative to serum of animal origin for clinical oncology applications.

To achieve the most representative models of neoplastic disease progression and treatment, it's vital to standardize cancer characterization protocols at each step of organoid derivation. Understanding distinctions between the environments where healthy and malignant stem cells thrive will be essential for effectively modeling cancer onset and preventing biases in clonal selection and expansion. In addition to soluble factor concentration, exploring physiochemical properties such as growth-factor signaling, pH, ECM composition, architecture, and oxygenation levels within the medium is essential. Current culture methods often fail to recapitulate the spatial heterogeneity of these factors in the *in vivo* TME. Future endeavors should be directed towards the development of technologies and platforms enabling the precise spatiotemporal control of medium in cancer organoid cultures (Broguiere *et al.,* 2020). As cancer organoid models grow in complexity by incorporating diverse cell types from the tumor microenvironment, determining the essential components of the medium required to sustain non-cancerous cells and facilitate interactions between different cell types will be of paramount importance.

Another crucial factor in organoid cultures is the intimate relationship between encapsulated cells and the ECM. In the recent past, the primary matrix for culture of 3D organoid systems has been EHS matrix, rich in cytokines, growth factors, and ECM molecules that support the cultivation and expansion of diverse cancerous as well as tumor

microenvironment cell types. However, the animal-derived nature of EHS matrix, which contains ill-defined xenogeneic impurities, leads to substantial heterogeneity between different batches impacting organoid phenotype unpredictably (Aisenbrey *et al.,* 2020; Hughes *et al.,* 2010). Additionally, its lack of tunability in biochemical and mechanical properties restricts its ability to recapitulate patient-specific tumor ECM characteristics (Acerbi *et al.,* 2015; SelectScience https://www.selectscience.net/application-articles/tuning-the-elastic-moduli-of-corning-matrigel-and-collagen-i-3d-matrices-by-varying-the-protein-concentration/?artid=46305). Collectively these limitations conceal underlying mechanisms governing matrix-influenced tumor cell behavior and, coupled with its comparatively high cost and ethical concerns, undermine EHS matrix use in high-throughput pharmaceutical screenings and clinical applications.

An alternative biomimetic approach, employing collagen type I matrices, has gained popularity as a more cost-effective option for tumror organoid systems *in vitro*. Nevertheless, similar to EHS matrix, collagen matrices derived from animal sources suffer from batch-to-batch inconsistencies, limited tunability, and contamination concerns. The microstructure of collagen gels, influenced by gelation conditions, can result in structural heterogeneity, affecting cell interactions with the matrix (Hapach *et al.,* 2015; Velez *et al.,* 2017). Attempts to control collagen matrix properties frequently necessitate the introduction of substances posing a health hazard or chemical alterations, disrupting native crosslinking and ligand availability (Hapach *et al.,* 2015). Numerous biomaterial frameworks have been created for the three-dimensional cultivation of cancer cell lines, spheroids as well as primate cancer tissues *in vitro*. However, these materials have not yet fully translated to applications in cultures of human cancer organoids and currently represent a future opportunity to understand ECM's role in regulating patient-specific cancers (Gu & Mooney, 2016; Liu & Vunjak-Novakovic, 2016). In one example, GBM organoids grown in synthetic polyethylene glycol (PEG) crosslinked to recombinant hyaluronic acid (HA) hydrogels showed distinct phenotypic responses, demonstrating the potential of adjustable matrix structures providing numerous insights into how the matrix influences tumor organoid phenotypes and pharmacotropic responses (Xiao *et al.,* 2018).

In summary, the advancement of cancer organoid culture protocols, while facing challenges related to variability in tissue collection and processing, holds great promise for enhancing the clinical relevance of these models. The combination of innovative technologies and a deeper understanding of intra- and inter-tumoral heterogeneity will pave the way for more accurate and personalized cancer organoid-based approaches in drug discovery and biomarker development. Additionally, advancements in engineered matrices tailored for human cancer organoid cultures offer promising avenues for improved 3D models, addressing the limitations associated with animal-derived matrices and providing tunable and customizable platforms to explore matrix-mediated cancer organoid phenotypes and drug responses. These innovative materials, when further refined and scaled, have the potential to enhance our understanding of tumor-ECM interactions and contribute to the development of reproducible, disease-specific *in vitro* models.

HUMAN INTESTINAL ORGANOIDS WITH AN AUTOLOGOUS TISSUE-RESIDENT IMMUNE COMPARTMENT

Timothy Recaldin[2*], Bruno Gjeta[1,4*], Linda Steinacher[2,5*], Marius F. Harter[1,3], Lukas Adam[1], Mikhail Nikolaev[1], Rok Krese[1], Umut Kilik[1,4], Doris Popovic[1], Marina Bellavista[1], Kristina Kromer[1], Michael Bscheider[2], Lauriane Cabon[1], J. Gray Camp[1], Nikolche Gjorevski[1#]

[1] Institute of Human Biology (IHB), Roche Pharma Research and Early Development

[2] Roche Innovation Center Basel, Roche Pharma Research and Early Development

[3] Gustave Roussy Cancer Campus, University Paris-Saclay, Paris, France

[4] University of Basel, Basel, Switzerland

[5] Hannover Medical School, Institute of Immunology, Hannover, Germany

[*] These authors contributed equally

[#] Corresponding author

Contribution

This chapter represents work that has been published as a pre-print (https://www.biorxiv.org/content/10.1101/2023.10.04.560810v1) and has been submitted for peer-review. I performed all single-cell genomic data analysis presented in this manuscript.

BACKGROUND

The human intestine, with its single layer of columnar epithelial cells, has evolved for efficient nutrient absorption, but this design also renders it vulnerable to pathogens (Hooper & Macpherson, 2010). Rapid turnover of the epithelium, driven by stem cells located in the intestinal crypts, maintains tissue health but also leaves it susceptible to tumorigenesis (van der Flier & Clevers, 2009). Mutations in the WNT signaling pathway, which regulates stem cell proliferation, are frequently implicated in colorectal tumors (Fodde *et al.,* 2001; Rawla *et al.,* 2019; Zhang & Shay, 2017), contributing to colorectal cancer's ranking as the third most common cancer globally. To preserve homeostasis and protect against pathogenesis, the intestinal mucosal immune compartment, housing the largest pool of immune cells in the human body (Holmgren & Czerkinsky, 2005), plays a critical role in closely monitoring the intestinal epithelium. Intra-epithelial lymphocytes (IELs), a subgroup of tissue-resident memory (TRM) T cells found in peripheral tissues (Masopust & Soerens, 2019), are specifically responsible for constant surveillance, safeguarding the intestinal epithelium against infection and malignant transformation (Cheroutre *et al.,* 2011; Hayday, 2009). Uncontrolled responses to food antigens and invading bacteria are characteristic features of prevalent autoimmune conditions affecting the gut, such as Celiac disease and inflammatory bowel syndrome (Barker & Liu, 2008; Hugot *et al.,* 2001; Parzanese *et al.,* 2017; Sartor, 2006). Despite our reliance on *in vivo* models to understand the immune-epithelial interaction, *in vitro* culturing of gut-derived tissue-resident memory (TRM) T cells

remains a challenge (Beura *et al.,* 2018; Swamy *et al.,* 2015). Utilizing human material offers a platform for treatment with species-specific therapeutic compounds and subsequent experimental tracking, enabling drug efficacy and safety screening (Xu *et al.,* 2018). However, achieving donor matching of immune cells and epithelial cells is challenging yet essential due to the highly alloreactive nature of gut-derived T cells, which significantly influences the study of intestinal homeostasis and disease progression (Fu *et al.,* 2019). Organoids derived from adult stem cells (ASCs) have emerged as valuable models for understanding various aspects of human physiology, including genetic disorders, infectious diseases, cancer, regenerative medicine, and drug discovery (Bartfeld *et al.,* 2015; Huch *et al.,* 2015; Lukonin *et al.,* 2020; Schutgens & Clevers, 2020; van de Wetering *et al.,* 2015; Yui *et al.,* 2012). While intestinal organoids accurately model differentiation and function of major epithelial cell types, they lack a functional and tissue-specific immune compartment, limiting their ability to capture essential aspects of intestinal homeostasis and disease (Sato *et al.,* 2009; Sato *et al.,* 2011; Sato *et al.,* 2013; Schutgens & Clevers, 2020). Incorporating a mucosal lymphocyte compartment into these organoids has proven to be a challenging endeavor (Beura *et al.,* 2018; Swamy *et al.,* 2015), despite previous co-culturing of adult human intestinal epithelium with blood-derived innate immune cells (Jowett *et al.,* 2022; Noel *et al.,* 2017).

OBJECTIVES

In this project, we created a tractable immunocompetent intestinal organoid (IIO) model containing a tissue-resident and donor-matched immune repertoire starting from readily available human clinical samples (Fig. 1a). We benchmarked cell states in IIOs through comparison to reference atlases using single-cell transcriptomes, and used IIOs to explore the effects of drug treatment that has important implications for back-translation.

RESULTS

In our efforts to introduce a functional and relevant lymphocyte compartment into intestinal organoids, we focus on tissue-resident memory T cells (TRMs). TRMs are antigen-experienced T-cell populations, which take permanent residence in the intestinal mucosa, providing front-line defense against invading pathogens (Cheroutre *et al.,* 2011; Masopust & Soerens, 2019). Given the absence of recirculation, they are an appropriate lymphocyte type to stably incorporate into organoid models. Furthermore, their prior antigen exposure and memory character ensures functionality in the absence of antigen-presenting cells, lymphoid structures and the remaining immune cell recirculation machinery. TRMs are difficult to incorporate into *in vitro* systems, owing to their poor viability upon enzymatic removal from the tissue (Beura *et al.,* 2018; Swamy *et al.,* 2015). Therefore, we adapted an enzyme-free scaffold-based crawl-out protocol to isolate large numbers of healthy intestinal immune cells (Clark *et al.,* 2006) (Fig. 21a). We found that, even in the complete absence of cytokine or T-cell receptor (TCR) stimulation, our approach liberated significantly more cells than enzymatic digestion-based protocols, while retaining similar proportions of immune cell types (Fig. 22a-b).

We deemed this lack of cytokine exposure crucial for retaining the tissue-like physiological properties of the intestine-derived lymphocytes. Indeed, flow cytometry analysis showed that the isolated cells expressed TRM markers pertinent to the intestine, including CD161 (IL-17A production (Maggi *et al.,* 2010)) and CD117 (notch signaling

(Massa *et al.,* 2006)) (Fig. 22c), as well as surface molecules associated with tissue retention (CD69 (Kumar *et al.,* 2017)), extracellular matrix association (CD49a (Bank *et al.,* 1994)) and epithelial cell integration (CD103 (Cepk *et al.,* 1994)), all of which were undetectable on blood-derived lymphocytes (Fig. 21b-c). We generated organoids and TRMs from human intestinal specimens, additionally collecting matched peripheral blood mononuclear cells (PBMCs) from the same donor. Once established, organoids were combined with TRMs or PBMCs within three-dimensional (3D) extracellular matrix (ECM) at physiologically-relevant cellular concentrations (Fu *et al.,* 2019), and in the absence of external stimulation. Confocal microscopy and 3D reconstruction revealed that, after 24h coculture, TRMs were viable and closely associated with the organoids (Fig. 21d). To examine the organoid-TRM interactions in greater detail, we generated histological sections of the models and visualized the epithelial and immune cells (Fig. 21e-g).

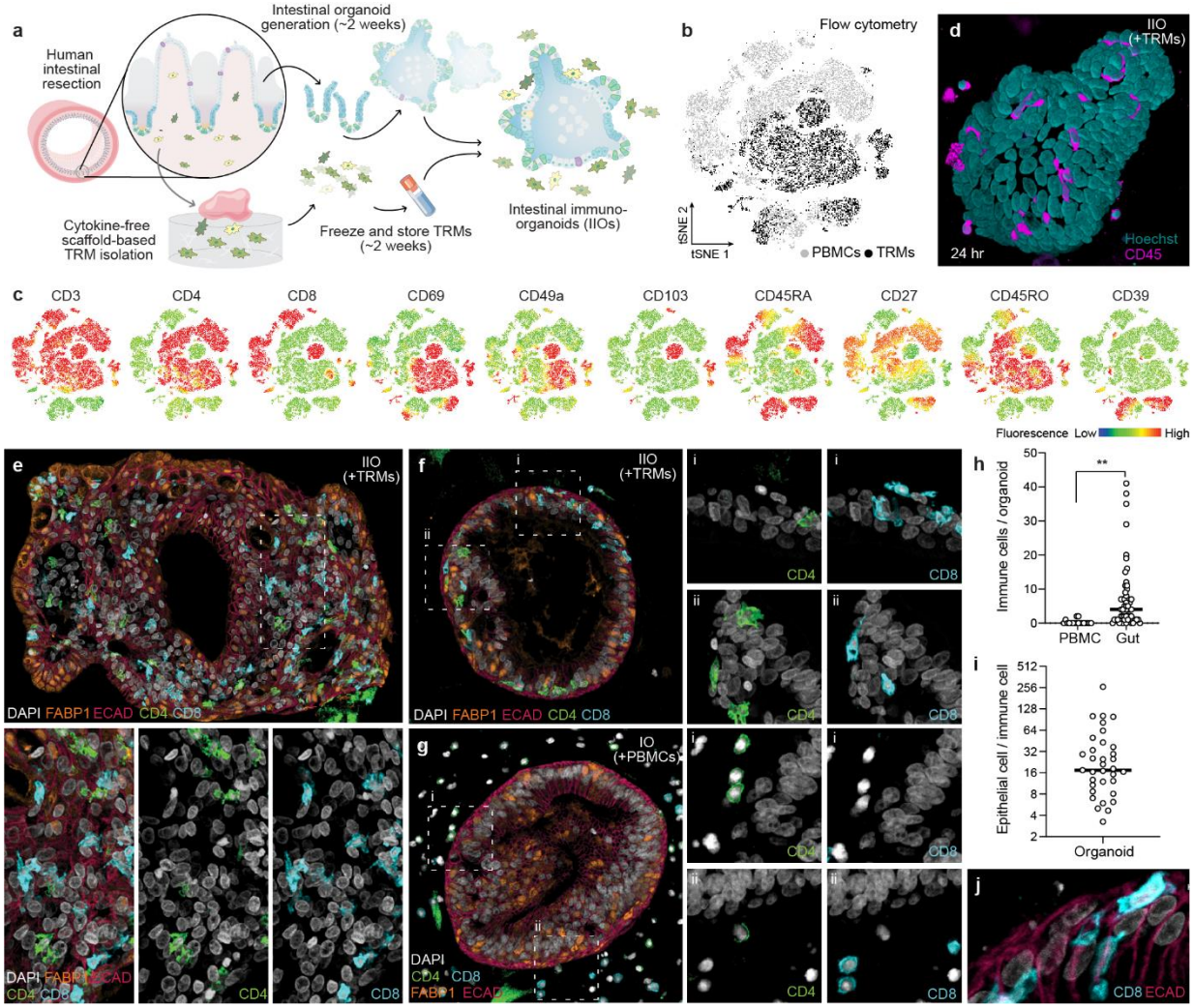

Figure 21: Intestine-derived tissue-resident lymphocytes (TRMs) integrate homeostatically into autologous organoids to form intestinal immuno-organoids (IIOs). *a, Schematic overview for establishing autologous IIOs. b-c, Flow cytometry-based tSNE analysis of gut (TRM) and circulating (PBMC) T cell subgroups based on surface marker expression. tSNE plot colored by original source of the T cells (b, light grey for PBMC and dark grey for TRM) and expression of 10 individual markers of naivety, memory or tissue residency (c). d, Fluorescent still from live imaging 24 hours after IIO coculture with autologous TRMs (nuclei = teal, T cells = pink). e-g, Fluorescent IHC staining of IIO cultures 24 hours after coculture with autologous TRMs (e-f) or PBMCs (g). h, Detected immune cell count per organoid, each data point represents 1 individual organoid. **P < 0.01, unpaired T-test. i, Ratio of epithelial cells to immune cells within each organoid, following organoid supplementation with autologous TRM cells. j, Elongated flossing T cell inserting between basal-lateral epithelial cell junctions.*

We found that, whereas PBMCs occupied the ECM space without apparent interactions with the epithelial cells (Fig. 21g), a sub-population of TRMs infiltrated the organoids and integrated within the epithelial barrier in the absence of stimulation, strikingly resembling the behavior of intestinal intraepithelial lymphocytes (IELs) (Hoytema van Konijnenburg *et al.,* 2017) (Fig. 21e-f, h). We estimated a median integration ratio of 16 epithelial cells per immune cell (Fig. 21i) – highly similar to observations in the intestinal tract of healthy humans (Sergi *et al.,* 2017). Intraepithelial lymphocytes displayed an elongated morphology of ~ 60 µm in length (Fig. 21j, Fig. 22d), around 10 times the length of a naïve blood-derived T cell (Tasnim *et al.,* 2018), and reminiscent of the "flossing" behavior described for transgenic murine IELs imaged *in vivo* (Hoytema van Konijnenburg *et al.,* 2017). With low-level cytokine support, immune-organoid cultures could be maintained across at least three passages, albeit with a diminishing ratio of immune cells to epithelial cells (Fig. 22e). This model provides the first example of self-organization between human immune cells and epithelial organoids to form an organoid system with a tissue-resident immune compartment. We termed these structures intestinal immuno-organoids (IIOs).

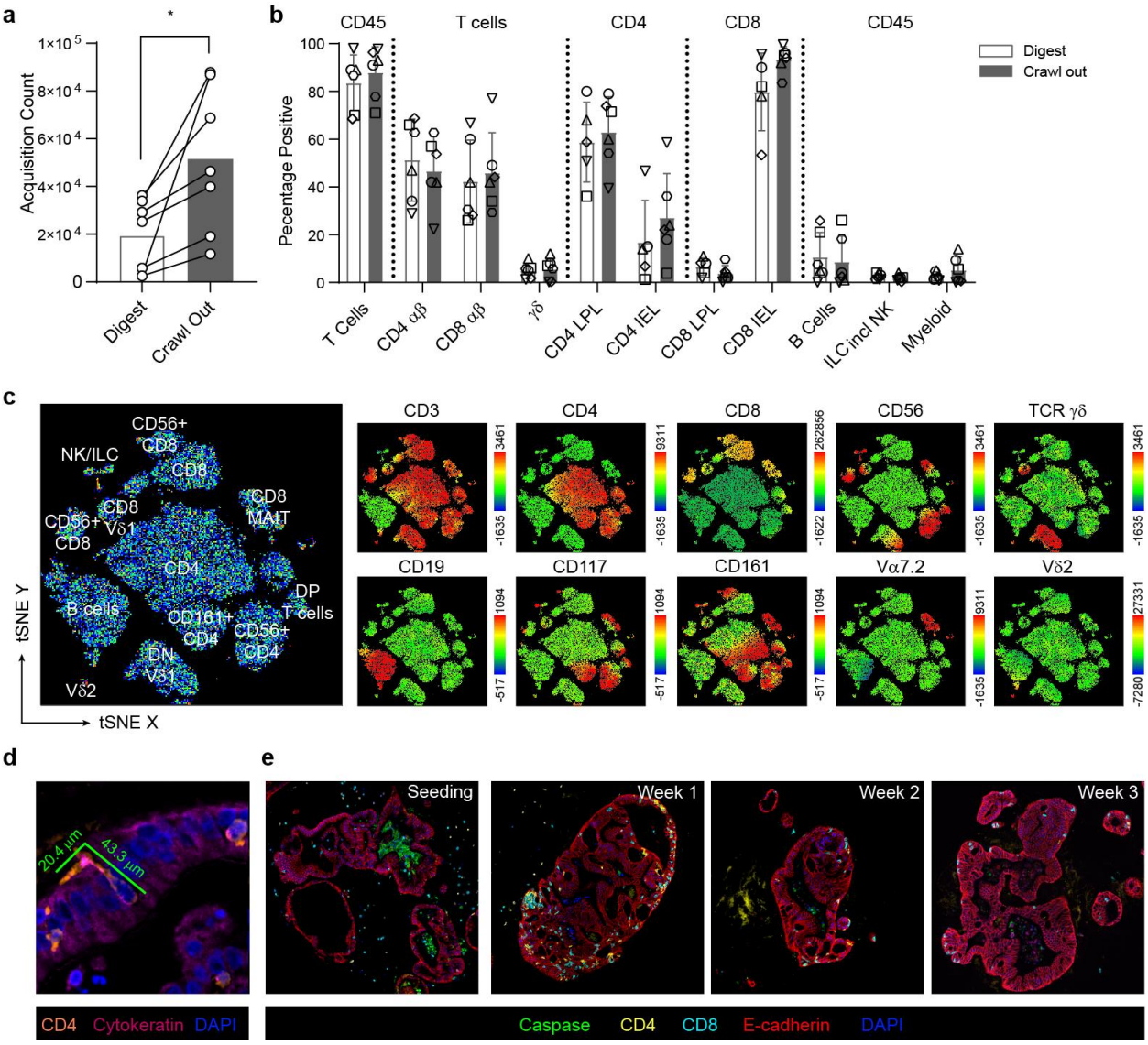

Figure 22: Intestinal TRM isolation and comparison to circulating T cells. *a, Comparison of viable CD45 count in matched donors subjected to either digestion- or crawl out- based isolation. *P < 0.05, paired T-test. b, Comparison of immune cell proportions subjected to either digestion- or crawl out- based isolation. Values represent percentages of parent population listed*

above each bar. LPL lamina propria lymphocyte, IEL intraepithelial lymphocyte, DP double positive, DN double negative. c, tSNE analysis of a typical intestinal lymphocyte isolation incorporating standard lineage defining immune cell markers. The leftmost plot represents annotated cell populations with smaller plots displaying heatmaps for each of the 10 key surface markers assessed. d, Elongated flossing T cell inserting itself between basal-lateral epithelial cell junctions. The diameter of the T cell from head to tail is listed. e, Fluorescent IHC staining of the IIO culture over time.

Elegant *in vivo* studies have dissected the dynamics of murine TCRγδ IELs and their interaction with the intestinal epithelium (Hoytema van Konijnenburg *et al.,* 2017). Owing to their poor survival *in vitro*, similar studies of human IEL behavior have been challenging (Beura *et al.,* 2018; Swamy *et al.,* 2015) resulting in poorly elucidated mechanisms driving human-specific IEL integration. To understand how TRMs and IELs are capable of interaction and integration with intestinal epithelial cells *in vitro*, and how they differ from PBMCs in that regard, we used single-cell RNA sequencing (scRNA-seq) to analyze donor-matched tissue-resident and blood-derived immune cells alone, or cocultured with organoids (Fig. 23a). After dissociating the cultures, we prepared scRNA-seq libraries of TRMs and PBMCs, with a focus on CD3+ T cells, given the TRM predominance within the tissue-derived population. Heterogeneity analysis and visualization using UMAP embedding demonstrated the presence of 3 distinct populations, representing blood-derived naive, blood-derived memory and gut-derived tissue-resident memory T cells (Fig. 23b, Fig. 24).

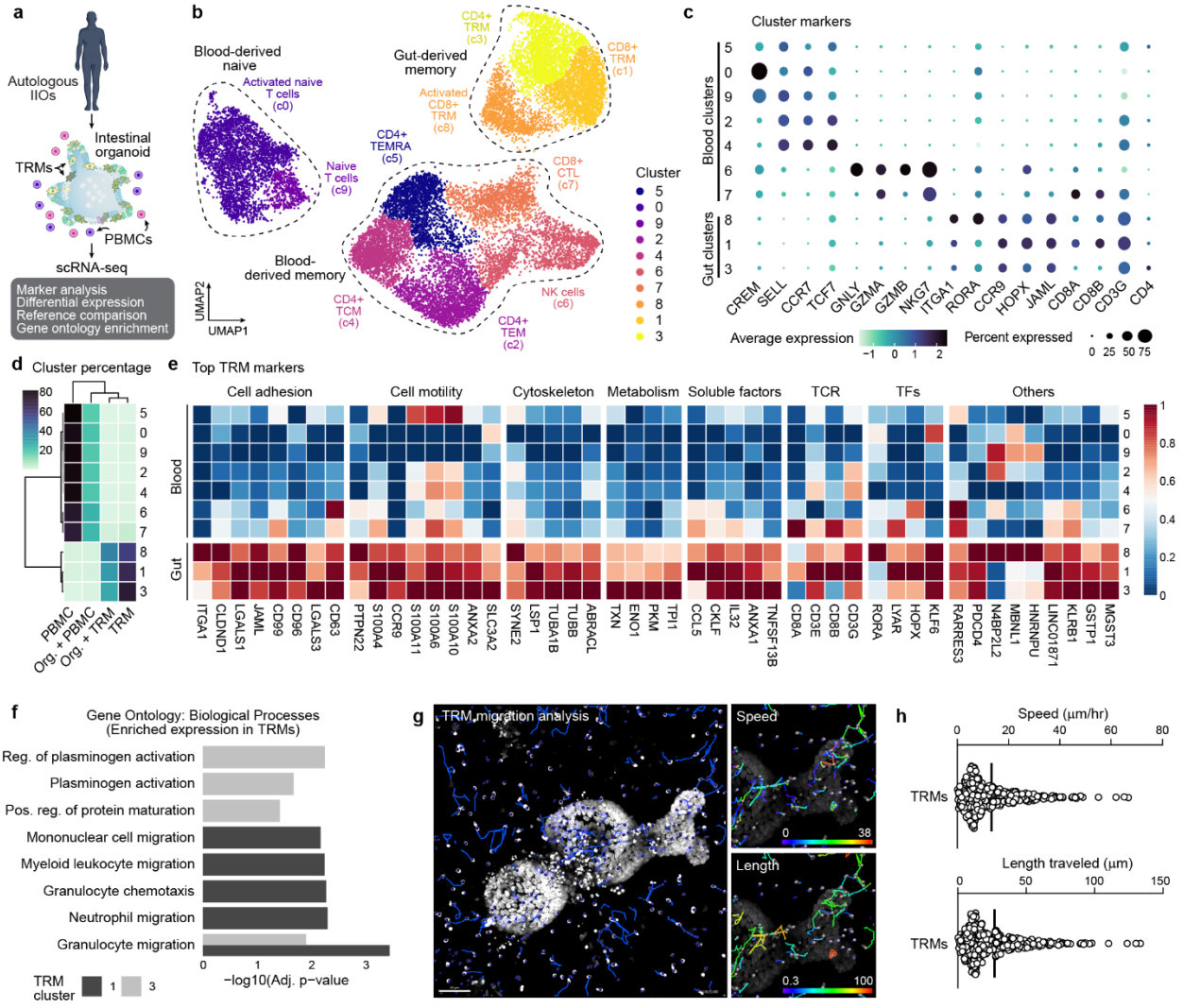

Figure 23: Tissue-resident transcriptomic signatures and migratory behavior underlie TRM epithelial insertion and IIO formation. *a, Overview of single-cell transcriptome analysis of IIOs containing patient-matched TRMs and*

PBMCs. b, Integrated UMAP embedding of transcriptome data shows 10 distinct cell clusters (colors, numbers) labeled based on analysis of marker genes. c, Dotplot summarizing marker gene expression across the different clusters. d, Heatmap representing proportional sample distribution in each cluster. e, Heatmap representing TRM-specific genes grouped by functional category. TFs transcription factors, TCR T-cell receptor. f, Barplot showing significantly enriched gene ontology (GO) biological processes of genes marking TRM clusters 1 (CD8+) and 3 (CD4+). g, Images showing migration analysis from IIO time-lapse imaging. Tracks are shown in blue (left) and colored by speed (top left) and length (bottom right). Nuclei are labeled with Hoechst (white). h, Distribution of TRM speed (top) and length traveled (bottom) from IIO time-lapse imaging.

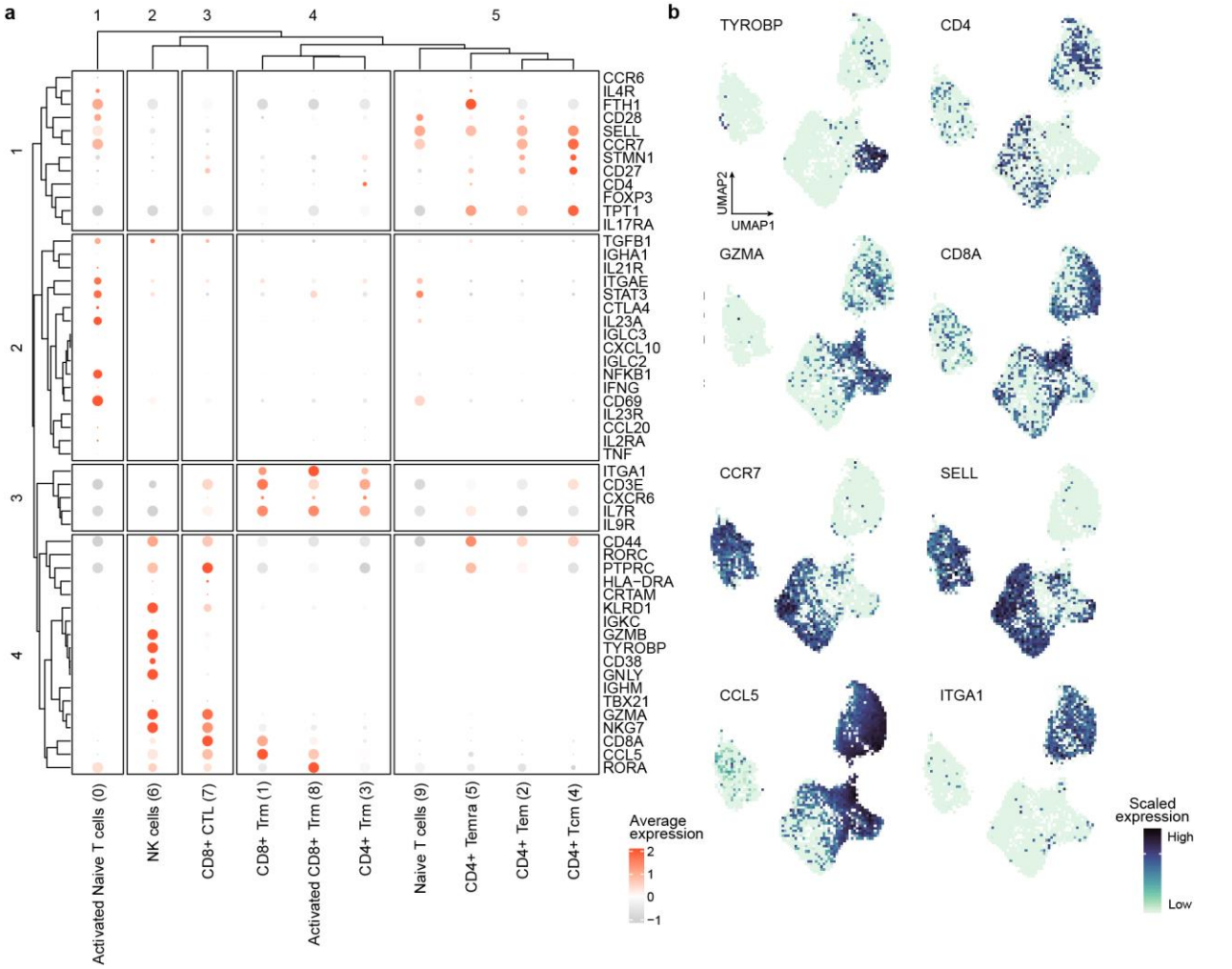

Figure 24: Immune cell cluster annotation. *a, Dotplots showing the z-scored average expression of curated T cell subset marker genes for each cluster introduced in Fig. 23b. The size of the dot encodes the percentage of positive cells within a cluster for the respective gene. Subsets were classified into CD4+ and CD8+ populations using the aggregated expression values for CD4 and CD8A. Activated populations were identified using the expression of RORA (Haim-Vilmovsky et al., 2021). Tissue-residency of memory cells was determined based on the expression of ITGA1 and ITGAE, which are expressed by most TRMs (Mackay et al., 2013). Final annotations were then designated based on the combinatorial expression of multiple markers. Source data detailing averaged expression values for T cell subset marker genes are provided in the source data file. b, Feature plot showing the scaled expression of representative marker genes.*

Further interrogation of the T cell populations based on previously published markers (Andreatta *et al.,* 2021; Luoma *et al.,* 2020; Szabo *et al.,* 2019; Wang *et al.,* 2022) revealed that TRMs, unlike their matched blood-derived counterparts, were transcriptomically defined by: (i) the absence of receptors necessary for lymph node homing (*SEL*, *CCR7*), indicative of their non-circulating tissue-residence status, (ii) intrinsically high expression of intestinal integration factors (*ITGA1*, *CCR9*, *JAML*), and (iii) a complete absence of cytotoxic granules (GZMA, GZMB, GNLY, NKG7) despite their function as highly differentiated effector T cells (Fig. 23c). We observed that populations c1, c3 and c8 were uniquely enriched in gut-derived TRMs (Fig. 23d).

To identify the main functional differences between TRMs and PBMCs, we considered the top differentially regulated TRM genes, and observed a dominance of genes governing cell adhesion, motility and cytoskeletal rearrangements (Fig. 23e). Gene ontology analysis suggested enrichment in transcriptomic programs related to immune cell chemotaxis and migration within TRMs compared with PBMCs (Fig. 23f), which may explain the different propensities for movement toward and integration within the epithelium between these two populations. Indeed, live imaging experiments in which donor-matched TRMs and PBMCs were tracked over time (Fig. 23g) showed a striking difference in morphologies and migratory behaviors between the two populations. Whereas PBMCs were largely static and morphologically round, TRMs exhibited asymmetric, elongated shapes with front-rear polarity, and migrated dynamically within both the epithelial layers and ECM, with speeds of up to 80 μm/h (Fig. 23h). TRM migration was not directional, suggesting that TRMs in this system integrate within organoids through random movement and encounters of epithelial cells, rather than through chemotaxis. Indeed, TRMs appeared to be as likely to move towards and within organoids as they were to move out and away. We note that intestinal organoids are a sterile system and the introduction of luminal microbes may lead to altered modes of migration and interaction with the epithelium, as described in mice (Hoytema van Konijnenburg *et al.,* 2017).

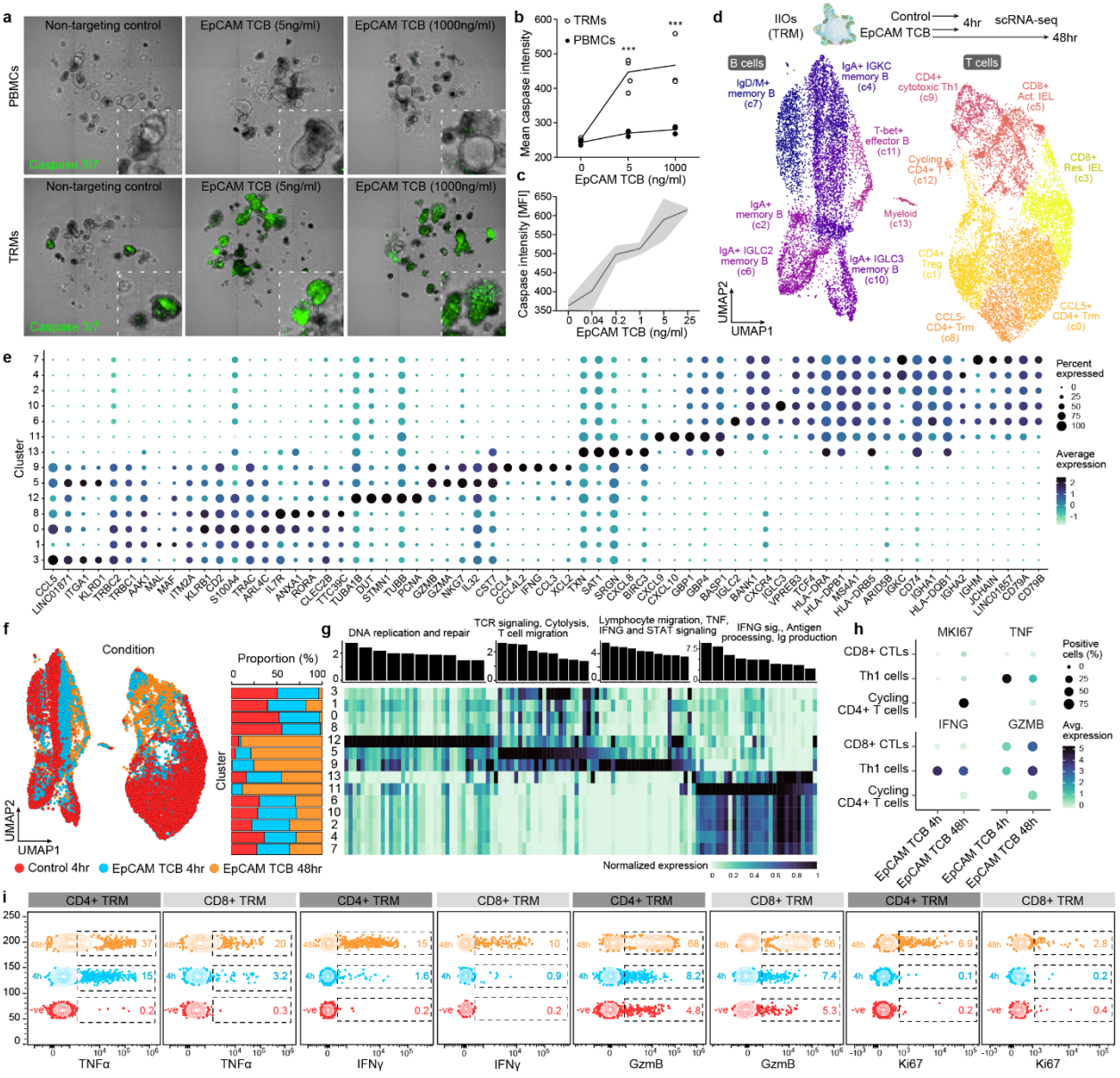

Figure 25: IIOs recapitulate clinically manifested intestinal inflammation associated with T cell bispecific antibodies (TCBs). *a, Representative images examining induction of green caspase 3/7 signal within IIO cocultures 24h after supplementation with EpCAM TCB. b, Quantification of the caspase 3/7 signal from (a). ***P < 0.001, two-way ANOVA with Sidak's multiple comparisons test correction. c, Quantification of the caspase 3/7 signal in IIO cocultures treated for 72h across a range of EpCAM TCB, n = 3. d, Single cell transcriptomic profiles of gut-derived immune cells from IIO model were integrated and grouped into 14 distinct cell states as represented by the colors in the UMAP embedding. e, Dotplot summarizing the expression patterns of representative genes across the clusters identified in (d). f, Integrated UMAP embedding (left) and proportional distribution (right) of gut-derived immune cells from IIO model colored by treatment and profiling time. g, Barplot showing significantly enriched GO biological processes for activated cell states (top) and heatmap showing average expression profiles of corresponding associated genes (bottom). h, Dotplot summarizing the expression pattern of representative genes involved in proliferation, signaling and cytotoxicity in the activated T cell populations as captured by scRNA-seq snapshots at different timepoints and treatment conditions. i, Flow cytometry plots visualizing expression of TNFα, IFNγ, GzmB and Ki67 across the different timepoints within CD4+ and CD8+ TRM cells isolated from IIO cultures.*

Next, we tested whether differential transcriptomes and migration behaviors between TRMs and PBMCs translated into differences in effector function within IIOs. In particular, we investigated whether IIOs can recapitulate clinical toxicities associated with cancer immunotherapy that manifest as severe intestinal inflammation and were not predicted by conventional preclinical models (Amann *et al.*, 2008; Kebenko *et al.*, 2018). We focused on solitomab – a bispecific T-cell engager intended to crosslink activated T cells to solid tumors

via EpCAM – which induced rapid and aggressive unintentional intestinal inflammation in patients, preventing escalation to therapeutic doses and ultimately leading to program termination (Elmentaite *et al.,* 2021). Given the rapid onset of the side effects, IELs localized within the basolateral epithelial junctions have been hypothesized to elicit the damage (Kebenko *et al.,* 2018). To assess whether IEL-containing IIOs could have predicted targeting of the healthy epithelium, we treated IIOs with an EpCAM-targeting T-cell bispecific (TCB) molecule at concentrations relevant to those detected in the serum of patients of the solitomab trial (Kebenko *et al.,* 2018).

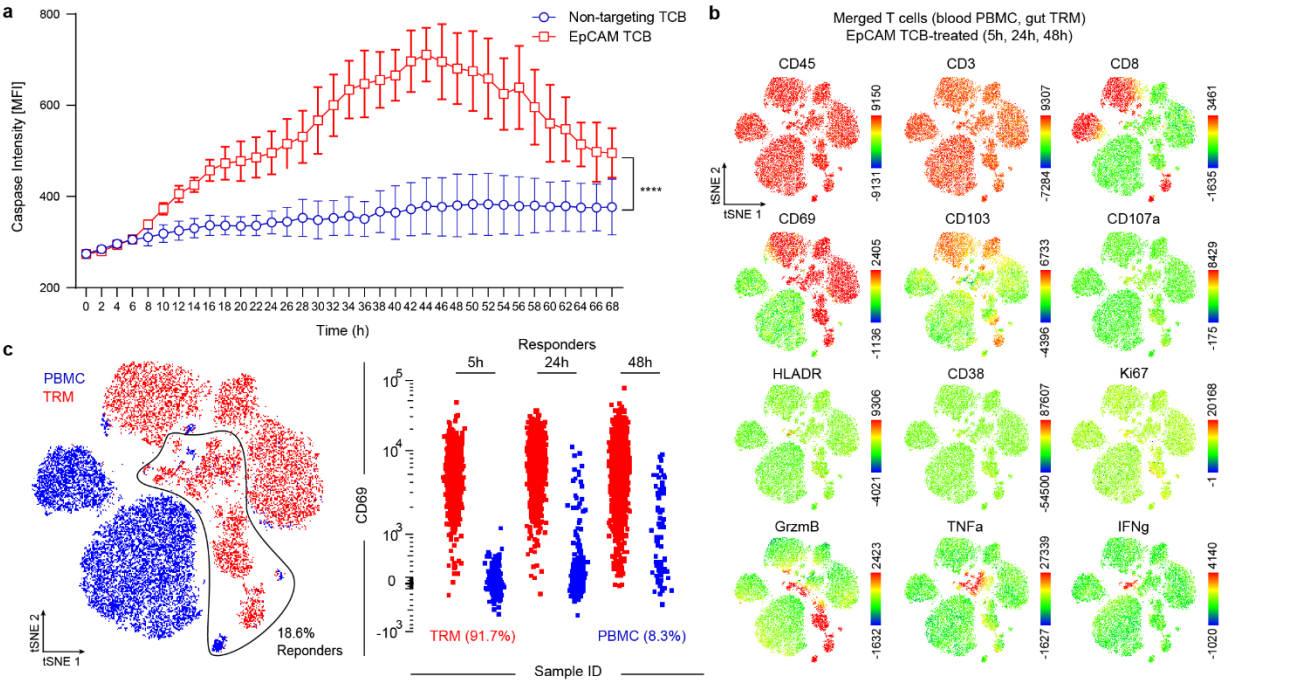

Figure 26: TRMs exhibit rapid and aggressive targeting of healthy epithelium following EpCAM-TCB treatment. *a, 8hourly quantification of caspase 3/7 signal in IIO cocultures for 68h treated with either 5 ng/ml EpCAM TCB or a non-targeting control molecule, n = 3, mean ± SD. ****P < 0.0001, T-test of the two AUCs. b, tSNE analysis of all T cells at all timepoints, derived from IIO cocultures with TRMs or PBMCs treated with 5 ng/ml EpCAM TCB. Plots display heatmaps for each of the 12 surface and intracellular markers assessed by flow cytometry. c, gating strategy for identifying responder cells (those that expressed TNFα, IFNγ or GzmB), and the ungating of the concatenated flow cytometry files to reveal the original source of responder T cells.*

Unlike organoids cultured with PBMCs, IIOs were aggressively targeted in a TCB-dose-dependent manner at concentrations as low as 40 pg/mL, as demonstrated by the detection of caspase 3/7 (Fig. 25a-c). A time-course of epithelial cell targeting showed induction of caspase by TRMs as early as 8h after treatment (Fig. 26a), mirroring clinical observations that were not predicted with classical *in vivo* models. We assessed T cell behavior at early (5h), mid (24h) and late (48h) timepoints by digesting and staining IIOs for surface and intracellular markers of T-cell activation and cytotoxicity (Fig. 26b). Identification of effector populations, based on the expression of TNFα, IFNγ and granzyme B, revealed that over 90% of responding cells were intestinal TRMs (Fig. 26c). This demonstrated that TRMs were approximately 10 times as likely to induce a detectable response to TCB treatment than their blood T-cell counterparts, emphasizing the necessity to include appropriate cell types within *in vitro* tissue-specific models.

The mechanisms of severe rapid-onset toxicities caused by T-cell targeted therapies are unclear, as patients who experience them are not biopsied in the acute phase. IIOs, which we show can recapitulate clinical outcomes, provide the opportunity for in-depth

analysis of the underlying cellular and molecular events. We used scRNA-seq to interrogate the transcriptomic dynamics underlying TCB-dependent TRM activity at the onset (4h) and peak (48h) of epithelial cell targeting. Lymphocyte populations within the integrated dataset were annotated using differential gene expression together with previously published signatures and surface markers (Andreatta *et al.,* 2021; Elmentaite *et al.,* 2021; Luoma *et al.,* 2020; Szabo *et al.,* 2019; Wang *et al.,* 2022), revealing diverse T cell, macrophage and B cell populations (Fig. 25d-e). TCB treatment induced a time-dependent shift in proportions of both the T cell and B cell states relative to the non-targeting control (Fig. 25f). This transition was driven by the emergence of several effector populations at both timepoints. Particularly prominent at 4h was a CD4+ T helper 1-like (Th1) population (c9) (Fig. 25f), characterized by rapid induction of *TNF* and *IFNG* signaling that became down-modulated over time (Fig. 25g-h). At 48h, we observed the emergence of an activated CD8+ IEL population (c5) (Fig. 25f), expressing genes related to cytotoxicity (such as *GZMB*), TCR signaling and T cell migration (Fig. 25g-h). Concurrently, a population of cycling (*MKI67*-expressing) CD4+ T cells (c12) and an activated population of B cells (c11) appeared, whereas the Treg population (c1) diminished (Fig. 25d-g). Importantly, key gene expression changes detected by scRNA-seq were mirrored by changes at the protein level, obtained by flow cytometry (Fig. 25i). In particular, we observed early induction of TNFα in CD4+ cells at 4h (corresponding to c9), whereas the cytotoxic granzyme B was upregulated at the 48h time point, consistent with the appearance of c5. Likewise, Ki67 was strongly upregulated within a subset of CD4+ cells at 48h, co-occurring with the appearance of c12 within the scRNA-seq analysis. IIO cell heterogeneity dynamics bear striking similarities to those observed within primary samples from patients experiencing spontaneous and immune checkpoint inhibitor (ICI)-induced intestinal inflammation. For example, the emergence of a cytotoxic CD8+ T-cell population was one of the main features of patients experiencing ICI-induced colitis (Luoma *et al.,* 2020; Sasson *et al.,* 2021). Likewise, Treg depletion and the appearance of an activated IFNγ-responsive B-cell population were reported in clinical samples from colitis patients (Mohammadnia-Afrouzi *et al.,* 2015; Smillie *et al.,* 2019). These similarities suggest that IIOs may be used to recapitulate and study intestinal inflammation in a tractable *in vitro* setting.

Next, we set out to chart the dynamics of clinically relevant populations that appear in IIOs, focusing first on the progression of CD8+ T-cell activation. Using Diffusion Maps (Hagverdi *et al.,* 2016) we computed a pseudo-temporal ordering of CD8+ populations (c3 and c5) (Fig. 27a, Fig. 28a) and observed a striking correlation with experimental time (Fig. 27b). This reconstructed activation trajectory allowed for characterization of the transcriptional dynamics underlying CD8+ TRM lymphocyte activation (Fig. 28c). In particular, we observed strong induction of glycolytic regulators *ENO1* and *HIF1A*, with concurrent suppression of *TCF7* and *ZBTB32* (Chen *et al.,* 2019; Finlay *et al.,* 2012; Gemta *et al.,* 2019; Shin *et al.,* 2017) to likely facilitate the appropriate metabolic profile for full CD8+ TRM cell cytotoxic activity. Simultaneously, *CCL5*, important for immune cell recruitment and early inflammatory responses (Zeng *et al.,* 2022), and *IL7R*, which captures proinflammatory signals to mediate cytotoxic activation (Micevic *et al.,* 2023), correlated with induction of cytotoxicity effector molecules *GZMA*, *GZMB* and *NKG7*. Sequencing of inflamed colonic biopsies of patients suffering from drug-induced colitis demonstrated the presence of both cytotoxic (CTL) and IEL CD8+ T cell populations (Luoma *et al.,* 2020). By cross referencing TCB-treated IIOs to this dataset, we found that IIO CD8+ T cells acquired gene signatures related to a cytotoxic and IEL state, mirroring those observed in clinical

samples (Fig. 28d-e). The concurrent increase in lymphocyte-epithelium association and cytotoxicity may underscore the severe clinical adverse events triggered by these molecules.

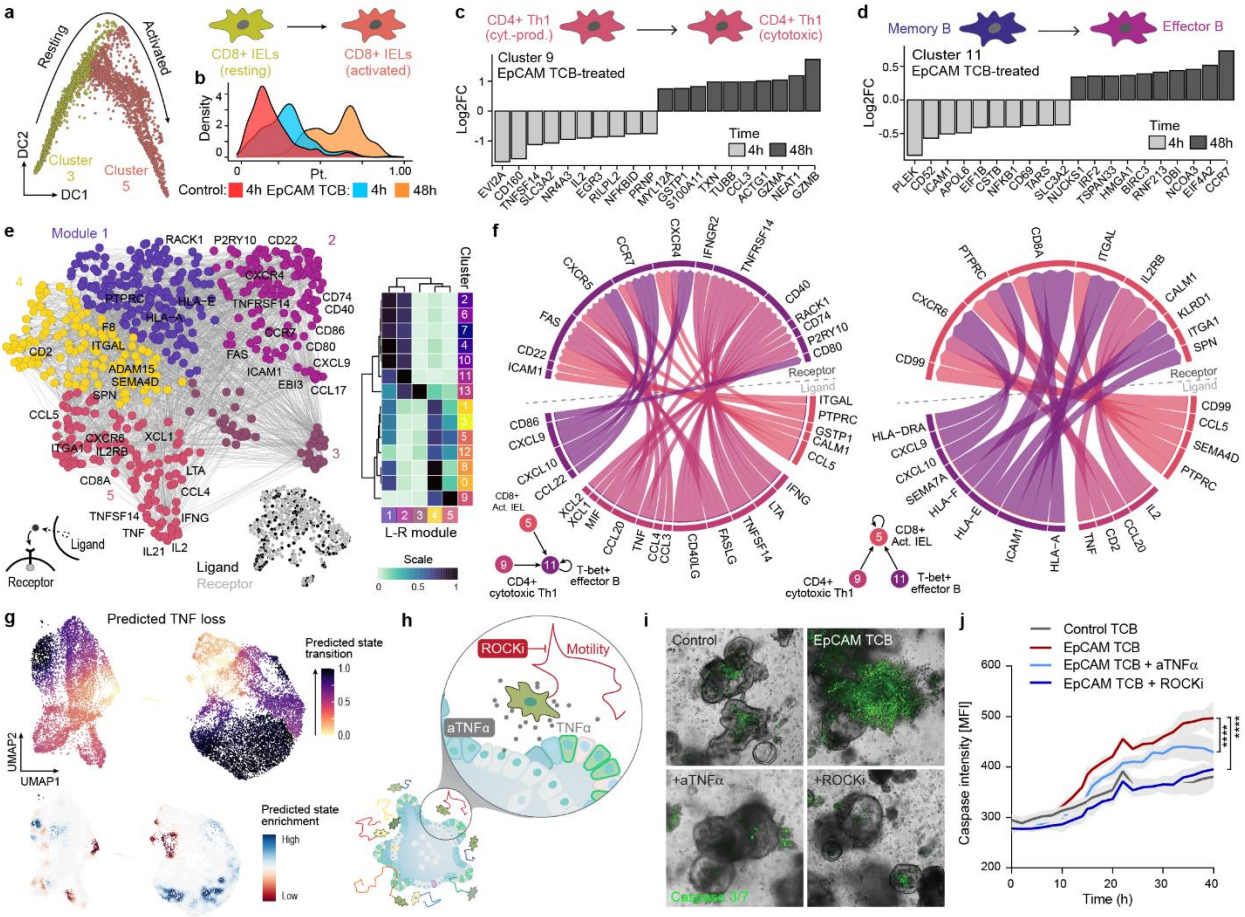

Figure 27: Transcriptomic analyses elucidate the immune dynamics underlying TCB-mediated inflammation and help identify mitigation strategies. *a, CD8+ T cell activation in IIO model was analyzed with diffusion maps. Plot represents CD8+ T cells on the first two diffusion components colored by cell state. b, Density plot showing distribution of CD8+ T cells along the reconstructed pseudotime (x-axis) grouped by treatment condition and time point. c-d, Barplot showing differentially expressed genes for CD4+ cytotoxic Th1 population (c9) (c) and T-bet+ effector B cells (c11) (d) at 4h (light grey) and 48h (dark grey) after EpCAM TCB treatment. e, Ligand-receptor pairing analysis of IIO immune cell populations. Ligands and receptors are colored based on co-expression module, with some representative genes labeled. Heatmap (right) shows the average expression of each gene within a module across each cell cluster. f, Circle plots describe signaling interactions received by the T-bet+ effector B cells (c11) (left) and the CD8+ Act. IELs (c5) (right). g, In silico perturbation analysis simulating the loss (KO) of TNF in IIO model treated with EpCAM TCB. Plots show predicted perturbation-induced state transition (top) or enrichment (bottom). Note that the activated immune cell states are predicted to fall back to homeostatic conditions. h, Schematic of experiments to inhibit TNFα signaling and cell migration. i, Representative images examining induction of green caspase 3/7 signal within IIO cocultures 40h after supplementation with either a non-targeting control TCB or 5 ng/ml EpCAM TCB with or without 1 mM Y27362 (ROCKi) or a TNFα blocking antibody. j, Bihourly quantification of caspase 3/7 signal in IIO cultures in treatment conditions, n = 3. ****P < 0.0001, T-test of the AUC compared to the EpCAM TCB condition.*

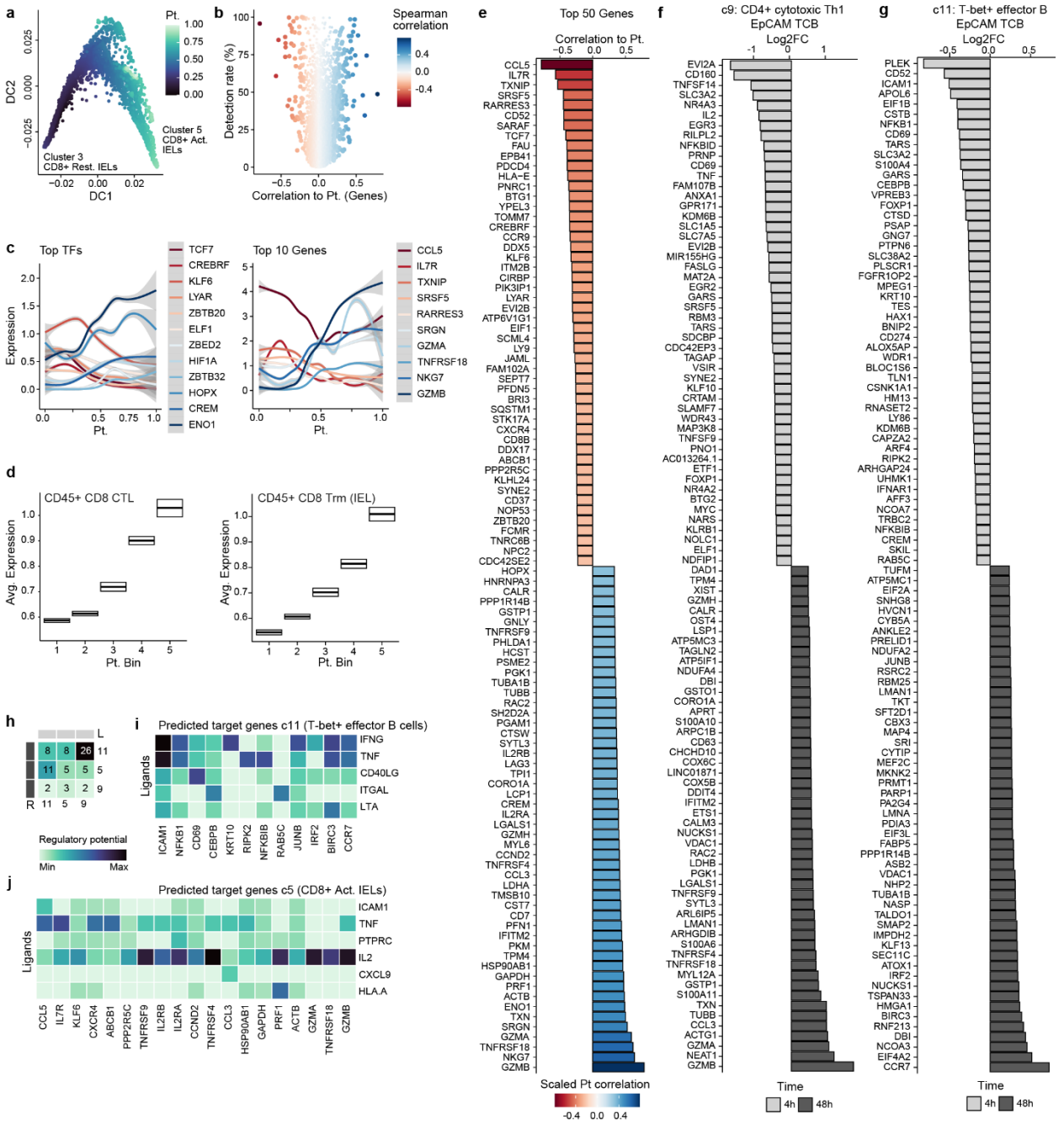

Figure 28: Extended analysis of cell states and interactions in IIOs after treatment. *a, Plot represents IIO CD8+ T cells on the first two diffusion components colored by reconstructed diffusion pseudotime. b, Volcano plot showing variable genes along reconstructed CD8+ T cell trajectory. x-axis represents spearman correlation value between gene expression and pseudotime value, y-axis represents detection rates of genes in the CD8+ T cell populations. c, Expression patterns of most variable TFs (left) and effector genes (right) along the reconstructed CD8+ T cell trajectory. d, Boxplot summarizing the expression pattern of CD8+ CTL (left) and CD8+ Trm IEL (right) gene signatures described in Luoma et al., 2020 along the reconstructed activation trajectory of IIO CD8+ T cells. x-axis represents 5 equidistant bins of the reconstructed pseudotime. e-g, Barplot showing differentially expressed genes in the CD8+ T cell trajectory (e), in the CD4+ cytotoxic Th1 population (c9) (f) and in the T-bet+ effector B cells (c11) (g) at 4h and 48h after EpCAM TCB treatment. h, Heatmap summarizes directed ligand-receptor pairing interactions of T-bet+ effector B cells (c11) and T cell populations (clusters 5 and 9) in the IIO model. i-j, Predicted regulatory potential of CD4+ cytotoxic Th1 cells (c9) ligands towards signature genes of T-bet+ effector B cells (c11) (i) and CD8+ activated IELs (c5) (j).*

Together with CD8+ CTLs, other populations displayed clinically relevant dynamics of early- vs. late- transcriptional hallmarks. Consistent with clinical reports (Riaz *et al.*, 2016), a Th1 population (c9) shifted from a cytokine- (*TNF*, *IFNG* and *IL2*)- producing state to a cytotoxic, *GZM*-producing state (Fig. 27c, Fig. 28f). Likewise, the early *IFN*-responsive B

cell population (c11) showed a transcriptional landscape distinct from that of the late, activated state (Fig 4d, Fig. 28g). We performed a receptor-ligand pairing analysis and inspected how activated phenotypes may emerge via intercellular signaling (Fig. 27e). Our model implicates Th1 cells (c9) as a major organizational hub, instructing B cells (c11) and CD8+ T cells (c5) through the secretion of numerous signaling factors (Fig. 27f, Fig. 28h). In particular, chemokines (*CCL3, CCL4, CCL5* and *CCL20*) and pro-inflammatory molecules (IFNG, CD40LG and *TNFSF14*) expressed by T cell clusters 5 and 9 likely encouraged close association with, and then full activation of B cells via reciprocal receptors (Fig 4f, Fig. 28i). Meanwhile, CD4 T cell (c9) expression of *TNF* corresponded to increased *CALM1* expression in activated CD8+ IELs (c5), potentially augmenting TCR-induced calcium signaling and full T-cell maturation (Trebak & Kinet, 2019) (Fig. 27f, Fig. 28j). Ligand-to-target signaling models and network propagation analysis (Browaeys *et al.,* 2020) reaffirmed these observations, suggesting that Th1-produced *IFNG* may mediate the up-regulation of activation-related genes within B cells, while *TNF* and *IL2* act in tandem to orchestrate cytotoxic CD8+ cell maturation (Fig. 28h-i).

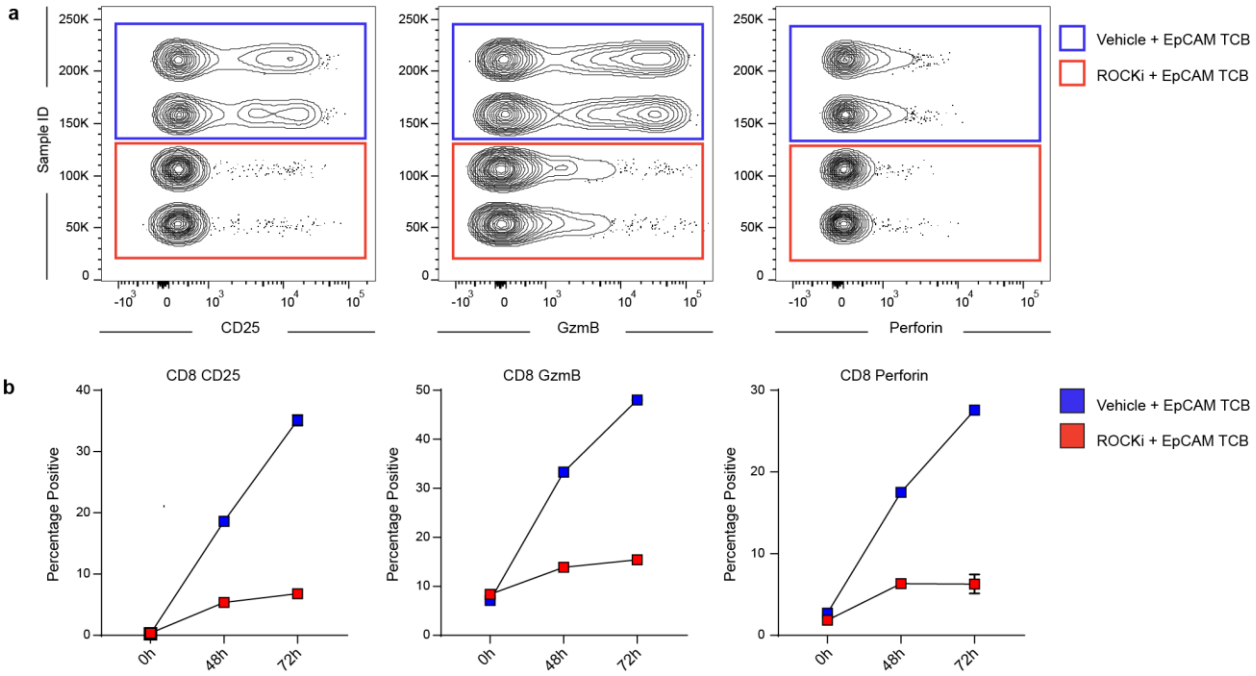

Figure 29: Inhibition of ROCK1/2 pathway quells TRM-driven intestinal inflammation. *a, flow cytometry plots comparing expression of CD25, GzmB and perforin in CD8 T cells isolated from IIO cocultures 72h after treatment with 5 ng/ml EpCAM-targeting T-cell bispecific antibodies with or without 1 mM Y27362 (ROCKi) b, Line graphs quantifying expression of CD25, GzmB and perforin in CD8 T cells isolated from IIO cocultures at baseline, at 48h and at 72h after treatment with 5 ng/ml EpCAM-targeting T-cell bispecific antibodies with or without 1 mM Y27362 (ROCKi).*

A key advantage of human model systems is their amenability to direct experimental manipulation as a means to define the roles of putative regulators. Given the function of TNFα as an instigator of inflammation, the effectiveness of TNFα-blocking antibodies in the treatment of autoimmune disease (Jang *et al.,* 2021), and its prominent early induction in our model (Fig. 25h-i), we investigated the role of this cytokine in promoting differentiation and activation profiles. *In silico* perturbation analysis simulating the complete removal of *TNF* from IIOs predicted that *TNF* depletion would prevent the emergence of activated immune cell populations and ultimately reduce the cytotoxic response (Fig. 27g). Antibody-neutralization of TNFα in IIOs confirmed these predictions, significantly reducing epithelial cell apoptosis following TCB treatment (Fig. 27h-j). Having confirmed the impact of

neutralizing a clinically-validated pathway, we used the transcriptomic data defining TRM identity (Fig. 23) to suggest novel TRM-specific factors that could be manipulated to quell unwanted TCB-mediated inflammation. Given the TRM cytoskeletal transcriptomic signature and their rapid locomotion within the ECM, we hypothesized that T-cell motility and cytoskeletal rearrangements may be in part responsible for the outcome. To test this hypothesis, we used the ROCK1/2 inhibitor (ROCKi) Y27632 to abrogate cell motility (Mrass *et al.,* 2017) within TCB-treated IIOs. Strikingly, we found that ROCK inhibition reduced epithelial cell apoptosis even more efficiently than TNFα blockade (Fig. 27h-j), simultaneously suppressing the induction of T-cell activation markers such as CD25, as well as cytolytic molecules such as perforin and granzyme B (Fig. 29).

We thus describe human intestinal immuno-organoids (IIOs), comprising human sample-derived intestinal epithelium and autologous tissue-resident lymphocytes (TRMs), a sub-population of which are directly integrated within the IIO epithelial barrier, reflecting IEL inclusion within the native intestine. IIO formation was driven by extensive TRM migration and interaction with epithelial cells, as orchestrated by TRM-enriched transcriptomic programs governing cell motility and adhesion. Crucially, IIOs formed upon coculture with TRMs, but not blood-derived lymphocytes, which lacked the migratory properties of the former and failed to interact with organoids.

The inclusion of a tissue-appropriate immune compartment extends the utility of organoids far beyond epithelium-centered questions and applications. We use IIOs to recapitulate intestinal inflammation caused by cancer-targeted bispecific antibodies (TCBs) in phase I clinical trials. IIOs treated with TCBs at clinically relevant concentrations undergo rapid apoptosis, consistent with early-onset diarrhea and epithelial lesions in patients (Kebenko *et al.,* 2018). Importantly, whereas cocultures with PBMCs have been shown to capture similar outcomes, effects become apparent only at concentrations 1000-fold higher than clinical doses and, even then, with a delayed onset [MFH, TR, MB, NG, manuscript in preparation]. Dissecting the transcriptomic changes induced by TCB treatment, we uncover that the adverse outcomes are underpinned by elaborate and dynamic inter-lineage immune interactions. The events we documented within our model closely parallel mechanisms associated with checkpoint inhibitor-induced intestinal inflammation and inflammatory bowel disease, which were identified using primary patient samples (Luoma *et al.,* 2020; Riaz *et al.,* 2016; Sasson *et al.,* 2021).

Aside from affording the possibility for real-time, dynamic observation of TRM-related processes and immune-epithelial interaction, our model provides the advantage of direct perturbation and hypothesis testing. Whereas multi-omics analyses of primary patient samples provide rich catalogs of differences between baseline and diseased states, the exact roles of differentially regulated parameters are difficult to ascertain without manipulating them in a relevant context. After demonstrating that IIOs capture known mechanisms of drug-induced inflammation and recapitulate well-described mitigation strategies, we use them to identify novel approaches for the management of TCB-mediated toxicities. Specifically, we find that blocking TRM motility through the Rho pathway helps dampen inflammation. Intriguingly, small molecules that target this pathway are being developed as fibrosis inhibitors for inflammatory bowel disease (Holvoet *et al.,* 2017). Our data suggest that an additional benefit of inhibiting Rho signaling could be the quenching of T-cell-driven inflammation, by reducing the motility, contractility and ability of patrolling IELs to respond to TCR stimulation and engage with epithelial cells. Bearing in mind that our

simple model recapitulates both the phenotypic outcomes and the multi-compartment cellular interactions that mediate them, IIOs can be instrumental in investigating tissue-resident immune responses in contexts far beyond drug-induced inflammation, including tumorigenesis, infectious and autoimmune diseases.

CHALLENGES AND FUTURE PERSPECTIVES

Positioned within barrier sites such as the skin, lungs, and intestines, immune cells assume a crucial role by providing localized defense against invading pathogens at their primary entry points. This strategic placement establishes a formidable protective barricade between the body and the external environment. The innate immune system employs specialized cells like macrophages and dendritic cells that seamlessly integrate into barrier tissues during their developmental stages. Conversely, T cells, pivotal orchestrators of adaptive immunity, populate these barrier regions upon recognizing antigens. Some of these T cells persist as tissue-resident memory (TRM) cells, a distinct subset formed after encountering site-specific infections caused by a diverse array of pathogens, including viruses, bacteria, parasites, and fungi (Cheroutre *et al.,* 2011; Masopust & Soerens, 2019). Delving into the mechanisms underlying the adaptation and persistence of TRM cells within human barrier sites becomes profoundly consequential for fostering robust protective immunity and preempting potential dysfunctions.

The realm of organoids, complex 3D tissue constructs cultivated from stem cells, has surfaced as a profoundly promising avenue spanning a myriad of biomedical research applications (Bartfeld *et al.,* 2015; Huch *et al.,* 2015; Lukonin *et al.,* 2020; Schutgens & Clevers, 2020; van de Wetering *et al.,* 2015; Yui *et al.,* 2012). As strides in organoid research forge ahead, the prospect of integrating an immune cell component into these structures emerges as a transformative opportunity for scrutinizing the safety of immunotherapies in the context of human biology (Neal *et al.,* 2018; Schnalzger *et al.,* 2019). Nonetheless, a constellation of challenges mandates thorough consideration to unlock the full potential of immune cell-infused organoids, thereby enabling comprehensive assessments of immunotherapeutic safety.

Sourcing and orchestrating the integration of immune cells into organoids represents a multifaceted challenge (Beura *et al.,* 2018; Swamy *et al.,* 2015). The diverse phenotypic and functional spectrum of immune cells demands meticulous differentiation protocols to faithfully capture this intricate diversity within organoids. Navigating the complexities of generating substantial quantities of functional immune cells within a three-dimensional context adds an extra layer of intricacy to the process. Immune responses are innately context-dependent and intimately entwined with the surrounding microenvironment (Poon *et al.,* 2023). Reproducing the precise physiological milieu necessary to elicit potent immune responses within organoids remains a formidable task. Complicating matters further, the vitality of organoids can be compromised over extended periods due to the absence of a functional vascular network, impairing sustained nutrient and oxygen exchange (Cakir *et al.,* 2019; Popova *et al.,* 2021). Variations in the lifespan and metabolic requisites of immune cells may further impact both the organoid's overall viability and the functionality of its immune compartment.

Innovations that integrate vascular networks into organoids hold immense potential, ushering in improved nutrient and oxygen exchange, thereby facilitating prolonged culture

and cultivating more physiologically relevant interactions between immune players and their target counterparts (Cakir *et al.,* 2019; Popova *et al.,* 2021). The advent of multi-organoid systems that harmoniously interlace various tissues, encompassing tumors, stroma, and immune constituents, holds the potential to yield a comprehensive panorama of the impacts of immunotherapies (Neal *et al.,* 2018; Schnalzger *et al.,* 2019). Pioneering avenues such as microfluidic methodologies (Brandenberg *et al.,* 2020; Chen *et al.,* 2017; Haase *et al.,* 2020; Horowitz *et al.,* 2021; Li *et al.,* 2014) and bioengineering strategies (Cakir *et al.,* 2019; Cakir *et al.,* 2022) appear as beacons of promise in this endeavor providing a unique assessment of immune cell extravasation and tissue adaptation in response to drug delivery or homing signal processes at specific clonal or subpopulation resolution. Innovative technologies that facilitate the deliberate spatial arrangement of distinct cell types, coupled with their orchestrated communication, are poised to amplify the precision of immune responses within organoids.

Establishing a robust and quantitative analytical framework to assess immune reactions within these systems emerges as a linchpin (Luoma *et al.,* 2020; Poon *et al.,* 2023; Szabo *et al.,* 2019). This encompasses vigilant tracking of cytokine profiles, markers of immune cell activation, and antigen-specific responses, all of which collectively furnish the bedrock for evaluating the safety of immunotherapeutic interventions. Propelling this endeavor forward, automation and high-throughput screening methodologies have the potential to expedite the evaluation of immunotherapeutic safety. By leveraging miniaturized organoid platforms in tandem with advanced single-cell genomics technologies and imaging modalities (Camp *et al.,* 2015; Kanton *et al.,* 2019; Mayr *et al.,* 2019; Quadrato *et al.,* 2017; Velasco *et al.,* 2019), the swift assessment of numerous immunotherapeutic agents and their dynamic effects on immune responses becomes an achievable reality.

In conclusion, while organoids harboring an immune cell compartment hold promise as models for assessing immunotherapy safety in humans, challenges related to immune system complexity, microenvironment mimicry, and functional integration must be addressed. Advances in co-culture techniques, vascularization, multi-organoid systems, and functional readouts offer exciting avenues for improving the fidelity and utility of immune cell-containing organoids in immunotherapy research. These efforts could revolutionize our ability to predict human immune responses and enhance the safety profile of novel immunotherapeutic interventions.

CONCLUSIVE REMARKS

The integration of organoids and single-cell genomics technologies heralds a transformative era in biomedical research, offering remarkable potential to address pressing therapeutic needs across diverse fields. These advancements promise to deepen our understanding of complex diseases, personalize treatments, and expedite drug discovery. However, this promising journey is not without its share of critical challenges.

In the realm of cancer research, patient-derived organoids hold immense promise as dynamic models that capture the intricacies of individual tumors. Their ability to recapitulate the tumor microenvironment and heterogeneity offers a platform for targeted drug development and precision medicine. Yet, standardizing organoid cultures and overcoming sourcing variability remain paramount hurdles. Additionally, there is a crucial need to bridge the gap between organoid modeling and the *in vivo* temporal evolution of cancer.

The incorporation of immune cells into organoids represents a frontier in immunotherapy research. These models can provide insights into immunotherapeutic safety and efficacy, paving the way for more precise treatments. Nevertheless, orchestrating immune cell integration, recreating physiological contexts, and addressing organoid viability challenges demand concerted efforts. The quest for accurate, high-throughput analytical frameworks to assess immune reactions within these systems further underscores the complexity of this endeavor.

As we forge ahead, it is clear that these challenges are not insurmountable obstacles but rather steppingstones toward unlocking the full potential of organoids and single-cell genomics technologies. Collaboration between researchers, clinicians, and engineers will be pivotal in developing innovative solutions. Automation, advanced scaffolding strategies, and scaling up production processes will contribute to more robust and reproducible models. Moreover, the creation of comprehensive organoid atlases, incorporating diverse data modalities, will provide holistic insights into human biology and disease.

In conclusion, the synergy between organoids and single-cell genomics technologies holds immense promise for revolutionizing biomedical research. These tools have the potential to reshape our understanding of diseases and accelerate therapeutic advancements. While challenges persist, they serve as beacons guiding us towards more precise, personalized, and impactful biomedical solutions. As we navigate this exciting frontier, it is with determination and collaboration that we will unlock the full potential of these groundbreaking technologies.

APPENDIX

METHODS FOR PDAC TUMOROID PROJECT

Establishment of cystic organoid and fibroblast cultures

The clinical specimens used to establish organoids and stromal cells were obtained from patients at the Kanagawa Cancer Center with informed consent after approval by the ethical review. Tumor tissue and healthy tissue were collected by surgical resection. The cancer cyst organoid (CCO) culture method from PDAC tumor specimens is briefly described below (Boj *et al.,* 2015). The surgical tissue is washed several times with Dulbecco's phosphate buffered saline (DPBS). The tissue was finely chopped using surgical scissors and a scalpel. The tissue was transferred to a 50 ml tube and washed again with DPBS. The washed tissue was digested with LiberaseTM (Roche) at 37 °C for 40-60 minutes. Tissues were enzymatically treated and then washed with DMEM containing 10% fetal bovine serum (FBS, Sigma) to stop the enzymatic reaction. The obtained pancreatic cancer cells were embedded in growth factor reduced (GFR) Matrigel (Corning) and cultured in the following complete medium. DMEM/F12(Thermo), Primocine (1mg/ml, InvivoGen), GlutaMAX (1x, Invitrogen), 1x B27(1x, Invitrogen), Gastrin, N-acetyl-L-cysteine (1mM, Sigma), Nicotinamide (10mM, Sigma), A83-01(Tocris, 0.5uM), Noggin (Peprotech, 0.1ug/ml), R-Spondin1 (Peprotech, 100ng/ml), Wnt3A(R&D, 50ng/ml), EGF (Peprotech, 50 ng/ml), FGF10 (Peprotech, 100ng/ml). Y-27632 (Sigma, 10uM) was added for only one day after starting the organoid culture, and on the following day, the cells were cultured in a complete medium without Y-27632. The medium was changed 2 to 3 times a week. For establishment of fibroblasts, healthy pancreatic tissue and cancer tissue were treated with Liberase and the collected cells were washed with DPBS several times. Subsequently, cells were suspended in Mesenchymal stem cell growth media (MSCGM, Lonza) and seeded on a culture plate. The media was changed 2-3 times a week. All cells were cultured under 5% CO2 in 20%O2 at 37°C.

Tumoroid culture method

To establish a stroma-rich pancreatic tumoroid, pancreatic CCO cells, fibroblasts and human umbilical vein endothelial cells (HUVECs) were separately expanded and cultured. Pancreatic CCO cells were incubated with Triple EX (Gibco) for 7 minutes, and fibroblasts and HUVECs were incubated for 3 minutes at 37°C to generate a cellular suspension. To stop the enzymatic reaction by Triple EX, the cells were washed with DMEM/F12 medium containing 10% FBS and 1% Penicillin-Streptomycin (P/S, Gibco). The obtained cells were counted separately, and then 3x10 ^ 4 cancer cells, 1.2x10 ^ 4 HUVECs, 8x10 ^ 4 fibroblasts were transferred to a tube coated with bovine serum albumin (1% BSA), mixed and centrifuged at 300 g. After removal of the supernatant, cell pellets were gently resuspended and 1.2 x10 ^ 5 cells were then seeded in 96 well plates coated with 50% Matrigel (Corning). The three types of cells made cell-cell interactions with each other and showed self organisation during the period of 24-48 hours. The reconstituted stromal-rich pancreatic tumoroid were cultured with 50% Endothelial Cell Growth Media (Lonza) and 50% DMEM/F12 medium. Culture mediums were exchanged every 24 hours. Tumoroid were cultured under 5% CO2 in 20% O2 at 37°C.

Generation of reporter lines

For live imaging, HUVECs were infected with retroviruses expressing Kusabira-Orange (KO) and cancer cells were infected with a lentivirus expressing enhanced green fluorescent protein (EGFP) (Koike *et al.,* 2004). Briefly, Human Embryonic Kidney (HEK) 283T cells were transfected with the retroviral vector pGCDNsam IRES-EGFP or KOFP (M. Onodera) for packaging at 293gag / pol (gp) and 293gpg (gp and VSV-G) to induce viral particle production. The culture supernatant of the retrovirus-producing cells was passed through a 0.45 mm filter (Whatman, GE Healthcare) and immediately used for infection. The firefly luciferase gene was subcloned into the CSII-EF-MCS-EGFP vector (RIKEN BRC) to generate the CSII-EF-Luc-IRES-EGFP construct. CSII-EF-Luc-IRES-EGFP plasmid and helper plasmid (293T cells were transfected with calcium phosphate using pCAG-HIVgp and pCMV-VSV-G-RSV-Rev, RIKEN BRC) to produce VSV-G pseudotyped lentivirus. The virus supernatant was recovered 46 hours after transfection, and filtered with a 0.45 μm filter. The virus supernatant was concentrated by ultracentrifugation.

Whole-mount clearing and FFPE tissue slice imaging

Tumoroids were washed several times with PBS and fixed with 200ul of 4% (wt/vol) paraformaldehyde (PFA). Tumoroids were incubated on a horizontal shaker at 4ºC for 24 hours. PFA was then completely removed and fixed tumoroids were washed several times with PBT buffer (0.1% Tween (vol / vol)). Tumoroid washing buffer (TWB: 100ml of PBS with 0.2 g of BSA and 0.1% Triton X-100) was added to the wells and incubated on a horizontal shaker at 4ºC for 1 day to block tumoroid. The next day, the blocking reagent was completely removed from the well, and then 100 ul of TWB with primary antibodies(1/100) was added to the wells and incubated on a horizontal shaker at 4ºC for 2 days. After immuno-labeling the tumoroid with the primary antibody, these reagents were removed from the wells, and then fresh TWB was added to the wells and was incubated on a horizontal shaker at 4ºC for 2 hours. This process was performed 3 times to completely remove the antibodies from organoids. After the tumoroid were sufficiently washed with TWB, 100ul of TWB with secondary antibodies(1/200) was added to the wells and incubated on a horizontal shaker at 4ºC for 1 day. After immuno-labeling the tumoroid with the secondary antibody, the secondary antibodies were removed from the wells and then fresh TWB was added to the wells and washed three times. Subsequently, 50ul of the fructose–glycerol clearing solution(Dekkers *et al.,* 2019) was added to the well and incubated on a horizontal shaker at 4ºC, overnight. Cleared organoids were placed on a glass slide or in a glass-bottom plate and imaged on a spinning disc confocal microscope (Olympus SpinSR10 spinning disk confocal super resolution microscope, objective x10,x20,x30,x40,x60). In immunofluorescence staining (IF) for FFPE tissue slide, PDAC tumor tissue was fixed with 4% PFA, embedded in paraffin and cleaved. A cutted tissue section was deparaffinized with xylene and rehydrated with a gradual alcohol. After heating with a citric acid buffer, antigen recovery is complete. The tissues were incubated with primary antibodies at 4ºC, overnight. The next day, the tissue was washed with PBS, 3 times and then incubated with secondary antibodies(1/200) at room temperature 1h. After antibodies were washed with PBS, it was images with Slide scanner. We used the following antibodies: anti-GFP (1:400; Abcam, ab13970), anti-Cytokeratin 7 (1:00; Agilent Technologies, M701829-2), anti-Cytokeratin 19 (1:100; Abcam, ab7754), anti-PPARG (1:100, Thermo Scientific, PA3-821A), anti-Collagen I (1:100; Abcam, ab34710), anti-Fibronectin (1:100, Abcam, ab2413), anti-AKAP12 (1:100, Thermo Scientific, PA5-52281), anti-Trefoil Factor 3 (1:100, Abcam, ab108599), anti-

Lipocalin-2 (1:100, Abcam, ab23477), anti-E-cadherin (1:100, R&D Systems, AF748), anti-Syndecan-1 (1:100, Abcam, ab128936), anti-MIF (1:100, Abcam, ab187064), anti-Collagen III (1:100, Abcam, ab6310), anti-AGR2 (1:100, Sigma-Aldrich, HPA007912), anti-CEACAM6 (1:100, Thermo Scientific, MA5-29144), anti-MUC1 (1:100, Thermo Scientific, MA5-11202), Donkey anti-Goat IgG (H+L) Highly Cross-Adsorbed Secondary Antibody, Alexa Fluor Plus 405 (1:200, Thermo Scientific, A48259), Donkey anti-Mouse IgG (H+L) Highly Cross-Adsorbed Secondary Antibody, Alexa Fluor Plus 555 (1:200, Thermo Scientific, A32773), Donkey anti-Rabbit IgG (H+L) Highly Cross-Adsorbed Secondary Antibody, Alexa Fluor Plus 647 (1:200, Thermo Scientific, A32795), Goat Anti-Armenian hamster IgG H&L (1:200,Abcam, ab173004), Goat anti-Chicken IgY (H+L) Cross-Adsorbed Secondary Antibody, Alexa Fluor Plus 488 (1:800, Thermo Scientific, A32931), Molecular Probes DAPI (4',6 Diamidino 2 Phenylindole, Dihydrochloride) (1:500, Thermo Scientific, D1306).

SDC1 inhibition assays

For antibody treatment with anti-SDC1 (Abcam) on long-term cultured tumoroid, the co-cultured culture medium was completely removed from the wells and changed to 200ul of the co-cultured medium with 20ul anti-SDC1 added in the wells. The tumoroid were cultured under 5% CO2 in 20%O2 at 37°C. The antibody mixed medium was changed daily with a fresh one and the tumoroid had imaging after 5 days. A 200ul medium containing 20ul of isotype control antibody (Mouse IgG1, kappa monoclonal, Abcam) was used as a control medium.

Single-cell RNA-seq experiments

All samples were dissociated to single cells by specific enzymatic treatment. The cultured medium for stroma-rich tumoroid was removed from the wells and tumoroids washed three times with 1xDPBS. The tumoroids were collected in 5 ml tubes, after the DPBS was completely removed from the tube, TrypLE™ Select (Thermo) was added and incubated at 37ºC for 8 minutes(Gehart *et al.,* 2019). After the incubation step, tumoroids were further dissociated by trituration. This incubation and trituration process was repeated 3 times to obtain a single cell suspension. The enzymatic dissociation was stopped by addition of cold BE-PBS (Cold PBS 1 ml with 0.04% BSA / (0.1 mM EDTA)) and remaining cellular clumps were removed by using 70um and 40um strainers. Fibroblasts and HUVECs were cultured on a 10 cm dish and dissociated to a single cell suspension using the same procedure as described above. Single cell suspensions were adjusted to an appropriate concentration to obtain approximately 2000-10000 cells per lane of a 10x Genomics microfluidic Chip G. Libraries were generated using 10x Genomics 3’ Gene Expression Kit (v3.1), following recommended protocol, and subsequently sequenced on NextSeq500, using 28-9-0-91 Read Configuration, as recommended by for Single Index libraries.

Single-cell RNA-seq data preprocessing

CellRanger (v3.1.0, 10x Genomics) was used to extract unique molecular identifiers, cell barcodes, and genomic reads from the sequencing results of 10x Chromium experiments. Then, count matrices, including both protein coding and non-coding transcripts, were constructed aligning against the annotated human reference genome (GRCh38, v3.0.0, 10x Genomics). In order to remove potentially damaged or unhealthy cells and improve data quality, the following filtering steps were performed in addition to the built-in CellRanger filtering pipeline. Cells associated with over 20,000 transcripts, usually less

than 1% of the total number of samples, were removed. Cells associated with a low number of transcripts (<1% of the total number of samples) were removed. Cells with over 15% of mitochondrial transcripts were removed. Transcripts mapping to ribosomal protein coding genes were ignored. Cells with <800 unique transcripts (<1% of the total number of samples) were removed together with transcripts detected in less than 10 samples.

Normalization with Seurat

For normalization and variance stabilization of each scRNA-seq experiment's molecular count data, we employed the modeling framework of SCTransform in Seurat v3 (Hafemeister & Satija, 2019). In brief, a model of technical noise in scRNA-seq data is computed using 'regularized negative binomial regression'. The residuals for this model are normalized values that indicate divergence from the expected number of observed UMIs for a gene in a cell given the gene's average expression in the population and cellular sequencing depth. Additionally, a curated list of cell cycle associated genes, available within Seurat, was used to estimate the contribution of cell cycle and remove this source of biological variation from each dataset in order to increase the signal deriving from more interesting processes. The residuals for the top 2,000 variable genes were used directly as input to computing the top 100 Principal Components (PCs) by PCA dimensionality reduction through the RunPCA() function in Seurat. Corrected UMI, which are converted from Pearson residuals and represent expected counts if all cells were sequenced at the same depth, were log-transformed and used for visualization and differential expression (DE) analysis. Primary PDAC biopsy samples as well as metastatic PDAC biopsy samples were processed as described above. However, they did not undergo any cell filtering as quality control steps had already been performed in the respective published studies.

Doublet removal with DoubletFinder

For each scRNA-seq experiment DoubletFinder (McGinnis *et al.,* 2019) was used to predict doublets in the sequencing data. In brief, this tool generates artificial doublets from existing scRNA-seq data by merging randomly selected cells which are then pre-processed together with real data and jointly embedded on a PCA space that serves as basis to find each cell's proportion of artificial k nearest neighbors (pANN). For this step we restricted the dimension space to the top 50 PCs. Finally, pANN values are rank ordered according to the expected number of doublets and optimal cutoff is selected through ROC analysis across pN-pK parameter sweeps for each scRNA-seq dataset; pN describes the proportion of generated artificial doublets while pK defines the PC neighborhood size. In order to achieve maximal doublet prediction accuracy, mean-variance normalized bimodality coefficient (BCmvn) was leveraged. This provides a ground-truth-agnostic metric that coincides with pK values that maximize AUC in the data. To overcome DoubletFinder's limited sensitivity to homotypic doublets, we consider doublet number estimates based on Poisson statistics with homotypic doublet proportion adjustment assuming 1/50,000 doublet formation rate the 10x Chromium droplet microfluidic cell loading.

Data integration

Individual datasets, after preprocessing and doublet removal, were aggregated according to specific criterias (e.g. patient id, timepoint, culture condition) and went through an additional step of mild processing in order to mitigate technical confounding factors, which also served as means for selection of a set of meaningful 2,000 most variable global

genes prior to data integration. Integration of different conditions (cell lines and timepoints) was performed using the log-normalized corrected UMI count data. We used the first 30 PCs and the Pearson residuals to integrate the different timepoints (or cell lines) in the datasets using the Cluster Similarity Spectrum method (CSS) (He *et al.,* 2020). In brief, clustering is applied to cells within each sample label separately and similarities, by Spearman correlation, of one cell to those clusters are calculated and normalized. Integration of primary and metastatic datasets was performed Harmony (Korsunsky et al. 2019) algorithm. In particular, we used the RunHarmony() function on the first 30 PCs and other default parameters which initiates an iterative process of soft cluster assignments to group cells from different samples based on biological similarities. To obtain a two-dimensional (2D) representation of the data we performed Uniform Manifold Approximation and Projection (UMAP (McInnes *et al.,* 2018) using RunUMAP() with default parameters on the CSS matrix or the first 30 Harmony vectors. Integrated datasets were then clustered according to the shared neighborhood graph on lower dimensional space using the Louvain algorithm (Blondel *et al.,* 2018) through either the Seurat function FindClusters() with resolution 0.2.

Pseudotime reconstruction

PCA is an eigenvector-based multivariate analysis that defines a new orthogonal coordinate system that optimally describes variance in a dataset. It learns a linear transformation where the PCs form an orthogonal basis for the features that are uncorrelated (Bengio *et al.,* 2013). By construction, this transformation can encode the original data in a latent (lower dimensional) space concentrating much of the signal into the first few principal components and achieve a higher signal-to-noise ratio while minimizing the total squared reconstruction error. Given its strength, we sought at using PCA to learn time-dependent variability in our tumoroid system and optimally describe heterogeneity in the scRNA-seq time course data by reconstructing a differentiation trajectory for each cell type in the 2D PCA space. Cells were subsequently aligned along that trajectory.

Dynamic Time Warping (DTW) analysis

DTW is an algorithm that enables measuring the similarity between two sequences independent of non-linear variations. The algorithm computes the optimal match path that minimizes the sum of absolute differences between pairs of mapped elements. We used this feature to align the tumoroid CAF state trajectories to the reference primary CAF state trajectory by invoking the dtw() function, as implemented by dtw (Giorgino, 2009) package in R. with default parameters.

CAF-tumor communication

To investigate ligand-receptor (LR) mediated cell-cell communications during cancer progression in our multi-lineage tumoroids, we focused on the signals exchanged between CAF and cancer cells. For this analysis we extracted genes labeled as either ligands or receptors from curated databases (Browaeys *et al.,* 2020) and required that genes were expressed in at least 10 percent of either CAF or cancer cells. We then computed a UMAP embedding on LR genes and clustered them into modules that were assigned to each cell type, based on average expression score, in order to retrieve directional information about the signal exchange. Among all significant LR pairs, we focused first on CAF to cancer signaling, thus considering CAF as the signal source, expressing ligands, and cancer as the signal target, expressing receptors. We then looked also at signals being delivered by

cancer to CAF receptors. In order to model dynamic communication during cancer progression we emphasized LR pairs characterized by significant incremental expression change along pseudotime alignment. This analysis identified ligand-receptor (LR) pairs which significantly co-expressed along CAF-cancer trajectories, and therefore potentially mediated the communications between cell populations. A similar approach was followed to uncover signal exchanges in the microenvironment of primary PDAC resection data from Peng et al. Here, LR genes were required to be expressed in at least 10% of any of the 20 cell clusters we identified and, after UMAP embedding and module detection, they were assigned to specific cell types of the primary tumor samples (cancer, CAF, endothelial cell or immune cell).

Functional enrichment analysis

To understand mechanisms underlying phenotypes in our data, differentially expressed genes were analyzed for cancer hallmark and gene onthology biological process (GOBP) enrichment using one-sided hypergeometric testing. P-values were adjusted for multiple testing hypotheses by the Bonferroni method and only enrichment results below a 5% significance level threshold were considered. The hallmarks are a collection of curated gene sets, within MSigDB, refined to convey a specific biological state or process and display coherent expression (Liberzon *et al.,* 2015). Cell populations were evaluated for over representation or change in biologically related functional gene sets. For this analysis we only considered hallmarks consisting of sets with more then 10 but less then 300 mapped genes.

Gene regulatory network inference in tumoroids

To gain biological insights into mechanisms driving time-dependent cellular heterogeneity in pancreatic cancer, we resorted to utilizing the Single-Cell rEgulatory Network Inference and Clustering (SCENIC) workflow (Aibar *et al.,* 2017). This is a computational method to infer gene regulatory networks (GRNs) and cell types from single-cell RNA-seq data. In brief, we initialized SCENIC options by selecting the latest versions (v9) of two motif annotation datasets, 500 base pairs (bp) upstream and 100 bp downstream of transcription start site (TSS) as well as 10k bp centered TSS, on human genome (hg38) and 20 processing units; otherwise default parameters. To infer potential transcription factor targets, we imputed Pearson residuals of the most variable genes expressed in at least 10% of the cells and built a co-expression network via GENIE3 (Huynh-Thu *et al.,* 2010) with default parameters. GENIE3 is a Random Forest based method capable of detecting non-linear dependencies. In order to distinguish activation from repression we took advantage of the Spearman correlation between transcription factors and respective target genes. Finally, the activity of the inferred GRNs was computed by aggregating the expression of the target genes within each single cell. We then identified top variable GNRs by assessing their activity along the pseudotime.

Bulk RNA-seq data processing

Pancreas adenocarcinoma (PAAD) related samples from The Cancer Genome Atlas (TCGA) were downloaded via the Genomic Data Common (GDC) website. The R package TGAbiolinks was used to connect to GDC data transfer tool client and GDC API in order to query and download the raw gene expression profiles, metadata and available clinical data for 177 tumor samples as well as 4 normal pancreatic tissue samples. The data was filtered

by removing subsequent occurrences of probes matching the same gene symbol as well as probes matching no known genes at all. Raw HTSEQ counts data was then normalized for sequencing depth using estimateSizeFactors() and variance-stabilized through regularized-logarithm transformation to remove spurious effects from aberrant gene counts with rlog() function in DESeq2 (Love *et al.,* 2014). For the regularized-logarithm transformation the blind parameter was set to false. This, to ensure that variables in the design formula will not contribute to the expected variance-mean trend of the experiment; otherwise default parameters were used.

Survival analysis

Individual samples were divided into higher and lower categories based on normalized expression of the gene of interest. A quartile cutoff based on expression was considered to group the samples into two categories. The long-term survival probability was analyzed by utilizing the Kaplan-Meier survival plot. Log-rank test (Harrington and Fleming, 1982), as implemented within the survdiff() function, was applied to assess the difference between the cohorts. Analysis of survival time was performed using the survival (Therneau & Grambsch, 2000) package in R statistical software.

Differential expression analysis

Gene differential expression (DE) analysis between distinct cell populations in scRNA-seq data was assessed by performing Wilcoxon rank sum tests and auROC analysis as implemented by Presto (Ilya *et al.,* 2019) package in R. Log-transformed corrected UMIs were used as input for the DE statistical tests, and genes were called differentially expressed if associated adjusted p-value (Bonferroni method) was lower than 0.05, AUC value was above 0.6 and log fold change was greater than 0.15. In addition, we also set thresholds on detection rates of DE genes. In particular, a given gene was assigned as over-expressed in the analyzed group if it was detected in at least 30% of the samples of that group, while the detection rate in the background samples was at most 70% of the detection rate of the analyzed group. Differential expression analysis on bulk RNA-seq data was performed in accordance with the DESeq2 pipeline on row counts with DESeq() function and default parameters. Genes were then considered up-regulated if they were assigned an adjusted p-value below 0.05 and a log fold change greater than 0.5.

Association to worse survival phenotype

In order to link tumoroid cell populations to a clinically relevant phenotype and identify critical cell subpopulations that can drive survival outcome in PDAC, we resorted in using Single-Cell Identification of Subpopulations with Bulk Sample Phenotype Correlation (Scissor). In brief, we employed the bulk RNA-seq PDAC samples from TCGA with associated clinical survival time annotations and our integrated normal fibroblast- and CAF-cultured tumoroid scRNA-seq dataset introduced in Fig. 12. The reasoning behind using both tumoroid models was to understand and validate differential association to clinical outcomes arising from the culture systems. Scissor performs a quantification of the correlation between single-cells and bulk samples followed by the optimization of a regression model, constrained by a graph regularization and a sparse penalty. We used Cox proportional hazard regression to determine the association of our single-cells with survival time based on expression of a common gene set between the tumoroid and bulk samples, otherwise Scissor analysis was performed with default parameters. The coefficients in a Cox

regression relate to hazard. In particular, a positive coefficient indicates worse prognosis conversely a negative coefficient relates to a protective effect. Single-cells having a coefficient equal to zero are indicated as 'unselected' as they do not show a strong correlation to the phenotype. Finally, to control for false associations we performed a reliability significance test with 3-fold cross-validation (CV) and 100 random permutations of the bulk samples' phenotype annotations as described in the Scissor study.

Reference-based annotation

Reference-based integration was applied to SCTransform-normalized datasets by specifying the integrated primary cancer cell (Peng *et al.,* 2019) and PDAC metastatic cells (Raghavan *et al.,* 2021) dataset as the 'reference' while the integrated tumoroid cancer cell dataset introduced in Fig. 19 was designated as 'query'. This workflow identifies anchors between reference-query pairs and projects the PCA structure of the reference onto the query. Specifically, we applied FindTransferAnchors() function in Seurat by specifying reference and query arguments as well as leading 30 PCs (dims argument). After finding anchors, we used the TransferData() function to classify the query cells based on reference data tissue labels. TransferData() returns a matrix with predicted IDs and prediction scores, which we used to assess similarity between tumoroid cancer cells and PDAC metastasis cancer biopsy cells.

METHODS FOR IIO PROJECT

Isolation of tissue-resident memory cells and donor-matched crypts for organoid generation

Human intestinal tissue samples and annotated data were obtained and experimental procedures performed within the framework of the non-profit foundation HTCR (Munich, Germany) including informed patient's consent. Tissue was first processed by removing the underlying muscularis, serosa and fat from the basal side of the tissue by pinching with forceps and trimming away with scissors. The remaining mucosal tissue was washed with PBS (supplemented with penicillin [1500U/ml], streptomycin [1500 µg/ml], gentamicin [500 µg/ml]) multiple times before using a scalpel to remove excess mucus from the luminal side and blood vessels from the basal side. Trimmed, cleaned tissue was then cut into square explants approximately 5 mm by 5 mm with a scalpel. Two methodologies were used to isolate intestinal tissue-resident memory cells. For the scaffold-based egression protocol (adapted from29) each explant was loaded onto a 9x9x1.5 mm tantalum-coated carbon based scaffold (Ultramet), and cultured in 24-well plates containing 1 mL of cytokine-free, cell culture media (RPMI 1640 10% FCS, penicillin [1500U/ml], streptomycin [1500 µg/ml], gentamicin [500 µg/ml] and amphotericin [12.5 µg/ml]). 24 hours later, scaffolds and tissue were removed, and egressed cells were harvested from the bottom of the culture well via pipetting. For the enzymatic digestion protocol, explants were digested using the Human Tumour Dissociation Kit with the gentleMACS Octo Dissociator program 37C_h_TDK_1 (Miltenyi Biotec), as per the manufacturer's instructions, reducing Enzyme R content by 80% to minimize surface antigen cleavage. Cells were then counted, phenotyped by flow cytometry and frozen prior to use in downstream applications. To isolate donor-matched crypts for organoid generation, a lamelle was scraped over a 3 cm2 piece of trimmed tissue to remove intestinal protrusions/villi. Tissue was then incubated in ice cold PBS + 10 mM EDTA with vigorous shaking for 30 minutes to break down epithelial cell junctions. The tissue was retrieved and a lamelle was used to scrape off crypts into DMEM-F12 1% BSA collection

buffer. Crypts were centrifuged, resuspended in Matrigel Matrix GFR (Corning) and cultured in IntestiCult™ Organoid Growth Medium with 10 uM Y-27362 (STEMCELL Technologies).

Preparation and culture of intestinal immune-organoids

In-passage organoids, approximately 2 weeks to 1 month after initial isolation, were cultured for 4 days post-split in IntestiCult™ Organoid Growth Medium and then switched IntestiCult™ Organoid Differentiation Medium (STEMCell Technologies) for 72 hours to promote epithelial stem cell differentiation. On the day of coculture setup, media was aspirated from the well, organoids were washed with PBS and treated with ice cold Cell Recovery Solution (Corning) for 40 minutes. The solution was collected and centrifuged to harvest the liberated organoids. Donor-matched TRM or PBMCs were thawed, and combined with the liberated organoids and resuspended in either Matrigel Matrix GFR (Corning), or if the cocultures were to be formalin-fixed, a 50:50 mixture of Matrigel Matrix GF and 4 mg/ml Cultrex Rat Collagen I (R&D Systems). For time-lapse live imaging experiments, immune cells were labelled with CellTrace Far Red or CFSE (ThermoFisher) prior to mixing with organoids. Organoids were used at a concentration double to their standard passaging density, whereby a 20 ul dome was harvested and resuspended in 10 ul of matrix, while immune cells were used at a density of 15,000 cell per mm3 of resuspension volume. A 50:50 ratio of RPMI 1640 10% FCS and IntestiCult™ Organoid Differentiation Medium was used for culture. For assessment of TCB-based cytotoxicity, an EpCAM-CD3 bispecific antibody, or its associated non-targeting control (which contains a CD3 binder on one arm and a non-specific DP47 arm), was supplemented into the culture medium upon coculture setup, typically at a concentration of 5 ng/ml. When used, blocking antibodies to TNFa (MAb-1, Biolegend) were added at a concentration of 1 ug/mL. To investigate the role of ROCK signaling on TRM activation, 10 uM Y-27362 was added daily for the duration of the coculture. For the month-long cocultures, the media was supplemented with IL-2 [10 IU/mL] (Roche) and IL-15 [2 ng/ml] (BioLegend), media change 3 times per week and culture splitting 1 time per week. Cultures were supplemented with 10 uM Y-27362 (STEMCELL Technologies) after splitting.

Flow cytometry analysis of immune-organoids

Triplicate wells of immuno-organoid cocultures from each condition were harvested 5h, 24h and 48h post-treatment. 4h prior to culture harvest at each timepoint, wells were treated with Protein Transport Inhibitor Cocktail (Thermo Fisher) to facilitate intracellular accumulation of cytokine protein. Cocultures were washed with PBS and then digested to single cells using Accutase solution (STEMCELL Technologies) at room temperature for approximately 30 minutes. Cell suspensions were passed through a 70 um strainer and stained for surface proteins (Extended Data Table 3). Cells were then fixed and permeabilized using the Foxp3 Transcription Factor Staining Buffer Set (Thermo Fisher), and subsequently stained for intracellular and intranuclear proteins. Stained cell suspensions were acquired on a BD Fortessa X-20 and analysed using FlowJo v10. To facilitate visual representation across one plot, samples from different time points and treatments were concatenated and separated along the y-axis.

Caspase-3/7 based epithelial cell cytotoxicity assay

IIO cultures were prepared in 4 ul Matrigel Matrix GF per well of a PhenoPlate™ 96-well microplate (Phenoplate), with cell ratios and media as described above. Apoptosis was

assessed using the CellEvent Caspase-3/7 Detection Reagent (Invitrogen) over TCB-treatment duration or at specific intervals. CellEvent Caspase-3/7 Detection Reagent was to the culture media at 1:1000. Samples were imaged in confocal mode at 5x magnification (Air objective) with the Operetta CLS (Perkin Elmer) covering approximately a 450 µm Z-stack, starting at -150 µm. Distance between Z-stacks was set to the minimum of 27 µm for the 5x objective (Autofocus: Two Peak; Binning: 2). Channels selected were brightfield and the predefined AlexaFluor 488. Per well, 5 fields were acquired, covering nearly the entire surface of the 96-well PhenoPlate plate. CO2 was set to 5%, temperature to 37°C. Caspase 3/7 fluorescence signal intensity was quantified using the Opera Harmony software (PerkinElmer). Briefly, segmentation of organoids was done by using “Find Texture Regions” based on the bright-field signal only, followed by “Select Region” and “Find Image Region” to segment single organoids as objects. Next, “Calculate Morphology Parameters” was performed to select objects >10000 µm 2 with “Select Population”. Next, the Caspase 3/7 fluorescence signal per individual organoid was determined using “Calculate Intensity Properties” of the AF 488 channel within these objects.

Time-lapse imaging of IIOs

The time-lapse live imaging was performed with a Leica SP8 confocal microscope using a 20x dry objective (HC PL APO CS2 20x/0.75 DRY) and 0.75 zoom. A 119.93µm thick Z-stack (step size: 3.98µm) was imaged every 10 minutes. During imaging the samples were in an incubation chamber (The Box, Life Imaging Services) at 37°C and 5% CO2. After acquisition maximum intensity projections were generated with the Leica Las X software and later exported as AVI files using ImageJ.

FFPE-embedding of cocultures

To FFPE-embed the cocultures, the samples were seeded in a 50% (v/v) Matrigel-Collagen I matrix. Wells were washed once with 1X DPBS before fixation with 4% paraformaldehyde (PFA) in the 24-well Clear TC-treated plate. After 30 min of fixation at RT, the wells were washed three more times before complete aspiration of the 1X DPBS. 400 µL preliquefied HistoGel (Thermo Scientific) was dispensed into the 24-well Clear TC-treated plates. After polymerization of the HistoGel (10min in 4°C fridge), the organoid-HistoGel ‘platelet’ was carefully lifted out of the 24-well Clear TC-treated plate using a thin metallic spatula. The samples were then distributed into biopsy cassettes and dehydrated overnight using a Vacuum filter processor (Sakura, TissueTek VIP5). On the next day, the samples were embedded in liquid paraffin.

Microtome sectioning

FFPE blocks were – in general – sectioned at a thickness of 5 µm and transferred on Superfrost Plus Adhesion microscope slides (Epredia). Where indicated, thickness differs. Slides were incubated in a slide oven overnight at 37°C.

Staining – FFPE-based multiplex immunofluorescence (mIF)

mIF staining of FFPE slides was performed using Ventana Discovery Ultra automated tissue stainer (Roche Tissue Diagnostics, Tucson AZ USA). Slides were baked first at 60°C for 8 min and subsequently further heated up to 69°C for 8 min for subsequent deparaffinization. This cycle was repeated twice. Heat-induced antigen retrieval was performed with Tris-EDTA buffer pH 7.8 (Ventana) at 92°C for 32 min. After each blocking

step with Discovery Inhibitor (Ventana) for 16 min, the Discovery Inhibitor was neutralized. Primary antibodies were diluted in 1X Plus Automation Amplification Diluent (Akoya Biosciences). Primaries were detected using according anti-species secondary antibodies conjugated to HRP (OmniMap Ventana) (Extended Data Table 3). Subsequently, the relevant Opal dye (Akoya Biosciences) was applied. After every application of a primary, respective secondary antibody and opal dye, an antibody neutralization and HRP-denaturation step was applied to remove residual antibodies and HRP, before starting the staining cycle again with the Discovery Inhibitor blocking step. Lastly, samples were counterstained with 4',6- Diamidino-2-phenylindol (DAPI, Roche).

FFPE-based mIFe

mIF stainings using the Opal dyes from Akoya were digitized with multispectral imaging by the Vectra® Polaris™ (PerkinElmer) using the MOTiF™ technology at 20x magnification for all 7 colors (Opal 480, Opal 520, Opal 570, Opal 620, Opal 690, Opal 780 and DAPI). Slides were scanned in a batch manner to ensure same imaging settings and cross-comparability for later image analysis with HALO AI. Next, unmixing of the channels and tiling of the images was performed with PhenoChart (v1.0.12) and inForm (v2.4). Tiles were fused in HALO (Indica labs, v3.2.1851.328).

High-resolution mIF were obtained using a STELLARIS 8 microscope (Leica) with a 40X1.1 NA water-immersion objective (HC FLUOTAR L VISIR 25x/0.95 WATER) and 1.0 zoom. The white light laser (WLL: 440 nm-790 nm) allowed to image all opal dyes mentioned above, channels were acquired sequentially to reduce crosstalk. Images were obtained in bidirectional mode with 2048 x 2048 pixels (pixel size: 273.8nm x 273.83 nm) at 600 Hz. Where indicated, images were acquired with z-stacks between 10-15 µm (z-steps: 1 µm) and 3D-reconstructed and displayed in ‘Maximum’-mode using the Leica Application Suite X software (Leica).

Image Analysis – FFPE-based mIF

Image analysis of the mIF images was performed with HALO AI (Indica Labs, v3.2.1851.328). Briefly, single organoids were automatically detected using a Deep Learning algorithm trained to distinguish matrix and organoids (iterations: 5000; cross entropy: 0.32; DenseNet AI V2 Plugin). After quick validation, organoids were annotated as individual ROIs, objects. Only objects >7500 µm2 were considered positive.

The HighPlex FL v4.1.3 module was used to perform nuclear segmentation based on DAPI+ cells. For quantification, DAPI+ nuclei and markers for each distinct cell type of interest were merged. Thereby, secondary-only negative controls on the tissue of origin served as a negative signal threshold in order to prevent biased adjustments. The analysis module was deployed on ROIs per single object (organoid).

Single-cell dissociation of IIO

IIO were dissociated as described previously by (Yu *et al.,* 2021). In short, organoids were dislodged and mechanically broken up and transferred to 1% BSA-coated tubes. The organoid fragments were centrifuged at 400g, 4min, RT. The supernatant was removed and the enzymes of the neural tissue dissociation kit (Miltenyi Biotec) were mixed in HBSS-1%BSA buffer. The organoid fragments were dissociated to single cells for a total of 30 min with through pipetting every 7 minutes. Next, cells were filtered through a 40uM filter and

single cells were centrifuged at 450g, 4min, RT and subsequently resuspended in DPBS 1% BSA. The single cell libraries were prepared with the 10x Genomics platform using the Chromium Next GEM Single Cell 3' Kit v3.1.

Single-cell RNA-seq data preprocessing

CellRanger (v6.0.2, 10x Genomics) was used to extract unique molecular identifiers, cell barcodes, and genomic reads from the sequencing results of 10x Chromium experiments. Then, count matrices, including both protein coding and non-coding transcripts, were constructed aligning against the annotated human reference genome (GRCh38, v3.0.0, 10x Genomics). In order to remove potentially damaged or unhealthy cells and improve data quality, the following filtering steps were performed in addition to the built-in CellRanger filtering pipeline. Cells associated with over 50,000 transcripts, usually less than 1% of the total number of samples, were removed. Cells associated with a low number of unique transcripts, less than 500 unique transcripts detected (1% of the total number of samples), were removed. Cells with over 20% of mitochondrial transcripts were removed. Transcripts mapping to ribosomal protein coding genes as well as mitochondrial genes were removed together with transcripts detected in less than 10 samples.

Normalization with SCTransform

For normalization and variance stabilization of each scRNA-seq experiment's molecular count data, we employed the modeling framework of SCTransform in Seurat v3 (Hafemeister & Satija, 2019). In brief, a model of technical noise in scRNA-seq data is computed using 'generalized gamma poisson regression' (Ahlmann-Eltze & Huber, 2021). The residuals for this model are normalized values that indicate divergence from the expected number of observed UMIs for a gene in a cell given the gene's average expression in the population and cellular sequencing depth. Additionally, a curated list of cell cycle associated genes, available within Seurat, was used to estimate the contribution of cell cycle and remove this source of biological variation from each dataset in order to increase the signal deriving from more interesting processes. The residuals for the top 2,000 variable genes were used directly as input to computing the top 100 Principal Components (PCs) by PCA dimensionality reduction through the RunPCA() function in Seurat. Corrected UMI, which are converted from Pearson residuals and represent expected counts if all cells were sequenced at the same depth, were log-transformed and used for visualization and differential expression (DE) analysis. Primary immune cells from intestinal biopsy samples were processed as described above. However, they did not undergo any cell filtering as quality control steps had already been performed in the respective published studies.

Doublet removal with DoubletFinder

For each scRNA-seq experiment DoubletFinder (McGinnis *et al.,* 2019) was used to predict doublets in the sequencing data. In brief, this tool generates artificial doublets from existing scRNA-seq data by merging randomly selected cells which are then pre-processed together with real data and jointly embedded on a PCA space that serves as basis to find each cell's proportion of artificial k nearest neighbors (pANN). For this step we restricted the dimension space to the top 50 PCs. Finally, pANN values are rank ordered according to the expected number of doublets and optimal cutoff is selected through ROC analysis across pN-pK parameter sweeps for each scRNA-seq dataset; pN describes the proportion of generated artificial doublets while pK defines the PC neighborhood size. In order to achieve

maximal doublet prediction accuracy, mean-variance normalized bimodality coefficient (BCmvn) was leveraged. This provides a ground-truth-agnostic metric that coincides with pK values that maximize AUC in the data. To overcome DoubletFinder's limited sensitivity to homotypic doublets, we consider doublet number estimates based on Poisson statistics with homotypic doublet proportion adjustment assuming 1/50,000 doublet formation rate the 10x Chromium droplet microfluidic cell loading.

Ambient mRNA signal removal

After doublet prediction and removal, we analyzed each scRNA-seq dataset in order to estimate the extent of ambient mRNA contamination in every single cell and correct it. We used the R package Cellular Latent Dirichlet Allocation (CELDA) (Wang *et al.,* 2022) which contains DecontX, a method based on Bayesian statistical framework to computationally estimate and remove RNA contamination in individual cells without empty droplet information. We applied the DecontX() function in CELDA to the raw count matrices with default parameters. Subsequently, we removed all cells with contamination values above 0.5 and we used the decontaminated count matrices resulting from DecontX() for downstream analysis.

Data integration

Individual datasets, after preprocessing, doublet removal and ambient mRNA regression, were aggregated according to specific criterias (e.g. tissue of origin, profiling time, culture condition) and went through a joint normalization step with SCTransform in order to mitigate technical confounding factors, which also served as means for selection of a set of meaningful 2,000 most variable global genes prior to data integration. Integration of different conditions (culture model, treatment and timepoints) was performed using the log-normalized corrected UMI count data in two steps. First, the residuals for the top 2,000 global variable genes were used as input to computing the top 100 Principal Components (PCs) through the RunPCA() function in Seurat. The leading 30 PCs and 50 nearest neighbors were then used to define the shared neighborhood graph with the FindNeighbors() function in Seurat. Subsequently, datasets were clustered according to the shared neighborhood graph using the Louvain algorithm (Blondel *et al.,* 2008) through the Seurat function FindClusters() with resolution 0.8. Finally, we used these high-resolution clusters to define a restricted, noise reduced and cell state specific set of genes through differential expression analysis (see Methods section below). In the second step of the integration process, we compiled a list consisting of the ensemble of the top 30 DEGs for each cluster and used it to focus and repeat PCA dimensionality reduction. The first 30 PC vectors of the new PCA space served as basis to obtain a two-dimensional (2D) representation of the data through Uniform Manifold Approximation and Projection (UMAP) (McInnes *et al.,* 2018) implemented in RunUMAP() with 50 nearest neighbors. We then computed a shared neighborhood graph on the UMAP lower-dimensional space and computed the final integrated clusters with resolution parameter 0.2.

Differential expression analysis

Gene differential expression (DE) analysis between distinct cell populations in scRNA-seq data was assessed by performing Wilcoxon rank sum tests and auROC analysis as implemented by Presto (Ilya *et al.,* 2019) package in R. Log-transformed corrected UMIs were used as input for the DE statistical tests, and genes were called differentially expressed

if associated adjusted p-value (Bonferroni method) was lower than 0.05, AUC value was above 0.6 and log fold change was greater than 0.15. In addition, we also set thresholds on detection rates of DE genes. In particular, a given gene was assigned as over-expressed in the analyzed group if it was detected in at least 30% of the samples of that group, while the detection rate in the background samples was at most 70% of the detection rate of the analyzed group.

CD8+ T cell activation trajectory reconstruction

To reconstruct the continuum of the CD8+ T cell activation trajectory in IIO models challenged with bispecific antibodies we took advantage of diffusion pseudotime (DPT) as implemented by the destiny (Angerer *et al.,* 2016) package In R. In brief, DPT uses random-walk-based distance, computed on the leading eigenvectors of a transition matrix, to order scRNA-seq data according to differentiation stages (Hagverdi *et al.,* 2016). Concretely, we used the DiffusionMap() function in destiny package on the space identified by the leading 30 PC vectors of the integrated PCA embedding of the CD8+ clusters. Pseudotime values were then computed with the DTP() function in destiny on the diffusion map object using default parameters. Similarly, the global pseudotime, following TNF perturbation simulation, was based on a random walk approach on the cell state transition matrix.

Intercellular communication analysis

To investigate ligand-receptor (LR) mediated cell-cell communications during immune cell activation in our IIO models, we focused on the signals exchanged between Th1 cells, activated t-bet B cells and CD8+ CTLs. For this analysis we extracted genes labeled as either ligands or receptors from curated databases (Browaeys *et al.,* 2020) and required that genes were differentially expressed between the three populations under investigation, which facilitated retrieval of directional information about the signal exchange. To gain insights into functional cell-cell communication, we used the NicheNet pipeline which considers the influence of sender-cell ligands on receiver-cell gene expression58. NicheNet's analysis pipeline provided us with a ranking of predicted ligands that most likely affect gene expression in activated t-bet B cells and CD8+ CTLs highlighting the role of critical Th1-secreted factors in driving immune cell phenotypes within IIOs.

Functional enrichment analysis

To understand mechanisms underlying phenotypes in our data, differentially expressed genes were analyzed for gene ontology biological process (GOBP) enrichment using one-sided hypergeometric testing. P-values were adjusted for multiple testing hypotheses by the Bonferroni method and only enrichment results below a 5% significance level threshold were considered. For this analysis, we only considered biological processes consisting of sets with more than 10 but less than 300 mapped genes.

In silico perturbation analysis

To simulate dynamic shifts in cell identity resulting from ligand signaling cascade activation, we employed Nichenet’s prior model58. The first step involved generating simulated values by applying the gene regulatory network (GRN) as a function and propagating the relative changes in gene expression after k-nearest neighbor imputation of the gene expression data. This iterative (3 times) signal propagation enabled us to calculate the broad, downstream effects of ligand perturbation, thereby estimating the global

transcriptional shift. The estimation of cell-identity transition probability was accomplished by comparing this gene expression shift to that of local neighbors, utilizing a likelihood-based dynamical model. By doing so, we could establish a measure of how cell identities transition in response to ligand perturbation. Finally, the transition probabilities were transformed into a weighted local average vector map, encoding the simulated directionality of cell-state transition for each cell. This workflow results from an adaptation and integration of CellOracle (Kamimoto *et al.,* 2023) and scVelo (Bergen *et al.,* 2020).

REFERENCES

Acerbi, I., et al. “Human Breast Cancer Invasion and Aggression Correlates with ECM Stiffening and Immune Cell Infiltration.” *Integrative Biology*, vol. 7, no. 10, Oct. 2015, pp. 1120–34. *DOI.org (Crossref)*, https://doi.org/10.1039/c5ib00040h.

Aibar, Sara, et al. “SCENIC: Single-Cell Regulatory Network Inference and Clustering.” *Nature Methods*, vol. 14, no. 11, Nov. 2017, pp. 1083–86. *DOI.org (Crossref)*, https://doi.org/10.1038/nmeth.4463.

Aiello, Leslie C., and Peter Wheeler. “The Expensive-Tissue Hypothesis: The Brain and the Digestive System in Human and Primate Evolution.” *Current Anthropology*, vol. 36, no. 2, Apr. 1995, pp. 199–221. *DOI.org (Crossref)*, https://doi.org/10.1086/204350.

Aisenbrey, Elizabeth A., and William L. Murphy. “Synthetic Alternatives to Matrigel.” *Nature Reviews Materials*, vol. 5, no. 7, May 2020, pp. 539–51. *DOI.org (Crossref)*, https://doi.org/10.1038/s41578-020-0199-8.

Akl, Mohamed R., et al. “Molecular and Clinical Profiles of Syndecan-1 in Solid and Hematological Cancer for Prognosis and Precision Medicine.” *Oncotarget*, vol. 6, no. 30, Oct. 2015, pp. 28693–715. *DOI.org (Crossref)*, https://doi.org/10.18632/oncotarget.4981.

Amann, Maria, et al. “Therapeutic Window of MuS110, a Single-Chain Antibody Construct Bispecific for Murine EpCAM and Murine CD3.” *Cancer Research*, vol. 68, no. 1, Jan. 2008, pp. 143–51. *DOI.org (Crossref)*, https://doi.org/10.1158/0008-5472.CAN-07-2182.

Andreatta, Massimo, et al. “Interpretation of T Cell States from Single-Cell Transcriptomics Data Using Reference Atlases.” *Nature Communications*, vol. 12, no. 1, May 2021, p. 2965. *DOI.org (Crossref)*, https://doi.org/10.1038/s41467-021-23324-4.

Argelaguet, Ricard, et al. “Computational Principles and Challenges in Single-Cell Data Integration.” *Nature Biotechnology*, vol. 39, no. 10, Oct. 2021, pp. 1202–15. *DOI.org (Crossref)*, https://doi.org/10.1038/s41587-021-00895-7.

Australian Pancreatic Cancer Genome Initiative, Peter Bailey, et al. “Genomic Analyses Identify Molecular Subtypes of Pancreatic Cancer.” *Nature*, vol. 531, no. 7592, Mar. 2016, pp. 47–52. *DOI.org (Crossref)*, https://doi.org/10.1038/nature16965.

Australian Pancreatic Cancer Genome Initiative, Nicola Waddell, et al. “Whole Genomes Redefine the Mutational Landscape of Pancreatic Cancer.” *Nature*, vol. 518, no. 7540, Feb. 2015, pp. 495–501. *DOI.org (Crossref)*, https://doi.org/10.1038/nature14169.

Babbitt, Courtney C., et al. “Genomic Signatures of Diet-Related Shifts during Human Origins.” *Proceedings of the Royal Society B: Biological Sciences*, vol. 278, no. 1708, Apr. 2011, pp. 961–69. *DOI.org (Crossref)*, https://doi.org/10.1098/rspb.2010.2433.

Badia-i-Mompel, Pau, et al. “Gene Regulatory Network Inference in the Era of Single-Cell Multi-Omics.” *Nature Reviews Genetics*, June 2023. *DOI.org (Crossref)*, https://doi.org/10.1038/s41576-023-00618-5.

Bagley, Joshua A., et al. “Fused Cerebral Organoids Model Interactions between Brain Regions.” *Nature Methods*, vol. 14, no. 7, July 2017, pp. 743–51. *DOI.org (Crossref)*, https://doi.org/10.1038/nmeth.4304.

Bank, Ilan, et al. “Functional Role of VLA-1 (CD49A) in Adhesion, Cation-Dependent Spreading, and Activation of Cultured Human T Lymphocytes.” *Cellular Immunology*, vol. 156, no. 2, July 1994, pp. 424–37. *DOI.org (Crossref)*, https://doi.org/10.1006/cimm.1994.1187.

Barcellos-Hoff, M. H., et al. “Functional Differentiation and Alveolar Morphogenesis of Primary Mammary Cultures on Reconstituted Basement Membrane.” *Development*, vol. 105, no. 2, Feb. 1989, pp. 223–35. *DOI.org (Crossref)*, https://doi.org/10.1242/dev.105.2.223.

Barker, Jennifer M., and Edwin Liu. “Celiac Disease: Pathophysiology, Clinical Manifestations, and Associated Autoimmune Conditions.” *Advances in Pediatrics*, vol. 55, no. 1, Sept. 2008, pp. 349–65. *DOI.org (Crossref)*, https://doi.org/10.1016/j.yapd.2008.07.001.

Barker, Nick, et al. “Lgr5+ve Stem Cells Drive Self-Renewal in the Stomach and Build Long-Lived Gastric Units *In vitro*.” *Cell Stem Cell*, vol. 6, no. 1, Jan. 2010, pp. 25–36. *DOI.org (Crossref)*, https://doi.org/10.1016/j.stem.2009.11.013.

Bartfeld, Sina, et al. “*In vitro* Expansion of Human Gastric Epithelial Stem Cells and Their Responses to Bacterial Infection.” *Gastroenterology*, vol. 148, no. 1, Jan. 2015, pp. 126-136.e6. *DOI.org (Crossref)*, https://doi.org/10.1053/j.gastro.2014.09.042.

Beccari, Leonardo, et al. “Multi-Axial Self-Organization Properties of Mouse Embryonic Stem Cells into Gastruloids.” *Nature*, vol. 562, no. 7726, Oct. 2018, pp. 272–76. *DOI.org (Crossref)*, https://doi.org/10.1038/s41586-018-0578-0.

Bengio, Yoshua, et al. *Estimating or Propagating Gradients Through Stochastic Neurons for Conditional Computation*. arXiv, 15 Aug. 2013. *arXiv.org*, https://doi.org/10.48550/arXiv.1308.3432.

Benton, Mary Lauren, et al. “The Influence of Evolutionary History on Human Health and Disease.” *Nature Reviews Genetics*, vol. 22, no. 5, May 2021, pp. 269–83. *DOI.org (Crossref)*, https://doi.org/10.1038/s41576-020-00305-9.

Bergen, Volker, et al. “Generalizing RNA Velocity to Transient Cell States through Dynamical Modeling.” *Nature Biotechnology*, vol. 38, no. 12, Dec. 2020, pp. 1408–14. *DOI.org (Crossref)*, https://doi.org/10.1038/s41587-020-0591-3.

Bertero, Thomas, et al. “Tumor-Stroma Mechanics Coordinate Amino Acid Availability to Sustain Tumor Growth and Malignancy.” *Cell Metabolism*, vol. 29, no. 1, Jan. 2019, pp. 124-140.e10. *DOI.org (Crossref)*, https://doi.org/10.1016/j.cmet.2018.09.012.

Beura, Lalit K., et al. “Intravital Mucosal Imaging of CD8+ Resident Memory T Cells Shows Tissue-Autonomous Recall Responses That Amplify Secondary Memory.” *Nature Immunology*, vol. 19, no. 2, Feb. 2018, pp. 173–82. *DOI.org (Crossref)*, https://doi.org/10.1038/s41590-017-0029-3.

Biankin, Andrew V., and Anirban Maitra. “Subtyping Pancreatic Cancer.” *Cancer Cell*, vol. 28, no. 4, Oct. 2015, pp. 411–13. *DOI.org (Crossref)*, https://doi.org/10.1016/j.ccell.2015.09.020.

Birey, Fikri, et al. “Assembly of Functionally Integrated Human Forebrain Spheroids.” *Nature*, vol. 545, no. 7652, May 2017, pp. 54–59. *DOI.org (Crossref)*, https://doi.org/10.1038/nature22330.

Blasco, María Teresa, et al. “Complete Regression of Advanced Pancreatic Ductal Adenocarcinomas upon Combined Inhibition of EGFR and C-RAF.” *Cancer Cell*, vol. 35, no. 4, Apr. 2019, pp. 573-587.e6. *DOI.org (Crossref)*, https://doi.org/10.1016/j.ccell.2019.03.002.

Boisset, Jean-Charles, et al. “Mapping the Physical Network of Cellular Interactions.” *Nature Methods*, vol. 15, no. 7, July 2018, pp. 547–53. *DOI.org (Crossref)*, https://doi.org/10.1038/s41592-018-0009-z.

Boj, Sylvia F., et al. “Organoid Models of Human and Mouse Ductal Pancreatic Cancer.” *Cell*, vol. 160, no. 1–2, Jan. 2015, pp. 324–38. *DOI.org (Crossref)*, https://doi.org/10.1016/j.cell.2014.12.021.

Boretto, Matteo, et al. “Patient-Derived Organoids from Endometrial Disease Capture Clinical Heterogeneity and Are Amenable to Drug Screening.” *Nature Cell Biology*, vol. 21, no. 8, Aug. 2019, pp. 1041–51. *DOI.org (Crossref)*, https://doi.org/10.1038/s41556-019-0360-z.

Brandenberg, Nathalie, et al. “High-Throughput Automated Organoid Culture via Stem-Cell Aggregation in Microcavity Arrays.” *Nature Biomedical Engineering*, vol. 4, no. 9, June 2020, pp. 863–74. *DOI.org (Crossref)*, https://doi.org/10.1038/s41551-020-0565-2.

Bray, Eric R., et al. “Thrombospondin-1 Mediates Axon Regeneration in Retinal Ganglion Cells.” *Neuron*, vol. 103, no. 4, Aug. 2019, pp. 642-657.e7. *DOI.org (Crossref)*, https://doi.org/10.1016/j.neuron.2019.05.044.

Broguiere, Nicolas, et al. “Morphogenesis Guided by 3D Patterning of Growth Factors in Biological Matrices.” *Advanced Materials*, vol. 32, no. 25, June 2020, p. 1908299. *DOI.org (Crossref)*, https://doi.org/10.1002/adma.201908299.

Broutier, Laura, et al. “Human Primary Liver Cancer–Derived Organoid Cultures for Disease Modeling and Drug Screening.” *Nature Medicine*, vol. 23, no. 12, Dec. 2017, pp. 1424–35. *DOI.org (Crossref)*, https://doi.org/10.1038/nm.4438.

Browaeys, Robin, et al. “NicheNet: Modeling Intercellular Communication by Linking Ligands to Target Genes.” *Nature Methods*, vol. 17, no. 2, Feb. 2020, pp. 159–62. *DOI.org (Crossref)*, https://doi.org/10.1038/s41592-019-0667-5.

Buenrostro, Jason D., et al. “Single-Cell Chromatin Accessibility Reveals Principles of Regulatory Variation.” *Nature*, vol. 523, no. 7561, July 2015, pp. 486–90. *DOI.org (Crossref)*, https://doi.org/10.1038/nature14590.

Butler, Andrew, et al. “Integrating Single-Cell Transcriptomic Data across Different Conditions, Technologies, and Species.” *Nature Biotechnology*, vol. 36, no. 5, May 2018, pp. 411–20. *DOI.org (Crossref)*, https://doi.org/10.1038/nbt.4096.

Butler, Colin R., et al. “Rapid Expansion of Human Epithelial Stem Cells Suitable for Airway Tissue Engineering.” *American Journal of Respiratory and Critical Care Medicine*, vol. 194, no. 2, July 2016, pp. 156–68. *DOI.org (Crossref)*, https://doi.org/10.1164/rccm.201507-1414OC.

Cakir, Bilal, Yangfei Xiang, et al. “Engineering of Human Brain Organoids with a Functional Vascular-like System.” *Nature Methods*, vol. 16, no. 11, Nov. 2019, pp. 1169–75. *DOI.org (Crossref)*, https://doi.org/10.1038/s41592-019-0586-5.

Cakir, Bilal, Yoshiaki Tanaka, et al. “Expression of the Transcription Factor PU.1 Induces the Generation of Microglia-like Cells in Human Cortical Organoids.” *Nature Communications*, vol. 13, no. 1, Jan. 2022, p. 430. *DOI.org (Crossref)*, https://doi.org/10.1038/s41467-022-28043-y.

Camp, J. Gray, Farhath Badsha, et al. “Human Cerebral Organoids Recapitulate Gene Expression Programs of Fetal Neocortex Development.” *Proceedings of the National Academy of Sciences*, vol. 112, no. 51, Dec. 2015, pp. 15672–77. *DOI.org (Crossref)*, https://doi.org/10.1073/pnas.1520760112.

Camp, J. Gray, Keisuke Sekine, et al. “Multilineage Communication Regulates Human Liver Bud Development from Pluripotency.” *Nature*, vol. 546, no. 7659, June 2017, pp. 533–38. *DOI.org (Crossref)*, https://doi.org/10.1038/nature22796.

Campbell, Peter J., et al. “The Patterns and Dynamics of Genomic Instability in Metastatic Pancreatic Cancer.” *Nature*, vol. 467, no. 7319, Oct. 2010, pp. 1109–13. *DOI.org (Crossref)*, https://doi.org/10.1038/nature09460.

Cao, Junyue, et al. “Comprehensive Single-Cell Transcriptional Profiling of a Multicellular Organism.” *Science*, vol. 357, no. 6352, Aug. 2017, pp. 661–67. *DOI.org (Crossref)*, https://doi.org/10.1126/science.aam8940.

Cao, Zhi-Jie, and Ge Gao. “Multi-Omics Single-Cell Data Integration and Regulatory Inference with Graph-Linked Embedding.” *Nature Biotechnology*, vol. 40, no. 10, Oct. 2022, pp. 1458–66. *DOI.org (Crossref)*, https://doi.org/10.1038/s41587-022-01284-4.

Castellanos, Emily, et al. “Current Treatment Options for Pancreatic Carcinoma.” *Current Oncology Reports*, vol. 13, no. 3, June 2011, pp. 195–205. *DOI.org (Crossref)*, https://doi.org/10.1007/s11912-011-0164-1.

Cepek, Karyn L., et al. “Adhesion between Epithelial Cells and T Lymphocytes Mediated by E-Cadherin and the αEβ7 Integrin.” *Nature*, vol. 372, no. 6502, Nov. 1994, pp. 190–93. *DOI.org (Crossref)*, https://doi.org/10.1038/372190a0.

Chal, Jérome, and Olivier Pourquié. “Making Muscle: Skeletal Myogenesis *in vivo* and *in vitro*.” *Development*, vol. 144, no. 12, June 2017, pp. 2104–22. *DOI.org (Crossref)*, https://doi.org/10.1242/dev.151035.

Chan-Seng-Yue, Michelle, et al. “Transcription Phenotypes of Pancreatic Cancer Are Driven by Genomic Events during Tumor Evolution.” *Nature Genetics*, vol. 52, no. 2, Feb. 2020, pp. 231–40. *PubMed*, https://doi.org/10.1038/s41588-019-0566-9.

Chen, Kok Hao, et al. “Spatially Resolved, Highly Multiplexed RNA Profiling in Single Cells.” *Science*, vol. 348, no. 6233, Apr. 2015, p. aaa6090. *DOI.org (Crossref)*, https://doi.org/10.1126/science.aaa6090.

Chen, Michelle B., et al. “On-Chip Human Microvasculature Assay for Visualization and Quantification of Tumor Cell Extravasation Dynamics.” *Nature Protocols*, vol. 12, no. 5, May 2017, pp. 865–80. *DOI.org (Crossref)*, https://doi.org/10.1038/nprot.2017.018.

Chen, Song, et al. “High-Throughput Sequencing of the Transcriptome and Chromatin Accessibility in the Same Cell.” *Nature Biotechnology*, vol. 37, no. 12, Dec. 2019, pp. 1452–57. *DOI.org (Crossref)*, https://doi.org/10.1038/s41587-019-0290-0.

Chen, Xidong, et al. “The HPA/SDC1 Axis Promotes Invasion and Metastasis of Pancreatic Cancer Cells by Activating EMT via FGF2 Upregulation.” *Oncology Letters*, Nov. 2019. *DOI.org (Crossref)*, https://doi.org/10.3892/ol.2019.11121.

Chen, Zeyu, et al. “TCF-1-Centered Transcriptional Network Drives an Effector versus Exhausted CD8 T Cell-Fate Decision.” *Immunity*, vol. 51, no. 5, Nov. 2019, pp. 840-855.e5. *DOI.org (Crossref)*, https://doi.org/10.1016/j.immuni.2019.09.013.

Cheroutre, Hilde, et al. “The Light and Dark Sides of Intestinal Intraepithelial Lymphocytes.” *Nature Reviews Immunology*, vol. 11, no. 7, July 2011, pp. 445–56. *DOI.org (Crossref)*, https://doi.org/10.1038/nri3007.

Chichagova, Valeria, et al. “Incorporating Microglia-like Cells in Human Induced Pluripotent Stem Cell-derived Retinal Organoids.” *Journal of Cellular and Molecular Medicine*, vol. 27, no. 3, Feb. 2023, pp. 435–45. *DOI.org (Crossref)*, https://doi.org/10.1111/jcmm.17670.

Ciruna, Brian, and Janet Rossant. “FGF Signaling Regulates Mesoderm Cell Fate Specification and Morphogenetic Movement at the Primitive Streak.” *Developmental Cell*, vol. 1, no. 1, July 2001, pp. 37–49. *DOI.org (Crossref)*, https://doi.org/10.1016/S1534-5807(01)00017-X.

Clark, Iain C., et al. “Microfluidics-Free Single-Cell Genomics with Templated Emulsification.” *Nature Biotechnology*, Mar. 2023. *DOI.org (Crossref)*, https://doi.org/10.1038/s41587-023-01685-z.

Clark, Rachael A., et al. “A Novel Method for the Isolation of Skin Resident T Cells from Normal and Diseased Human Skin.” *Journal of Investigative Dermatology*, vol. 126, no. 5, May 2006, pp. 1059–70. *DOI.org (Crossref)*, https://doi.org/10.1038/sj.jid.5700199.

Clevers, Hans. “Modeling Development and Disease with Organoids.” *Cell*, vol. 165, no. 7, June 2016, pp. 1586–97. *DOI.org (Crossref)*, https://doi.org/10.1016/j.cell.2016.05.082.

Cohen, Merav, et al. “Lung Single-Cell Signaling Interaction Map Reveals Basophil Role in Macrophage Imprinting.” *Cell*, vol. 175, no. 4, Nov. 2018, pp. 1031-1044.e18. *DOI.org (Crossref)*, https://doi.org/10.1016/j.cell.2018.09.009.

Cowan, Cameron S., et al. “Cell Types of the Human Retina and Its Organoids at Single-Cell Resolution.” *Cell*, vol. 182, no. 6, Sept. 2020, pp. 1623-1640.e34. *DOI.org (Crossref)*, https://doi.org/10.1016/j.cell.2020.08.013.

Dahl-Jensen, Svend, and Anne Grapin-Botton. “The Physics of Organoids: A Biophysical Approach to Understanding Organogenesis.” *Development*, vol. 144, no. 6, Mar. 2017, pp. 946–51. *DOI.org (Crossref)*, https://doi.org/10.1242/dev.143693.

Daviaud, Nicolas, et al. “Vascularization and Engraftment of Transplanted Human Cerebral Organoids in Mouse Cortex.” *Eneuro*, vol. 5, no. 6, Nov. 2018, p. ENEURO.0219-18.2018. *DOI.org (Crossref)*, https://doi.org/10.1523/ENEURO.0219-18.2018.

Dijkstra, Krijn K., et al. “Challenges in Establishing Pure Lung Cancer Organoids Limit Their Utility for Personalized Medicine.” *Cell Reports*, vol. 31, no. 5, May 2020, p. 107588. *DOI.org (Crossref)*, https://doi.org/10.1016/j.celrep.2020.107588.

Dong, Xin, et al. “Human Cerebral Organoids Establish Subcortical Projections in the Mouse Brain after Transplantation.” *Molecular Psychiatry*, vol. 26, no. 7, July 2021, pp. 2964–76. *DOI.org (Crossref)*, https://doi.org/10.1038/s41380-020-00910-4.

Driehuis, Else, et al. “Establishment of Patient-Derived Cancer Organoids for Drug-Screening Applications.” *Nature Protocols*, vol. 15, no. 10, Oct. 2020, pp. 3380–409. *DOI.org (Crossref)*, https://doi.org/10.1038/s41596-020-0379-4.

Drost, Jarno, et al. “Sequential Cancer Mutations in Cultured Human Intestinal Stem Cells.” *Nature*, vol. 521, no. 7550, May 2015, pp. 43–47. *DOI.org (Crossref)*, https://doi.org/10.1038/nature14415.

Drost, Jarno, and Hans Clevers. “Organoids in Cancer Research.” *Nature Reviews Cancer*, vol. 18, no. 7, July 2018, pp. 407–18. *DOI.org (Crossref)*, https://doi.org/10.1038/s41568-018-0007-6.

Duan, Bin, et al. “Model-Based Understanding of Single-Cell CRISPR Screening.” *Nature Communications*, vol. 10, no. 1, May 2019, p. 2233. *DOI.org (Crossref)*, https://doi.org/10.1038/s41467-019-10216-x.

Dunne, Richard F., and Aram F. Hezel. “Genetics and Biology of Pancreatic Ductal Adenocarcinoma.” *Hematology/Oncology Clinics of North America*, vol. 29, no. 4, Aug. 2015, pp. 595–608. *DOI.org (Crossref)*, https://doi.org/10.1016/j.hoc.2015.04.003.

Dye, Briana R., et al. “*In vitro* Generation of Human Pluripotent Stem Cell Derived Lung Organoids.” *eLife*, vol. 4, Mar. 2015, p. e05098. *DOI.org (Crossref)*, https://doi.org/10.7554/eLife.05098.

Ebbing, Eva A., et al. “Stromal-Derived Interleukin 6 Drives Epithelial-to-Mesenchymal Transition and Therapy Resistance in Esophageal Adenocarcinoma.” *Proceedings of the National Academy of Sciences*, vol. 116, no. 6, Feb. 2019, pp. 2237–42. *DOI.org (Crossref)*, https://doi.org/10.1073/pnas.1820459116.

Efremova, Mirjana, et al. “CellPhoneDB: Inferring Cell–Cell Communication from Combined Expression of Multi-Subunit Ligand–Receptor Complexes.” *Nature Protocols*, vol. 15, no. 4, Apr. 2020, pp. 1484–506. *DOI.org (Crossref)*, https://doi.org/10.1038/s41596-020-0292-x.

Eiraku, Mototsugu, Kiichi Watanabe, et al. “Self-Organized Formation of Polarized Cortical Tissues from ESCs and Its Active Manipulation by Extrinsic Signals.” *Cell Stem Cell*, vol. 3, no. 5, Nov. 2008, pp. 519–32. *DOI.org (Crossref)*, https://doi.org/10.1016/j.stem.2008.09.002.

Eiraku, Mototsugu, Nozomu Takata, et al. “Self-Organizing Optic-Cup Morphogenesis in Three-Dimensional Culture.” *Nature*, vol. 472, no. 7341, Apr. 2011, pp. 51–56. *DOI.org (Crossref)*, https://doi.org/10.1038/nature09941.

Elmentaite, Rasa, et al. “Cells of the Human Intestinal Tract Mapped across Space and Time.” *Nature*, vol. 597, no. 7875, Sept. 2021, pp. 250–55. *DOI.org (Crossref)*, https://doi.org/10.1038/s41586-021-03852-1.

Fan, Shaohua, et al. “Going Global by Adapting Local: A Review of Recent Human Adaptation.” *Science*, vol. 354, no. 6308, Oct. 2016, pp. 54–59. *DOI.org (Crossref)*, https://doi.org/10.1126/science.aaf5098.

Fatehullah, Aliya, et al. “Organoids as an *in vitro* Model of Human Development and Disease.” *Nature Cell Biology*, vol. 18, no. 3, Mar. 2016, pp. 246–54. *DOI.org (Crossref)*, https://doi.org/10.1038/ncb3312.

Fausett, Sarah R., et al. “BMP Antagonism by Noggin Is Required in Presumptive Notochord Cells for Mammalian Foregut Morphogenesis.” *Developmental Biology*, vol. 391, no. 1, July 2014, pp. 111–24. *DOI.org (Crossref)*, https://doi.org/10.1016/j.ydbio.2014.02.008.

Finlay, David K., et al. “PDK1 Regulation of mTOR and Hypoxia-Inducible Factor 1 Integrate Metabolism and Migration of CD8+ T Cells.” *Journal of Experimental Medicine*, vol. 209, no. 13, Dec. 2012, pp. 2441–53. *DOI.org (Crossref)*, https://doi.org/10.1084/jem.20112607.

Fleck, Jonas Simon, et al. “Inferring and Perturbing Cell Fate Regulomes in Human Brain Organoids.” *Nature*, Oct. 2022. *DOI.org (Crossref)*, https://doi.org/10.1038/s41586-022-05279-8.

Fodde, Riccardo, et al. “Mutations in the APC Tumour Suppressor Gene Cause Chromosomal Instability.” *Nature Cell Biology*, vol. 3, no. 4, Apr. 2001, pp. 433–38. *DOI.org (Crossref)*, https://doi.org/10.1038/35070129.

Fowler, Jonas L., et al. “A Critical Look: Challenges in Differentiating Human Pluripotent Stem Cells into Desired Cell Types and Organoids.” *WIREs Developmental Biology*, vol. 9, no. 3, May 2020. *DOI.org (Crossref)*, https://doi.org/10.1002/wdev.368.

Fu, Ya-Yuan, et al. “T Cell Recruitment to the Intestinal Stem Cell Compartment Drives Immune-Mediated Intestinal Damage after Allogeneic Transplantation.” *Immunity*, vol. 51, no. 1, July 2019, pp. 90-103.e3. *DOI.org (Crossref)*, https://doi.org/10.1016/j.immuni.2019.06.003.

Fujii, Masayuki, et al. “A Colorectal Tumor Organoid Library Demonstrates Progressive Loss of Niche Factor Requirements during Tumorigenesis.” *Cell Stem Cell*, vol. 18, no. 6, June 2016, pp. 827–38. *DOI.org (Crossref)*, https://doi.org/10.1016/j.stem.2016.04.003.

Gadue, Paul, et al. “Wnt and TGF-Beta Signaling Are Required for the Induction of an *in vitro* Model of Primitive Streak Formation Using Embryonic Stem Cells.” *Proceedings of the National Academy of Sciences of the United States of America*, vol. 103, no. 45, Nov. 2006, pp. 16806–11. *PubMed*, https://doi.org/10.1073/pnas.0603916103.

Ganesh, Karuna, et al. “A Rectal Cancer Organoid Platform to Study Individual Responses to Chemoradiation.” *Nature Medicine*, vol. 25, no. 10, Oct. 2019, pp. 1607–14. *DOI.org (Crossref)*, https://doi.org/10.1038/s41591-019-0584-2.

Gao, Dong, et al. “Organoid Cultures Derived from Patients with Advanced Prostate Cancer.” *Cell*, vol. 159, no. 1, Sept. 2014, pp. 176–87. *DOI.org (Crossref)*, https://doi.org/10.1016/j.cell.2014.08.016.

Garvey, Colleen M., et al. “Anti-EGFR Therapy Induces EGF Secretion by Cancer-Associated Fibroblasts to Confer Colorectal Cancer Chemoresistance.” *Cancers*, vol. 12, no. 6, May 2020, p. 1393. *DOI.org (Crossref)*, https://doi.org/10.3390/cancers12061393.

Gemta, Lelisa F., et al. “Impaired Enolase 1 Glycolytic Activity Restrains Effector Functions of Tumor-Infiltrating CD8 $^{+}$ T Cells.” *Science Immunology*, vol. 4, no. 31, Jan. 2019, p. eaap9520. *DOI.org (Crossref)*, https://doi.org/10.1126/sciimmunol.aap9520.

Giorgino, Toni. “Computing and Visualizing Dynamic Time Warping Alignments in *R* : The **Dtw** Package.” *Journal of Statistical Software*, vol. 31, no. 7, 2009. *DOI.org (Crossref)*, https://doi.org/10.18637/jss.v031.i07.

González-Blas, Carmen Bravo, et al. *SCENIC+: Single-Cell Multiomic Inference of Enhancers and Gene Regulatory Networks*. preprint, Bioinformatics, 19 Aug. 2022. *DOI.org (Crossref)*, https://doi.org/10.1101/2022.08.19.504505.

Greggio, Chiara, et al. “Artificial Three-Dimensional Niches Deconstruct Pancreas Development *in vitro*.” *Development*, vol. 140, no. 21, Nov. 2013, pp. 4452–62. *DOI.org (Crossref)*, https://doi.org/10.1242/dev.096628.

Grünwald, Barbara T., et al. “Spatially Confined Sub-Tumor Microenvironments in Pancreatic Cancer.” *Cell*, vol. 184, no. 22, Oct. 2021, pp. 5577-5592.e18. *DOI.org (Crossref)*, https://doi.org/10.1016/j.cell.2021.09.022.

Gu, Luo, and David J. Mooney. “Biomaterials and Emerging Anticancer Therapeutics: Engineering the Microenvironment.” *Nature Reviews Cancer*, vol. 16, no. 1, Jan. 2016, pp. 56–66. *DOI.org (Crossref)*, https://doi.org/10.1038/nrc.2015.3.

Haase, Kristina, et al. “Endothelial Regulation of Drug Transport in a 3D Vascularized Tumor Model.” *Advanced Functional Materials*, vol. 30, no. 48, Nov. 2020, p. 2002444. *DOI.org (Crossref)*, https://doi.org/10.1002/adfm.202002444.

Hafemeister, Christoph, and Rahul Satija. “Normalization and Variance Stabilization of Single-Cell RNA-Seq Data Using Regularized Negative Binomial Regression.” *Genome Biology*, vol. 20, no. 1, Dec. 2019, p. 296. *DOI.org (Crossref)*, https://doi.org/10.1186/s13059-019-1874-1.

Haghverdi, Laleh, Aaron T. L. Lun, et al. “Batch Effects in Single-Cell RNA-Sequencing Data Are Corrected by Matching Mutual Nearest Neighbors.” *Nature Biotechnology*, vol. 36, no. 5, May 2018, pp. 421–27. *DOI.org (Crossref)*, https://doi.org/10.1038/nbt.4091.

Haghverdi, Laleh, Florian Buettner, et al. “Diffusion Maps for High-Dimensional Single-Cell Analysis of Differentiation Data.” *Bioinformatics (Oxford, England)*, vol. 31, no. 18, Sept. 2015, pp. 2989–98. *PubMed*, https://doi.org/10.1093/bioinformatics/btv325.

Haghverdi, Laleh, Maren Büttner, et al. “Diffusion Pseudotime Robustly Reconstructs Lineage Branching.” *Nature Methods*, vol. 13, no. 10, Oct. 2016, pp. 845–48. *DOI.org (Crossref)*, https://doi.org/10.1038/nmeth.3971.

Haim-Vilmovsky, Liora, et al. “Mapping Rora Expression in Resting and Activated CD4+ T Cells.” *PLOS ONE*, edited by Scott N. Mueller, vol. 16, no. 5, May 2021, p. e0251233. *DOI.org (Crossref)*, https://doi.org/10.1371/journal.pone.0251233.

Hapach, Lauren A., et al. “Manipulation of *in vitro* Collagen Matrix Architecture for Scaffolds of Improved Physiological Relevance.” *Physical Biology*, vol. 12, no. 6, Dec. 2015, p. 061002. *DOI.org (Crossref)*, https://doi.org/10.1088/1478-3975/12/6/061002.

Harrington, David P., and Thomas R. Fleming. “A Class of Rank Test Procedures for Censored Survival Data.” *Biometrika*, vol. 69, no. 3, 1982, pp. 553–66. *JSTOR*, https://doi.org/10.2307/2335991.

Harrison, Rose G., et al. “Observations of the Living Developing Nerve Fiber.” *The Anatomical Record*, vol. 1, no. 5, June 1907, pp. 116–28. *DOI.org (Crossref)*, https://doi.org/10.1002/ar.1090010503.

Harrison, Sarah Ellys, et al. “Assembly of Embryonic and Extraembryonic Stem Cells to Mimic Embryogenesis *in vitro*.” *Science*, vol. 356, no. 6334, Apr. 2017, p. eaal1810. *DOI.org (Crossref)*, https://doi.org/10.1126/science.aal1810.

Hashimshony, Tamar, et al. “CEL-Seq2: Sensitive Highly-Multiplexed Single-Cell RNA-Seq.” *Genome Biology*, vol. 17, Apr. 2016, p. 77. *PubMed*, https://doi.org/10.1186/s13059-016-0938-8.

Hayday, Adrian C. “Γδ T Cells and the Lymphoid Stress-Surveillance Response.” *Immunity*, vol. 31, no. 2, Aug. 2009, pp. 184–96. *DOI.org (Crossref)*, https://doi.org/10.1016/j.immuni.2009.08.006.

He, Zhisong, et al. “CSS: Cluster Similarity Spectrum Integration of Single-Cell Genomics Data.” *Genome Biology*, vol. 21, no. 1, Dec. 2020, p. 224. *DOI.org (Crossref)*, https://doi.org/10.1186/s13059-020-02147-4.

Heinz, Sven, et al. “Simple Combinations of Lineage-Determining Transcription Factors Prime Cis-Regulatory Elements Required for Macrophage and B Cell Identities.” *Molecular Cell*, vol. 38, no. 4, May 2010, pp. 576–89. *DOI.org (Crossref)*, https://doi.org/10.1016/j.molcel.2010.05.004.

Hill, Sarah J., et al. “Prediction of DNA Repair Inhibitor Response in Short-Term Patient-Derived Ovarian Cancer Organoids.” *Cancer Discovery*, vol. 8, no. 11, Nov. 2018, pp. 1404–21. *DOI.org (Crossref)*, https://doi.org/10.1158/2159-8290.CD-18-0474.

Hinoda, Yuji, et al. “Increased Expression of MUC1 in Advanced Pancreatic Cancer.” *Journal of Gastroenterology*, vol. 38, no. 12, Dec. 2003, pp. 1162–66. *DOI.org (Crossref)*, https://doi.org/10.1007/s00535-003-1224-6.

Holmgren, Jan, and Cecil Czerkinsky. “Mucosal Immunity and Vaccines.” *Nature Medicine*, vol. 11, no. S4, Apr. 2005, pp. S45–53. *DOI.org (Crossref)*, https://doi.org/10.1038/nm1213.

Holvoet, Tom, et al. “Treatment of Intestinal Fibrosis in Experimental Inflammatory Bowel Disease by the Pleiotropic Actions of a Local Rho Kinase Inhibitor.” *Gastroenterology*, vol. 153, no. 4, Oct. 2017, pp. 1054–67. *DOI.org (Crossref)*, https://doi.org/10.1053/j.gastro.2017.06.013.

Hooper, Lora V., and Andrew J. Macpherson. “Immune Adaptations That Maintain Homeostasis with the Intestinal Microbiota.” *Nature Reviews Immunology*, vol. 10, no. 3, Mar. 2010, pp. 159–69. *DOI.org (Crossref)*, https://doi.org/10.1038/nri2710.

Horowitz, Lisa F., et al. “Microdissected ‘Cuboids’ for Microfluidic Drug Testing of Intact Tissues.” *Lab on a Chip*, vol. 21, no. 1, 2021, pp. 122–42. *DOI.org (Crossref)*, https://doi.org/10.1039/D0LC00801J.

Hoytema Van Konijnenburg, David P., et al. “Intestinal Epithelial and Intraepithelial T Cell Crosstalk Mediates a Dynamic Response to Infection.” *Cell*, vol. 171, no. 4, Nov. 2017, pp. 783-794.e13. *DOI.org (Crossref)*, https://doi.org/10.1016/j.cell.2017.08.046.

Hubert, Christopher G., et al. “A Three-Dimensional Organoid Culture System Derived from Human Glioblastomas Recapitulates the Hypoxic Gradients and Cancer Stem Cell Heterogeneity of Tumors Found *In vivo*.” *Cancer Research*, vol. 76, no. 8, Apr. 2016, pp. 2465–77. *DOI.org (Crossref)*, https://doi.org/10.1158/0008-5472.CAN-15-2402.

Huch, Meritxell, Craig Dorrell, et al. “*In vitro* Expansion of Single Lgr5+ Liver Stem Cells Induced by Wnt-Driven Regeneration.” *Nature*, vol. 494, no. 7436, Feb. 2013, pp. 247–50. *DOI.org (Crossref)*, https://doi.org/10.1038/nature11826.

Huch, Meritxell, Helmuth Gehart, et al. “Long-Term Culture of Genome-Stable Bipotent Stem Cells from Adult Human Liver.” *Cell*, vol. 160, no. 1–2, Jan. 2015, pp. 299–312. *DOI.org (Crossref)*, https://doi.org/10.1016/j.cell.2014.11.050.

Huch, Meritxell, Paola Bonfanti, et al. “Unlimited *in vitro* Expansion of Adult Bi-Potent Pancreas Progenitors through the Lgr5/R-Spondin Axis.” *The EMBO Journal*, vol. 32, no. 20, Sept. 2013, pp. 2708–21. *DOI.org (Crossref)*, https://doi.org/10.1038/emboj.2013.204.

Hughes, Chris S., et al. “Matrigel: A Complex Protein Mixture Required for Optimal Growth of Cell Culture.” *PROTEOMICS*, vol. 10, no. 9, May 2010, pp. 1886–90. *DOI.org (Crossref)*, https://doi.org/10.1002/pmic.200900758.

Hugot, Jean-Pierre, et al. “Association of NOD2 Leucine-Rich Repeat Variants with Susceptibility to Crohn’s Disease.” *Nature*, vol. 411, no. 6837, May 2001, pp. 599–603. *DOI.org (Crossref)*, https://doi.org/10.1038/35079107.

Huynh-Thu, Vân Anh, et al. “Inferring Regulatory Networks from Expression Data Using Tree-Based Methods.” *PLoS ONE*, edited by Mark Isalan, vol. 5, no. 9, Sept. 2010, p. e12776. *DOI.org (Crossref)*, https://doi.org/10.1371/journal.pone.0012776.

Iakobachvili, Nino, and Peter J. Peters. “Humans in a Dish: The Potential of Organoids in Modeling Immunity and Infectious Diseases.” *Frontiers in Microbiology*, vol. 8, Dec. 2017, p. 2402. *DOI.org (Crossref)*, https://doi.org/10.3389/fmicb.2017.02402.

Islam, Saiful, et al. “Characterization of the Single-Cell Transcriptional Landscape by Highly Multiplex RNA-Seq.” *Genome Research*, vol. 21, no. 7, July 2011, pp. 1160–67. *DOI.org (Crossref)*, https://doi.org/10.1101/gr.110882.110.

Jacob, Fadi, et al. “A Patient-Derived Glioblastoma Organoid Model and Biobank Recapitulates Inter- and Intra-Tumoral Heterogeneity.” *Cell*, vol. 180, no. 1, Jan. 2020, pp. 188-204.e22. *DOI.org (Crossref)*, https://doi.org/10.1016/j.cell.2019.11.036.

Jacomy, Mathieu, et al. “ForceAtlas2, a Continuous Graph Layout Algorithm for Handy Network Visualization Designed for the Gephi Software.” *PLoS ONE*, edited by Mark R. Muldoon, vol. 9, no. 6, June 2014, p. e98679. *DOI.org (Crossref)*, https://doi.org/10.1371/journal.pone.0098679.

Jacquemin, Guillaume, et al. “Paracrine Signalling between Intestinal Epithelial and Tumour Cells Induces a Regenerative Programme.” *eLife*, edited by Wafik S El-Deiry and Lindsey Carlsen, vol. 11, May 2022, p. e76541. *eLife*, https://doi.org/10.7554/eLife.76541.

Jaitin, D. A., et al. “Massively Parallel Single-Cell RNA-Seq for Marker-Free Decomposition of Tissues into Cell Types.” *Science*, vol. 343, no. 6172, Feb. 2014, pp. 776–79. *DOI.org (Crossref)*, https://doi.org/10.1126/science.1247651.

Jamal-Hanjani, Mariam, et al. “Tracking the Evolution of Non–Small-Cell Lung Cancer.” *New England Journal of Medicine*, vol. 376, no. 22, June 2017, pp. 2109–21. *DOI.org (Crossref)*, https://doi.org/10.1056/NEJMoa1616288.

Janda, Claudia Y., et al. “Surrogate Wnt Agonists That Phenocopy Canonical Wnt and β-Catenin Signalling.” *Nature*, vol. 545, no. 7653, May 2017, pp. 234–37. *DOI.org (Crossref)*, https://doi.org/10.1038/nature22306.

Jang, Dan-in, et al. “The Role of Tumor Necrosis Factor Alpha (TNF-α) in Autoimmune Disease and Current TNF-α Inhibitors in Therapeutics.” *International Journal of Molecular Sciences*, vol. 22, no. 5, Mar. 2021, p. 2719. *DOI.org (Crossref)*, https://doi.org/10.3390/ijms22052719.

Jansen, Camden, et al. “Building Gene Regulatory Networks from scATAC-Seq and scRNA-Seq Using Linked Self Organizing Maps.” *PLOS Computational Biology*, edited by Christina S. Leslie, vol. 15, no. 11, Nov. 2019, p. e1006555. *DOI.org (Crossref)*, https://doi.org/10.1371/journal.pcbi.1006555.

Jgamadze, Dennis, et al. “Structural and Functional Integration of Human Forebrain Organoids with the Injured Adult Rat Visual System.” *Cell Stem Cell*, vol. 30, no. 2, Feb. 2023, pp. 137-152.e7. *DOI.org (Crossref)*, https://doi.org/10.1016/j.stem.2023.01.004.

Jiang, Junyao, et al. “IReNA: Integrated Regulatory Network Analysis of Single-Cell Transcriptomes and Chromatin Accessibility Profiles.” *SSRN Electronic Journal*, 2022. *DOI.org (Crossref)*, https://doi.org/10.2139/ssrn.4071022.

Jin, Suoqin, et al. “Inference and Analysis of Cell-Cell Communication Using CellChat.” *Nature Communications*, vol. 12, no. 1, Feb. 2021, p. 1088. *DOI.org (Crossref)*, https://doi.org/10.1038/s41467-021-21246-9.

Joost, Simon, et al. “Single-Cell Transcriptomics of Traced Epidermal and Hair Follicle Stem Cells Reveals Rapid Adaptations during Wound Healing.” *Cell Reports*, vol. 25, no. 3, Oct. 2018, pp. 585-597.e7. *DOI.org (Crossref)*, https://doi.org/10.1016/j.celrep.2018.09.059.

Jowett, Geraldine M., et al. “Organoids Capture Tissue-Specific Innate Lymphoid Cell Development in Mice and Humans.” *Cell Reports*, vol. 40, no. 9, Aug. 2022, p. 111281. *DOI.org (Crossref)*, https://doi.org/10.1016/j.celrep.2022.111281.

Kadoshima, Taisuke, et al. “Self-Organization of Axial Polarity, inside-out Layer Pattern, and Species-Specific Progenitor Dynamics in Human ES Cell–Derived Neocortex.” *Proceedings of the National Academy of Sciences*, vol. 110, no. 50, Dec. 2013, pp. 20284–89. *DOI.org (Crossref)*, https://doi.org/10.1073/pnas.1315710110.

Kamimoto, Kenji, et al. “Dissecting Cell Identity via Network Inference and *in silico* Gene Perturbation.” *Nature*, vol. 614, no. 7949, Feb. 2023, pp. 742–51. *DOI.org (Crossref)*, https://doi.org/10.1038/s41586-022-05688-9.

Kanton, Sabina, et al. “Organoid Single-Cell Genomic Atlas Uncovers Human-Specific Features of Brain Development.” *Nature*, vol. 574, no. 7778, Oct. 2019, pp. 418–22. *DOI.org (Crossref)*, https://doi.org/10.1038/s41586-019-1654-9.

Kartha, Vinay K., et al. “Functional Inference of Gene Regulation Using Single-Cell Multi-Omics.” *Cell Genomics*, vol. 2, no. 9, Sept. 2022, p. 100166. *DOI.org (Crossref)*, https://doi.org/10.1016/j.xgen.2022.100166.

Kassis, Timothy, et al. “OrgaQuant: Human Intestinal Organoid Localization and Quantification Using Deep Convolutional Neural Networks.” *Scientific Reports*, vol. 9, no. 1, Aug. 2019, p. 12479. *DOI.org (Crossref)*, https://doi.org/10.1038/s41598-019-48874-y.

Kebenko, Maxim, et al. “A Multicenter Phase 1 Study of Solitomab (MT110, AMG 110), a Bispecific EpCAM/CD3 T-Cell Engager (BiTE®) Antibody Construct, in Patients with Refractory Solid Tumors.” *OncoImmunology*, Mar. 2018, p. e1450710. *DOI.org (Crossref)*, https://doi.org/10.1080/2162402X.2018.1450710.

Kim, Minsuh, et al. “Patient-Derived Lung Cancer Organoids as *in vitro* Cancer Models for Therapeutic Screening.” *Nature Communications*, vol. 10, no. 1, Sept. 2019, p. 3991. *DOI.org (Crossref)*, https://doi.org/10.1038/s41467-019-11867-6.

Kim, Seungsoo, and Joanna Wysocka. “Deciphering the Multi-Scale, Quantitative Cis-Regulatory Code.” *Molecular Cell*, vol. 83, no. 3, Feb. 2023, pp. 373–92. *DOI.org (Crossref)*, https://doi.org/10.1016/j.molcel.2022.12.032.

Klein, Allon M., et al. “Droplet Barcoding for Single-Cell Transcriptomics Applied to Embryonic Stem Cells.” *Cell*, vol. 161, no. 5, May 2015, pp. 1187–201. *DOI.org (Crossref)*, https://doi.org/10.1016/j.cell.2015.04.044.

Kodack, David P., et al. “Primary Patient-Derived Cancer Cells and Their Potential for Personalized Cancer Patient Care.” *Cell Reports*, vol. 21, no. 11, Dec. 2017, pp. 3298–309. *DOI.org (Crossref)*, https://doi.org/10.1016/j.celrep.2017.11.051.

Kong, Say Li, et al. “Cellular Reprogramming by the Conjoint Action of ERα, FOXA1, and GATA3 to a Ligand-inducible Growth State.” *Molecular Systems Biology*, vol. 7, no. 1, Jan. 2011, p. 526. *DOI.org (Crossref)*, https://doi.org/10.1038/msb.2011.59.

Kopper, Oded, et al. “An Organoid Platform for Ovarian Cancer Captures Intra- and Interpatient Heterogeneity.” *Nature Medicine*, vol. 25, no. 5, May 2019, pp. 838–49. *DOI.org (Crossref)*, https://doi.org/10.1038/s41591-019-0422-6.

Korsunsky, Ilya, et al. “Fast, Sensitive and Accurate Integration of Single-Cell Data with Harmony.” *Nature Methods*, vol. 16, no. 12, Dec. 2019, pp. 1289–96. *DOI.org (Crossref)*, https://doi.org/10.1038/s41592-019-0619-0.

Kozlowski, Mark T., et al. “Towards Organoid Culture without Matrigel.” *Communications Biology*, vol. 4, no. 1, Dec. 2021, p. 1387. *DOI.org (Crossref)*, https://doi.org/10.1038/s42003-021-02910-8.

Krebs, Angela M., et al. “The EMT-Activator Zeb1 Is a Key Factor for Cell Plasticity and Promotes Metastasis in Pancreatic Cancer.” *Nature Cell Biology*, vol. 19, no. 5, May 2017, pp. 518–29. *DOI.org (Crossref)*, https://doi.org/10.1038/ncb3513.

Kubo, Atsushi, et al. “Development of Definitive Endoderm from Embryonic Stem Cells in Culture.” *Development*, vol. 131, no. 7, Apr. 2004, pp. 1651–62. *DOI.org (Crossref)*, https://doi.org/10.1242/dev.01044.

Kumar, Brahma V., et al. “Human Tissue-Resident Memory T Cells Are Defined by Core Transcriptional and Functional Signatures in Lymphoid and Mucosal Sites.” *Cell Reports*, vol. 20, no. 12, Sept. 2017, pp. 2921–34. *DOI.org (Crossref)*, https://doi.org/10.1016/j.celrep.2017.08.078.

Kumar, Manu P., et al. “Analysis of Single-Cell RNA-Seq Identifies Cell-Cell Communication Associated with Tumor Characteristics.” *Cell Reports*, vol. 25, no. 6, Nov. 2018, pp. 1458-1468.e4. *DOI.org (Crossref)*, https://doi.org/10.1016/j.celrep.2018.10.047.

Kurmann, Anita A., et al. “Regeneration of Thyroid Function by Transplantation of Differentiated Pluripotent Stem Cells.” *Cell Stem Cell*, vol. 17, no. 5, Nov. 2015, pp. 527–42. *DOI.org (Crossref)*, https://doi.org/10.1016/j.stem.2015.09.004.

Kuzawa, Christopher W., et al. “Metabolic Costs and Evolutionary Implications of Human Brain Development.” *Proceedings of the National Academy of Sciences*, vol. 111, no. 36, Sept. 2014, pp. 13010–15. *DOI.org (Crossref)*, https://doi.org/10.1073/pnas.1323099111.

La Manno, Gioele, et al. “RNA Velocity of Single Cells.” *Nature*, vol. 560, no. 7719, Aug. 2018, pp. 494–98. *DOI.org (Crossref)*, https://doi.org/10.1038/s41586-018-0414-6.

Lancaster, Madeline A., et al. “Cerebral Organoids Model Human Brain Development and Microcephaly.” *Nature*, vol. 501, no. 7467, Sept. 2013, pp. 373–79. *DOI.org (Crossref)*, https://doi.org/10.1038/nature12517.

Lancaster, Madeline A., and Meritxell Huch. “Disease Modelling in Human Organoids.” *Disease Models & Mechanisms*, vol. 12, no. 7, July 2019, p. dmm039347. *DOI.org (Crossref)*, https://doi.org/10.1242/dmm.039347.

Lancaster, Madeline A., and Juergen A. Knoblich. “Organogenesis in a Dish: Modeling Development and Disease Using Organoid Technologies.” *Science*, vol. 345, no. 6194, July 2014, p. 1247125. *DOI.org (Crossref)*, https://doi.org/10.1126/science.1247125.

Langfelder, Peter, and Steve Horvath. “WGCNA: An R Package for Weighted Correlation Network Analysis.” *BMC Bioinformatics*, vol. 9, no. 1, Dec. 2008, p. 559. *DOI.org (Crossref)*, https://doi.org/10.1186/1471-2105-9-559.

Lee, Suk Hyung, et al. “Tumor Evolution and Drug Response in Patient-Derived Organoid Models of Bladder Cancer.” *Cell*, vol. 173, no. 2, Apr. 2018, pp. 515-528.e17. *DOI.org (Crossref)*, https://doi.org/10.1016/j.cell.2018.03.017.

Lehuédé, Camille, et al. “Metabolic Plasticity as a Determinant of Tumor Growth and Metastasis.” *Cancer Research*, vol. 76, no. 18, Sept. 2016, pp. 5201–08. *DOI.org (Crossref)*, https://doi.org/10.1158/0008-5472.CAN-16-0266.

LeSavage, Bauer L., et al. “Next-Generation Cancer Organoids.” *Nature Materials*, vol. 21, no. 2, Feb. 2022, pp. 143–59. *DOI.org (Crossref)*, https://doi.org/10.1038/s41563-021-01057-5.

Li, Jin-Tao, Yi-Ping Wang, et al. “Metabolism Remodeling in Pancreatic Ductal Adenocarcinoma.” *Cell Stress*, vol. 3, no. 12, Dec. 2019, pp. 361–68. *DOI.org (Crossref)*, https://doi.org/10.15698/cst2019.12.205.

Li, Xiaodun, et al. “Organoid Cultures Recapitulate Esophageal Adenocarcinoma Heterogeneity Providing a Model for Clonality Studies and Precision Therapeutics.” *Nature Communications*, vol. 9, no. 1, July 2018, p. 2983. *DOI.org (Crossref)*, https://doi.org/10.1038/s41467-018-05190-9.

Li, Xingnan, et al. “Oncogenic Transformation of Diverse Gastrointestinal Tissues in Primary Organoid Culture.” *Nature Medicine*, vol. 20, no. 7, July 2014, pp. 769–77. *DOI.org (Crossref)*, https://doi.org/10.1038/nm.3585.

Li, Zhijian, James S. Nagai, et al. “scMEGA: Single-Cell Multi-Omic Enhancer-Based Gene Regulatory Network Inference.” *Bioinformatics Advances*, edited by Marieke Lydia Kuijjer, vol. 3, no. 1, Jan. 2023, p. vbad003. *DOI.org (Crossref)*, https://doi.org/10.1093/bioadv/vbad003.

Liberzon, Arthur, et al. “The Molecular Signatures Database (MSigDB) Hallmark Gene Set Collection.” *Cell Systems*, vol. 1, no. 6, Dec. 2015, pp. 417–25. *PubMed*, https://doi.org/10.1016/j.cels.2015.12.004.

Liu, Longqi, et al. “Deconvolution of Single-Cell Multi-Omics Layers Reveals Regulatory Heterogeneity.” *Nature Communications*, vol. 10, no. 1, Jan. 2019, p. 470. *DOI.org (Crossref)*, https://doi.org/10.1038/s41467-018-08205-7.

Liu, Zen, and Gordana Vunjak-Novakovic. “Modeling Tumor Microenvironments Using Custom-Designed Biomaterial Scaffolds.” *Current Opinion in Chemical Engineering*, vol. 11, Feb. 2016, pp. 94–105. *DOI.org (Crossref)*, https://doi.org/10.1016/j.coche.2016.01.012.

Loomans, Cindy J. M., et al. “Expansion of Adult Human Pancreatic Tissue Yields Organoids Harboring Progenitor Cells with Endocrine Differentiation Potential.” *Stem Cell Reports*, vol. 10, no. 3, Mar. 2018, pp. 712–24. *DOI.org (Crossref)*, https://doi.org/10.1016/j.stemcr.2018.02.005.

Love, Michael I., et al. “Moderated Estimation of Fold Change and Dispersion for RNA-Seq Data with DESeq2.” *Genome Biology*, vol. 15, no. 12, 2014, p. 550. *PubMed*, https://doi.org/10.1186/s13059-014-0550-8.

Luca, Vincent C., et al. “Surrogate R-Spondins for Tissue-Specific Potentiation of Wnt Signaling.” *PLOS ONE*, edited by Chunming Liu, vol. 15, no. 1, Jan. 2020, p. e0226928. *DOI.org (Crossref)*, https://doi.org/10.1371/journal.pone.0226928.

Luecken, Malte D., and Fabian J. Theis. “Current Best Practices in Single-cell RNA-seq Analysis: A Tutorial.” *Molecular Systems Biology*, vol. 15, no. 6, June 2019, p. e8746. *DOI.org (Crossref)*, https://doi.org/10.15252/msb.20188746.

Lui, Jan H., et al. “Development and Evolution of the Human Neocortex.” *Cell*, vol. 146, no. 1, July 2011, pp. 18–36. *DOI.org (Crossref)*, https://doi.org/10.1016/j.cell.2011.06.030.

Lukonin, Ilya, et al. “Phenotypic Landscape of Intestinal Organoid Regeneration.” *Nature*, vol. 586, no. 7828, Oct. 2020, pp. 275–80. *DOI.org (Crossref)*, https://doi.org/10.1038/s41586-020-2776-9.

Luoma, Adrienne M., et al. “Molecular Pathways of Colon Inflammation Induced by Cancer Immunotherapy.” *Cell*, vol. 182, no. 3, Aug. 2020, pp. 655-671.e22. *DOI.org (Crossref)*, https://doi.org/10.1016/j.cell.2020.06.001.

Maaten, Laurens van der, and Geoffrey Hinton. “Visualizing Data Using T-SNE.” *Journal of Machine Learning Research*, vol. 9, no. 86, 2008, pp. 2579–605. *www.jmlr.org*, http://jmlr.org/papers/v9/vandermaaten08a.html.

Mackay, Laura K., et al. “The Developmental Pathway for CD103+CD8+ Tissue-Resident Memory T Cells of Skin.” *Nature Immunology*, vol. 14, no. 12, Dec. 2013, pp. 1294–301. *DOI.org (Crossref)*, https://doi.org/10.1038/ni.2744.

Macosko, Evan Z., et al. “Highly Parallel Genome-Wide Expression Profiling of Individual Cells Using Nanoliter Droplets.” *Cell*, vol. 161, no. 5, May 2015, pp. 1202–14. *DOI.org (Crossref)*, https://doi.org/10.1016/j.cell.2015.05.002.

Maggi, Laura, et al. “CD161 Is a Marker of All Human IL-17-Producing T-Cell Subsets and Is Induced by RORC.” *European Journal of Immunology*, vol. 40, no. 8, Aug. 2010, pp. 2174–81. *DOI.org (Crossref)*, https://doi.org/10.1002/eji.200940257.

Magwene, Paul M., et al. “Reconstructing the Temporal Ordering of Biological Samples Using Microarray Data.” *Bioinformatics*, vol. 19, no. 7, May 2003, pp. 842–50. *DOI.org (Crossref)*, https://doi.org/10.1093/bioinformatics/btg081.

Makohon-Moore, Alvin, and Christine A. Iacobuzio-Donahue. “Pancreatic Cancer Biology and Genetics from an Evolutionary Perspective.” *Nature Reviews Cancer*, vol. 16, no. 9, Sept. 2016, pp. 553–65. *DOI.org (Crossref)*, https://doi.org/10.1038/nrc.2016.66.

Makohon-Moore, Alvin P., et al. “Limited Heterogeneity of Known Driver Gene Mutations among the Metastases of Individual Patients with Pancreatic Cancer.” *Nature Genetics*, vol. 49, no. 3, Mar. 2017, pp. 358–66. *DOI.org (Crossref)*, https://doi.org/10.1038/ng.3764.

Mansour, Abed AlFatah, et al. “An *in vivo* Model of Functional and Vascularized Human Brain Organoids.” *Nature Biotechnology*, vol. 36, no. 5, May 2018, pp. 432–41. *DOI.org (Crossref)*, https://doi.org/10.1038/nbt.4127.

Martínez, Salvador, et al. “Molecular Regionalization of the Developing Neural Tube.” *The Mouse Nervous System*, Elsevier, 2012, pp. 2–18. *DOI.org (Crossref)*, https://doi.org/10.1016/B978-0-12-369497-3.10001-9.

Martinez-Ferre, Almudena, and Salvador Martinez. “Molecular Regionalization of the Diencephalon.” *Frontiers in Neuroscience*, vol. 6, 2012. *DOI.org (Crossref)*, https://doi.org/10.3389/fnins.2012.00073.

Martins-Costa, Catarina, et al. *Morphogenesis and Development of Human Telencephalic Organoids in the Absence and Presence of Exogenous ECM*. preprint, Developmental Biology, 7 Dec. 2022. *DOI.org (Crossref)*, https://doi.org/10.1101/2022.12.06.519271.

Masopust, David, and Andrew G. Soerens. “Tissue-Resident T Cells and Other Resident Leukocytes.” *Annual Review of Immunology*, vol. 37, no. 1, Apr. 2019, pp. 521–46. *DOI.org (Crossref)*, https://doi.org/10.1146/annurev-immunol-042617-053214.

Massa, Steffen, et al. “Critical Role for C-Kit (CD117) in T Cell Lineage Commitment and Early Thymocyte Development*in vitro*.” *European Journal of Immunology*, vol. 36, no. 3, Mar. 2006, pp. 526–32. *DOI.org (Crossref)*, https://doi.org/10.1002/eji.200535760.

Matano, Mami, et al. “Modeling Colorectal Cancer Using CRISPR-Cas9–Mediated Engineering of Human Intestinal Organoids.” *Nature Medicine*, vol. 21, no. 3, Mar. 2015, pp. 256–62. *DOI.org (Crossref)*, https://doi.org/10.1038/nm.3802.

Mayr, Urs, et al. “Exploring Single Cells in Space and Time during Tissue Development, Homeostasis and Regeneration.” *Development*, edited by Allon Klein and Barbara Treutlein, vol. 146, no. 12, June 2019, p. dev176727. *DOI.org (Crossref)*, https://doi.org/10.1242/dev.176727.

McCauley, Heather A., and James M. Wells. “Pluripotent Stem Cell-Derived Organoids: Using Principles of Developmental Biology to Grow Human Tissues in a Dish.” *Development*, vol. 144, no. 6, Mar. 2017, pp. 958–62. *DOI.org (Crossref)*, https://doi.org/10.1242/dev.140731.

McCracken, Kyle W., et al. “Modelling Human Development and Disease in Pluripotent Stem-Cell-Derived Gastric Organoids.” *Nature*, vol. 516, no. 7531, Dec. 2014, pp. 400–04. *DOI.org (Crossref)*, https://doi.org/10.1038/nature13863.

McInnes, Leland, et al. “UMAP: Uniform Manifold Approximation and Projection.” *Journal of Open Source Software*, vol. 3, no. 29, Sept. 2018, p. 861. *DOI.org (Crossref)*, https://doi.org/10.21105/joss.00861.

Miao, Yi, et al. “Next-Generation Surrogate Wnts Support Organoid Growth and Deconvolute Frizzled Pleiotropy *In vivo*.” *Cell Stem Cell*, vol. 27, no. 5, Nov. 2020, pp. 840-851.e6. *DOI.org (Crossref)*, https://doi.org/10.1016/j.stem.2020.07.020.

Micevic, Goran, et al. “IL-7R Licenses a Population of Epigenetically Poised Memory CD8 $^{+}$ T Cells with Superior Antitumor Efficacy That Are Critical for Melanoma Memory.” *Proceedings of the National Academy of Sciences*, vol. 120, no. 30, July 2023, p. e2304319120. *DOI.org (Crossref)*, https://doi.org/10.1073/pnas.2304319120.

Michels, Birgitta E., et al. “Pooled *In vitro* and *In vivo* CRISPR-Cas9 Screening Identifies Tumor Suppressors in Human Colon Organoids.” *Cell Stem Cell*, vol. 26, no. 5, May 2020, pp. 782-792.e7. *DOI.org (Crossref)*, https://doi.org/10.1016/j.stem.2020.04.003.

Mihara, Emiko, et al. “Active and Water-Soluble Form of Lipidated Wnt Protein Is Maintained by a Serum Glycoprotein Afamin/α-Albumin.” *eLife*, vol. 5, Feb. 2016, p. e11621. *DOI.org (Crossref)*, https://doi.org/10.7554/eLife.11621.

Moerman, Thomas, et al. “GRNBoost2 and Arboreto: Efficient and Scalable Inference of Gene Regulatory Networks.” *Bioinformatics*, edited by Janet Kelso, vol. 35, no. 12, June 2019, pp. 2159–61. *DOI.org (Crossref)*, https://doi.org/10.1093/bioinformatics/bty916.

Moffitt, Richard A., et al. “Virtual Microdissection Identifies Distinct Tumor- and Stroma-Specific Subtypes of Pancreatic Ductal Adenocarcinoma.” *Nature Genetics*, vol. 47, no. 10, Oct. 2015, pp. 1168–78. *DOI.org (Crossref)*, https://doi.org/10.1038/ng.3398.

Mohammadnia-Afrouzi, Mousa, et al. “Decrease of CD4 $^{+}$ CD25 $^{+}$ CD127 ^{low} FoxP3 $^{+}$ Regulatory T Cells with Impaired Suppressive Function in Untreated Ulcerative Colitis Patients.” *Autoimmunity*, vol. 48, no. 8, Nov. 2015, pp. 556–61. *DOI.org (Crossref)*, https://doi.org/10.3109/08916934.2015.1070835.

Moncada, Reuben, et al. “Integrating Microarray-Based Spatial Transcriptomics and Single-Cell RNA-Seq Reveals Tissue Architecture in Pancreatic Ductal Adenocarcinomas.” *Nature Biotechnology*, vol. 38, no. 3, Mar. 2020, pp. 333–42. *DOI.org (Crossref)*, https://doi.org/10.1038/s41587-019-0392-8.

Mora-Bermúdez, Felipe, et al. “Differences and Similarities between Human and Chimpanzee Neural Progenitors during Cerebral Cortex Development.” *eLife*, vol. 5, Sept. 2016, p. e18683. *DOI.org (Crossref)*, https://doi.org/10.7554/eLife.18683.

Morris, Brett A., et al. “Collagen Matrix Density Drives the Metabolic Shift in Breast Cancer Cells.” *EBioMedicine*, vol. 13, Nov. 2016, pp. 146–56. *DOI.org (Crossref)*, https://doi.org/10.1016/j.ebiom.2016.10.012.

Mrass, Paulus, et al. “ROCK Regulates the Intermittent Mode of Interstitial T Cell Migration in Inflamed Lungs.” *Nature Communications*, vol. 8, no. 1, Oct. 2017, p. 1010. *DOI.org (Crossref)*, https://doi.org/10.1038/s41467-017-01032-2.

Nanki, Kosaku, Kohta Toshimitsu, et al. “Divergent Routes toward Wnt and R-Spondin Niche Independency during Human Gastric Carcinogenesis.” *Cell*, vol. 174, no. 4, Aug. 2018, pp. 856-869.e17. *DOI.org (Crossref)*, https://doi.org/10.1016/j.cell.2018.07.027.

Nanki, Kosaku, Masayuki Fujii, et al. “Somatic Inflammatory Gene Mutations in Human Ulcerative Colitis Epithelium.” *Nature*, vol. 577, no. 7789, Jan. 2020, pp. 254–59. *DOI.org (Crossref)*, https://doi.org/10.1038/s41586-019-1844-5.

Nayak, Richa, and Yasha Hasija. “A Hitchhiker’s Guide to Single-Cell Transcriptomics and Data Analysis Pipelines.” *Genomics*, vol. 113, no. 2, Mar. 2021, pp. 606–19. *DOI.org (Crossref)*, https://doi.org/10.1016/j.ygeno.2021.01.007.

Neal, James T., et al. “Organoid Modeling of the Tumor Immune Microenvironment.” *Cell*, vol. 175, no. 7, Dec. 2018, pp. 1972-1988.e16. *DOI.org (Crossref)*, https://doi.org/10.1016/j.cell.2018.11.021.

Neureiter, Daniel. “Epigenetics and Pancreatic Cancer: Pathophysiology and Novel Treatment Aspects.” *World Journal of Gastroenterology*, vol. 20, no. 24, 2014, p. 7830. *DOI.org (Crossref)*, https://doi.org/10.3748/wjg.v20.i24.7830.

Ni, Wei-Dong, et al. “Tenascin-C Is a Potential Cancer-Associated Fibroblasts Marker and Predicts Poor Prognosis in Prostate Cancer.” *Biochemical and Biophysical Research Communications*, vol. 486, no. 3, May 2017, pp. 607–12. *DOI.org (Crossref)*, https://doi.org/10.1016/j.bbrc.2017.03.021.

Nichterwitz, Susanne, et al. “Laser Capture Microscopy Coupled with Smart-Seq2 for Precise Spatial Transcriptomic Profiling.” *Nature Communications*, vol. 7, no. 1, July 2016, p. 12139. *DOI.org (Crossref)*, https://doi.org/10.1038/ncomms12139.

Noel, Gaelle, et al. “A Primary Human Macrophage-Enteroid Co-Culture Model to Investigate Mucosal Gut Physiology and Host-Pathogen Interactions.” *Scientific Reports*, vol. 7, no. 1, Mar. 2017, p. 45270. *DOI.org (Crossref)*, https://doi.org/10.1038/srep45270.

Öhlund, Daniel, Abram Handly-Santana, et al. “Distinct Populations of Inflammatory Fibroblasts and Myofibroblasts in Pancreatic Cancer.” *Journal of Experimental Medicine*, vol. 214, no. 3, Mar. 2017, pp. 579–96. *DOI.org (Crossref)*, https://doi.org/10.1084/jem.20162024.

Öhlund, Daniel, Ela Elyada, et al. “Fibroblast Heterogeneity in the Cancer Wound.” *Journal of Experimental Medicine*, vol. 211, no. 8, July 2014, pp. 1503–23. *DOI.org (Crossref)*, https://doi.org/10.1084/jem.20140692.

Olabi, Safiah, et al. “Integrin-Rac Signalling for Mammary Epithelial Stem Cell Self-Renewal.” *Breast Cancer Research*, vol. 20, no. 1, Dec. 2018, p. 128. *DOI.org (Crossref)*, https://doi.org/10.1186/s13058-018-1048-1.

Orkin, R. W., et al. “A Murine Tumor Producing a Matrix of Basement Membrane.” *The Journal of Experimental Medicine*, vol. 145, no. 1, Jan. 1977, pp. 204–20. *DOI.org (Crossref)*, https://doi.org/10.1084/jem.145.1.204.

Pardo-Saganta, Ana, et al. “Injury Induces Direct Lineage Segregation of Functionally Distinct Airway Basal Stem/Progenitor Cell Subpopulations.” *Cell Stem Cell*, vol. 16, no. 2, Feb. 2015, pp. 184–97. *DOI.org (Crossref)*, https://doi.org/10.1016/j.stem.2015.01.002.

Parzanese, Ilaria, et al. “Celiac Disease: From Pathophysiology to Treatment.” *World Journal of Gastrointestinal Pathophysiology*, vol. 8, no. 2, 2017, p. 27. *DOI.org (Crossref)*, https://doi.org/10.4291/wjgp.v8.i2.27.

Paşca, Anca M., et al. “Functional Cortical Neurons and Astrocytes from Human Pluripotent Stem Cells in 3D Culture.” *Nature Methods*, vol. 12, no. 7, July 2015, pp. 671–78. *DOI.org (Crossref)*, https://doi.org/10.1038/nmeth.3415.

Pașca, Sergiu P. “The Rise of Three-Dimensional Human Brain Cultures.” *Nature*, vol. 553, no. 7689, Jan. 2018, pp. 437–45. *DOI.org (Crossref)*, https://doi.org/10.1038/nature25032.

Pavličev, Mihaela, et al. “Single-Cell Transcriptomics of the Human Placenta: Inferring the Cell Communication Network of the Maternal-Fetal Interface.” *Genome Research*, vol. 27, no. 3, Mar. 2017, pp. 349–61. *DOI.org (Crossref)*, https://doi.org/10.1101/gr.207597.116.

Peng, Junya, et al. “Author Correction: Single-Cell RNA-Seq Highlights Intra-Tumoral Heterogeneity and Malignant Progression in Pancreatic Ductal Adenocarcinoma.” *Cell Research*, vol. 29, no. 9, Sept. 2019, pp. 777–777. *DOI.org (Crossref)*, https://doi.org/10.1038/s41422-019-0212-1.

Picelli, Simone, Omid R. Faridani, et al. “Full-Length RNA-Seq from Single Cells Using Smart-Seq2.” *Nature Protocols*, vol. 9, no. 1, Jan. 2014, pp. 171–81. *DOI.org (Crossref)*, https://doi.org/10.1038/nprot.2014.006.

Picelli, Simone, Åsa K. Björklund, et al. “Smart-Seq2 for Sensitive Full-Length Transcriptome Profiling in Single Cells.” *Nature Methods*, vol. 10, no. 11, Nov. 2013, pp. 1096–98. *DOI.org (Crossref)*, https://doi.org/10.1038/nmeth.2639.

Pollen, Alex A., Aparna Bhaduri, et al. “Establishing Cerebral Organoids as Models of Human-Specific Brain Evolution.” *Cell*, vol. 176, no. 4, Feb. 2019, pp. 743-756.e17. *DOI.org (Crossref)*, https://doi.org/10.1016/j.cell.2019.01.017.

Pollen, Alex A., Umut Kilik, et al. “Human-Specific Genetics: New Tools to Explore the Molecular and Cellular Basis of Human Evolution.” *Nature Reviews Genetics*, Feb. 2023. *DOI.org (Crossref)*, https://doi.org/10.1038/s41576-022-00568-4.

Poon, Maya M. L., et al. “Tissue Adaptation and Clonal Segregation of Human Memory T Cells in Barrier Sites.” *Nature Immunology*, vol. 24, no. 2, Feb. 2023, pp. 309–19. *DOI.org (Crossref)*, https://doi.org/10.1038/s41590-022-01395-9.

Popova, Galina, et al. “Human Microglia States Are Conserved across Experimental Models and Regulate Neural Stem Cell Responses in Chimeric Organoids.” *Cell Stem Cell*, vol. 28, no. 12, Dec. 2021, pp. 2153-2166.e6. *DOI.org (Crossref)*, https://doi.org/10.1016/j.stem.2021.08.015.

Puelles, L., and S. Martinez. “Patterning of the Diencephalon.” *Patterning and Cell Type Specification in the Developing CNS and PNS*, Elsevier, 2013, pp. 151–72. *DOI.org (Crossref)*, https://doi.org/10.1016/B978-0-12-397265-1.00048-4.

Puram, Sidharth V., et al. “Single-Cell Transcriptomic Analysis of Primary and Metastatic Tumor Ecosystems in Head and Neck Cancer.” *Cell*, vol. 171, no. 7, Dec. 2017, pp. 1611-1624.e24. *DOI.org (Crossref)*, https://doi.org/10.1016/j.cell.2017.10.044.

Qian, Xuyu, et al. “Brain-Region-Specific Organoids Using Mini-Bioreactors for Modeling ZIKV Exposure.” *Cell*, vol. 165, no. 5, May 2016, pp. 1238–54. *DOI.org (Crossref)*, https://doi.org/10.1016/j.cell.2016.04.032.

Quadrato, Giorgia, et al. “Cell Diversity and Network Dynamics in Photosensitive Human Brain Organoids.” *Nature*, vol. 545, no. 7652, May 2017, pp. 48–53. *DOI.org (Crossref)*, https://doi.org/10.1038/nature22047.

Raghavan, Srivatsan, et al. “Microenvironment Drives Cell State, Plasticity, and Drug Response in Pancreatic Cancer.” *Cell*, vol. 184, no. 25, Dec. 2021, pp. 6119-6137.e26. *DOI.org (Crossref)*, https://doi.org/10.1016/j.cell.2021.11.017.

Rahib, Lola, et al. “Projecting Cancer Incidence and Deaths to 2030: The Unexpected Burden of Thyroid, Liver, and Pancreas Cancers in the United States.” *Cancer Research*, vol. 74, no. 11, June 2014, pp. 2913–21. *PubMed*, https://doi.org/10.1158/0008-5472.CAN-14-0155.

Ranga, Adrian, et al. “Neural Tube Morphogenesis in Synthetic 3D Microenvironments.” *Proceedings of the National Academy of Sciences*, vol. 113, no. 44, Nov. 2016. *DOI.org (Crossref)*, https://doi.org/10.1073/pnas.1603529113.

Raphael, Benjamin J., et al. “Integrated Genomic Characterization of Pancreatic Ductal Adenocarcinoma.” *Cancer Cell*, vol. 32, no. 2, Aug. 2017, pp. 185-203.e13. *DOI.org (Crossref)*, https://doi.org/10.1016/j.ccell.2017.07.007.

Rawla, Prashanth, Tagore Sunkara, and Adam Barsouk. “Epidemiology of Colorectal Cancer: Incidence, Mortality, Survival, and Risk Factors.” *Gastroenterology Review*, vol. 14, no. 2, 2019, pp. 89–103. *DOI.org (Crossref)*, https://doi.org/10.5114/pg.2018.81072.

Rawla, Prashanth, Tagore Sunkara, and Vinaya Gaduputi. “Epidemiology of Pancreatic Cancer: Global Trends, Etiology and Risk Factors.” *World Journal of Oncology*, vol. 10, no. 1, 2019, pp. 10–27. *DOI.org (Crossref)*, https://doi.org/10.14740/wjon1166.

Revah, Omer, et al. “Maturation and Circuit Integration of Transplanted Human Cortical Organoids.” *Nature*, vol. 610, no. 7931, Oct. 2022, pp. 319–26. *DOI.org (Crossref)*, https://doi.org/10.1038/s41586-022-05277-w.

Rheinwatd, James G., and Howard Green. “Seria Cultivation of Strains of Human Epidemal Keratinocytes: The Formation Keratinizin Colonies from Single Cell Is.” *Cell*, vol. 6, no. 3, Nov. 1975, pp. 331–43. *DOI.org (Crossref)*, https://doi.org/10.1016/S0092-8674(75)80001-8.

Riaz, Tahira, et al. “Quantitative Proteomics of Gut-Derived Th1 and Th1/Th17 Clones Reveal the Presence of CD28+ NKG2D- Th1 Cytotoxic CD4+ T Cells.” *Molecular & Cellular Proteomics*,

vol. 15, no. 3, Mar. 2016, pp. 1007–16. *DOI.org (Crossref)*, https://doi.org/10.1074/mcp.M115.050138.

Ringel, Till, et al. "Genome-Scale CRISPR Screening in Human Intestinal Organoids Identifies Drivers of TGF-β Resistance." *Cell Stem Cell*, vol. 26, no. 3, Mar. 2020, pp. 431-440.e8. *DOI.org (Crossref)*, https://doi.org/10.1016/j.stem.2020.02.007.

Roerink, Sophie F., et al. "Intra-Tumour Diversification in Colorectal Cancer at the Single-Cell Level." *Nature*, vol. 556, no. 7702, Apr. 2018, pp. 457–62. *DOI.org (Crossref)*, https://doi.org/10.1038/s41586-018-0024-3.

Rookmaaker, Maarten B., et al. "Development and Application of Human Adult Stem or Progenitor Cell Organoids." *Nature Reviews Nephrology*, vol. 11, no. 9, Sept. 2015, pp. 546–54. *DOI.org (Crossref)*, https://doi.org/10.1038/nrneph.2015.118.

Rosenberg, Alexander B., et al. "Single-Cell Profiling of the Developing Mouse Brain and Spinal Cord with Split-Pool Barcoding." *Science*, vol. 360, no. 6385, Apr. 2018, pp. 176–82. *DOI.org (Crossref)*, https://doi.org/10.1126/science.aam8999.

Rossi, Giuliana, et al. "Progress and Potential in Organoid Research." *Nature Reviews Genetics*, vol. 19, no. 11, Nov. 2018, pp. 671–87. *DOI.org (Crossref)*, https://doi.org/10.1038/s41576-018-0051-9.

Ryan, David P., et al. "Pancreatic Adenocarcinoma." *New England Journal of Medicine*, vol. 371, no. 11, Sept. 2014, pp. 1039–49. *DOI.org (Crossref)*, https://doi.org/10.1056/NEJMra1404198.

Sachs, Norman, Joep De Ligt, et al. "A Living Biobank of Breast Cancer Organoids Captures Disease Heterogeneity." *Cell*, vol. 172, no. 1–2, Jan. 2018, pp. 373-386.e10. *DOI.org (Crossref)*, https://doi.org/10.1016/j.cell.2017.11.010.

Sachs, Norman, Angelos Papaspyropoulos, et al. "Long-term Expanding Human Airway Organoids for Disease Modeling." *The EMBO Journal*, vol. 38, no. 4, Feb. 2019, p. e100300. *DOI.org (Crossref)*, https://doi.org/10.15252/embj.2018100300.

Sahai, Erik, et al. “A Framework for Advancing Our Understanding of Cancer-Associated Fibroblasts.” *Nature Reviews Cancer*, vol. 20, no. 3, Mar. 2020, pp. 174–86. *DOI.org (Crossref)*, https://doi.org/10.1038/s41568-019-0238-1.

Sartor, R. Balfour. “Mechanisms of Disease: Pathogenesis of Crohn’s Disease and Ulcerative Colitis.” *Nature Clinical Practice Gastroenterology & Hepatology*, vol. 3, no. 7, July 2006, pp. 390–407. *DOI.org (Crossref)*, https://doi.org/10.1038/ncpgasthep0528.

Sasagawa, Yohei, et al. “Quartz-Seq: A Highly Reproducible and Sensitive Single-Cell RNA Sequencing Method, Reveals Non-Genetic Gene-Expression Heterogeneity.” *Genome Biology*, vol. 14, no. 4, Apr. 2013, p. 3097. *DOI.org (Crossref)*, https://doi.org/10.1186/gb-2013-14-4-r31.

Sasai, Yoshiki. “Cytosystems Dynamics in Self-Organization of Tissue Architecture.” *Nature*, vol. 493, no. 7432, Jan. 2013, pp. 318–26. *DOI.org (Crossref)*, https://doi.org/10.1038/nature11859.

Sasson, Sarah C., et al. “Interferon-Gamma–Producing CD8+ Tissue Resident Memory T Cells Are a Targetable Hallmark of Immune Checkpoint Inhibitor–Colitis.” *Gastroenterology*, vol. 161, no. 4, Oct. 2021, pp. 1229-1244.e9. *DOI.org (Crossref)*, https://doi.org/10.1053/j.gastro.2021.06.025.

Sato, Toshiro, Daniel E. Stange, et al. “Long-Term Expansion of Epithelial Organoids From Human Colon, Adenoma, Adenocarcinoma, and Barrett’s Epithelium.” *Gastroenterology*, vol. 141, no. 5, Nov. 2011, pp. 1762–72. *DOI.org (Crossref)*, https://doi.org/10.1053/j.gastro.2011.07.050.

Sato, Toshiro, Johan H. Van Es, et al. “Paneth Cells Constitute the Niche for Lgr5 Stem Cells in Intestinal Crypts.” *Nature*, vol. 469, no. 7330, Jan. 2011, pp. 415–18. *DOI.org (Crossref)*, https://doi.org/10.1038/nature09637.

Sato, Toshiro, Robert G. Vries, et al. “Single Lgr5 Stem Cells Build Crypt-Villus Structures *in vitro* without a Mesenchymal Niche.” *Nature*, vol. 459, no. 7244, May 2009, pp. 262–65. *DOI.org (Crossref)*, https://doi.org/10.1038/nature07935.

Sato, Toshiro, and Hans Clevers. “Growing Self-Organizing Mini-Guts from a Single Intestinal Stem Cell: Mechanism and Applications.” *Science*, vol. 340, no. 6137, June 2013, pp. 1190–94. *DOI.org (Crossref)*, https://doi.org/10.1126/science.1234852.

Schild, Tanya, et al. “Unique Metabolic Adaptations Dictate Distal Organ-Specific Metastatic Colonization.” *Cancer Cell*, vol. 33, no. 3, Mar. 2018, pp. 347–54. *DOI.org (Crossref)*, https://doi.org/10.1016/j.ccell.2018.02.001.

Schnalzger, Theresa E., et al. “3D Model for CAR -mediated Cytotoxicity Using Patient-derived Colorectal Cancer Organoids.” *The EMBO Journal*, vol. 38, no. 12, June 2019, p. e100928. *DOI.org (Crossref)*, https://doi.org/10.15252/embj.2018100928.

Schutgens, Frans, and Hans Clevers. “Human Organoids: Tools for Understanding Biology and Treating Diseases.” *Annual Review of Pathology: Mechanisms of Disease*, vol. 15, no. 1, Jan. 2020, pp. 211–34. *DOI.org (Crossref)*, https://doi.org/10.1146/annurev-pathmechdis-012419-032611.

Schwank, Gerald, et al. “Functional Repair of CFTR by CRISPR/Cas9 in Intestinal Stem Cell Organoids of Cystic Fibrosis Patients.” *Cell Stem Cell*, vol. 13, no. 6, Dec. 2013, pp. 653–58. *DOI.org (Crossref)*, https://doi.org/10.1016/j.stem.2013.11.002.

Schweiger, Pawel J., and Kim B. Jensen. “Modeling Human Disease Using Organotypic Cultures.” *Current Opinion in Cell Biology*, vol. 43, Dec. 2016, pp. 22–29. *DOI.org (Crossref)*, https://doi.org/10.1016/j.ceb.2016.07.003.

Seino, Takashi, et al. “Human Pancreatic Tumor Organoids Reveal Loss of Stem Cell Niche Factor Dependence during Disease Progression.” *Cell Stem Cell*, vol. 22, no. 3, Mar. 2018, pp. 454-467.e6. *DOI.org (Crossref)*, https://doi.org/10.1016/j.stem.2017.12.009.

SelectScience. *Tuning the Elastic Moduli of Corning Matrigel and Collagen I 3D Matrices by Varying the Protein Concentration | SelectScience*. https://www.selectscience.net/application-articles/tuning-the-elastic-moduli-of-corning-matrigel-and-collagen-i-3d-matrices-by-varying-the-protein-concentration/?artid=46305. Accessed 30 Aug. 2023.

Sergi, Consolato, et al. “Intraepithelial Lymphocytes, Scores, Mimickers and Challenges in Diagnosing Gluten-Sensitive Enteropathy (Celiac Disease).” *World Journal of Gastroenterology*, vol. 23, no. 4, 2017, p. 573. *DOI.org (Crossref)*, https://doi.org/10.3748/wjg.v23.i4.573.

Serra, Denise, et al. “Self-Organization and Symmetry Breaking in Intestinal Organoid Development.” *Nature*, vol. 569, no. 7754, May 2019, pp. 66–72. *DOI.org (Crossref)*, https://doi.org/10.1038/s41586-019-1146-y.

Shin, Hyun Mu, et al. “Transient Expression of ZBTB32 in Anti-Viral CD8+ T Cells Limits the Magnitude of the Effector Response and the Generation of Memory.” *PLOS Pathogens*, edited by Christopher M. Walker, vol. 13, no. 8, Aug. 2017, p. e1006544. *DOI.org (Crossref)*, https://doi.org/10.1371/journal.ppat.1006544.

Shirai, Hiroshi, et al. “Transplantation of Human Embryonic Stem Cell-Derived Retinal Tissue in Two Primate Models of Retinal Degeneration.” *Proceedings of the National Academy of Sciences of the United States of America*, vol. 113, no. 1, Jan. 2016, pp. E81-90. *PubMed*, https://doi.org/10.1073/pnas.1512590113.

Siegel, Rebecca L., et al. “Cancer Statistics, 2018.” *CA: A Cancer Journal for Clinicians*, vol. 68, no. 1, Jan. 2018, pp. 7–30. *PubMed*, https://doi.org/10.3322/caac.21442.

Simunovic, Mijo, and Ali H. Brivanlou. “Embryoids, Organoids and Gastruloids: New Approaches to Understanding Embryogenesis.” *Development*, vol. 144, no. 6, Mar. 2017, pp. 976–85. *DOI.org (Crossref)*, https://doi.org/10.1242/dev.143529.

Singh, Akaljot, et al. “Gastrointestinal Organoids: A next-Generation Tool for Modeling Human Development.” *American Journal of Physiology-Gastrointestinal and Liver Physiology*, vol. 319, no. 3, Sept. 2020, pp. G375–81. *DOI.org (Crossref)*, https://doi.org/10.1152/ajpgi.00199.2020.

Skelly, Daniel A., et al. “Single-Cell Transcriptional Profiling Reveals Cellular Diversity and Intercommunication in the Mouse Heart.” *Cell Reports*, vol. 22, no. 3, Jan. 2018, pp. 600–10. *DOI.org (Crossref)*, https://doi.org/10.1016/j.celrep.2017.12.072.

Smillie, Christopher S., et al. “Intra- and Inter-Cellular Rewiring of the Human Colon during Ulcerative Colitis.” *Cell*, vol. 178, no. 3, July 2019, pp. 714-730.e22. *DOI.org (Crossref)*, https://doi.org/10.1016/j.cell.2019.06.029.

Sousa, André M. M., et al. “Evolution of the Human Nervous System Function, Structure, and Development.” *Cell*, vol. 170, no. 2, July 2017, pp. 226–47. *DOI.org (Crossref)*, https://doi.org/10.1016/j.cell.2017.06.036.

Spence, Jason R., et al. “Directed Differentiation of Human Pluripotent Stem Cells into Intestinal Tissue *in vitro*.” *Nature*, vol. 470, no. 7332, Feb. 2011, pp. 105–09. *DOI.org (Crossref)*, https://doi.org/10.1038/nature09691.

Ståhl, Patrik L., et al. “Visualization and Analysis of Gene Expression in Tissue Sections by Spatial Transcriptomics.” *Science*, vol. 353, no. 6294, July 2016, pp. 78–82. *DOI.org (Crossref)*, https://doi.org/10.1126/science.aaf2403.

Stuart, Tim, et al. “Comprehensive Integration of Single-Cell Data.” *Cell*, vol. 177, no. 7, June 2019, pp. 1888-1902.e21. *DOI.org (Crossref)*, https://doi.org/10.1016/j.cell.2019.05.031.

Sun, Duanchen, et al. “Identifying Phenotype-Associated Subpopulations by Integrating Bulk and Single-Cell Sequencing Data.” *Nature Biotechnology*, vol. 40, no. 4, Apr. 2022, pp. 527–38. *DOI.org (Crossref)*, https://doi.org/10.1038/s41587-021-01091-3.

Sun, Xin-Yao, et al. “Generation of Vascularized Brain Organoids to Study Neurovascular Interactions.” *eLife*, vol. 11, May 2022, p. e76707. *DOI.org (Crossref)*, https://doi.org/10.7554/eLife.76707.

Swamy, Mahima, et al. “Intestinal Intraepithelial Lymphocyte Activation Promotes Innate Antiviral Resistance.” *Nature Communications*, vol. 6, no. 1, May 2015, p. 7090. *DOI.org (Crossref)*, https://doi.org/10.1038/ncomms8090.

Szabo, Peter A., et al. “Single-Cell Transcriptomics of Human T Cells Reveals Tissue and Activation Signatures in Health and Disease.” *Nature Communications*, vol. 10, no. 1, Oct. 2019, p. 4706. *DOI.org (Crossref)*, https://doi.org/10.1038/s41467-019-12464-3.

Tadokoro, Tomomi, et al. “IL-6/STAT3 Promotes Regeneration of Airway Ciliated Cells from Basal Stem Cells.” *Proceedings of the National Academy of Sciences*, vol. 111, no. 35, Sept. 2014. *DOI.org (Crossref)*, https://doi.org/10.1073/pnas.1409781111.

Taguchi, Atsuhiro, et al. “Redefining the *In vivo* Origin of Metanephric Nephron Progenitors Enables Generation of Complex Kidney Structures from Pluripotent Stem Cells.” *Cell Stem Cell*, vol. 14, no. 1, Jan. 2014, pp. 53–67. *DOI.org (Crossref)*, https://doi.org/10.1016/j.stem.2013.11.010.

Takasato, M., et al. “Directing Human Embryonic Stem Cell Differentiation towards a Renal Lineage Generates a Self-Organizing Kidney.” *Nature Cell Biology*, vol. 16, no. 1, Jan. 2014, pp. 118–26. *DOI.org (Crossref)*, https://doi.org/10.1038/ncb2894.

Tardaguila, Manuel, et al. “SQANTI: Extensive Characterization of Long-Read Transcript Sequences for Quality Control in Full-Length Transcriptome Identification and Quantification.” *Genome Research*, vol. 28, no. 3, Mar. 2018, pp. 396–411. *DOI.org (Crossref)*, https://doi.org/10.1101/gr.222976.117.

Tasnim, Humayra, et al. “Quantitative Measurement of Naïve T Cell Association With Dendritic Cells, FRCs, and Blood Vessels in Lymph Nodes.” *Frontiers in Immunology*, vol. 9, July 2018, p. 1571. *DOI.org (Crossref)*, https://doi.org/10.3389/fimmu.2018.01571.

Therneau, Terry M., and Patricia M. Grambsch. *Modeling Survival Data: Extending the Cox Model*. Springer, 2000.

Tiriac, Hervé, et al. “Organoid Profiling Identifies Common Responders to Chemotherapy in Pancreatic Cancer.” *Cancer Discovery*, vol. 8, no. 9, Sept. 2018, pp. 1112–29. *DOI.org (Crossref)*, https://doi.org/10.1158/2159-8290.CD-18-0349.

Topalovski, Mary, and Rolf A. Brekken. “Matrix Control of Pancreatic Cancer: New Insights into Fibronectin Signaling.” *Cancer Letters*, vol. 381, no. 1, Oct. 2016, pp. 252–58. *DOI.org (Crossref)*, https://doi.org/10.1016/j.canlet.2015.12.027.

Trapnell, Cole, et al. “The Dynamics and Regulators of Cell Fate Decisions Are Revealed by Pseudotemporal Ordering of Single Cells.” *Nature Biotechnology*, vol. 32, no. 4, Apr. 2014, pp. 381–86. *DOI.org (Crossref)*, https://doi.org/10.1038/nbt.2859.

Trebak, Mohamed, and Jean-Pierre Kinet. “Calcium Signalling in T Cells.” *Nature Reviews Immunology*, vol. 19, no. 3, Mar. 2019, pp. 154–69. *DOI.org (Crossref)*, https://doi.org/10.1038/s41577-018-0110-7.

Treutlein, Barbara, et al. “Reconstructing Lineage Hierarchies of the Distal Lung Epithelium Using Single-Cell RNA-Seq.” *Nature*, vol. 509, no. 7500, May 2014, pp. 371–75. *DOI.org (Crossref)*, https://doi.org/10.1038/nature13173.

Tsukamoto, A. S., et al. “Expression of the Int-1 Gene in Transgenic Mice Is Associated with Mammary Gland Hyperplasia and Adenocarcinomas in Male and Female Mice.” *Cell*, vol. 55, no. 4, Nov. 1988, pp. 619–25. *PubMed*, https://doi.org/10.1016/0092-8674(88)90220-6.

Turner, David A., et al. “Organoids and the Genetically Encoded Self-Assembly of Embryonic Stem Cells.” *BioEssays*, vol. 38, no. 2, Feb. 2016, pp. 181–91. *DOI.org (Crossref)*, https://doi.org/10.1002/bies.201500111.

Tuveson, David, and Hans Clevers. “Cancer Modeling Meets Human Organoid Technology.” *Science*, vol. 364, no. 6444, June 2019, pp. 952–55. *DOI.org (Crossref)*, https://doi.org/10.1126/science.aaw6985.

Tüysüz, Nesrin, et al. “Lipid-Mediated Wnt Protein Stabilization Enables Serum-Free Culture of Human Organ Stem Cells.” *Nature Communications*, vol. 8, no. 1, Mar. 2017, p. 14578. *DOI.org (Crossref)*, https://doi.org/10.1038/ncomms14578.

Umkehrer, Christian, et al. “Isolating Live Cell Clones from Barcoded Populations Using CRISPRa-Inducible Reporters.” *Nature Biotechnology*, vol. 39, no. 2, Feb. 2021, pp. 174–78. *DOI.org (Crossref)*, https://doi.org/10.1038/s41587-020-0614-0.

Urbischek, Manuela, et al. “Organoid Culture Media Formulated with Growth Factors of Defined Cellular Activity.” *Scientific Reports*, vol. 9, no. 1, Apr. 2019, p. 6193. *DOI.org (Crossref)*, https://doi.org/10.1038/s41598-019-42604-0.

Van Den Brink, Susanne C., et al. “Symmetry Breaking, Germ Layer Specification and Axial Organisation in Aggregates of Mouse Embryonic Stem Cells.” *Development*, vol. 141, no. 22, Nov. 2014, pp. 4231–42. *DOI.org (Crossref)*, https://doi.org/10.1242/dev.113001.

Van Der Flier, Laurens G., and Hans Clevers. “Stem Cells, Self-Renewal, and Differentiation in the Intestinal Epithelium.” *Annual Review of Physiology*, vol. 71, no. 1, Mar. 2009, pp. 241–60. *DOI.org (Crossref)*, https://doi.org/10.1146/annurev.physiol.010908.163145.

Van Der Valk, J., et al. “Optimization of Chemically Defined Cell Culture Media – Replacing Fetal Bovine Serum in Mammalian *in vitro* Methods.” *Toxicology in vitro*, vol. 24, no. 4, June 2010, pp. 1053–63. *DOI.org (Crossref)*, https://doi.org/10.1016/j.tiv.2010.03.016.

van de Wetering, Marc, et al. “Prospective Derivation of a Living Organoid Biobank of Colorectal Cancer Patients.” *Cell*, vol. 161, no. 4, May 2015, pp. 933–45. *DOI.org (Crossref)*, https://doi.org/10.1016/j.cell.2015.03.053.

Velasco, Silvia, et al. “Individual Brain Organoids Reproducibly Form Cell Diversity of the Human Cerebral Cortex.” *Nature*, vol. 570, no. 7762, June 2019, pp. 523–27. *DOI.org (Crossref)*, https://doi.org/10.1038/s41586-019-1289-x.

Vlachogiannis, Georgios, et al. “Patient-Derived Organoids Model Treatment Response of Metastatic Gastrointestinal Cancers.” *Science*, vol. 359, no. 6378, Feb. 2018, pp. 920–26. *DOI.org (Crossref)*, https://doi.org/10.1126/science.aao2774.

Walsh, Alex J., et al. “Author Correction: Drug Response in Organoids Generated from Frozen Primary Tumor Tissues.” *Scientific Reports*, vol. 9, no. 1, Apr. 2019, p. 6517. *DOI.org (Crossref)*, https://doi.org/10.1038/s41598-019-42133-w.

Wang, Haoyi, et al. ‘One-Step Generation of Mice Carrying Mutations in Multiple Genes by CRISPR/Cas-Mediated Genome Engineering’. *Cell*, vol. 153, no. 4, May 2013, pp. 910–18. *PubMed*, https://doi.org/10.1016/j.cell.2013.04.025.

Wang, Xuefei, et al. “Reinvestigation of Classic T Cell Subsets and Identification of Novel Cell Subpopulations by Single-Cell RNA Sequencing.” *The Journal of Immunology*, vol. 208, no. 2, Jan. 2022, pp. 396–406. *DOI.org (Crossref)*, https://doi.org/10.4049/jimmunol.2100581.

Welch, Joshua D., et al. “Single-Cell Multi-Omic Integration Compares and Contrasts Features of Brain Cell Identity.” *Cell*, vol. 177, no. 7, June 2019, pp. 1873-1887.e17. *PubMed*, https://doi.org/10.1016/j.cell.2019.05.006.

Werner, Steffen, et al. “Self-Organization in Development, Regeneration and Organoids.” *Current Opinion in Cell Biology*, vol. 44, Feb. 2017, pp. 102–09. *DOI.org (Crossref)*, https://doi.org/10.1016/j.ceb.2016.09.002.

Willert, Karl, et al. “Wnt Proteins Are Lipid-Modified and Can Act as Stem Cell Growth Factors.” *Nature*, vol. 423, no. 6938, May 2003, pp. 448–52. *DOI.org (Crossref)*, https://doi.org/10.1038/nature01611.

Wolf, F. Alexander, Fiona K. Hamey, et al. “PAGA: Graph Abstraction Reconciles Clustering with Trajectory Inference through a Topology Preserving Map of Single Cells.” *Genome Biology*, vol. 20, no. 1, Dec. 2019, p. 59. *DOI.org (Crossref)*, https://doi.org/10.1186/s13059-019-1663-x.

Wolf, F. Alexander, Philipp Angerer, et al. “SCANPY: Large-Scale Single-Cell Gene Expression Data Analysis.” *Genome Biology*, vol. 19, no. 1, Dec. 2018, p. 15. *DOI.org (Crossref)*, https://doi.org/10.1186/s13059-017-1382-0.

Workman, Michael J., et al. “Engineered Human Pluripotent-Stem-Cell-Derived Intestinal Tissues with a Functional Enteric Nervous System.” *Nature Medicine*, vol. 23, no. 1, Jan. 2017, pp. 49–59. *DOI.org (Crossref)*, https://doi.org/10.1038/nm.4233.

Xavier Da Silveira Dos Santos, Aline, and Prisca Liberali. “From Single Cells to Tissue Self-organization.” *The FEBS Journal*, vol. 286, no. 8, Apr. 2019, pp. 1495–513. *DOI.org (Crossref)*, https://doi.org/10.1111/febs.14694.

Xiang, Yangfei, Yoshiaki Tanaka, Benjamin Patterson, et al. “Fusion of Regionally Specified hPSC-Derived Organoids Models Human Brain Development and Interneuron Migration.” *Cell Stem Cell*,

vol. 21, no. 3, Sept. 2017, pp. 383-398.e7. *DOI.org (Crossref)*, https://doi.org/10.1016/j.stem.2017.07.007.

Xiang, Yangfei, Yoshiaki Tanaka, Bilal Cakir, et al. "hESC-Derived Thalamic Organoids Form Reciprocal Projections When Fused with Cortical Organoids." *Cell Stem Cell*, vol. 24, no. 3, Mar. 2019, pp. 487-497.e7. *DOI.org (Crossref)*, https://doi.org/10.1016/j.stem.2018.12.015.

Xiao, Weikun, et al. "Correction: Brain-Mimetic 3D Culture Platforms Allow Investigation of Cooperative Effects of Extracellular Matrix Features on Therapeutic Resistance in Glioblastoma." *Cancer Research*, vol. 79, no. 6, Mar. 2019, pp. 1260–1260. *DOI.org (Crossref)*, https://doi.org/10.1158/0008-5472.CAN-19-0265.

Xu, Hanxiao, et al. "Organoid Technology in Disease Modelling, Drug Development, Personalized Treatment and Regeneration Medicine." *Experimental Hematology & Oncology*, vol. 7, no. 1, Dec. 2018, p. 30. *DOI.org (Crossref)*, https://doi.org/10.1186/s40164-018-0122-9.

Yang, Hui, Haoyi Wang, and Rudolf Jaenisch. 'Generating Genetically Modified Mice Using CRISPR/Cas-Mediated Genome Engineering'. *Nature Protocols*, vol. 9, no. 8, Aug. 2014, pp. 1956–68. *PubMed*, https://doi.org/10.1038/nprot.2014.134.

Yang, Hui, Haoyi Wang, Chikdu S. Shivalila, et al. 'One-Step Generation of Mice Carrying Reporter and Conditional Alleles by CRISPR/Cas-Mediated Genome Engineering'. *Cell*, vol. 154, no. 6, Sept. 2013, pp. 1370–79. *PubMed*, https://doi.org/10.1016/j.cell.2013.08.022.

Yao, Wantong, et al. "Syndecan 1 Is a Critical Mediator of Macropinocytosis in Pancreatic Cancer." *Nature*, vol. 568, no. 7752, Apr. 2019, pp. 410–14. *DOI.org (Crossref)*, https://doi.org/10.1038/s41586-019-1062-1.

Yoon, Se-Jin, et al. "Reliability of Human Cortical Organoid Generation." *Nature Methods*, vol. 16, no. 1, Jan. 2019, pp. 75–78. *DOI.org (Crossref)*, https://doi.org/10.1038/s41592-018-0255-0.

Yu, Lijia, et al. "Benchmarking Clustering Algorithms on Estimating the Number of Cell Types from Single-Cell RNA-Sequencing Data." *Genome Biology*, vol. 23, no. 1, Feb. 2022, p. 49. *DOI.org (Crossref)*, https://doi.org/10.1186/s13059-022-02622-0.

Yu, Qianhui, et al. “Charting Human Development Using a Multi-Endodermal Organ Atlas and Organoid Models.” *Cell*, vol. 184, no. 12, June 2021, pp. 3281-3298.e22. *DOI.org (Crossref)*, https://doi.org/10.1016/j.cell.2021.04.028.

Yui, Shiro, et al. “Functional Engraftment of Colon Epithelium Expanded *in vitro* from a Single Adult Lgr5+ Stem Cell.” *Nature Medicine*, vol. 18, no. 4, Apr. 2012, pp. 618–23. *DOI.org (Crossref)*, https://doi.org/10.1038/nm.2695.

Zeng, Zhen, et al. “CCL5/CCR5 Axis in Human Diseases and Related Treatments.” *Genes & Diseases*, vol. 9, no. 1, Jan. 2022, pp. 12–27. *DOI.org (Crossref)*, https://doi.org/10.1016/j.gendis.2021.08.004.

Zhang, Lu, and Jerry W. Shay. “Multiple Roles of APC and Its Therapeutic Implications in Colorectal Cancer.” *JNCI: Journal of the National Cancer Institute*, vol. 109, no. 8, Aug. 2017. *DOI.org (Crossref)*, https://doi.org/10.1093/jnci/djw332.

Zhang, Yan, et al. “Prognostic Significance and Therapeutic Implications of Peroxisome Proliferator-Activated Receptor γ Overexpression in Human Pancreatic Carcinoma.” *International Journal of Oncology*, vol. 46, no. 1, Jan. 2015, pp. 175–84. *DOI.org (Crossref)*, https://doi.org/10.3892/ijo.2014.2709.

Zhang, Yu Shrike, et al. “Multisensor-Integrated Organs-on-Chips Platform for Automated and Continual in Situ Monitoring of Organoid Behaviors.” *Proceedings of the National Academy of Sciences*, vol. 114, no. 12, Mar. 2017. *DOI.org (Crossref)*, https://doi.org/10.1073/pnas.1612906114.

Zhao, Zixuan, et al. “Organoids.” *Nature Reviews Methods Primers*, vol. 2, no. 1, Dec. 2022, p. 94. *DOI.org (Crossref)*, https://doi.org/10.1038/s43586-022-00174-y.

Zheng, Grace X. Y., et al. “Massively Parallel Digital Transcriptional Profiling of Single Cells.” *Nature Communications*, vol. 8, no. 1, Jan. 2017, p. 14049. *DOI.org (Crossref)*, https://doi.org/10.1038/ncomms14049.

Zheng, Y., et al. “Dorsal-Ventral Patterned Neural Cyst from Human Pluripotent Stem Cells in a Neurogenic Niche.” *Science Advances*, vol. 5, no. 12, Dec. 2019, p. eaax5933. *DOI.org (Crossref)*, https://doi.org/10.1126/sciadv.aax5933.

Zuin, Jessica, et al. “Nonlinear Control of Transcription through Enhancer–Promoter Interactions.” *Nature*, vol. 604, no. 7906, Apr. 2022, pp. 571–77. *DOI.org (Crossref)*, https://doi.org/10.1038/s41586-022-04570-y.

RESUME

Bruno Gjeta

PhD, COMPUTATIONAL BIOLOGY

Basel, CH

+41 77908 19 60

bruno.gjeta@roche.com

About me

Curious scientist, passionate about studying the regulatory principles underlying cell fate decisions in complex multicellular systems. Interested in disease modeling and therapeutics. Expertise in computational and developmental biology of retina, central nervous system, and cancer systems.

Education and Industry Experience

2021-2023

Doctorate in Computational Biology

University of Basel

Most relevant courses: Statistical Models in Computational Biology, Machine Learning

GPA: 6/6

Dissertation: Unveiling Cellular Dynamics: Exploring Human Disease Progression and Therapeutic Potential through Organoid Models and Single-Cell Technologies

Advisor: Gray Camp

Gray Camp Lab (IHB-Roche)

PhD Candidate in Computational Biology

2020-2021

Gray Camp Lab (IOB-Novartis)

PhD Candidate in Computational Biology

2017-2020

MSc in Biotechnology

ETH Zurich

Most relevant courses: Advanced Imaging Technologies, Systems Genomic, Design of Experiments, Genome Engineering, Stem Cells: Biology and Therapeutic Manipulation, Data Mining I & II, Next-Generation Sequencing (Lab-course), Cellular Engineering Stem Cells (Lab-course)

GPA: 5.47/6

2014-2017

BSc in Biomolecular Sciences and Technologies

Università degli Studi di Trento (CIBIO)

GPA: 104/110

Research projects and internships

2019-2020 *Master Thesis Project*

Quantitative Developmental Biology Group - ETHZ

Supervisor(s): Prof. Dr. Barbara Treutlein (ETHZ) and Group Head Dr. Gray Camp (IOB)

2018-2019 *Research Scientist*

Computational Biology Group (CoBi) - ETHZ

Supervisor(s): Prof. Dr. Dagmar Iber

2018-2018 *Research Scientist*

Computational Systems Biology Group (CSB) – ETHZ

Supervisor(s): Prof. Dr. Joerg Stelling

2017-2017 *Internship*

Laboratory of Developmental and Regenerative Biology - CIBIO

Supervisor(s): Prof. Dr. Simona Casarosa

Publications

2023

- *Journal publication:* Timothy Recaldin, Bruno Gjeta, Linda Steinacher et al., "Human Intestinal Organoids with an Autologous Tissue-Resident Immune compartment", BioRxiv, 6 October 2023, 560810 (DOI link)

2022

- *Journal publication:* Ryo Okuda, Bruno Gjeta, et al., "Reconstructing cell interactions and state trajectories in pancreatic cancer stromal tumoroids", BioRxiv, 16 February 2022, 480334 ([DOI link](https://doi.org/10.1101 /2022.02.14.480334))
- *Journal publication:* Philipp Wahle, Giovanna Brancati, Christoph Harmel, Zhisong He et al., "Multimodal spatiotemporal phenotyping of human retinal organoid development“, Nat Biotechnol, 08 May 2023, (DOI link)

2019

- *Journal publication:* Roman Vetter, Marco Kokic, et al., "Aboave-Weaire’s Law in Epithelia Results from an Angle Constraint in Contiguous Polygonal Lattices“, BioRxiv, 27 March 2019, 591461 ([DOI link](https://doi.org/10.1101 /591461))

Selected technical skills

Genomics

- RNA sequencing

Microscopy

- Widefield and confocal fluorescence imaging of live and fixed cells, organoids, and embryos

Developmental Biology

- Genetic crossing, tissue dissection, embryo staging, and sorting

Cell Biology

- Immunofluorescence (IF)

Molecular Biology

- Molecular cloning, PCR, RT-qPCR, viral particle production

Model Systems

- Danio rerio, Xenopus laevis, Saccharomyces cerevisiae, HEK and HeLa cells, human ESCs and iPSCs, human organoids and tumoroids, Escherichia coli

Data Processing & Analysis

- Python, R and RStudio big data computation, CellRanger, SQANTi3, Matlab, UNIX and MS-DOS command line, MS-Office package, SnapGene, Blast, FlowJo, Benchling, Fiji (ImageJ), Kallisto

---

Languages

- **Albanian:** Native language
- **Italian:** Native language
- **English:** Proficient (IELTS 7.5)
